A GEOCHEMICAL, PETROGRAPHIC, AND METALLOGENIC

ANALYSIS OF VOLCANOGENIC SULPHIDE DEPOSITION

WITHIN THE CONNAIGRE BAY GROUP,

HERMITAGE PENINSULA, SOUTHERN NEWFOUNDLAND

WILLIAM ALEXANDER SEARS, B.Sc. (Hons.)

Canada

A GEOCHEMICAL, PETROGRAPHIC, AND METALLOGENIC ANALYSIS

OF VOLCANOGENIC SULPHIDE DEPOSITION WITHIN THE CONNAIGRE

BAY GROUP, HERMITAGE PENINSULA, SOUTHERN NEWFOUNDLAND.

By

© William Alexander Sears, B.Sc. (Hons.)

A thesis submitted to the School of Graduate
Studies in partial fulfillment of the
requirements for the degree of
Master of Science

Department of Earth Sciences,
Memorial University of Newfoundland

May, 1990

St. John's   Newfoundland

ABSTRACT

The Hermitage Peninsula, southern Newfoundland, is underlain by the late Precambrian Connaigre Bay Group, a sequence of felsic to mafic flows, tuffs, and associated volcaniclastic sedimentary rocks. The Connaigre Bay Group was intruded by the Ordovician or older Hermitage Bay Complex, Simmons Brook Batholith, and Straddling Granite, and by the Devonian or Carboniferous Pass Island Granite and Harbour Breton Granite.

The Connaigre Bay Group is host to two significant ($\geq$ 2-3% combined Zn+Pb$\pm$(Cu)) volcanogenic massive sulphide showings (Winter Hill and Frenchman Head) and several base-metal-poor massive pyrite occurrences. The mineralized zones occur within a limited stratigraphic interval consisting of the top sequences of the lowermost, dominantly felsic, Tickle Point Formation and the lower portions of the conformably overlying, mainly mafic volcanic, Sam Head Formation.

The main showing, Winter Hill, displays some characteristics similar to the world class Kuroko deposits. The showing can be divided into two distinct zones. The lower zone is a discordant stringer-zone containing chalcopyrite and pyrite in a gangue dominated by recrystallized quartz, along with minor cordierite, chlorite, and rare andalusite. The upper zone is concordant and contains disseminated to layered massive sphalerite-galena-pyrrhotite-pyrite $\pm$ chalcopyrite in

a carbonate- and Ca-Mg-silicate-rich gangue.

The showings and occurrences probably represent deposition during a hiatus in volcanism (i.e. a change from felsic-dominated to mafic-dominated volcanism). The mineralization is situated near, and parallel to, major faults, implying that the faults exerted a structural control on mineral deposition, and provided a conduit along which mineral-rich fluids could be focussed to the seawater-seafloor interface.

The Connaigre Bay Group displays transitional calcalkaline-tholeiitic characteristics (Tickle Point Fm.), and entirely tholeiitic characteristics (Sam Head Fm. and the conformably overlying mafic volcanic Doughball Point Fm.). Major, trace, and rare earth element chemistry, along with the regional geology, suggest that sulphide deposition occurred in an extensional environment within an island arc environment. Nb depletions and LREE-enriched patterns typify island arc environments, yet high (>3) Zr/Y ratios suggest that there is some crustal contamination within the arc system.

ACKNOWLEDGEMENTS

TABLE OF CONTENTS

CHAPTER 1

INTRODUCTION

CHAPTER 2

REGIONAL AND LOCAL GEOLOGY

CHAPTER 3

GEOCHEMISTRY OF THE UNALTERED ROCKS AND PETROCHEMICAL INTERPRETATION OF THEIR TECTONIC ENVIRONMENT

CHAPTER 4

MINERALIZATION

CHAPTER 5

GEOCHEMISTRY OF THE MINERALIZED ROCKS

CHAPTER 6

SUMMARY AND CONCLUSIONS

CHEMICAL ANALYSES

ANALYTICAL TECHNIQUES

LIST OF TABLES

LIST OF FIGURES

LIST OF PLATES

CHAPTER 1

INTRODUCTION

1.1 Location and Access

The study area is underlain by the Connaigre Bay Group which crops out in a northeast-southwest trending belt between latitudes 56° 55'N and 55° 30'N and longitudes 47° 43'E and 47° 30'E within the Gaultois map sheet (N.T.S. 1M/12). Access to the area is provided via Route 360 from Bishop Falls to Harbour Breton. An unpaved road (Route 364) forks from Route 360 approximately 25 km north of Harbour Breton and continues southwestward past the coastal village of Hermitage towards Pass Island. The two routes combine to provide an excellent crossection of the Connaigre Bay Group.

The majority of the studied pyrite mineralization occurs within a short distance of the roads, whereas the significant base-metal showings at Winter Hill and Frenchman Head are both approximately 2 km off the main highway. There are no logging roads in this area so these occurrences can only be reached by foot or by helicopter.

1.2 Previous Work

The Hermitage Peninsula was geologically mapped in detail first by Widmer (1950) between 1938-1940 and in 1946. He described and mapped local granites, and presented a general

stratigraphic sequence which included a description of the unit now known as the Connaigre Bay Group (O'Driscoll and Strong, 1979).

During the mid-1950's, NALCO Ltd. geologists, while undertaking reconnaissance exploration work, discovered two base-metal prospects; one at Frenchman Head, situated 15 km northeast of Hermitage along the Hermitage Bay coast; and the other along the Harbour Breton road. They trenched and drilled the Frenchman Head prospect in the 1960's following preliminary geochemical work (McKenzie, 1984).

Greene (1975) conducted reconnaissance mapping in the Harbour Breton (1M/5) and Gaultois (1M/12) map areas, followed by 1:50,000 mapping of the Harbour Breton map sheet. He concluded that the Connaigre Bay Group was late Precambrian in age due to lithological similarities with the late Precambrian Long Harbour Group (Williams, 1971) to the east (Widmer, 1950; Greene and O'Driscoll, 1976).

Greene and O'Driscoll (1976) mapped the part of the Gaultois map area southeast of Hermitage Bay. They succeeded in dividing the Connaigre Bay Group into four conformable formations. The Hermitage area was also the subject of an M.Sc. thesis by O'Driscoll (1977).

Strong (1977) suggested that the late Precambrian volcanic rocks of the Avalon Zone show an eastward change in composition from calc-alkaline near the western margin of the zone (represented by the Connaigre Bay Group) to more alkaline

eastward (e.g. Marystown Group and the Harbour Main Group). O'Driscoll and Strong (1979) reviewed the geology and geochemistry of the late Precambrian volcanic and intrusive rocks of the Hermitage Peninsula.

Substantial mineral exploration followed the release of a lake sediment survey from the Newfoundland Department of Mines and Energy in 1978 (Butler and Davenport, 1978). BP-Selco Resources Canada Ltd. geologists (McKenzie, 1984) conducted soil geochemistry plus VLF-EM and magnetic surveys over their claims between the upper reaches of Connaigre Bay and Northeast Arm (Harbour Breton). Geologists with Noranda Exploration Co. Ltd. (Graves, 1985 and 1986) conducted extensive geophysical work on their claims at Winter Hill, located approximately 3 km south of the head of Hermitage Bay, and at their claims at Frenchman Head. They also drilled 11 diamond drill holes (with a cumulative length of 1948.2 m); nine on the Winter Hill claims and two on the Frenchman Head claims.

1.3 Physiography and Climate

The topography within the study area is dominated by a barren peneplain exhibiting greater than 50% bedrock exposure. The plateau ranges in height between 300 and 400 metres (1000 - 1300 feet) and contains numerous small ponds and lakes that are generally elongate in a northeast-southwest direction and surrounded by thick stands of stunted

spruce trees, locally known as tuckamore. Drainage is toward either the north-northwest into Hermitage Bay or to the south-southeast toward Great Bay de l'eau.

Vegetation is sparse around the more exposed areas where it consists of a thin veneer of moss and grass. Hillsides bordering the uplands and the slopes surrounding the water bodies on the plateau are almost completely covered by thick vegetation and dense stands of small softwood trees.

The climate is moderately wetter and cooler than insular Newfoundland. Thick blankets of fog are very common and can persist for weeks at a time.

1.4 Methods

The initial stages of this study consisted of two months of detailed mapping of known and newly-found pyritic base-metal showings and occurrences. Detailed maps on a scale of 1:100 or less were produced across mineralized zones from unaltered host on one side to unaltered host on the opposite side (where possible). Reconnaissance regional mapping was conducted around most of the mineralized zones. Numerous samples were taken from each site and were shipped to St. John's. Samples representative of typical lithologies in and around mineralized horizons were selected for chemical and/or petrographic analysis.

Drill core owned by Noranda (stored at the government facility at Torbay and at a Noranda owned warehouse in Gander)

was also examined and study samples were taken for chemical analysis and/or thin section study.

Major and trace element analyses (analyzed at the Newfoundland Department of Mines and Energy labs in St. John's) were conducted on 209 samples. Au assays on 144 specimens (plus 5 duplicates) were performed by Chemex Ltd. Rare earth and selected trace elements were analyzed at Memorial University by ICP-MS techniques.

Thin sections were studied under transmitted and reflected light. Unknown minerals were analysed with an electron microprobe, and a scanning electron microscope which yielded semi-quantitative analyses.

1.5 Purpose and Scope

Much of the sulphide mineralization within the Connaigre Bay Group is limited to a stratigraphic horizon comprising the upper portion of the Tickle Point Formation and the basal section of the Sam Head Formation. The bulk of this thesis is a metallogenic, petrographic, and geochemical study of sulphide mineralization within this limited stratigraphy. This data is used to interpret a possible local and regional tectonic environment.

CHAPTER 2

REGIONAL AND LOCAL GEOLOGY

2.1 Regional Tectonic Setting

The Appalachian Orogen is a northeast-trending belt (Figure 2.1) of late Precambrian and lower Paleozoic rocks, portions of which were deformed during the late Precambrian (Avalonian Orogeny), middle Ordovician (Taconic Orogeny), Devonian (Acadian Orogeny), and Permian-Carboniferous (Alleghanian Orogeny) times (Williams, 1982). The Canadian section of the orogen is bounded to the northwest by the Canadian Shield and is covered by continental slope and rise sediments to the east.

Williams et al. (1972) divided the Canadian Appalachians into nine distinct zones based upon different depositional and/or structural histories. These nine zones were then coalesced by Williams (1978a,b) into five tectonostratigraphic zones: the Humber, Gander, Dunnage, Avalon, and Meguma zones (Figure 2.1). Only the Meguma Zone is not represented in Newfoundland.

According to Williams (1979), the Humber Zone records the development and destruction of an Atlantic-type continental margin at the ancient continental margin of eastern North America. The Dunnage Zone represents the remnants of sea floor from the Iapetus Ocean with later island arc sequences and melanges. Gander Zone lithologies record the development and
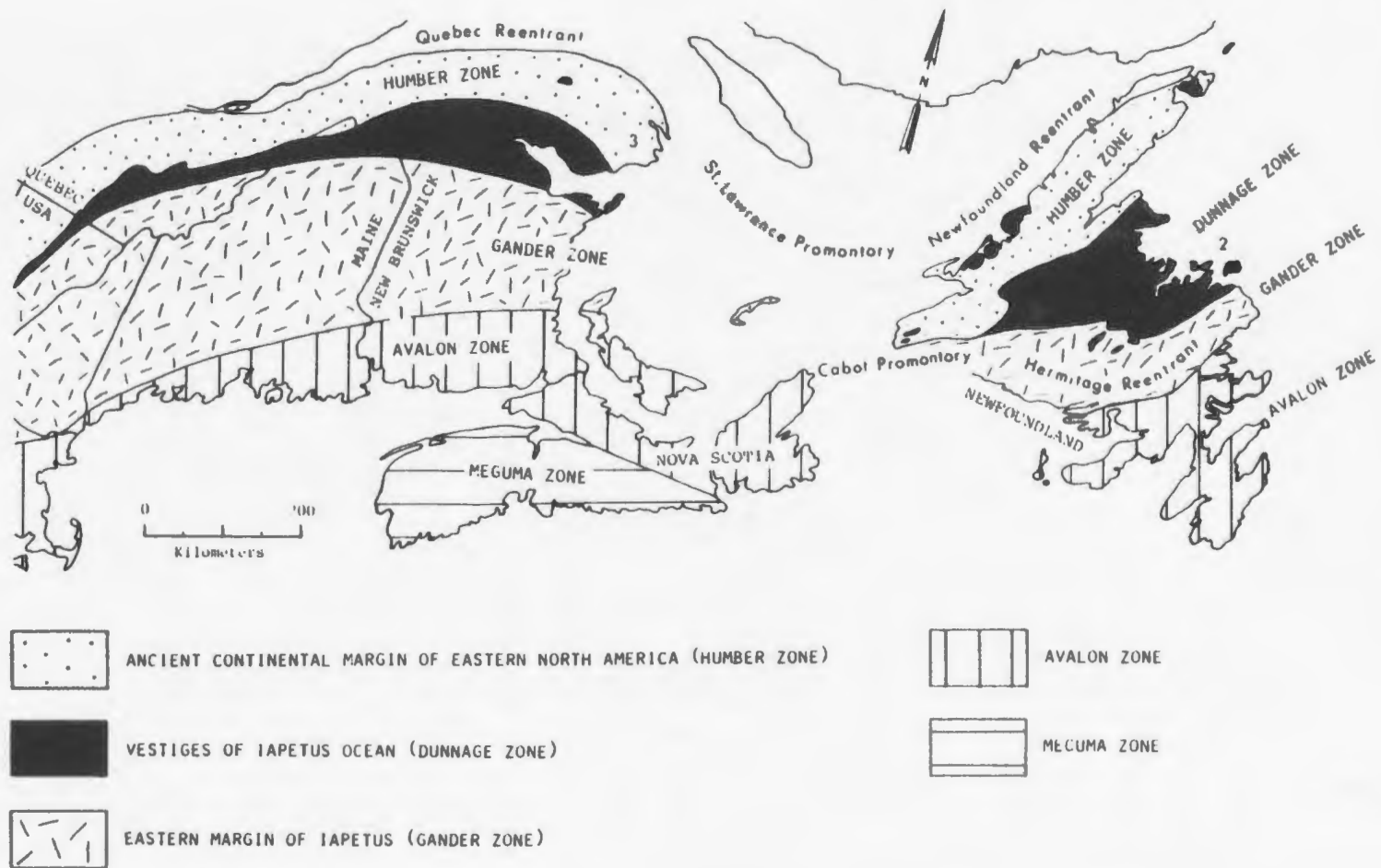
Figure 2.1. Tectonostratigraphic map of the Canadian Appalachians. Taken from Williams (1980).

destruction of a continental margin which lay to the east ofthe Iapetus Ocean. Development of the Precambrian Avalon Zone relates either to rifting and the subsequent initiation of Iapetus (Papezik, 1972), or to a subduction cycle that preceded Iapetus opening (Rast et al., 1976). The Avalon Zone was a stable platform or marine shelf during the Cambrian.

The boundaries between the earliest accreted zones (Humber, Dunnage, and Gander) are characterized by melanges and ophiolite complexes, whereas the Gander-Avalon and Avalon-Meguma Zone boundaries are marked by steep faults with broad zones of ductile deformation (Williams, 1982). The Hermitage Bay Fault, which separates the Gander and Avalon Zones in southern Newfoundland, is an exception, but the brittle deformation observed there may be a manifestation of later brittle movement along an originally ductile fault zone (Blackwood, 1975; Blackwood and O'Driscoll, 1976).

The Avalon Zone, which hosts the Connaigre Bay Group, consists of late Precambrian volcanic, sedimentary and plutonic rocks overlain by lower to mid-Paleozoic shallow marine and terrestrial sediments (Williams, 1978b; O'Brien et al., 1983). Correlatives of the Avalon Zone are found in Nova Scotia, New Brunswick, New England, Virginia, the Carolinas, and Georgia (O'Brien et al., 1983). The British Caledonides, the Hercynian-Alpine orogens of Europe, and the Pan-African belts of North America may also contain rocks with Avalon affinities (Hughes, 1972; Rast et al., 1976; Strong et al., 1978a).

The Avalon Zone is in contact with the Gander Zone along the Dover Fault (Blackwood and Kennedy, 1975) in the north and the Hermitage Bay Fault (Blackwood and O'Driscoll, 1976) in southern Newfoundland (Figure 2.2). The two fault systems are separated by the Ackley Granite which has been dated by 40Ar/39Ar techniques on biotite mineral separates at ca. 410 Ma (Kontak et al., 1988), thus constraining movement along the fault zone to pre-Devonian times. Blackwood and Kennedy (1975) suggest that the Dover Fault was last active during the late Precambrian, whereas Dallmeyer et al. (1981) describe an Acadian age for the last movement along the Hermitage Bay Fault. The Ackley Granite probably intruded during the waning stages of movement along the Hermitage Bay Fault since the fault can be traced only partially into the Ackley Granite. A late Precambrian age for the last movement along the Dover Fault would indicate that the Avalon and Gander Zones were already juxtaposed when Iapetus closed during the Paleozoic (Williams, 1978b).

The Precambrian development of the Avalon Zone precludes any genetic influence by the Paleozoic closing of the Iapetus Ocean, but it is thought that the late Precambrian Avalon lithologies may be related to rifting and the initial opening of Iapetus (Papezik, 1972). Another scenario may be that the Avalon Zone is a composite of volcanic terranes related to a subduction cycle which preceded the opening of Iapetus (Rast et al., 1976). If the Papezik (1972) theory is correct, then the Dunnage Zone formed behind a migrating Avalon
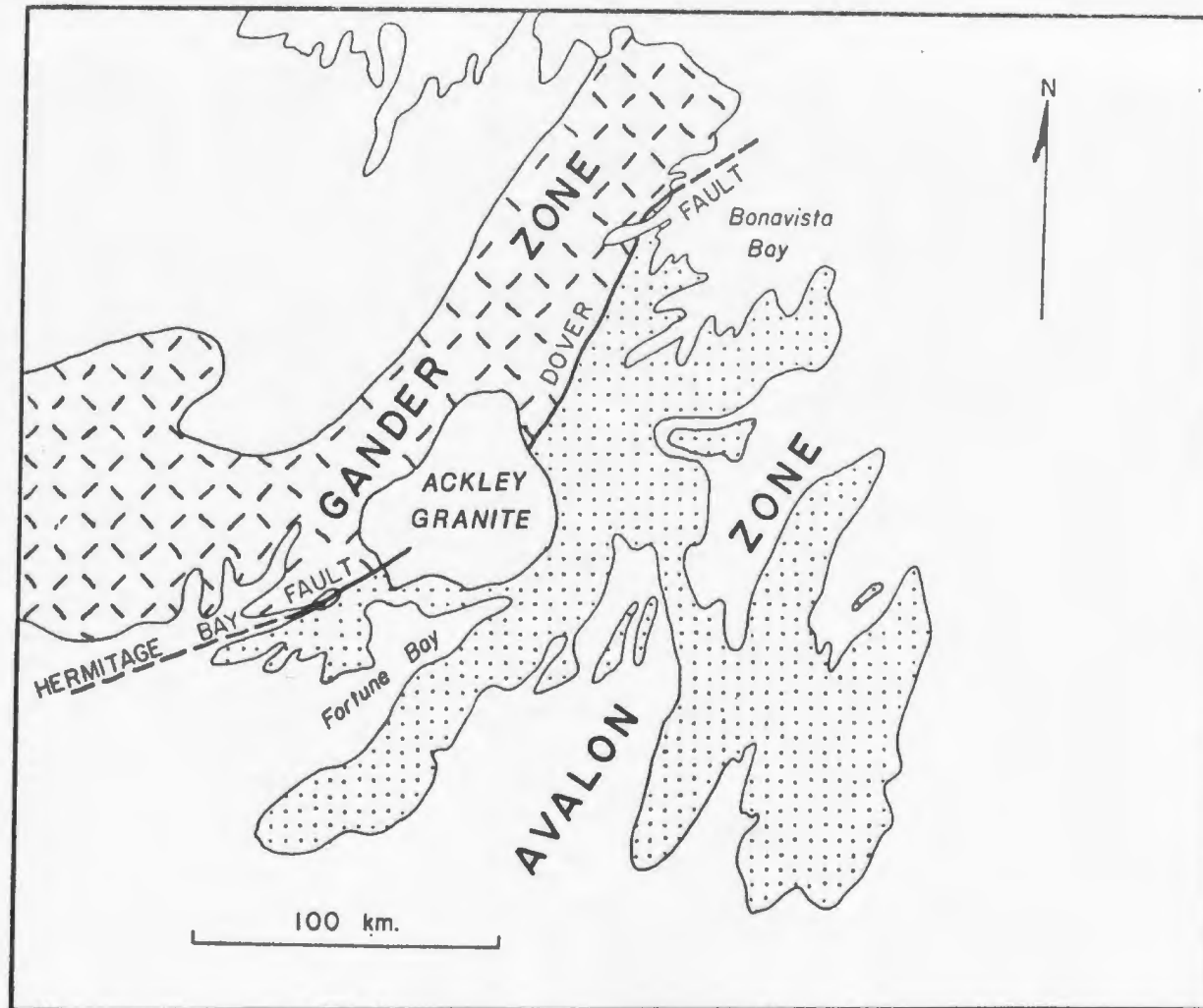
Figure 2.2. The Avalon-Gander Zone boundary and the respective positions of the Dover Fault, Hermitage Bay Fault, and the Ackley Granite. Modified from O'Driscoll (1977).

microcontinent (Schenk, 1971). The Rast et al. (1976) model suggests that the Avalon Zone evolved independently of the Humber-Dunnage assemblage and therefore its present position is due to random movement of microcontinents (Williams, 1978b).

Recent deep seismic reflection profiles across the Newfoundland Appalachians (Keen et al., 1986) have revealed a number of deep crustal relationships including: the Dover Fault is a deep structure that penetrates through the crust and appears to be unrelated to the Appalachian tectonic history; Grenvillian material extends approximately 70 km eastward under the Dunnage Zone; the Baie Verte-Brompton Line and the Gander River Ultrabasic Belt (GRUB Line) do not extend into the deep crust, therefore the Dunnage may be allochthonous, resting on both Humber and Gander Zone basement rocks and; the lower crust under the eastern Dunnage and Gander zones may have had a collisional relationship with the crust beneath the western Dunnage and Humber zones.

There is no known basement to Avalon Zone rocks in Newfoundland but there is a possible example on the French island of Miquelon (Williams, 1978b).

Direct correlation of the tectonostratigraphic zones in Newfoundland with those in other localities (e.g. Nova Scotia) is a major key and a major problem in attempting to understand the tectonic history of the Appalachian belt. Keppie (1979) included all the pre-Carboniferous rocks on Cape Breton Island and all pre-Carboniferous rocks in the Antigonish and Cobequid

Highlands of mainland Nova Scotia as part of the Avalon Zone. The Chedebucto Fault (Minas Geofracture) acts as the southern limit to the Avalon Zone, dividing it from the Meguma Zone (Keppie, 1979). Barr and Raeside (1989) subdivided pre-Carboniferous rocks of Cape Breton Island into four tectonostratigraphic terranes: the Blair River Complex, Aspy Terrane, Bras d'or Terrane, and the Mira Terrane (Figure 2.3). They conclude that only the Mira Terrane has Avalonian affinities. Their Aspy Terrane may be correlated with the Exploits and Notre Dame Subzones due to similar age ranges (i.e. mainly Ordovician to Silurian ages reported by Dunning et al. (1989) and Jamieson et al. (1986)). Crystalline rocks from the Blair River Complex give Grenvillian ages and would probably be equivalent to the rocks of the Long Range Inlier within the Humber Zone (Barr and Raeside, 1989).

The most recent tectonostratigraphic subdivisions within the Newfoundland Appalachians (William et al., 1988) affect only the Dunnage and Gander zones (Figure 2.4). The Dunnage Zone has been split into the Notre Dame and Exploits subzones. The Gander Zone is subdivided into the Gander Lake, Mount Cormack, and Meelpaeg subzones. Williams et al. (1988) suggest that some Gander Zone material may represent basement windows beneath the Exploits Subzone.

2.2 Geology of the Hermitage Peninsula

The Hermitage Peninsula is located along the southwestern margin of the Avalon Zone and is separated from the metamorphosed and polydeformed rocks of the Gander Zone by the

Figure 2.3. Tectonostratigraphic terrane map of Nova Scotia and Newfoundland and the inferred correlation. Taken from Barr and Raeside (1989).

Figure 2.4. Dunnage and Gander Zone subdivisions in Newfoundland, from Williams **et al.** (1988).

Hermitage Bay Fault (Williams, 1978b) (Figure 2.2). The peninsula is underlain by the Connaigre Bay Group, a conformable suite of late Precambrian volcanic and sedimentary rocks (Figure 2.5) (O'Driscoll, 1977; O'Driscoll and Strong, 1979) dated at 682.8 ± 1.6 Ma using the U-Pb method (Scott Swinden, 1990, pers. comm.). The Connaigre Bay Group was previously assigned a late Precambrian age due to lithological correlations with the Long Harbour Group (Williams, 1971) to the east (Widmer, 1950; Greene and O'Driscoll, 1976). The Long Harbour Group is assigned a late Precambrian age in spite of an Rb/Sr age of 515 ± 7 Ma (Williams, 1971) because it is lithologically similar to known Precambrian aged rocks of eastern Newfoundland (Williams, 1971).

All units within the Connaigre Bay Group are separated from other sedimentary sequences by faults or igneous intrusions (O'Driscoll, 1977).

The Connaigre Bay Group is intruded by the Hermitage complex which is divided into two phases: the Grole Diorite (a diorite-gabbro phase) and the Furby's Cove Granite (O'Driscoll, 1977). An age of ca. 450 Ma for the Hermitage Complex was obtained from hornblendes using the 40Ar/39Ar method (O'Driscoll, 1977). This represents a minimum age because the hornblende was possibly reset, resulting in a loss of Ar (V. Stukas, pers. comm. to O'Driscoll, 1977).

It is probable that the Hermitage Complex and the Connaigre Bay Group, together classified as a bimodal, calc-alkaline assemblage (O'Driscoll, 1977), are genetically

Figure 2.5. Geology of the Hermitage Peninsula with mineralized localities. Adapted from Sears and O'Driscoll (1989) after Greene and O'Driscoll (1976).

15

related because of geochemical and mineralogical similarities. Also, mafic and felsic dykes associated with the Hermitage Complex both cut and apparently feed the Connaigre Bay Group volcanic rocks (O'Driscoll, 1977; O'Driscoll and Strong, 1979).

The Straddling Granite, also named the Indian Point Granite by Elias and Strong (1982), is so named because it straddles the Avalon and Gander Zone boundary. It is a small intrusion, possibly related to the Hermitage Complex, located at the head of Hermitage Bay (O'Driscoll, 1977).

The Simmons Brook Batholith is a composite intrusion consisting of a range of rock types, from altered hornblende granite to hornblende-pyroxene gabbro (Colman-Sadd et al., 1979). Small gabbroic intrusions cut the Connaigre Bay Group along the south shore of upper Hermitage Bay and may also be related to the Hermitage Complex.

The Hermitage Complex was intruded by the Pass Island Granite (Widmer, 1950), a hornblende-biotite granite that is believed to be related to the ca. 410 Ma Ackley Granite.

Structural patterns on the Hermitage Peninsula are dominated by faults and broad open folds (O'Driscoll, 1977) (Plate 2.1). The faults strike in a north-northeast to northeast direction (see Figure 2.5) with steep dips to the northwest, while the open folds generally have northeast-southwest trending, gently southwest plunging axes (e.g. Salmonier Cove and Good Hill synclines) (O'Driscoll, 1977). O'Driscoll also noted that in a few localities older rocks

Plate 2.1. Broad, north-northeast trending open fold near Winter Hill. View is to the north.

Plate 2.2. Oscillatory zoned plagioclase crystal with albite twins from rhyolite belonging to the Tickle Point Formation. Sample SS88-422 (584199), magnification (mag.) = 26X, field of view (fov) = 4.0 mm (long dimension), X-nicols.

have been faulted upwards and over rocks of younger formations. Cleavage is not well developed except for an axial planar cleavage within the fine-grained sedimentary rocks of the Sam Head Formation (O'Driscoll, 1977) and a variably spaced fracture cleavage in the rocks in close proximity to the Hermitage Bay Fault.

Most, if not all, of the faults on the Hermitage Peninsula are directly or indirectly related to the Hermitage Bay Fault. This major zonal boundary is marked by a 50-100 m wide zone of brecciation which contains foliated Gander Zone fragments and unfoliated Avalon Zone fragments in a fine-grained matrix of crushed granitic and volcanic rocks (Blackwood and O'Driscoll, 1976; O'Driscoll, 1977). The fault is thought to be a high angle reverse fault (Widmer, 1950). This configuration is supported by the presence of sheared Gander Zone rocks, located near the head of Hermitage Bay, which were probably uplifted by a reverse fault (O'Driscoll, 1977).

2.3 Connaigre Bay Group - Field Relations and Petrography

2.3.1 Introduction

The late Precambrian Connaigre Bay Group is a predominantly bimodal volcanic assemblage with associated sedimentary rocks (Fig. 2.5). It can be divided into a conformable succession of four formations, viz.: Tickle Point (lowermost), Sam Head, Doughball Point, and Down's Point (uppermost) (O'Driscoll, 1977; Colman-Sadd et al., 1979)

(Figure 2.5).

2.3.2 Tickle Point Formation

The Tickle Point Formation crops out between the upper reaches of Connaigre Bay and Northeast Arm (Harbour Breton) and between Frenchman Cove and the head of Hermitage Bay. The formation consists of purple to pink, massive, flow banded and autobrecciated rhyolite and rhyolitic lithic-crystal tuff with lesser, interbedded, massive green andesite and basalt (Colman-Sadd et al., 1979) and minor argillite and cherty beds. The base of the Tickle Point Formation is unexposed, but from outcrop exposures the total thickness is at least 500 m (O'Driscoll, 1977).

Rhyolite and rhyolitic tuff are difficult to differentiate between in the field because they both contain a fine-grained matrix comprising variable amounts of crystals, and both weather to a buff colour. Flow banding in the rhyolite is not common. The rhyolites have a groundmass of very fine- to fine-grained anhedral quartz and laths of plagioclase. Where the rock is foliated, sericite is common and can be the dominant matrix mineral. Small amounts of carbonate are generally associated with sericite. The majority of the phenocrysts are plagioclase with lesser abundances of potassium feldspar and quartz. The phenocrysts are anhedral to subhedral and the plagioclase phenocrysts exhibit albite twinning and, less frequently, oscillatory zoning (Plate 2.2). There are also phenocrysts or crystal fragments with

myrmekitic or granophyric textures. In rare cases there are mafic phenocrysts, usually clinopyroxene, but also biotite. Garnet also appears infrequently as small phenocrysts. Spherulitic textures are sporadic and the spherulites are up to 1-2 cm in diameter but average a few mm in width (Plate 2.3). The spherulites are composed of fine-grained quartz and feldspar, plus sericite where alteration has taken place. Overall, the rhyolites contain 1-2% pyrite which is often oxidized to hematite.

Alteration consists of light to moderate sericite and saussurite ± carbonate alteration within the matrix component and the feldspar phenocrysts. There is minor chlorite and epidote alteration of the clinopyroxene phenocrysts. Rarely, quartz appears to replace pyrite, but must simply be secondary infilling of vacant pyrite cubes.

The rhyolite tuffs range from crystal-rich to lithic- and crystal-rich (Plate 2.4). The crystal fragments are usually quartz and K-feldspar with lesser abundance of plagioclase and minor amounts of clinopyroxene and hornblende. There are also crystal fragments of intergrown quartz and feldspar. Crystals may occasionally constitute 20-30% of a given thin section. Lithic fragments are generally subrounded and are composed of small plagioclase laths in a dark brown to black glassy matrix. Overall, lithic fragments are much less abundant than crystal fragments, but locally lithic fragments and crystal fragments are present in equal percentages. Both lithic and crystal fragments are set in a fine-grained matrix of quartz
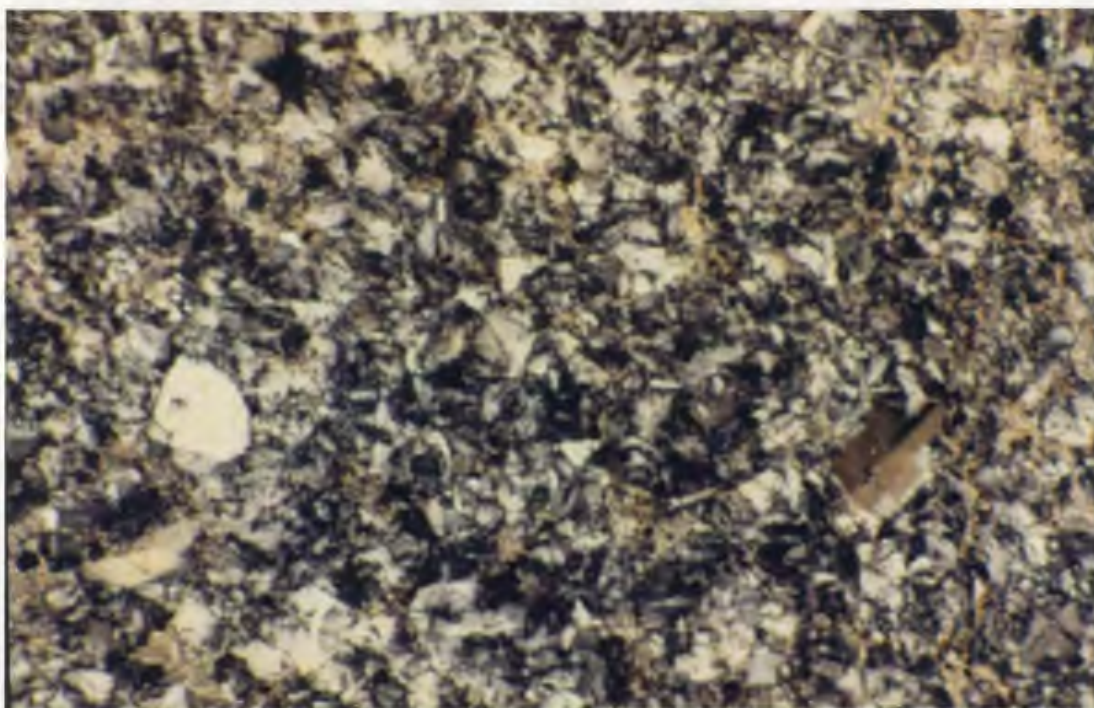
Plate 2.3. Spherulites in rhyolite from the Tickle Point Formation. Sample SS88-197 (584109), mag.= 8X, fov = 13.2 mm, X-nicols.

Plate 2.4. Lithic- and crystal-rich rhyolitic tuff from the Tickle Point Formation. Sample SS88-237 (584126), mag.= 6.3X, fov = 17.0 mm, X-nicols.

and feldspar.

Feldspars in the tuffs can range from being slightly to completely altered to sericite and/or saussurite, whereas the rare mafic crystals have minor chlorite and epidote alteration. The matrix is variably altered to chlorite, epidote and calcite. Pyrite cubes are now replaced by hematite and have feathery quartz growing around their perimeter.

The less abundant mafic rocks of the Tickle Point Formation are dominantly composed of plagioclase and pyroxene (clino and orthopyroxene) with lesser, but highly variable, amounts of quartz, potassium feldspar, hornblende, chlorite, epidote, olivine, serpentine, calcite, and opaques. Plagioclase occurs as small laths (altered to saussurite), while pyroxene occurs in the groundmass and as larger phenocrysts. Quartz is fine-grained and confined to the matrix. Both K-feldspar and hornblende are present as phenocrysts and as fine-grained matrix material. In some instances hornblende is an alteration product of clinopyroxene. Chlorite occurs as large bluish-purple clots whereas epidote is usually an alteration product of clinopyroxene and hornblende. Olivine is rare and has been altered to serpentine. These mafic rocks are frequently cut by veinlets of carbonate, quartz, and calc-silicates.

2.3.3 Sam Head Formation

Portions of the Sam Head Formation flanking Connaigre Bay are composed of laminated green and gray argillite with purple

conglomerate, sandstone, and shale at the base (O'Driscoll, 1977; Colman-Sadd et al., 1979). Limestone (marble) lenses, limey argillite layers, and chert and argillaceous cherty lenses are rare. Southeast of upper Hermitage Bay, the formation comprises interbedded mafic tuffs and tuffaceous sedimentary rocks (O'Driscoll, 1977). Carbonate/Ca-Mg-silicate lenses are present and are important, at least in one case (i.e. Winter Hill), as a site for significant base-metal accumulation. The total thickness of the Sam Head Formation is estimated to be at least 300 m (O'Driscoll, 1977).

The tuff-dominated portion of the Sam Head Formation is the more interesting because of the associated carbonate/calc-silicate lenses and accompanying base-metal mineralization. The tuffs range from lithic to crystal dominant. The crystal-lithic tuffs (Plate 2.5) contain fragments of plagioclase in a glassy matrix, lithic fragments of fine-grained pyroxene crystals, and crystal fragments of plagioclase and pyroxene (and rare biotite and hornblende), all in a fine-grained, dark brown matrix. The lithic fragments are generally round to oval and up to 1-2 cm in length. The lithic-crystal tuffs are variable with some thin sections dominated by plagioclase fragments and lesser quartz, whereas other specimens contain mostly K-feldspar and quartz crystal fragments. The crystal fragments are subhedral, broken, and usually set in a matrix similar to the matrix within the lithic-rich tuffs. There is light to moderate pervasive saussurite, epidote, sericite, and chlorite alteration.

Plate 2.5. Crystal-lithic tuff from the Sam Head Formation. Sample SS88-505 (584226), mag.= 6.3X, fov = 17.0 mm, X-nicols.

Plate 2.6. Green, fine-grained, laminated argillite from the Sam Head formation.

The carbonate/Ca-Mg-silicate lenses can be composed of several layers and incorporate a wide range of carbonate, calc-silicate, and mafic minerals. This rock type will be discussed at length in the following chapter.

The sedimentary rocks within the Sam Head Formation are monotonous, thick sequences of fine-grained argillite (Plate 2.6) overlying thin basal deposits of shale and conglomerate. The argillites contain a very fine- to fine-grained assemblage of quartz and sericite, with Ca-Mg-silicates, talc, and ± garnet present where the rock is carbonatized. There may be up to 5% opaques in some sections consisting mostly of pyrite with lesser hematite, sphalerite, and magnetite. A few sections display a "porphyritic" texture with larger plagioclase and hornblende crystals in a finer grained matrix (i.e. probably a tuff or tuffaceous rock). Bedding is thinly to thickly laminated with the laminations defined more by a grain-size variation and less so from changes in mineral composition. Some laminae contain possible spherulites of fine-grained quartz while other layers retain a ghost spherulite shape filled with sericite and quartz. Thin quartz ± carbonate veins are common.

Drill core from the Winter Hill area indicates the presence of spherulitic rocks in the structural footwall. The spherulites range in size from ≤ 1 mm to 1.5-2.0 cm and are composed of very fine- to fine-grained quartz ± feldspar set in a matrix of fine-grained sericite ± feldspar (Plate 2.7). The quartz within the spherulites generally has an

Plate 2.7. Relict spherulites composed of fine-grained quartz
and feldspar in a matrix of fine-grained sericite and
feldspar. Sample SS88-493 (584221), mag.= 7.5X, fov = 14.0
mm, X-nicols.

Plate 2.8. Relict spherulite containing fine-grained quartz-
rich cores, inner sericitic mantles, and outer sericite-and
opaque-rich mantles, in a very fine-grained sericite
groundmass. Sample SS88-515, mag.= 8X, fov = 13.2 mm, X-
nicols.

interlocking arrangement but there are rare examples where an actual spherulitic texture is visible. Boundaries between the spherulites and the matrix range from sharp, to irregular and nebulous, to boundaries where there is an outer sericitic rind between the spherulites and the groundmass (Plate 2.8).

Thin deposits of conglomerate mark the transition from the Tickle Point Formation to the Sam Head Formation. The conglomerates are polylithic with round to subround, pebble- to cobble-sized fragments. Rhyolite is the most abundant fragment with lesser argillite, mafic tuff, and granitic(?) fragments.

2.3.4 Doughball Point Formation

The Doughball Point Formation is a suite of mafic rocks which crops out around Connaigre Bay and Northeast Arm (Harbour Breton) and as small conformable or fault bounded slivers in the Good Hill area. Major rock types consist of green to gray massive andesite and basalt, fine to coarse mafic tuff and agglomerate, and minor interbedded silicic flows and tuffs (O'Driscoll, 1977; Colman-Sadd et al., 1979). At approximately 1500 m, the Doughball Point Formation is the thickest formation in the Connaigre Bay Group.

A limited number of samples of the Doughball Point Formation were examined and therefore the following may represent an incomplete description. O'Driscoll (1977) provides a more complete petrographic analysis.

Of the seven samples examined, all are mafic and

generally contain an alteration assemblage with varying amounts of chlorite, epidote, calcite, saussurite, ± talc, quartz, tremolite, and opaques. In some instances plagioclase and pyroxene crystals have been preserved with the plagioclase crystals frequently showing albite twinning and less frequently, oscillatory zoning. The crystals of plagioclase and pyroxene occur in a black, glassy groundmass (Plate 2.9). Carbonate ± epidote, garnet, quartz, zoisite, and calc-silicate rich veins are pervasive throughout the Doughball Point Formation.

2.3.5 Down's Point Formation

The Down's Point Formation consists of red, purple, and gray, graded and crossbedded sandstone and pebble to cobble conglomerate; red, thinly laminated argillite; and pink to purple massive rhyolite and silicic tuff (O'Driscoll, 1977; Colman-Sadd et al., 1979). This formation crops out along the northeast shore of upper Connaigre Bay and to the northeast of the head of Connaigre Bay. The estimated thickness of the formation is 1000 m but faulting within the thickest exposed section (southwest of Good Hill) may have caused either repetition or omission of part of the formation (O'Driscoll, 1977).

As with the Doughball Point Formation, only a limited number of samples were studied and therefore the reader is again directed to O'Driscoll (1977) for a more comprehensive petrographic analysis.
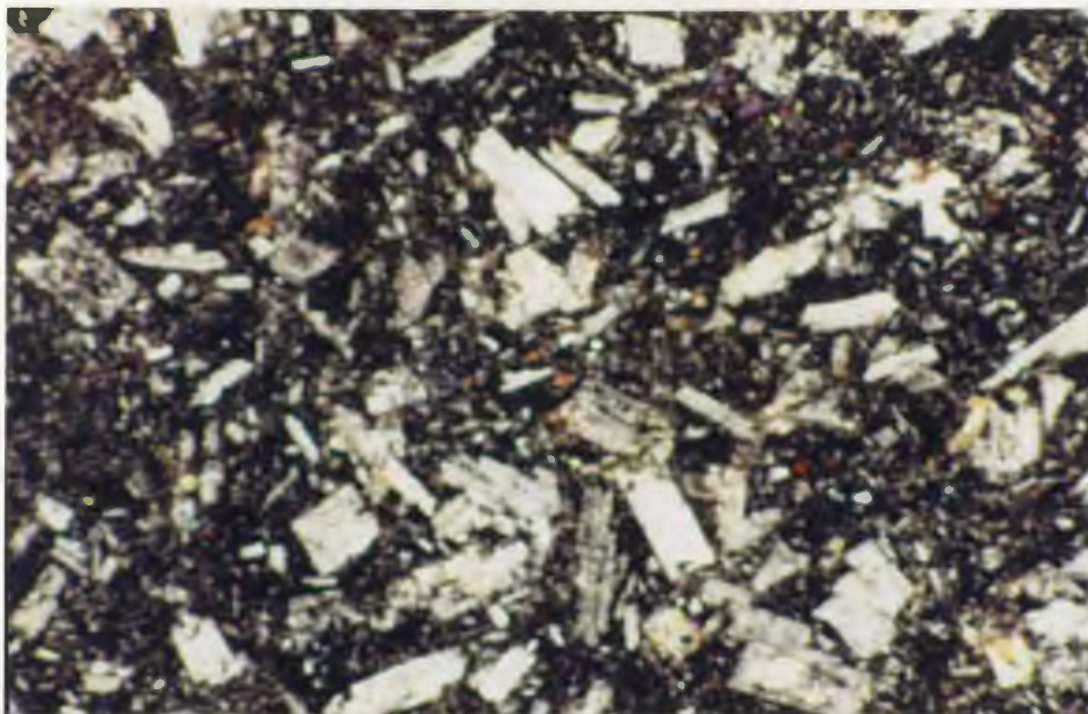
Plate 2.9. Mafic volcanic rock from the Doughball Point Formation containing plagioclase laths and small pyroxene crystals in a glassy matrix. Sample SS88-469 (584211), mag.= 20X, fov = 5.3 mm, X-nicols.

Plate 2.10. Lithic and crystal fragments in a lithic arkose from the Down's Point Formation. Sample SS88-458 (584208), mag.= 7X, fov = 15.0 mm, X-nicols.

Of four samples studied, two are arkosic and two felsic volcanic. The arkosic samples may be better described as a greywacke and a lithic arkose. The greywacke contains many fragments consisting of highly altered plagioclase laths in a very fine-grained "glassy" matrix of fine-grained calcite, chlorite, saussurite, and opaques. There is also a small percentage of crystal fragments, mostly quartz with some feldspar. The lithic arkose contains numerous quartz and feldspar crystal fragments, with lesser amounts of lithic fragments (Plate 2.10). These lithic fragments are glassy with visible plagioclase laths. The crystal and lithic fragments are set in a matrix similar to that of the greywacke. All feldspars are moderately to strongly altered to an assemblage of sericite, saussurite, and chlorite. The glassy nature of both of these samples may indicate a close volcanic association (i.e. the rocks may be pyroclastic and not epiclastic in origin).

The two felsic volcanic flow rocks examined consist of an equigranular groundmass of plagioclase and lesser quartz and K-feldspar with K-feldspar, plagioclase, and chlorite phenocrysts. The chlorite phenocrysts pseudomorph either clinopyroxene or hornblende. The feldspars are partially to wholly altered to sericite and saussurite.

Calcite veining is present in all thin sections.

2.4 Intrusive Rocks

2.4.1 Hermitage Complex (Grole Diorite)

The Grole Diorite is the major phase, in area, of the Hermitage Complex, comprising approximately 85% of the observed outcrop (O'Driscoll, 1977). This mafic phase crops out on the southwestern part of the Hermitage Peninsula while many related mafic dykes crop out regularly throughout the peninsula. The Grole Diorite is actually a composite of quartz diorite, diorite, and gabbro with minor occurrences of granodiorite (O'Driscoll, 1977). Hornblende separates from the gabbro have been dated at ca. 450 Ma (O'Driscoll, 1977, pers. comm. from P.H. Reynolds, 1975) by 40Ar/39Ar techniques. The hornblendes may have been reset (i.e. reheated so that Ar is lost) so the date represents a minimum age (O'Driscoll, 1977).

Outcrops are usually an assemblage of medium- to coarse-grained hornblende and plagioclase with varying amounts of biotite, quartz, potassium feldspar and minor to trace amounts of magnetite, pyrite, and chalcopyrite. Pegmatitic areas are common (Plate 2.11), especially near contacts with country rock. Also exposed at the contact in a roadside quarry between Partridge Cove and Hermitage Cove is a complex zone of partial assimilation of mafic country rock from the Doughball Point Formation. Some country rock inclusions are aligned and partially stretched whereas other inclusions are almost completely resorbed (O'Driscoll, 1977).

In thin section, hornblende and plagioclase comprise the bulk of the mineralogy with pyroxene, biotite, orthoclase, and

Plate 2.11. Late-stage (?) coarse-grained granitic phase cutting gabbro from the Hermitage Bay Complex.
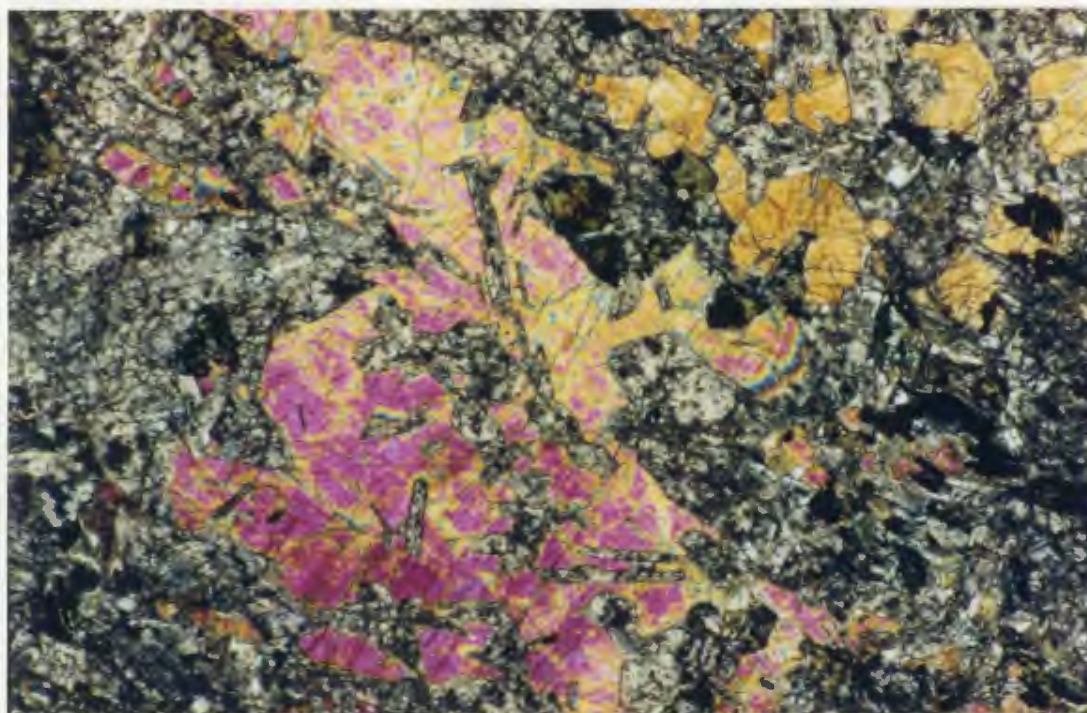
Plate 2.12. Ophitic to subophitic texture in a gabbroic phase of the Hermitage Bay Complex. Sample SS88-264 (584138), mag.= 17.5X, fov = 6.2 mm, X-nicols.

quartz ranging from minor to locally abundant. There are up to a few percent opaques, dominantly magnetite.

Plagioclase (andesine) is commonly partially to almost completely saussuritized. It displays an ophitic to subophitic texture in hornblende (altered clinopyroxene), and to a lesser extent in fresh clinopyroxene (Plate 2.12), but andesine generally occurs as randomly oriented lath-shaped crystals. Hornblende is anhedral to subhedral and pleochroic green to brown. It is mainly medium- to coarse-grained but in someplaces is found as fibrous masses (uralite) probably as a replacement product of clinopyroxene. It is also found replacing clinopyroxene along fractures within, and rims around, many clinopyroxene crystals (Plate 2.13). It is therefore difficult to determine how much (if any) of the hornblende is primary. Clinopyroxene (augite) occurs as large crystals often partially replaced by hornblende. Where augite is present, it is usually the dominant mineral. Biotite is much less common than hornblende or augite and occurs as anhedral crystals displaying dark brown pleochroism. Orthoclase and quartz occur mainly in the more felsic-rich phases as small anhedral crystals, rarely showing embayment textures. Orthoclase tends to be slightly altered to a fine-grained assemblage dominated by muscovite. Quartz is relatively fresh but is strained (i.e. displays undulose extinction). Opaque minerals constitute approximately 1-2% of the rocks with magnetite being the dominant opaque. Magnetite occurs as skeletal crystals and also as concentrations along

Plate 2.13. Hornblende (hb) replacing clinopyroxene (cpx) in a gabbroic phase of the Hermitage Bay Complex. Sample SS88-351 (584172), mag.= 20X, X-nicols.

Plate 2.14. Older rhyolite dyke containing plagioclase phenocrysts in a fine-grained quartzo-feldspathic matrix. Sample SS88-062 (584034), mag.= 6.3X, fov = 17.0 mm, X-nicols.

cleavage planes in hornblende and clinopyroxene, probably as a result of clinopyroxene breaking down to hornblende.

2.4.2 Simmons Brook Batholith

The Simmons Brook Batholith is a problem in the study area because of its similarities to the mafic phases of the Hermitage Complex (i.e. Grole Diorite). Small intrusive bodies located along the southern shore near the head of Hermitage Bay have been attributed to the Hermitage Complex (O'Driscoll, 1977) but are now included as part of the Simmons Brook Batholith (Colman-Sadd et al., 1979). The Simmons Brook Batholith is assigned an Ordovician (?) age, as is the Hermitage Complex, providing some basis that both intrusions may be related.

Rocks of the Simmons Brook Batholith range from hornblende-biotite granite to medium-grained, equigranular, altered hornblende-biotite granodiorite, to a fine- to coarse-grained diorite and hornblende-pyroxene gabbro (Colman-Sadd et al., 1979). Within the study area, diorite and gabbro are the only visible phases, which on an outcrop scale are indistinguishable from phases of the Grole Diorite. Thin section analyses reveal that the Simmons Brook Batholith samples appear to be more highly altered equivalents of the Grole Diorite.

2.4.3 Straddling Granite

The Straddling Granite (Indian Point Pluton, Elias and

Strong, 1982), is another Ordovician (?) intrusion thought to be genetically related to the Furby's Cove Granite (O'Driscoll, 1977). The Straddling Granite is composed of medium-grained, orange-pink to gray granite and granodiorite (O'Driscoll, 1977). It is situated near the head of Hermitage Bay and has been brittly deformed by the Hermitage Bay Fault.

The study by Elias and Strong (1982) concentrated on the part of the Straddling Granite north of the Hermitage Bay Fault. There is speculation over the relationship between the granite north (Gander Zone) of the fault and that south (Avalon Zone) of the fault (i.e. adjacent to the Hermitage Bay Fault, the Straddling Granite north and south are mylonitized and brecciated respectively). It is possible that the granite north of the fault represents a deeper level of erosion due to uplift on the Gander Zone side of the Hermitage Bay Fault.

2.5 Felsic and Mafic Dykes

2.5.1 Felsic Dykes

Two generations of felsic dykes combine to cut all the lithologies of the Connaigre Bay Group (O'Driscoll, 1977). The older dykes are related to the Furby's Cove Granite whereas the younger dykes cut the Devonian Pass Island Granite and are therefore assigned a Devonian or younger age (O'Driscoll, 1977). Both dyke sets are pink to orange, aphanitic, and porphyritic (Colman-Sadd et al., 1979). Since the dykes are texturally and geochemically similar, those mapped in the field were either assigned an Ordovician (?) age (i.e. related

to the Furbys Cove Granite) because they cut, or were cut by, equigranular diabase dykes from the Grole Diorite, or if they were cutting only Connaigre Bay Group lithologies their age was noted as being uncertain.

The felsic dykes are fine- to medium-grained masses of quartz and feldspar with only minor amounts of other minerals. The matrix component is an unoriented mixture of often equal amounts of quartz and feldspar with plagioclase being the dominant feldspar over orthoclase. Fine-grained muscovite can be prevalent as a matrix phase creating a slight fabric. The feldspars are partially altered to sericite and saussurite. Plagioclase (oligoclase) is the dominant phenocryst (Plate 2.14), with minor orthoclase and quartz. The phenocrysts can be up to 5 mm in length with plagioclase usually the larger phenocryst. Plagioclase and orthoclase, like their matrix component, are also partially altered to sericite and saussurite. Quartz phenocrysts are usually quite fresh but show a very distinctive undulose extinction pattern. Rare muscovite phenocrysts are also present. Radial clusters of quartz (spherulites ?) are also common in some of the dykes (Plate 2.15).

Accessory minerals include hornblende (now partially altered to chlorite and epidote) and pyrite. There are also rare grains of zircon and garnet.

2.5.2 Mafic Dykes

Mafic dykes, as with the felsic dykes, are ubiquitous
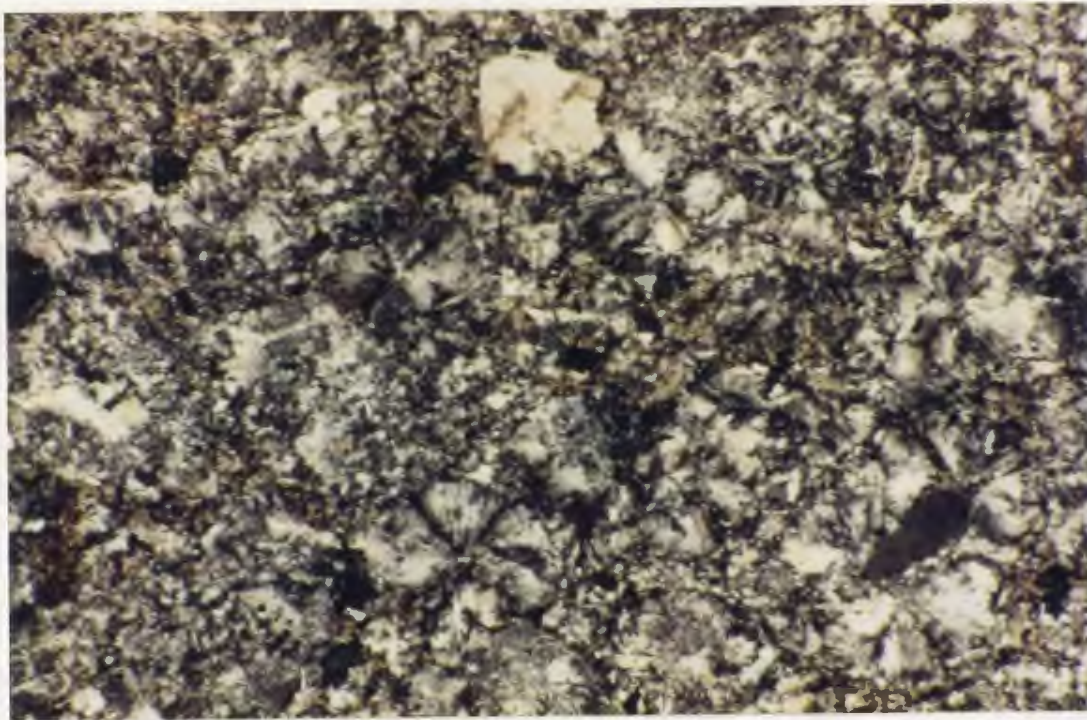
Plate 2.15. Spherulites in a rhyolite dyke. Sample SS88-502, mag.= 20X, fov = 5.3 mm, X-nicols.
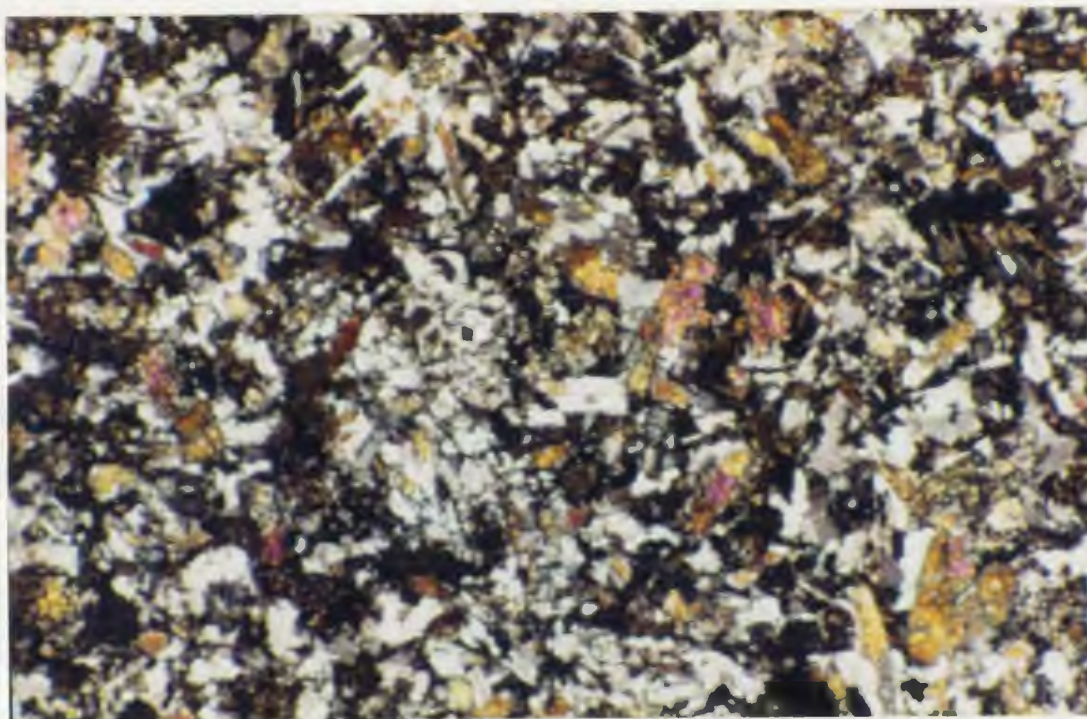
Plate 2.16. Equigranular texture from the older mafic dyke suite. Sample SS88-284 (584145), mag.=32X, fov = 3.3 mm, X-nicols.

throughout the Connaigre Bay Group. There are also two generations of dykes. The older set of dykes is related to the Grole Diorite thus giving it an Ordovician (?) age (O'Driscoll, 1977). The younger dyke set is petrologically and texturally different from the older set. It is given a Devonian or later age because it cuts the Devonian Pass Island Granite (O'Driscoll, 1977).

The older dykes are composed of almost equal amounts of clinopyroxene (now partially hornblende) and plagioclase (Plate 2.16). This subhedral to euhedral assemblage is usually equigranular but clinopyroxene can be present as phenocrysts. Less common, but locally abundant, minerals are orthopyroxene, epidote, chlorite, hornblende, K-feldspar, carbonate, quartz, and opaque minerals. Saussuritization and sericitization of the feldspars is common. Clinopyroxene is either colorless or faintly pink pleochroic and commonly fractured. Chlorite, epidote, and hornblende are common alteration minerals along these fractures, and are also found pseudomorphing primary mafic minerals. Quartz and carbonate occur in cross-cutting veins and less commonly as pods. The opaque minerals consist of cubic or skeletal crystals of pyrite and magnetite, respectively. These opaques may comprise up to 5% of the rock.

A few of these dykes exhibit a fine-grained equigranular texture with possible ghost amygdules outlined by a concentric arrangement of altered plagioclase crystals.

The younger dyke set is characterized by large plagioclase phenocrysts set in a fine-grained matrix. The

Plate 2.17. Altered plagioclase crystals with relict albite twins from the younger mafic dyke set. Sample SS88-366 (584177), mag.= 6.3X, fov = 17.0 mm, X-nicols.

plagioclase phenocrysts range from relatively unaltered oscillatory zoned crystals to completely saussuritized crystals with only minute relics of albite twins (Plate 2.17). The matrix component is mainly plagioclase and hornblende with lesser amounts of clinopyroxene, quartz, K-feldspar, opaques, and secondary epidote and chlorite. In a more felsic sample, quartz is quite common in the groundmass and occurs as free crystals and spherical aggregates with a radial texture.

CHAPTER 3

GEOCHEMISTRY OF UNALTERED ROCKS AND PETROCHEMICAL

INTERPRETATION OF THEIR TECTONIC ENVIRONMENT

3.1 Major and Trace Elements

3.1.1. Introduction

Extensive geochemistry was undertaken in this study. Two hundred and ten samples were analyzed for the following major oxide and trace elements:

major oxides - SiO_2, Al_2O_3, Fe_2O_3 (total Fe), MgO, CaO, Na_2O, K_2O, TiO_2, MnO, P_2O_5, and LOI (loss on ignition);

trace elements - Cr, Ni, Co, V, Cu, Pb, Zn, Cd, Mo, Ag, Au, Rb, Ba, Sr, Ga, Li, Nb, Zr, Y, Th, La, Ce, F, and Be.

Of the 210 samples, 145 were classified as unaltered or nonmineralized whereas the other 65 samples constitute mineralized and vein samples.

Also, 25 of these 210 samples (along with 19 other samples) were analysed for rare earth elements (REE) and varying trace elements, viz.:

REE - La, Ce, Pr, Nd, Sm, Eu, Gd, Tb, Dy, Ho, Er, Tm, Yb, and Lu;

trace elements - Sc, Pb, Bi, W, Mo, Rb, Cs, Ba, Sr, Tl, Li, Ta, Nb, Hf, Zr, Y, Th, U, and Be.

One hundred and one of the 145 samples were from the Connaigre Bay Group, with 66 volcanic rock specimens, 16

carbonate/Ca-Mg-silicate rock samples, and 19 miscellaneous sedimentary samples. The remainder of the rocks are mafic and felsic dykes (27 samples) and assorted coarser-grained intrusive rocks from the Grole Diorite, Simmons Brook Batholith, and the Straddling Granite (total of 17 samples).

This section will attempt to describe the geochemistry of "unaltered" rocks but, as will become apparent from the chemical analyses and discrimination diagrams, this section actually deals with the "least altered" rocks available. It is important to determine the original rock chemistry and certain elements provide more reliable data than other elements (i.e. the immobile and incompatible high field strength elements are preferred over the mobile and compatible low field strength elements). Elements such as Ta, Nb, Hf, Zr, Ti, Y, Th, and HREE are relatively unaffected by low grade of metamorphism (e.g. Pearce and Cann, 1973; Myers and Breitkopf, 1989), whereas the alkaline and alkaline earth elements (Na, K, Ca, Mg, Rb, Sr, Ba,) can be highly mobile when subjected to minor hydrothermal alteration or low grade metamorphism.

The aim of this section is not only to determine original rock chemistry, but also to determine the tectonic depositional environments. Although many relationships are discussed, only those deemed most important are illustrated.

The actual chemical analyses are listed in Appendices I, II, and IV, and the analytical methods are described in Appendix V. Average major and trace element compositions are

listed in Tables 3.1, 3.2, and 3.3.

3.1.2 Connaigre Bay Group

3.1.2.1 Introduction

A total of 66 volcanic rocks from the Connaigre Bay Group were analysed (Appendix I and Table 3.1). According to Winchester and Floyd's (1977) (Nb/Y) vs. (Zr/Ti) discrimination diagram (Figure 3.1), samples below the rhyodacite/dacite-andesite boundary are classified as mafic to intermediate in composition and those above the boundary are dacitic to felsic.

Although the rock types are equally represented (i.e. 33 samples from each classification), the different formations within the Connaigre Bay Group are not. Fifty-one of the 66 samples are from the Tickle Point Formation, eight are from the Sam Head Formation, five from the Doughball Point Formation, and one sample is a member of the Down's Point Formation. This sampling bias occurs because the bulk of the mineralization lies within the Tickle Point Formation. The most significant base-metal mineralization, however, is within the Sam Head Formation.

3.1.2.2 Mafic to Intermediate Volcanic Rocks

From the chemical analyses of these rocks (Appendix I and Table 3.1), it is apparent that normal values expected for many major and trace elements either exceed or are below the

Table 3.1. Average compositions for mafic to intermediate (1) and dacitic to felsic (2)
volcanic rocks, and sedimentary rocks (3) from the Connaigre Bay Group.
(-1 = less than one; nc = not calculated)

Sample #	1	2	3
SiO2 (wt.%)	53.25	71.55	65.36
TiO2	1.19	0.37	0.57
Al2O3	14.19	12.39	11.51
Fe2O3(total)	10.28	4.01	6.32
MnO	0.31	0.09	0.18
MgO	5.86	1.46	3.85
CaO	6.89	1.28	3.8
Na2O	1.98	3.72	1.95
K2O	1.34	1.79	1.3
P2O5	0.21	0.07	0.11
LOI	4.09	2.48	4.42
Total	99.59	99.2	99.38
Cr(ppm)	107	5	28
Ni	32	1	11
Co	28	3	9
V	220	37	76
Cu	143	9	120
Pb	43	24	55
Zn	351	68	234
Cd	0.8	0.2	1.3
Mo	5	4	6
Rb	25	35	37
Ba	628	694	671
Sr	216	89	113
Ga	23	16	17
Li	19	7	19
Nb	2	7	5
Ta	0.1	0.4	nc
Zr	108	262	206
Hf	2.9	7.1	nc
Y	23	35	33
Th	3	4	3
La	10	19	23
Ce	29	60	62
F	383	283	399
Be	1.1	1.5	1.4
Ag	0.45	0.17	0.34
Au(ppb)	-5	6	-5
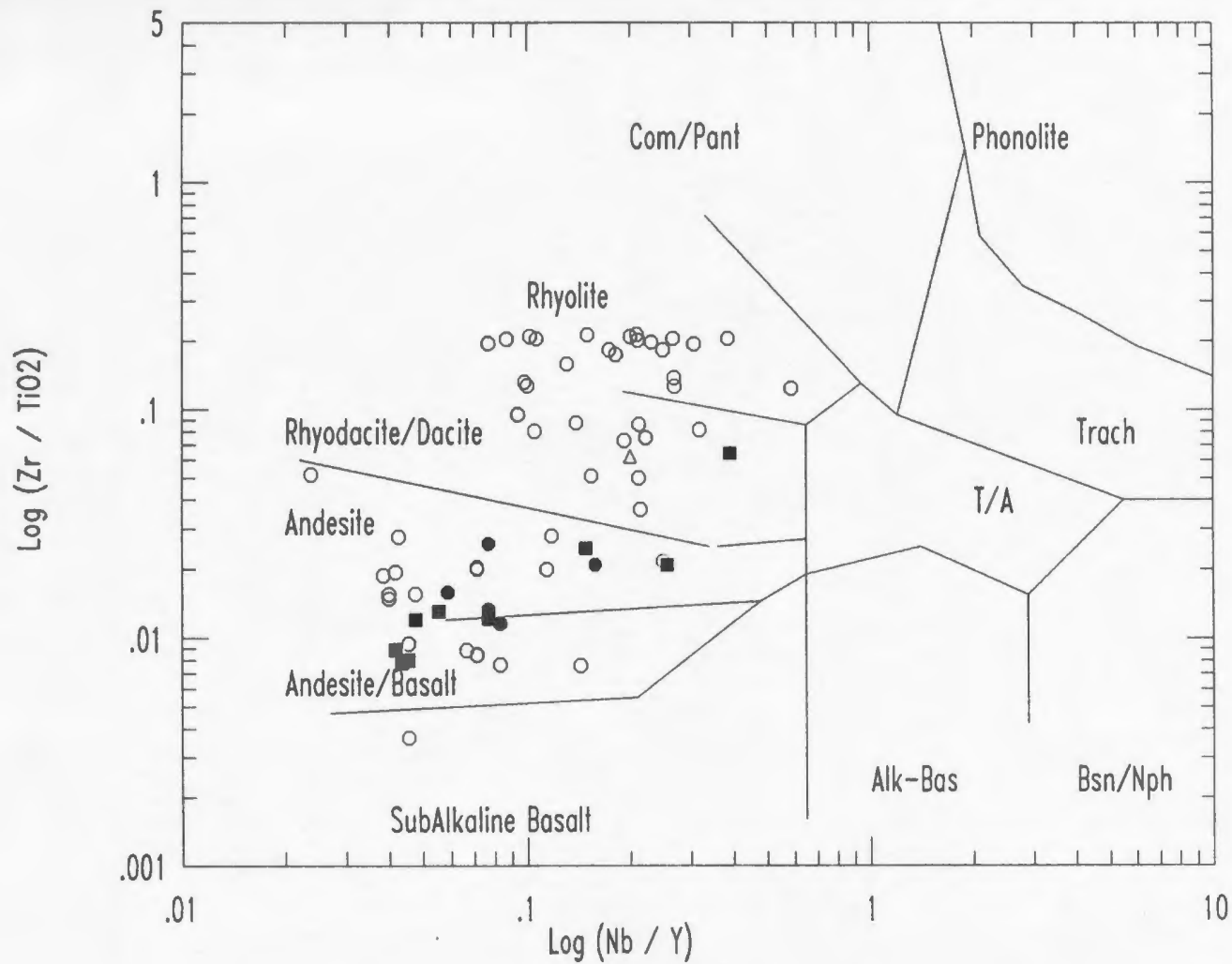
Figure 3.1. Nb/Y vs. Zr/Ti diagram from Winchester and Floyd (1977), with the 66 relatively unaltered volcanic rock samples plotted. Open circles = Tickle Pt. Fm., filled squares = Sam Head Fm., filled circles = Doughball Pt. Fm., and the open triangle = Down's Pt. Fm.

normal range (<u>i.e.</u> SiO_2 ranges from 41.00 wt.% to 76.10 wt.% but averages 53.25 wt.% which corresponds to the approximate boundary between basalt and andesite; Zr ranges from 32 ppm to 218 ppm and averages 108 ppm, which is slightly higher than the average values for tholeiitic basalts (Pearce, 1975; Wilson, 1989)). These data show that alteration has taken place, yet the overall chemical characteristics remain. (Since many samples were taken from in or around mineralized zones, small-scale local alteration may be inherent in many of the samples.)

Zr is immobile and increases with increasing magmatic differentiation because it is incompatible (Wilson, 1989). Hence Zr will be used to describe magmatic differentiation trends in this data.

The range in Zr values is caused essentially by magmatic differentiation, but such a large range as seen in this data is not expected. There is probably some limited mobility involved because the samples were collected from mineralized zones where the fluid flux was generally high.

Figure 3.2 consists of a series of plots of Zr vs. major elements. Zr shows the strongest positive correlations with the most immobile major elements, P_2O_5 and TiO_2. The trends are stronger for rocks from the Sam Head and Doughball Point Formations with limited scatter for rocks from the Tickle Point Formation. SiO_2 has a weak positive correlation with Zr whereas Fe_2O_{3total} and MgO have weak negative trends with
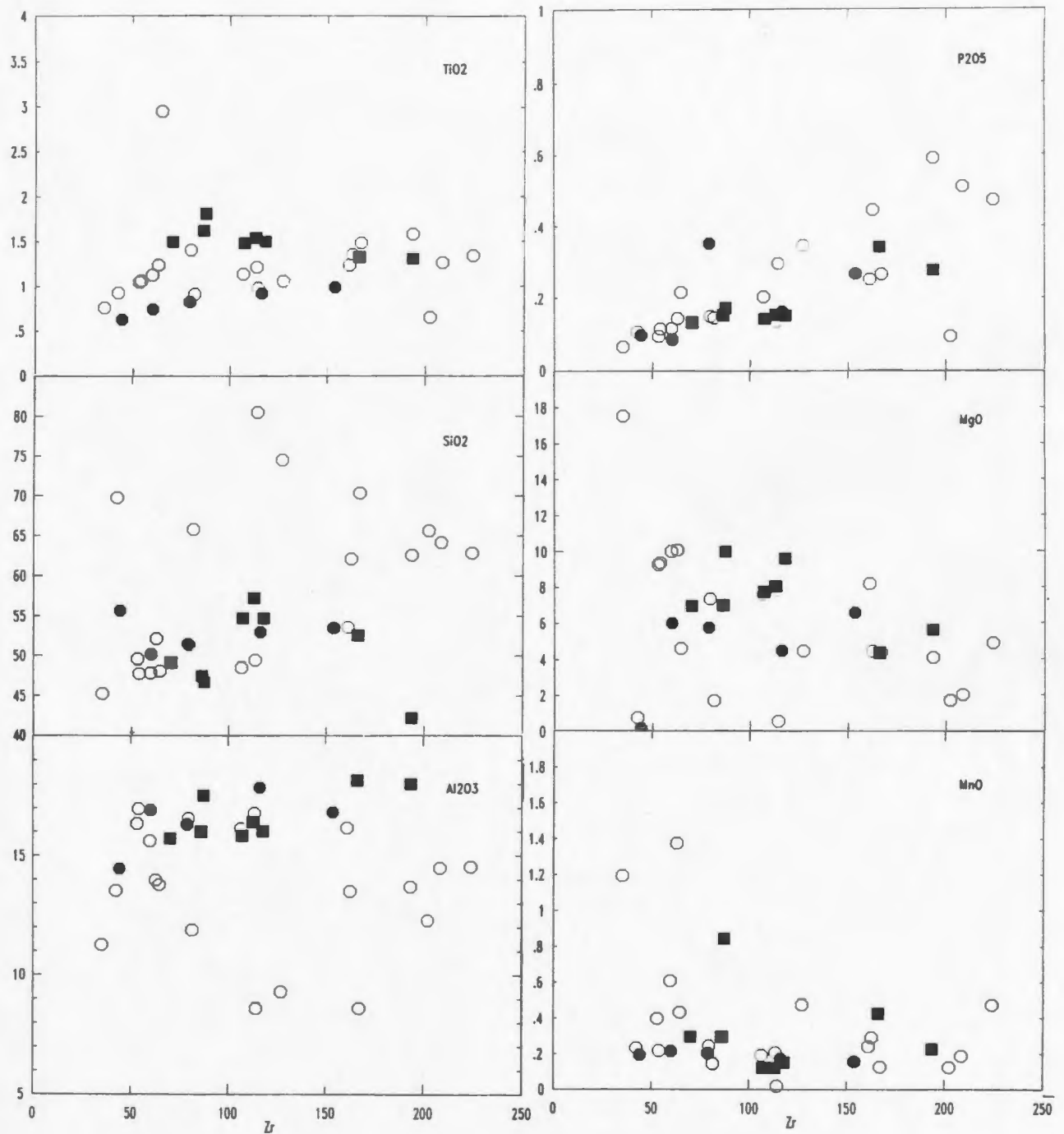
Figure 3.2. Variation diagrams involving Zr vs. the major elements for the mafic to intermediate rock samples. Symbols as in Figure 3.1.
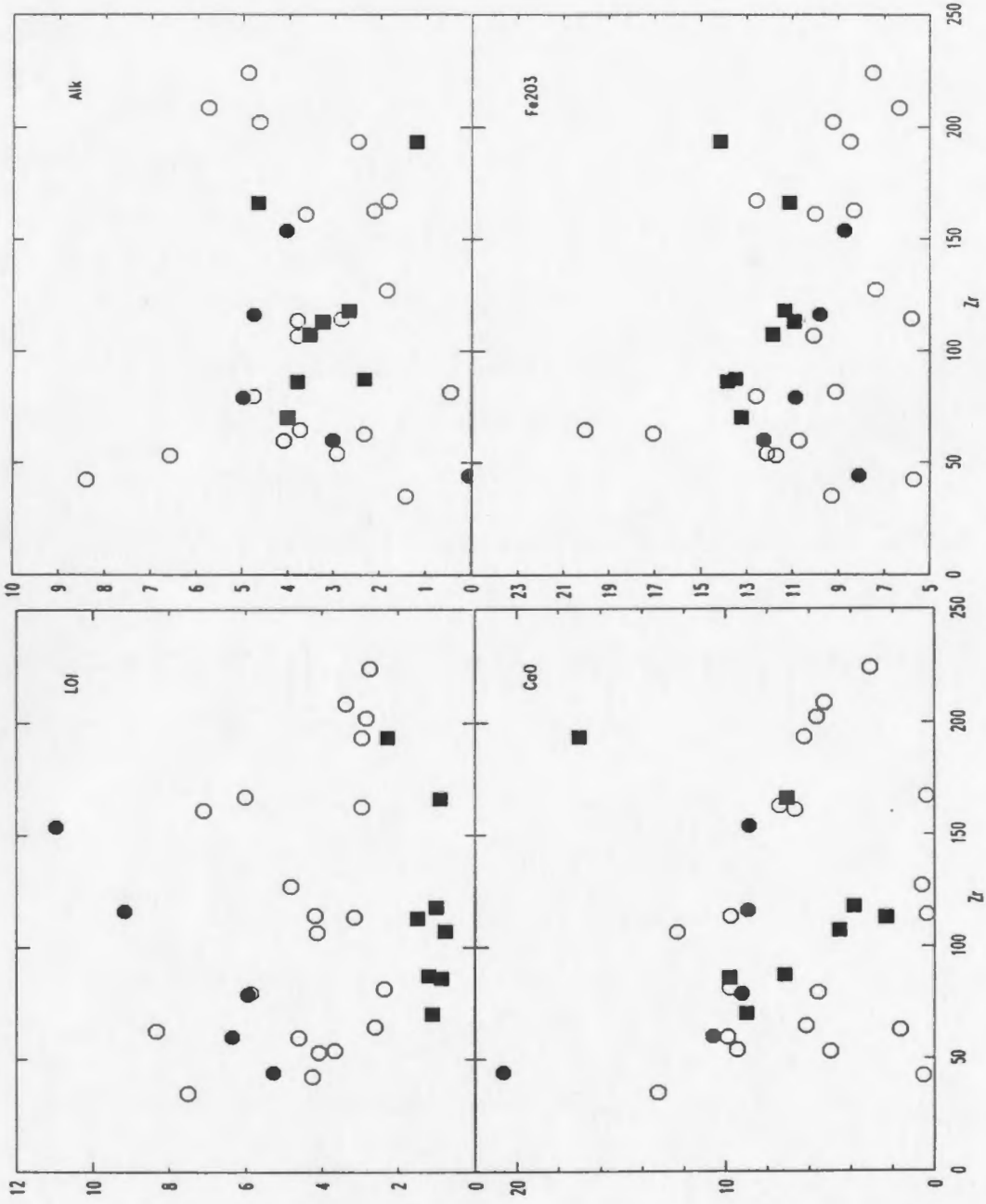
Figure 3.2. (continued)

increasing Zr. Samples with high a SiO_2 value are sample taken from near mineralized zones, and although the rocks appear, visually, to be mafic or intermediate in composition, they are silicified, thus yielding high SiO_2 values. Al_2O_3, MnO, CaO, alkalis, and LOI vs. Zr all illustrate widely scattered patterns, although rocks from the Sam Head and Doughball Point Formations have tighter patterns than samples from the Tickle Point Formation. This probably occurs because most of the mineralization and alteration occurred during deposition of the Tickle Point Formation and the lowermost sections of the Sam Head Formation.

Figure 3.3 shows Zr versus selected trace elements. Zr vs. Y (which behaves as a heavy REE), displays a strong positive correlation. Ce, a light REE, also has a positive trend with Zr. When Zr is plotted versus mobile elements such as Rb, there is a wide scatter in the data which is possibly a manifestation of variable and localized alteration. Zr vs. V (which parallels the behaviour of Ti) shows a weak to moderate trend of decreasing V with increasing Zr. Decreasing fractionation of Ti-Fe phases such as ilmenite or titanomagnetite (or possibly titaniferous clinopyroxene) with increasing magmatic differentiation (Wilson, 1989) may result in the Zr-V pattern.

The alteration of most of the major elements has rendered them much less useful as indicators of primary magmatic processes, but some possible igneous trends remain. MgO vs.
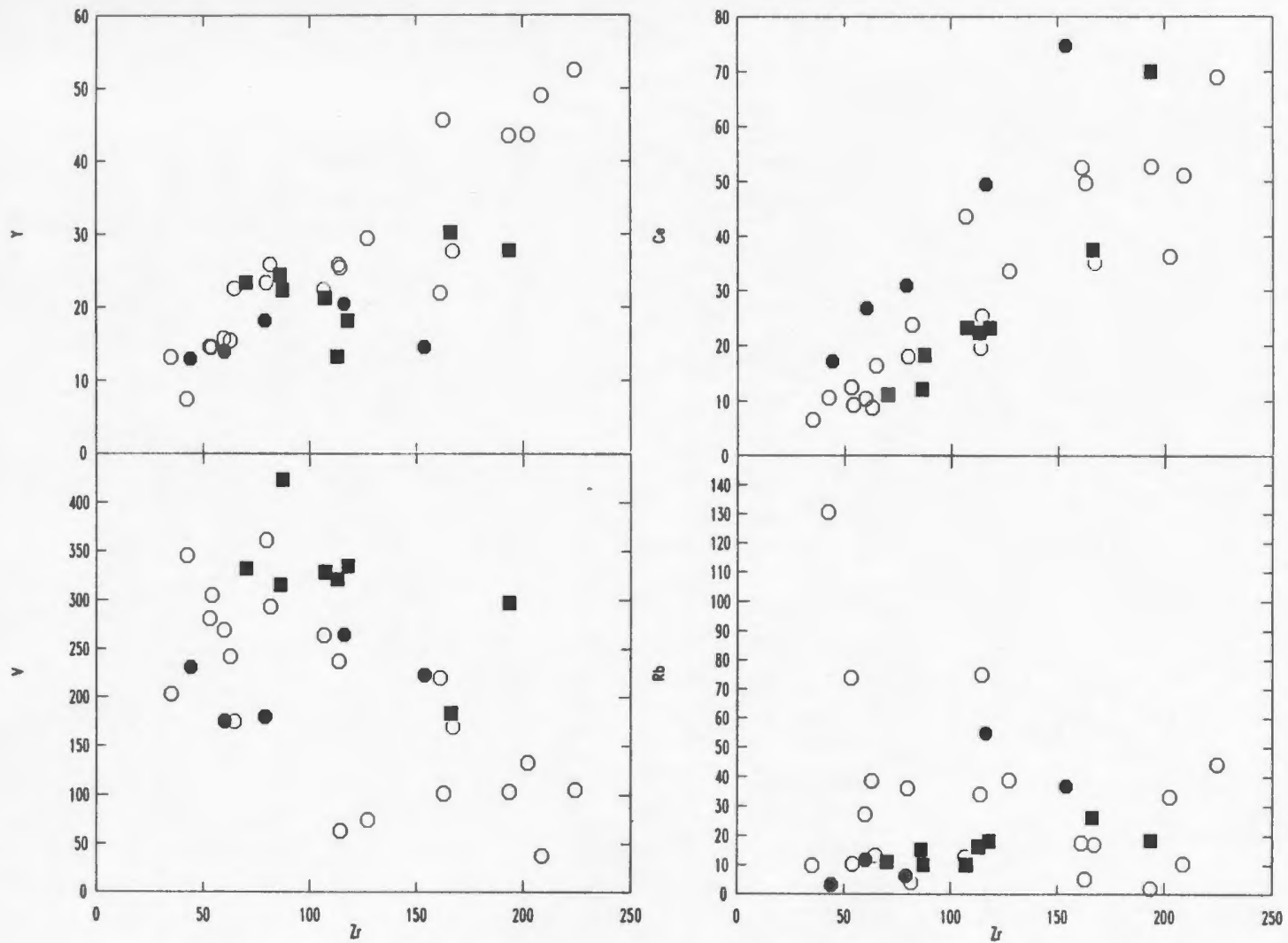
Figure 3.3. Variation diagrams of Zr vs. selected trace elements. Symbols as in Figure 3.1.

Fe_2O_{3total} and TiO_2 both have positive trends (Figure 3.4) and K_2O vs. Rb (Figure 3.5) also have a positive linear correlation. The mobile trace elements (Sr, Ba, Rb, Li) commonly create scatter diagrams when plotted against one another and other less mobile trace elements. Cr vs. Ni has a very strong positive correlation whereas Cr vs. Co and Ni vs. Co both have weak to moderate positive trends with no variation after 45 ppm Co.

According to Winchester and Floyd's (1977) SiO_2 vs. (Nb/Y) diagram, the rocks are subalkaline in character (Figure 3.6). SiO_2 alteration will not affect the alkalinity since the boundary between alkaline and subalkaline is parallel to the silica axis. Only a large change in the Nb/Y ratio will effect the alkalinity. Nb and Y are considered immobile, so the ratios probably represent primary magmatic ratios. These subalkaline rocks are generally confined to the tholeiitic series (Figure 3.7) as defined by Jensen's (1976) ternary diagram of Al_2O_3 - Fe_2O_{3total} + TiO_2 - MgO. Most of the sample plot in the high-Fe tholeiite field or the tholeiitic andesite field. When plotted on a Zr vs. P_2O_5 diagram (Figure 3.8), the rocks produce a flat slope typical of oceanic tholeiitic basalts (Floyd and Winchester, 1975).

3.1.2.3 Dacitic to Felsic Volcanic Rocks

Observation of the chemical analyses listed in Appendix I and Table 3.1, illustrates that the felsic rocks are not as
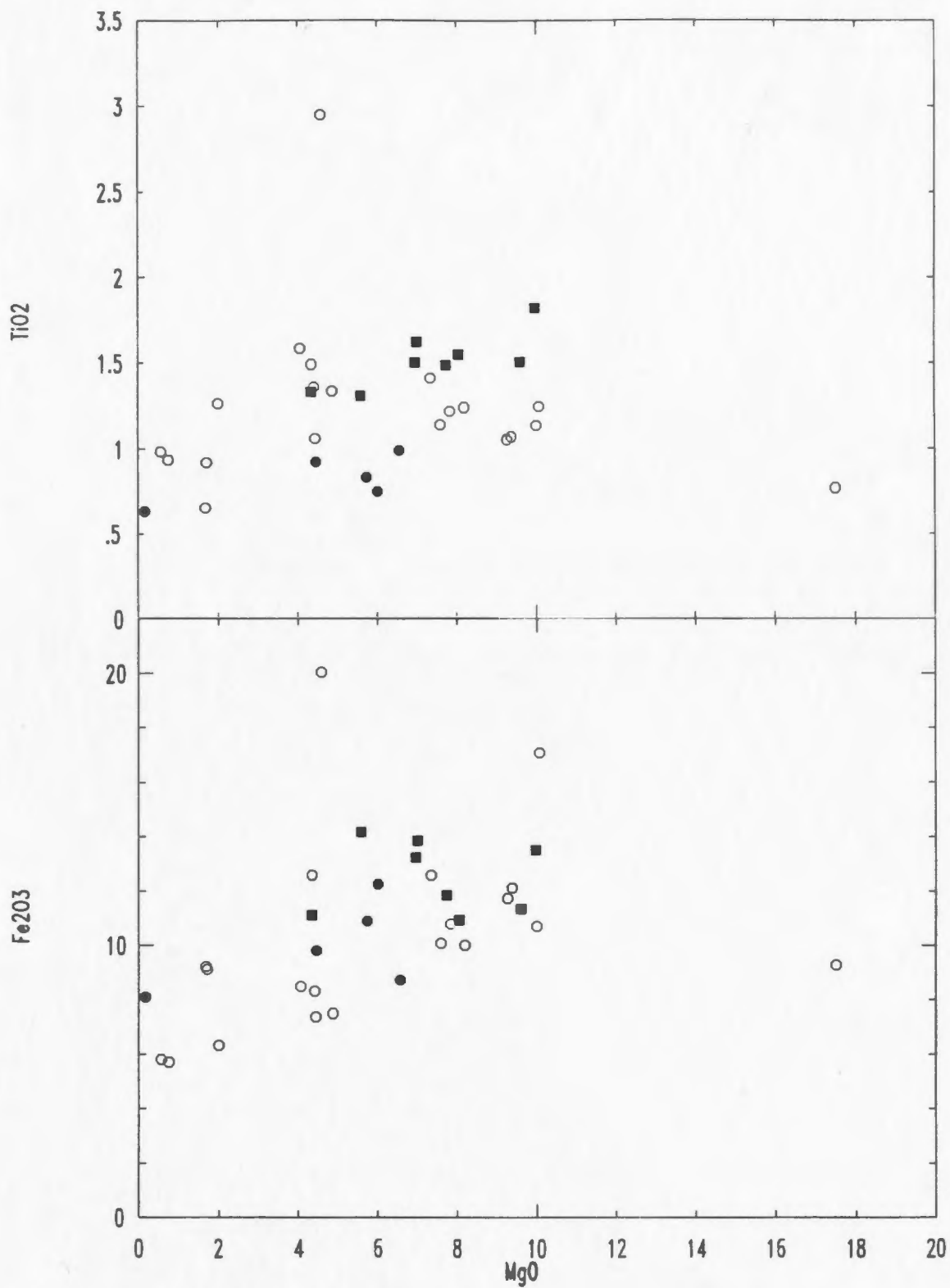
Figure 3.4. Variation diagrams of MgO vs. $Fe_2O_{3\,total}$ and TiO_2. Symbols as in Figure 3.1.
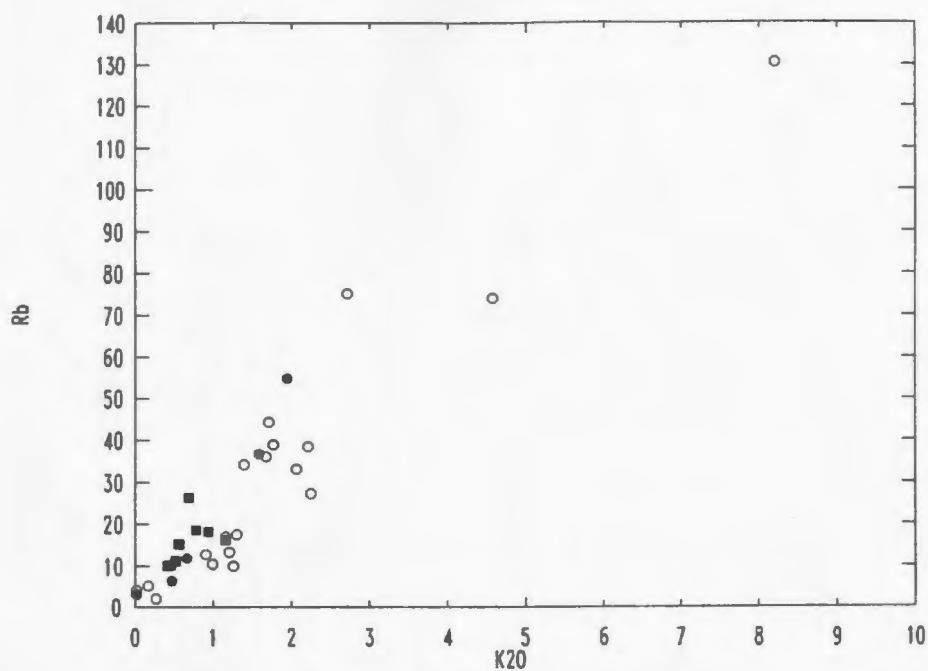
Figure 3.5. Plot of K_2O vs. Rb displaying a positive linear relationship. Symbols as in Figure 3.1.
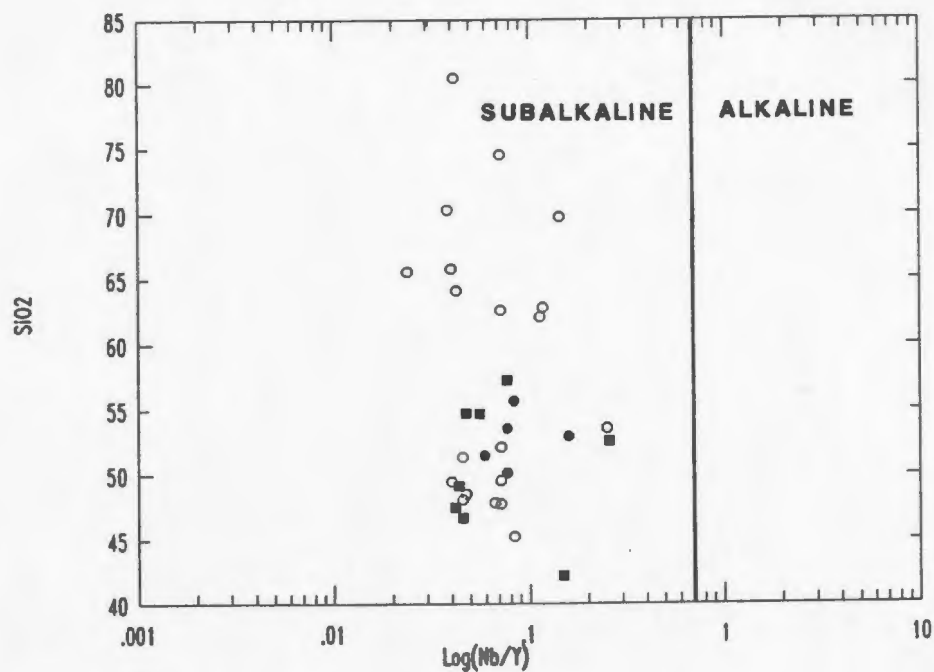
Figure 3.6. Nb/Y vs. SiO_2 diagram displaying the subalkaline and alkaline fields (adapted from Winchester and Floyd, 1977). The mafic to intermediate samples are subalkaline in character and variably silicified. Symbols as in Figure 3.1.
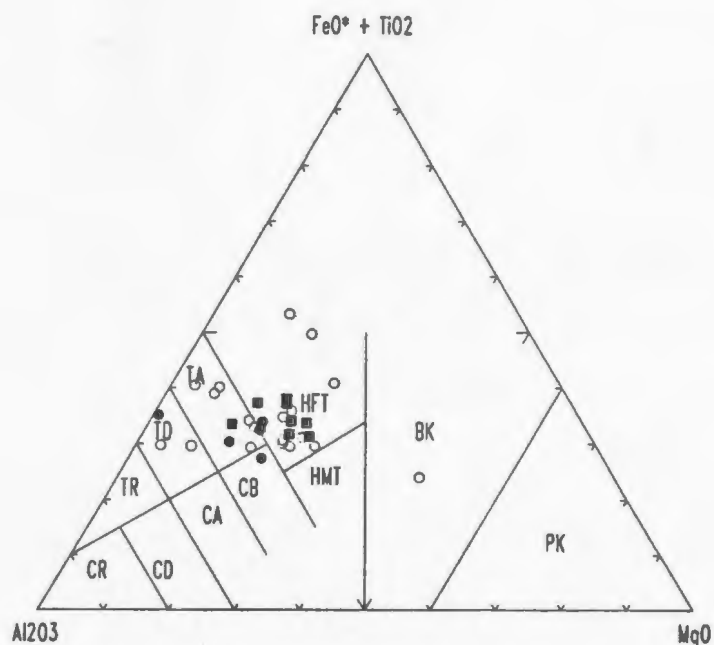
Figure 3.7. Al_2O_3 - FeO* (Fe total) + TiO_2 - MgO ternary diagram after Jensen (1976). This plot illustrates the tholeiitic nature of the mafic to intermediate rocks. Symbols as in Figure 3.1. CR, CD, CA, CB = calcalkaline rhyolite, dacite, andesite, basalt; TR, TD, TA = tholeiitic rhyolite, dacite, andesite; HFT = high Fe tholeiite; HMT = high Mg tholeiite; BK = basaltic komatiite; PK = picritic komatiite.
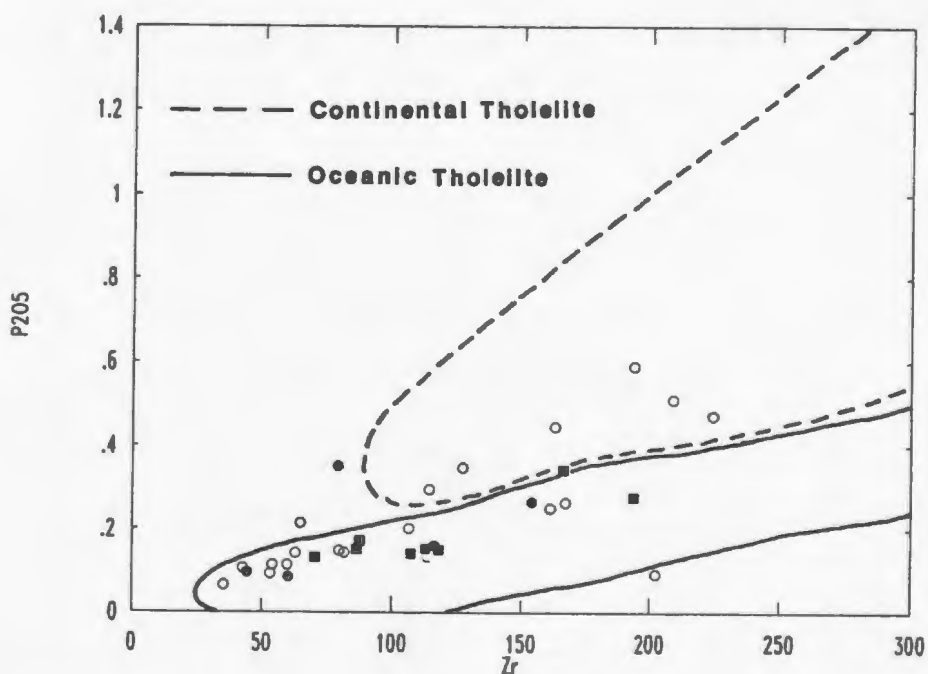
Figure 3.8. Plot of Zr vs. P_2O_5 and the respective fields for oceanic and continental tholeiites. The mafic to intermediate rocks have a strong oceanic character. Symbols as in Figure 3.1.

altered as the mafic to intermediate rocks. With the exception of the alkaline oxides (Figure 3.9) and some trace elements, distributions of the other elements and oxides appear relatively unaltered. Therefore, SiO_2 may be used as a base for describing magmatic differentiation.

A series of Harker diagrams are presented in Figure 3.10. Silica has strong negative correlations with Al_2O_3, TiO_2, and MnO, and a weak to moderate negative trend with P_2O_5. These oxides are usually considered to be the most immobile of the major elements and therefore may represent original igneous compositions. A negative correlation is then expected with increasing SiO_2 representing a fractionation trend. Chayes (1964) suggested that this negative trend is partially due to the constant sum effect, <u>i.e.</u> with increasing SiO_2, the other oxides must decrease in abundance to accommodate the higher SiO_2 values. CaO has a very weak negative trend against SiO_2 as does Fe_2O_{3total} and MgO, whereas LOI exhibits a wide scatter of points when plotted vs. SiO_2. The alkalis have a flat pattern with SiO_2 with an average alkali content near 6 wt.%. Both this plot and Figure 3.9 appear to show that even though the alkalis have been mobilized, mobilization appears to be localized and as one alkali is removed, the other replaces it on a 1:1 ratio (Figure 3.11).

With respect to the other major elements, Al_2O_3 vs. TiO_2 (Figure 3.11) display a strong positive correlation which is expected because both have strong negative correlations with
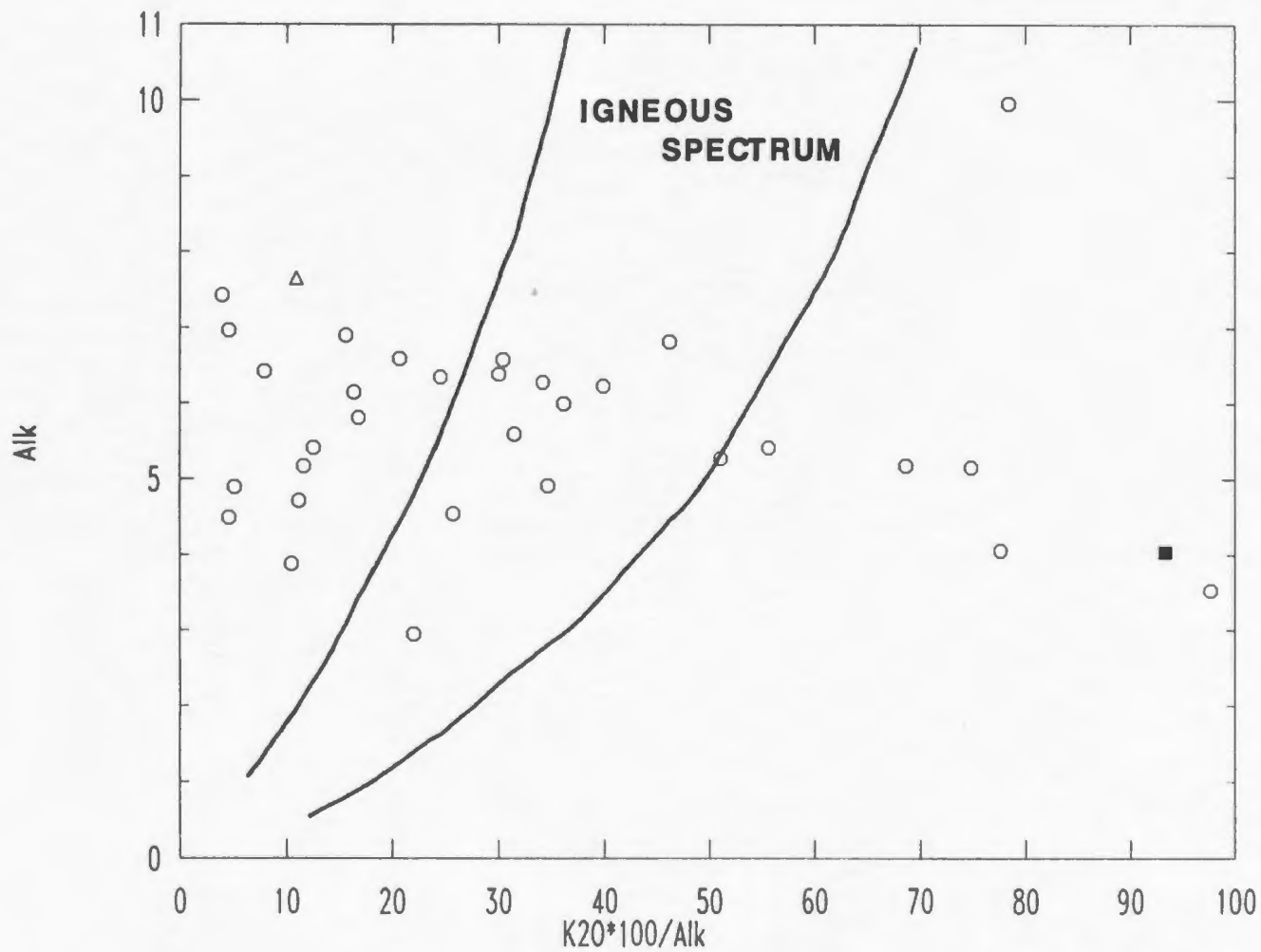
Figure 3.9. An "igneous spectrum" diagram taken from Hughes (1973). The felsic rocks are generally altered with respect to the K_2O and Na_2O, but the overall alkali content remains fairly constant between 4 and 7 wt.%. Symbols as in Figure 3.1.
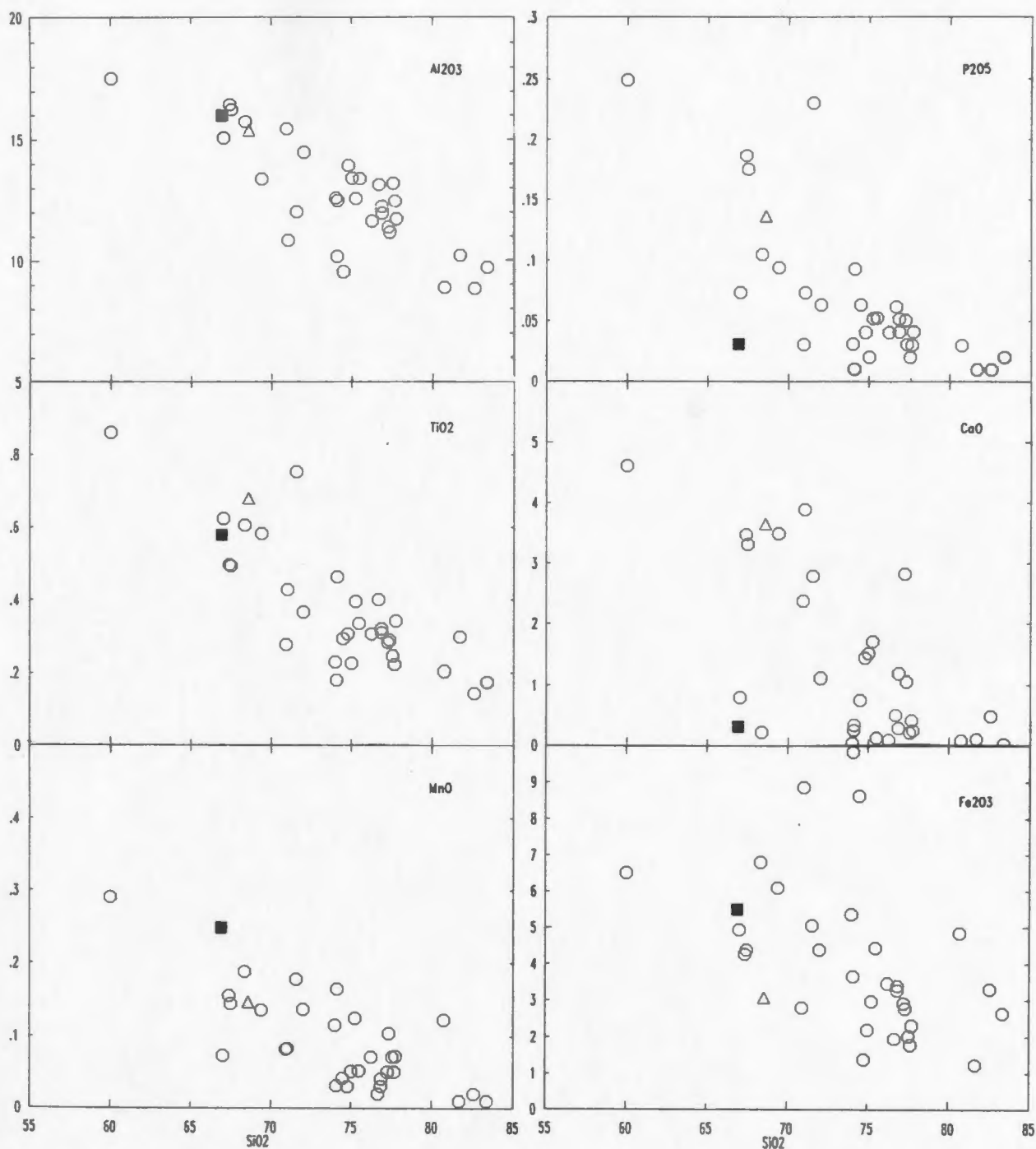
Figure 3.10. Variation diagrams involving SiO₂ vs. other major elements for the dacitic to felsic rock samples. Symbols as in Figure 3.1.

Figure 3.10. (continued)
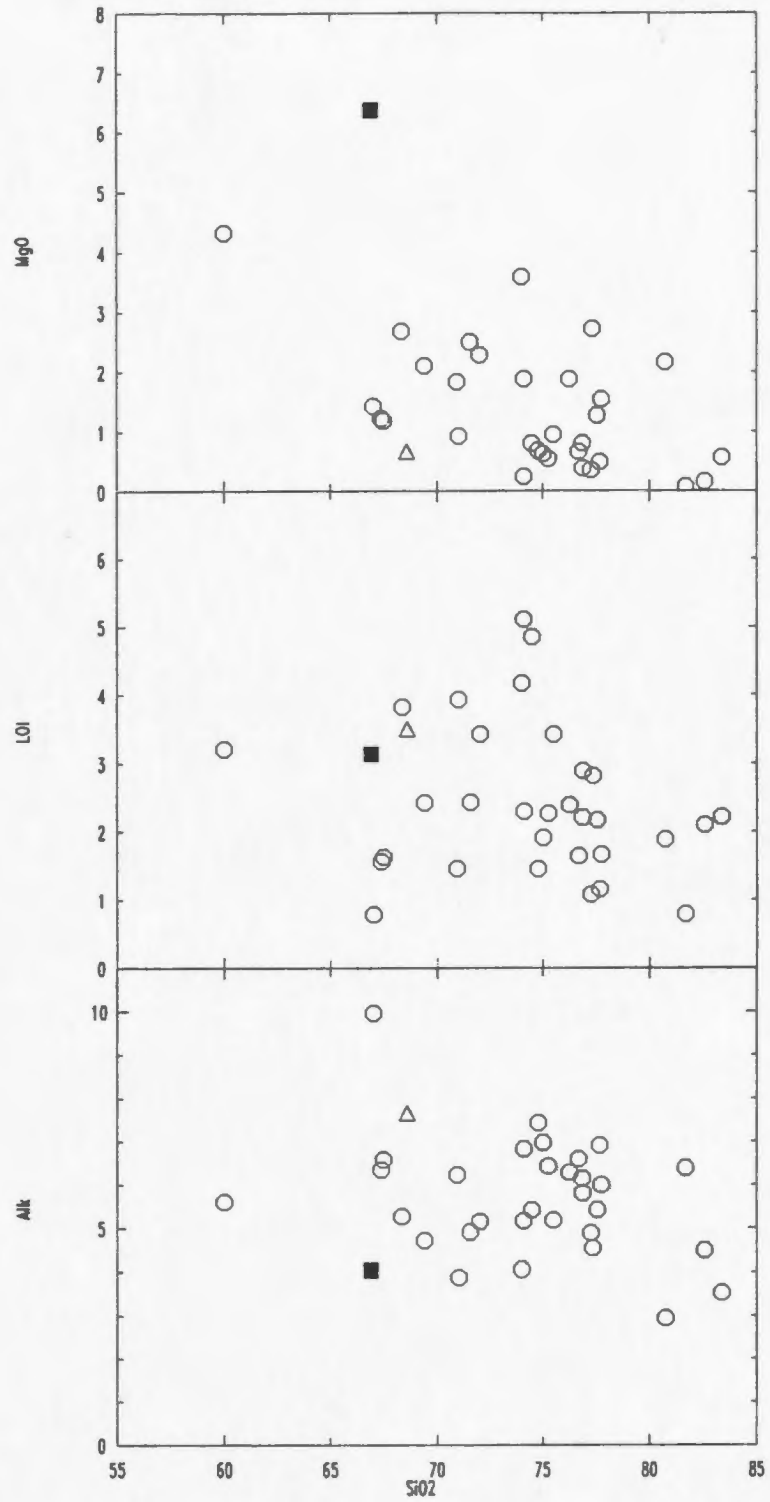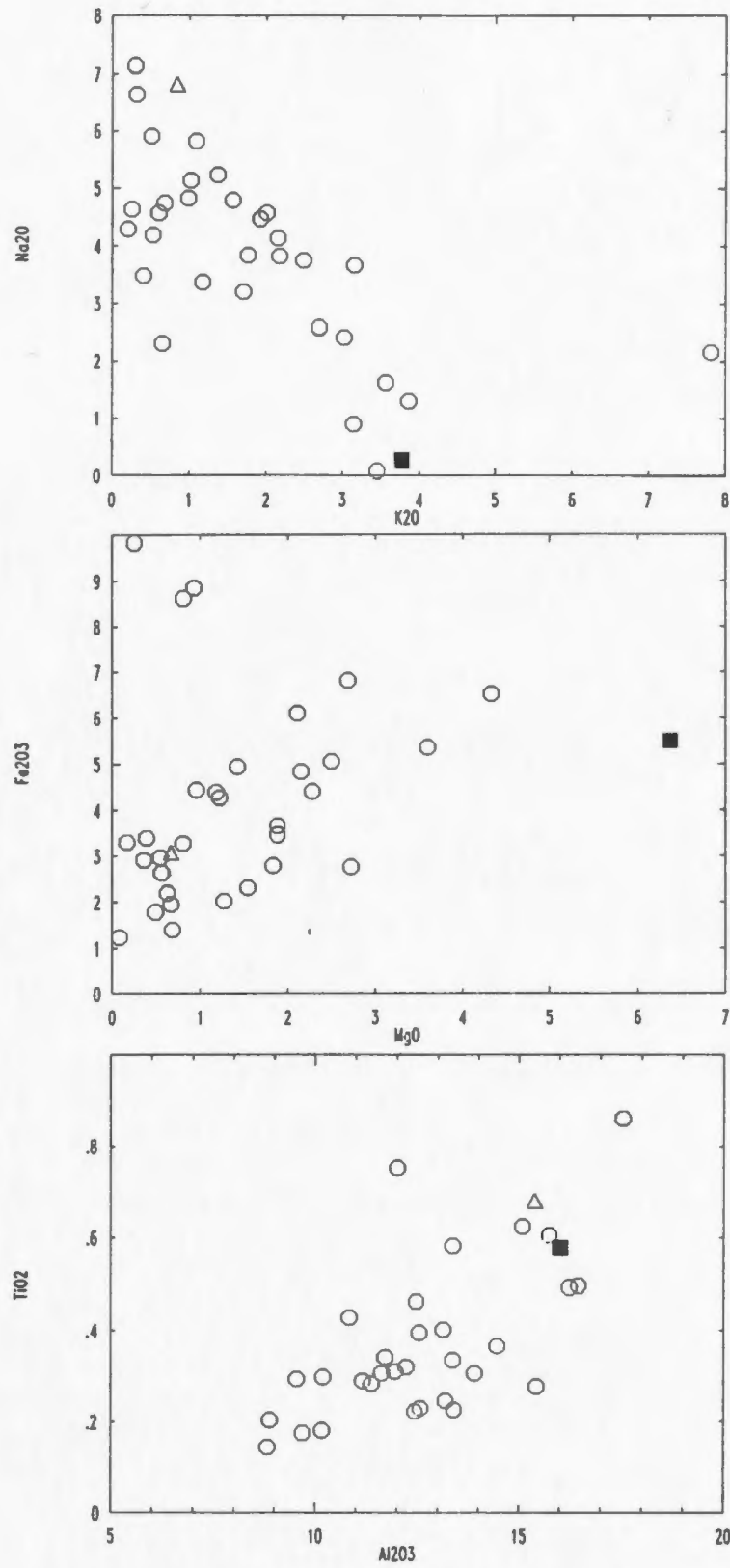
Figure 3.11. Major element variation plots. Symbols as in Figure 3.1.

SiO_2. There is also a moderate positive trend between MgO and total Fe (Figure 3.11). Both increase with decreasing SiO_2 reflecting the greater mafic character as silica decreases. The scatter on MgO vs Fe_2O_{3total} may be due to Fe contamination by pyrite from hydrothermal fluids which produced the nearby mineralized zones.

Using Zr as a base to plot other trace elements against (Figure 3.12), similar patterns emerge as seen in the mafic to intermediate volcanic rocks. Y and Ce (and La) display moderate to strong positive trends with increasing Zr, indicating a strong correlation between Zr and the HREE. Against Rb (plotted) and Sr, there is a wide array of data points. Even Th, thought to be generally immobile, exhibits a large scatter of points.

Amongst the highly mobile elements (Rb, Sr, Ba) there are no strong trends between any two. There is a strong negative correlation of Rb with Na_2O and a positive trend with K_2O. Neither Sr or Ba have any strong affinities with Na_2O or K_2O.

Assuming that the overall alkali content has remained relatively constant (i.e. alkalis have been locally mobilized but the overall K_2O + Na_2O total has remained relatively constant), there is some justification in using discrimination diagrams that use total alkalis as an end member. The felsic rocks are, therefore, strongly subalkaline in character (Figure 3.13) according to Irvine and Baragar's (1971) SiO_2 vs. alkalis plot.
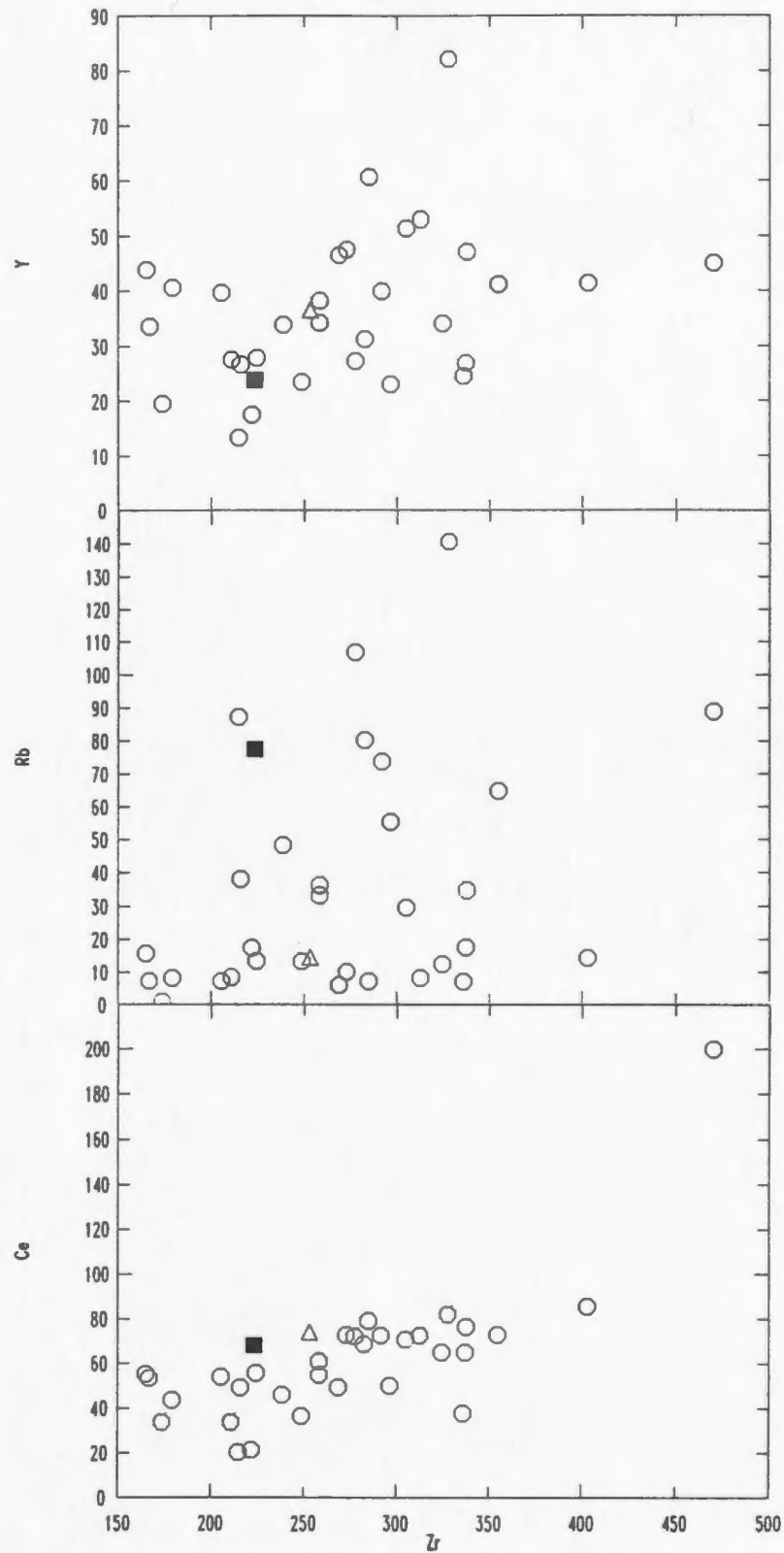
Figure 3.12. Trace element variation diagrams involving Zr and other selected elements. Symbols as in Figure 3.1.
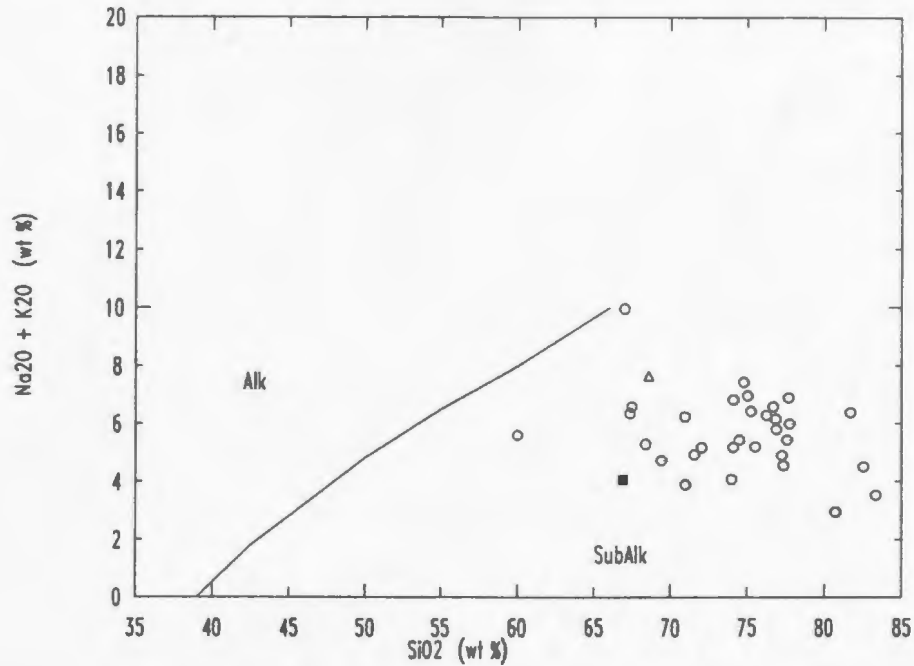
Figure 3.13. SiO$_2$ vs. alkalis diagram and the respective alkaline and subalkaline fields (taken from Irvine and Baragar, 1971). The dacitic to felsic rocks display a strong subalkaline character. Symbols as in Figure 3.1.
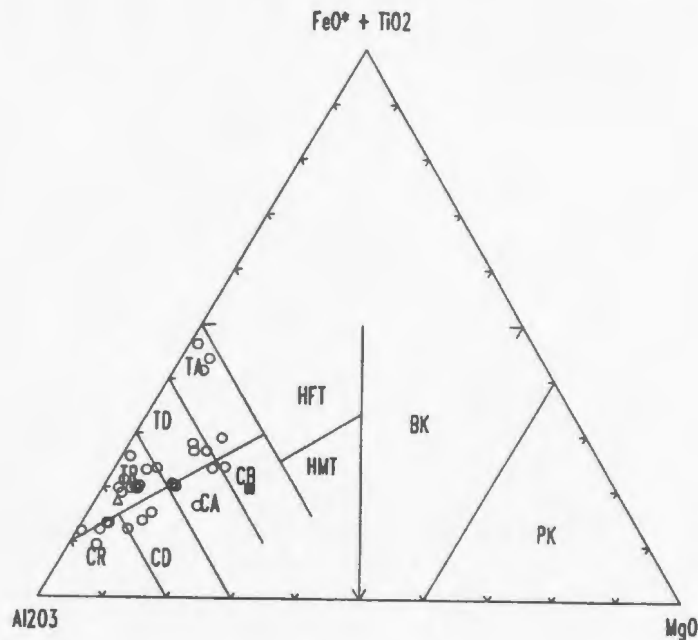
Figure 3.14. Al$_2$O$_3$ - FeO* (Fe total) + TiO$_2$ - MgO ternary diagram for the dacitic to felsic rocks. The rocks have an apparent transitional tholeiitic-calcalkaline character. Symbols as in Figure 3.1 and the fields are the same as in Figure 3.7.

There is some contradiction as to which series the rocks belong. On Jensen's (1976) diagram, the majority of the samples plot in the tholeiitic field (Figure 3.14), yet there are a number of samples in the calcalkaline series and almost all of the points lie close to the tholeiite-calcalkaline boundary. An AFM plot has all but four of the 33 samples plotting in the calcalkaline field (Figure 3.15). The Jensen (1976) plot is probably the more reliable, but the samples contain minor amounts of pyrite which would add to the Fe_2O_{3total}, pushing some samples into the tholeiitic field. It is assumed above that the overall alkali content remained constant, therefore lending credence to the AFM plot, but the alkalis are very mobile and must be used with caution.

3.1.2.4 Sedimentary Rocks

Chemical analyses for the sedimentary rocks from the Connaigre Bay Group are available in Appendix I and Table 3.1.

Of the 17 samples, nine are within the Sam Head Formation (fine-grained chert (with occasional spherulites) to argilaceous chert and argillite), six are from the Tickle Point Formation (chert and argillite), and the remaining two samples were taken from the Down's Point Formation (arkose and pebble conglomerate).

The cherts have SiO_2 values between 73 and 82 wt.% and Al_2O_3 values between 7 and 12 wt.% whereas the other oxide percentages are quite variable. Overall, the chemical analyses

for the cherts are similar to the analyses of the felsic tuffs and flows, suggesting a possible genetic link between the lithologies. The argillitic rocks are more intermediate in character ($\approx$ 60 wt.% SiO_2) with one carbonate-rich sample containing only 34.9 wt.% SiO_2. There is also a pyritic, black argillite sample (no. 584074) with low SiO_2 but high Al_2O_3, CaO, and MgO. The chemical analyses for these argillite samples are approximately the same as the analyses for the mafic to intermediate volcanic rocks from the Connaigre Bay Group.

The two samples from the Down's Point Formation contain many large-size (up to 2-3 cm) lithic fragments and therefore their chemical analyses are probably not representative of the formation due to possible local concentration of any one type of rock fragment. Nevertheless, they are chemically similar to the argillitic rocks.

Roser and Korsch (1986) devised a method of determining tectonic environment by examining the chemistry of mudstones and sandstones from ancient sedimentary suites. Figure 3.16 is a plot of SiO_2 vs. log (K_2O/Na_2O) with the respective tectonic fields. The sedimentary samples from this study create a large scatter yet there is a concentration of Sam Head Formation samples in the passive margin field, whereas the Tickle Point and the Down's Point Formation rocks concentrate in the active margin fields.

There is no problem with rock samples from the Tickle
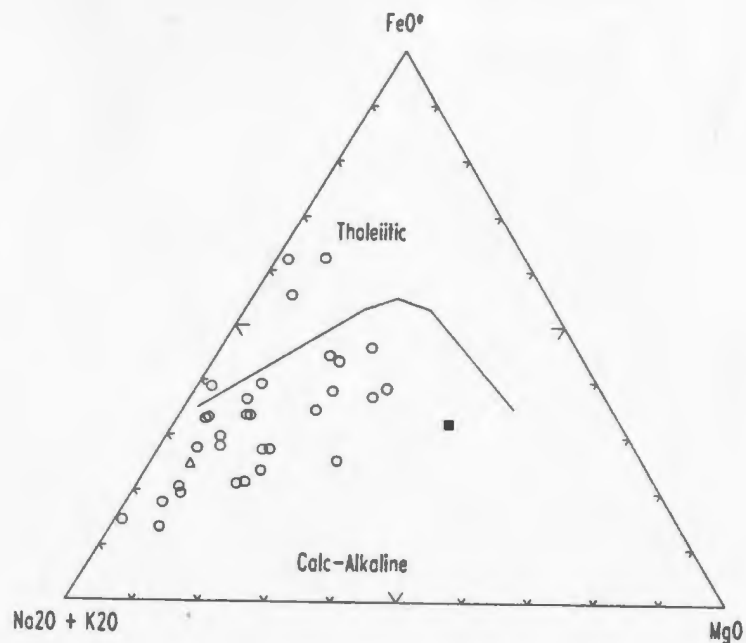
Figure 3.15. AFM diagram after Irvine and Baragar (1971). The dacitic to felsic samples display calcalkaline affinities. Symbols as in Figure 3.1. (FeO* = Fe total).
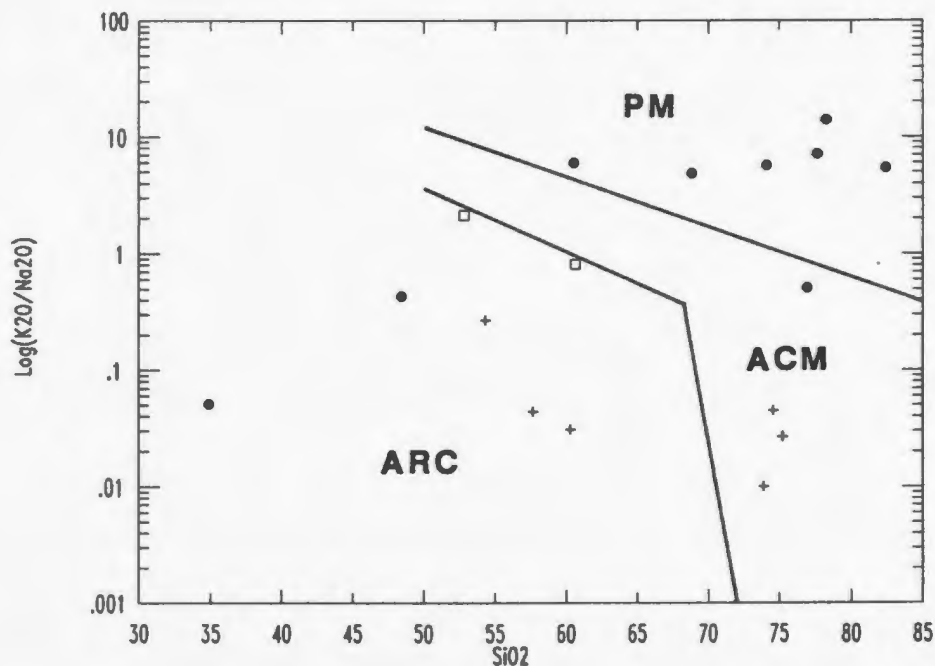
Figure 3.16. SiO$_2$ vs. K$_2$O/Na$_2$O plot taken from Roser and Korsch (1986), with the fields for passive margin (PM), active continental margin (ACM), and oceanic island arc (ARC) sedimentation. Closed circles = sedimentary rocks from the Sam Head Fm., crosses = sedimentary samples from the Tickle Pt. Fm., open squares = Doughball Pt. Fm. sedimentary rock samples.

Point and Down's Point Formations plotting in the active margin field because the geochemistry of the volcanic rocks suggests an island arc environment. One reason why sedimentary samples from the Sam Head Formation fall into the passive margin field is that most of the sedimentation occurred before the arc-rifting volcanism. Therefore the cherts (and other chemical sediments) were deposited in a quiet environment along a passive margin. Also, being behind the arc and moving away from the trench, K_2O values increase over Na_2O (Wilson, 1989) which may account for the elevated K_2O/Na_2O ratios within the Sam Head Formation samples, and also inferring a possible back-arc basin setting.

3.3.1 Intrusive Rocks

3.3.1.1 Grole Diorite, Simmons Brook Batholith, and the Straddling Granite

Little emphasis was placed on mapping and sampling the coarser grained intrusive rocks. Those samples collected were generally in close proximity to mineralized zones, therefore they probably incorporated altered country rock, resulting in an altered chemistry.

Most of the chemical analyses for the Grole Diorite and the Simmons Brook Batholith (Appendix II and Table 3.2) are gabbros while the two analyses for the Straddling Granite are similar to that of calcalkaline granite (sensu stricto) according to Ehlers and Blatt (1982).

Table 3.2. Average compositions for intrusive rocks from the Hermitage peninsula: Grole Diorite and Simmons Brook Batholith (1), Straddling Granite (2), older mafic dykes (3), younger mafic dykes (4), older felsic dykes (5), and younger felsic dykes (6). (-1 = less than one, nc = not calculated, na = not analysed)

Sample #	1	2	3	4	5	6
SiO2 (wt.%)	46.05	73.97	47.04	54.25	75.92	73.01
TiO2	0.68	0.29	1.41	0.95	0.24	0.04
Al2O3	14.98	12.45	14.94	19.32	11.35	14.92
Fe2O3(total)	12.06	2.6	11.28	7.99	1.91	0.94
MnO	0.19	0.04	0.41	0.13	0.21	0.07
MgO	8.42	1.29	7.11	2.64	1.98	0.4
CaO	10.18	1.02	9.58	4.54	0.99	1.1
Na2O	2.07	2.67	1.85	3.89	4.58	4.72
K2O	0.66	2.63	0.98	1.71	0.86	2.14
P2O5	0.11	0.02	0.16	0.2	0.03	0.09
LOI	4.03	1.72	5.19	3.82	1.09	1.58
Total	99.43	98.71	99.95	99.43	99.19	99.01
Cr(ppm)	306	9	142	6	4	4
Ni	200	2	53	4	1	1
Co	65	3	35	19	3	1
V	132	10	281	163	8	1
Cu	1615	12	83	33	18	7
Pb	17	14	133	11	43	12
Zn	101	62	316	100	277	133
Cd	0.4	0.3	0.7	0.1	2	0.4
Mo	5	3	4	5	3	3
Rb	11	67	16	89	15	56
Ba	573	365	439	434	269	484
Sr	201	32	277	284	71	152
Ga	23	16	26	20	13	15
Li	11	15	17	66	18	11
Nb	-1	6	-1	2	6	19
Ta	nc	nc	0.1	0.1	0.4	1.1
Zr	116	264	102	154	236	46
Hf	nc	nc	2.8	4.2	6.4	1.3
Y	23	35	24	22	38	9
Th	2	9	-1	-1	7	2
La	11	23	8	14	19	10
Ce	31	60	21	41	54	26
F	200	348	419	226	207	225
Be	0.9	1.5	1	1.4	1.3	2.1
Ag	1.67	-0.1	0.14	0.37	0.42	-0.1
Au(ppb)	14	na	-5	33	-5	na

SiO_2 is fairly constant between 45 and 47 wt.% within the gabbroic rocks. Sample 584092 has very low silica and high Fe_2O_3 because it is a magnetite-rich sample from a pegmatitic amphibole pod. The highest SiO_2 content (60.30 wt.%) is from a plagioclase-rich phase in which the chemistry is more reflective of plagioclase than gabbro. The data also show large variations in Al_2O_3 (4.93 to 22.07 wt.%), MgO (1.00 to 15.62 wt.%), Fe_2O_{3total} (2.33 to 18.29 wt.% - excluding the magnetite-rich sample), CaO (4.54 to 21.68 wt.%), and the total alkalis (0.12 to 6.78 wt.%).

SiO_2 plotted against Al_2O_3, Fe_2O_{3total}, and MgO generally form tight clusters for the Grole Diorite samples whereas the Simmons Brook Batholith samples commonly have widely scattered patterns. CaO and Na_2O vs. silica both have weak to moderate negative and positive correlations, respectively. TiO_2 is higher in the Grole Diorite whereas MnO, K_2O, P_2O_5, and LOI have scattered plots for both mafic intrusives, when plotted against SiO_2. The mafic trace elements (Cr, Co, Ni) increase and decrease respectively, but only Co has a positive trend with Fe_2O_{3total}. They all have a positive correlation with MgO.

The two Straddling Granite samples can be plotted on discrimination diagrams (figure 3 and 4 from Pearce et al. (1984)) to determine in which tectonic environment they were formed. Figure 3.17 has examples of both plots for the granitic and gabbroic samples. The granites (and gabbros) fall in the VAG field on the log Y + Nb vs. Rb diagram whereas they
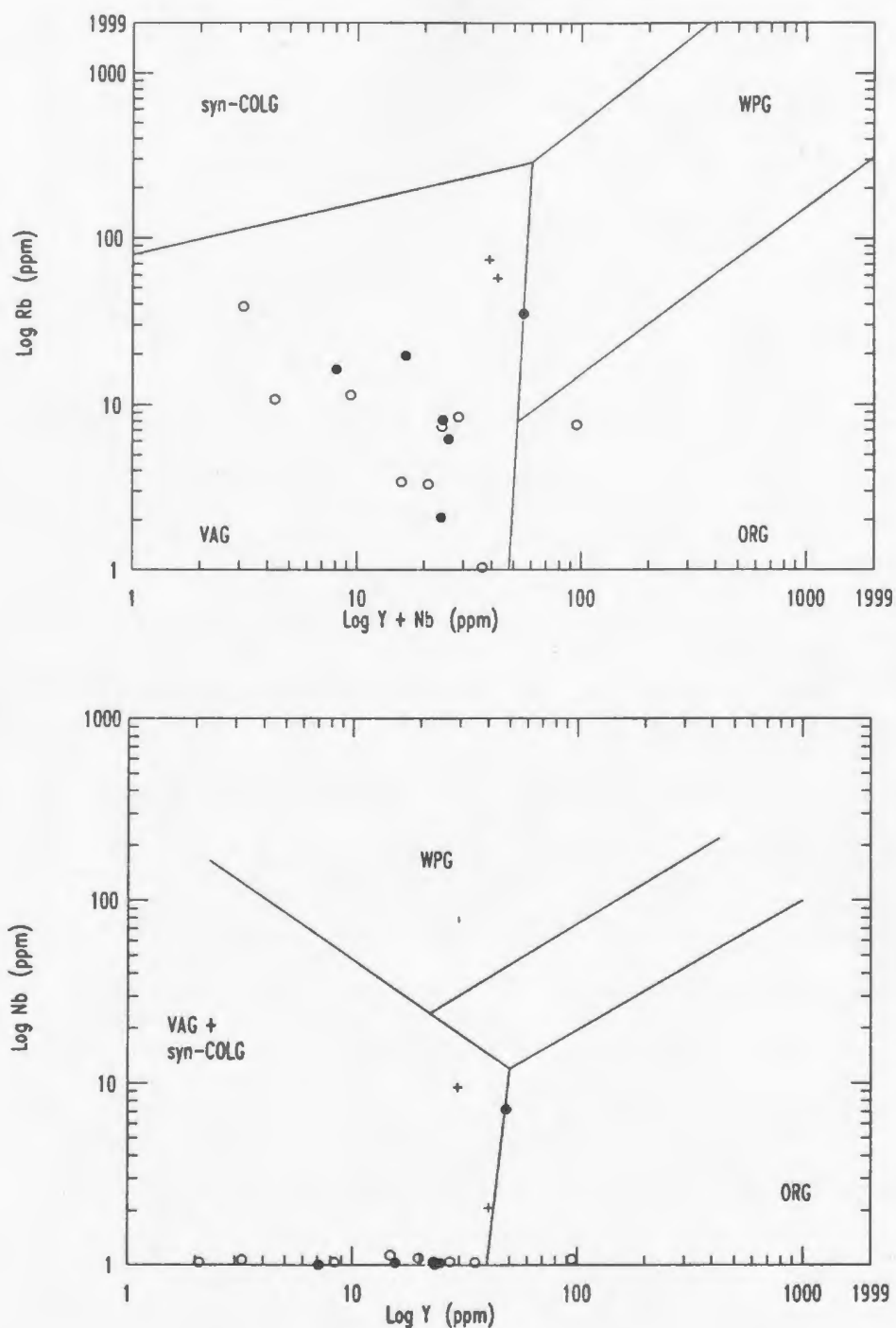
Figure 3.17. Y+Nb vs. Rb and Y vs. Nb plots, and the respective tectonic fields (from Pearce *et al.*, 1984). All samples but one plot in the volcanic arc granite field. Crosses = samples of the Straddling Granite, while the open and closed circles represent samples from the Simmons Brook Batholith and the Grole Diorite, respectively. WPG = within-plate granite, VAG = volcanic arc granite, syn-COLG = syn-collisional granite, and ORG = orogenic granite.

plot in the VAG and syn-COLG field on the Y vs. Nb diagram. There is more scatter on the Y + Nb vs. Rb plot due to the higher mobility of Rb. It is apparent that the rocks were intruded into an arc environment.

3.3.1.2 Mafic Dykes

The two mafic dyke sets cutting the Connaigre Bay Group are separable by the different textures and by slightly different mineralogy (see Chapter 2). Geochemical analyses enhance the distinction between the two dyke sets (Appendix II and Table 3.2).

The older dykes are characterized by lower SiO_2, Al_2O_3, Na_2O, and K_2O and higher percentages of Fe_2O_{3total}, MgO, and CaO compared to the younger dykes. TiO_2, MnO, P_2O_5, and LOI are similar in the two dyke sets. The differences reflect the larger percentage of plagioclase within the younger dykes and the larger proportion of clinopyroxene in the older dykes.

Trace elements concentrations are very similar between the dyke suites except for some of the transition elements (i.e. Cr, Ni, Co). Concentrations of Cr, Ni, and Co are much higher in the older dykes, again reflecting the greater abundance of clinopyroxene (these elements partition into clinopyroxene (Wilson, 1989)). Zr is also slightly elevated within the younger dykes.

A (Nb/Y) vs. (Zr/Ti) plot (Figure 3.18) further corroborates the geochemical features shown by the major
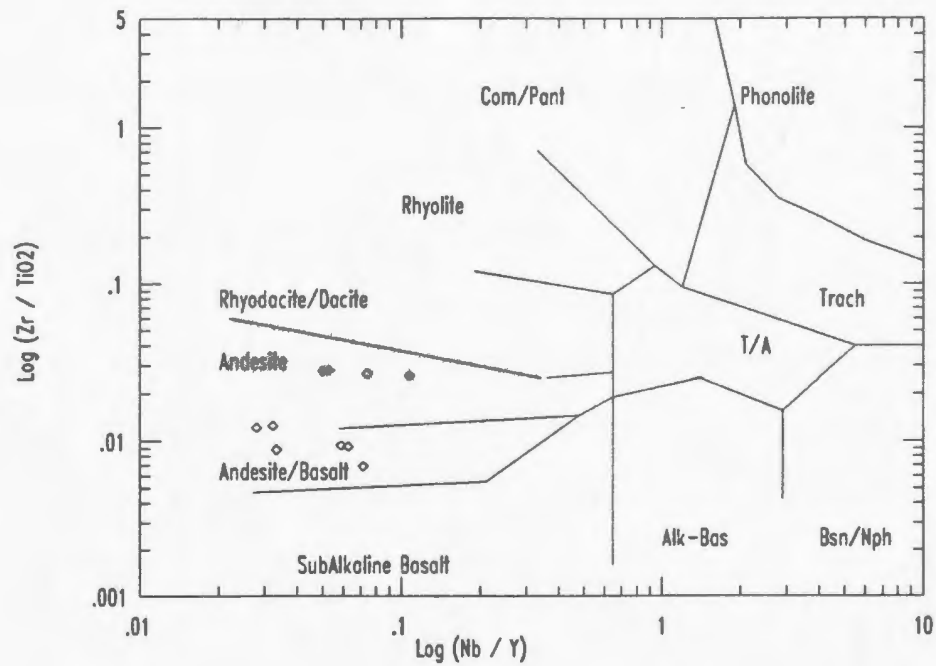
Figure 3.18. Nb/Y vs. Zr/Ti diagram illustrating the compositions of the older (open diamonds) and younger (filled diamonds) mafic dykes.
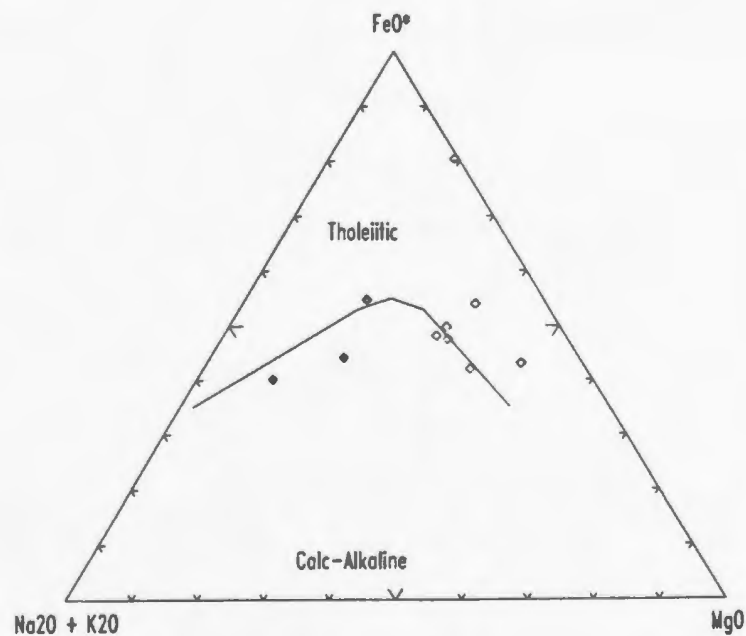
Figure 3.19. AFM diagram showing the transitional nature of the two mafic dyke suites. Symbols as in Figure 3.18. (FeO* = Fe total).

elements. The older dykes, with lower SiO_2 and higher MgO, Fe-total, and CaO, range in composition from basalt to basaltic andesite, whereas the younger dykes are solely andesitic. Both sets are subalkaline.

Expanding on the subalkaline character, when the samples are plotted on an AFM ternary diagram (Figure 3.19), both dyke sets straddle the boundary between the calcalakline and tholeiitic series of Irvine and Baragar (1971). On a different ternary diagram, from Jensen (1976), (Figure 3.20), all the samples plot in the tholeiitic fields with the older dykes in the high-Fe field whereas the younger dykes plot in the dacite-rhyolite field.

In comparison to the mafic volcanic tuffs and flows of the Connaigre Bay Group, the older dykes are very similar in composition, whereas the younger dykes have different chemical characteristics. This reinforces the hypothesis that the older dykes were feeders for the mafic volcanic rocks of the Connaigre Bay Group.

3.3.1.3 Felsic Dykes

Two generations of felsic dykes cut the Connaigre Bay Group and the younger set also cuts the Devonian(?) Pass Island Granite. Thin section analyses reveal that the two sets are similar and cannot be confidently separated by visual examination. However, using chemical analyses for the 17 samples (Appendix II and Table 3.2), they can be divided into
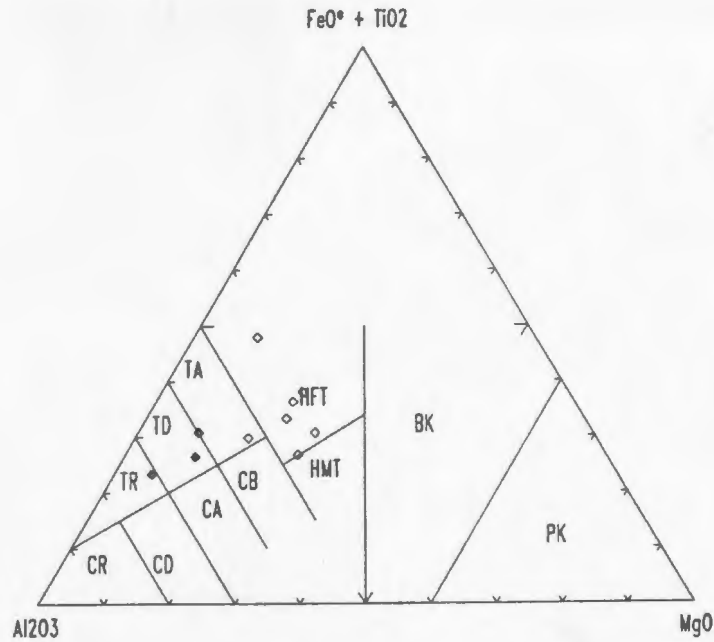
Figure 3.20. Al_2O_3 - FeO^* (Fe total) + TiO_2 - MgO diagram displaying the tholeiitic nature of both mafic dyke sets. Symbols as in Figure 3.18 and fields as in Figure 3.7.
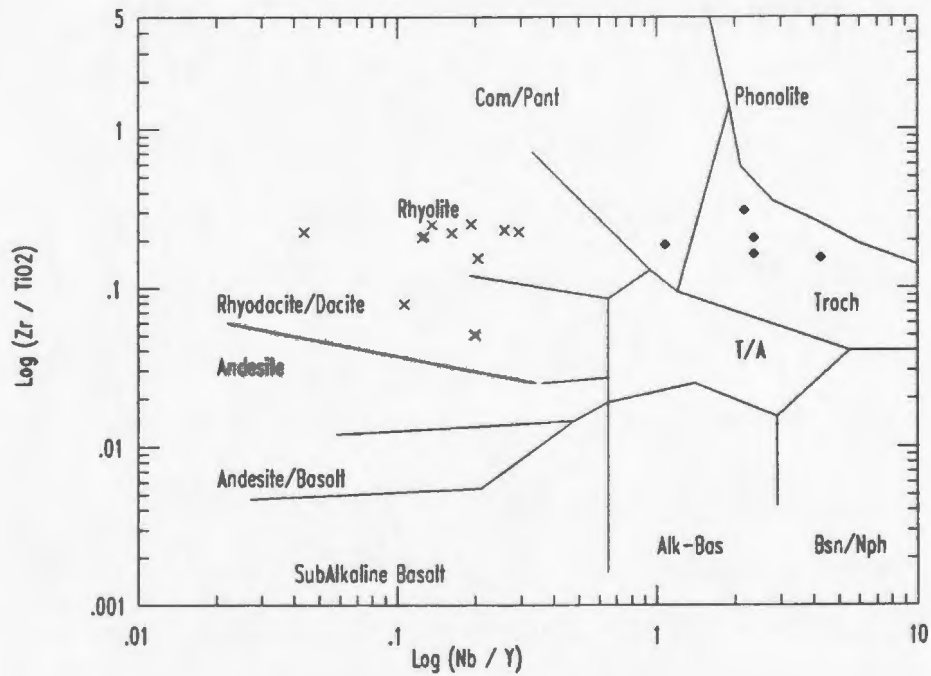
Figure 3.21. Nb/Y vs. Zr/Ti plot illustrating the dictinct chemical signatures between the older felsic dykes (X's) and the younger felsic dykes (filled diamonds).

two groups.

On a log (Nb/Y) vs. log (Zr/Ti) diagram (Figure 3.21), the older dyke set (12 samples) clusters in and around the subalkaline rhyolite field, and a group of five samples (younger dykes), plots in the strongly alkaline trachyte field (four samples) and in the mildly alkaline comendite/pantellerite field (one sample). A SiO_2 vs. alkalis diagram (Figure 3.22) indicates that all 17 samples plot in the subalkaline field far away from the alkaline-subalkaline boundary. On an AFM ternary diagram (Figure 3.23), the samples fall into the calcalkaline field, while the five alkaline samples plot near the alkalis apex. On an igneous spectrum diagram (Figure 3.24), the alkaline samples appear relatively fresh whereas the older samples are mostly Na-altered. Yet if the five alkaline rocks are trachytic (Figure 3.21), then there has been an addition of at least 15-20 wt.% SiO_2 and possibly a reduction of total alkali content by 5-7 wt.%.

The alkaline dykes not only have a higher Nb/Y ratio, their TiO_2 and Al_2O_3 contents are also distinct. An Al_2O_3 vs. TiO_2 plot (Figure 3.25) shows that the younger alkaline dyke set clusters around 15 wt.% Al_2O_3 and approximately 0.04 to 0.05 wt.% TiO_2. The older calcalkaline dykes have an average Al_2O_3 of 12 wt.% and a TiO_2 value of $\approx$ 0.25 wt.%. The alkaline rocks also have slightly lower SiO_2 and slightly higher P_2O_5 and K_2O wt. percentages. Na_2O is slightly higher in the calcalkaline dykes and MgO, MnO, CaO, Fe_2O_{3total}, and LOI are
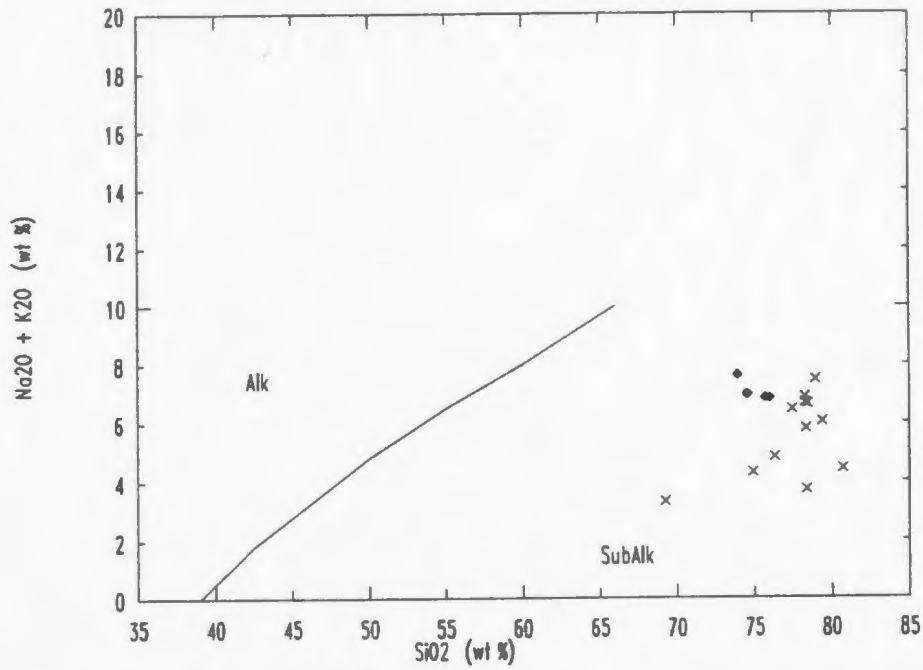
Figure 3.22. SiO$_2$ vs. alkalis diagram. Both felsic dyke suites have are subalkaline in character. Symbols as in Figure 3.21.
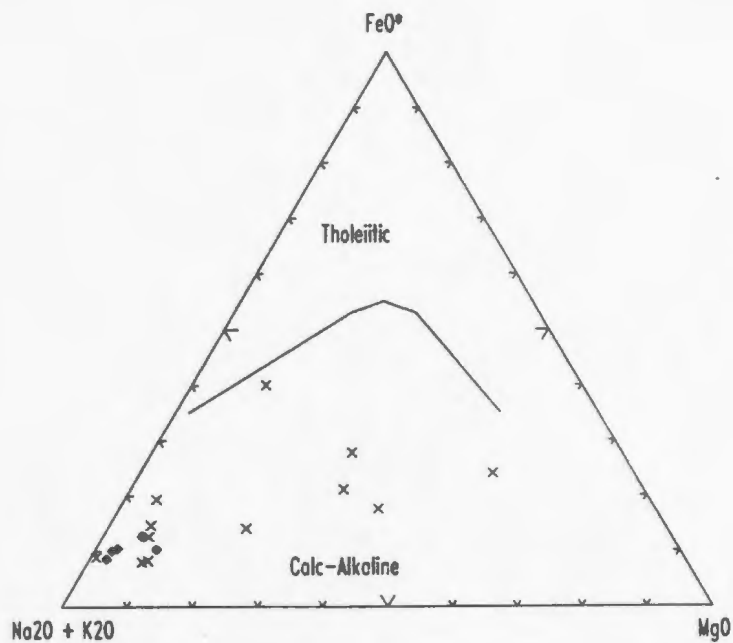
Figure 3.23. AFM diagram showing the calcalkaline character of the felsic dykes. Symbols as in Figure 3.21. (FeO* = Fe total).
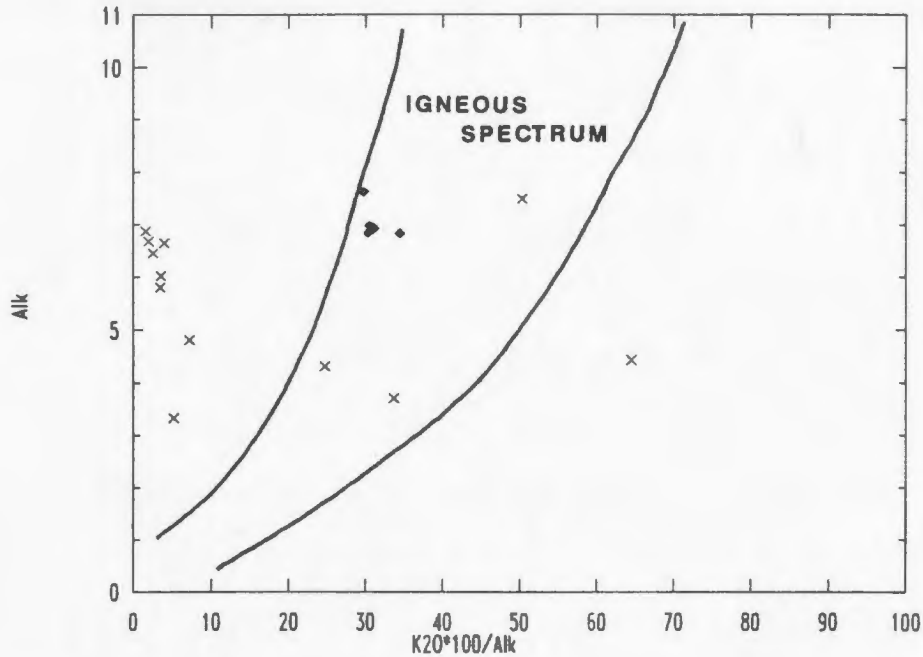
Figure 3.24. An "igneous spectrum" plot illustrating the apparently altered younger felsic dykes and the apparently Na-altered older felsic dyke suite. Symbols as in Figure 3.21.
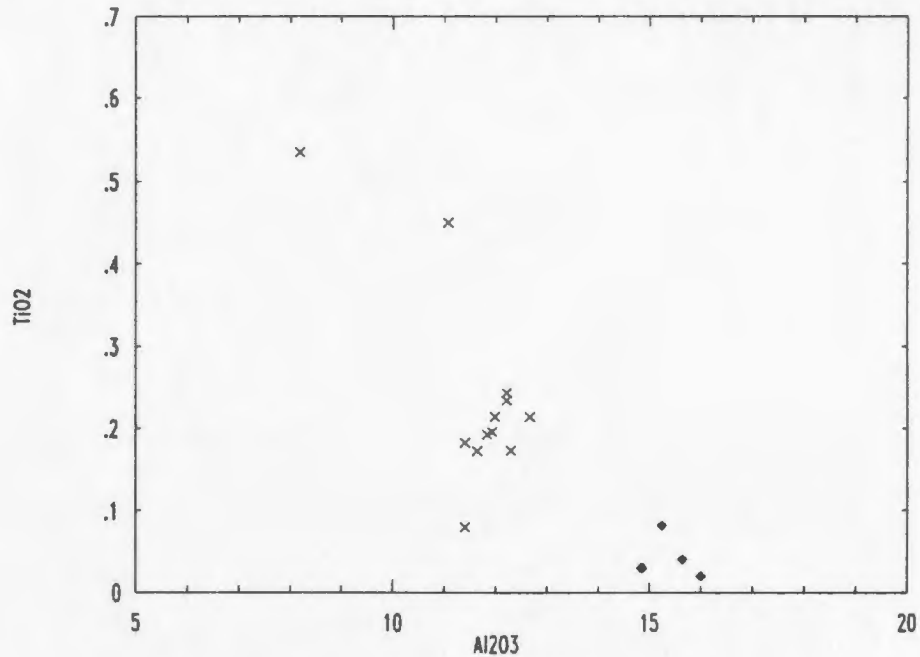
Figure 3.25. Al_2O_3 vs. TiO_2 variation diagram. The younger dyke suite is distinguished from the older suite by higher Al_2O_3 and lower TiO_2. Symbols as in Figure 3.21.

similar for both sets.

With respect to trace elements, the alkaline samples have lower incompatible concentrations than the calcalkaline rhyolite dykes. Zr, Y, Ce, and La have average concentrations of approximately 40, 10, 30, and 10 ppm respectively within the alkaline dykes, whereas the calcalkaline dykes have Zr, Y, Ce, and La averages of 250, 40, 60, and 20 ppm respectively. Nb is the only incompatible element that is more concentrated in the alkaline rocks; an average of $\approx$ 15 ppm against 6-7 ppm for the calcalkaline dykes.

The alkaline dykes are most likely related to the Pass Island Granite, but they do have chemical characteristics similar to both the Hermitage Complex (Furbys Cove Granite) and the Pass Island Granite. Each intrusive has high SiO_2 phases which also have low TiO_2 and relatively high Al_2O_3 (Appendix 2 and Tables 3 and 5 of O'Driscoll, 1977). Zr values for the alkaline rocks resemble those for phases of the Pass Island Granite whereas Nb values more closely approximate those for the Hermitage Complex. Within the Connaigre Bay Group there are no felsic rocks with an alkaline signature, therefore suggesting that the alkaline dykes are not related to the volcanic rocks. Also, the lack of a continuum between the calcalkaline samples and the alkaline rocks suggest a separate origin for the two groups.

3.2 Rare Earth Elements (REE) and Associated Trace Elements

3.2.1 Introduction

Rare earth elements (REE) and associated trace elements serve as important petrogenetic and tectonic indicators (Henderson, 1984; Wilson, 1989; Swinden et al., 1989). Different tectonic environments have distinct REE and extended REE patterns (not including any post generation effects) which are a direct result of igneous processes in the zone of magma generation. Therefore, by comparing patterns from the study to traditional patterns from known tectonic regimes, a tectonic environment may be postulated.

Forty-four (44) samples were analysed for the 14 REE and selected trace elements (Appendix IV and Table 3.3) using induced coupled plasma/mass spectrometry (ICP/MS) techniques (Appendix V). Due to analytical difficulties, Zr (and Hf) and Ta values are suspect and should not be used. To get around this difficulty, Ta is recalculated from Nb using the ratio Ta = Nb/17 (Jochum et al., 1986). Zr values for 25 of the 44 samples were also analysed by ICP/ES, therefore these Zr values will be used. Hf can be recalculated from Zr using the ratio Hf = Zr/37 (Jochum et al., 1986).

Of the 23 relatively unaltered rocks analysed, eight are mafic to intermediate volcanic tuffs and flows, 10 are dacitic to felsic volcanic rock samples, with three rhyolite dyke and two mafic dyke samples. Partial extended REE patterns for 5 of the younger felsic and 3 of the younger mafic dykes are also

Table 3.3. Average ICP-MS REE and selected trace element contents for rock samples from the Hermitage Peninsula: mafic tuffs and flows (1), felsic tuffs and flows (2), mafic dykes (3), felsic dykes (4), mineralized Tickle Point Fm. samples (5), and mineralized Sam Head fm. samples (6). (ca = check Appendix IV - incomplete data)

Sample #	1	2	3	4	5	6
Sc(ppm)	29	10	27	7	8	10
Pb	142	11	7	33	132	3452
Bi	0.16	1.14	0.03	0.05	4.34	1.86
W	105.17	443.6	127.6	2.74	58.06	94.11
Mo	0.81	3.35	1.8	0.9	12.81	11.64
Rb	30	39	128	7	19	29
Cs	2.09	0.75	1.11	2.11	0.37	7.45
Ba	776	400	230	196	240	161
Sr	158	66	262	71	40	27
Tl	1.92	0.49	0.51	0.44	0.62	10.41
Li	17.26	12.39	11	19	7.39	41.01
Ta	0.16	0.29	0.25	0.4	0.2	0.2
Nb	2.8	4.9	4.2	6.7	3.3	3.5
Hf	ca	ca	ca	7.38	3.67	ca
Zr	ca	ca	ca	273	135	ca
Y	22	37.2	28	33.3	22	10.8
Th	0.87	4.21	1.41	5.19	2.54	1.39
U	0.18	0.81	0.35	0.96	0.56	0.39
Be	0.82	1.2	0.9	1.15	0.75	1.95
La	6.55	21.65	9.46	18.21	8.76	6.24
Ce	16.1	51.42	22.2	42.31	20.65	14.83
Pr	2.4	6.8	3.16	5.77	2.76	2.03
Nd	10.6	26.92	14.03	22.43	10.98	8.32
Sm	3.28	6.86	4.13	5.61	3.04	2.17
Eu	1.1	1.5	1.26	0.85	0.85	0.58
Gd	3.8	6.26	4.45	4.82	3.41	1.95
Tb	0.68	1.14	0.82	0.9	0.65	0.33
Dy	4.38	7.13	5.17	5.84	4.17	2.06
Ho	0.9	1.48	1.09	1.27	0.87	0.43
Er	2.25	4.45	3.21	4.27	2.59	1.34
Tm	0.35	0.66	0.45	0.66	0.38	0.2
Yb	2.16	4.25	2.9	4.62	2.46	1.38
Lu	0.3	0.63	0.43	0.75	0.37	0.22

utilized in this section.

Extended REE diagrams are normalized to primitive mantle values and normal REE plot are normalized to chondrite values (Table 3.4).

3.2.2 Connaigre Bay Group
3.2.2.1 Mafic to Intermediate Volcanic Rocks

Eight mafic to intermediate rock analyses are plotted on REE and extended REE patterns. Six are from the Tickle Point Formation and two are from the Sam Head Formation.

Figure 3.26 illustrates that the extended REE patterns are very similar in shape and there is only 10X difference between extremes for any given element. This plot also shows Nb and Ta depletions with respect to La, and slight negative Eu anomalies, with respect to Sm and Gd, in three of the samples. The sample with the largest Eu anomaly is a sheared carbonatized and chloritized mafic rock below the mineralized zone at Frenchman Head. Alteration of plagioclase feldspar to sericite and sausserite may have resulted in a loss of Eu or there may have been little original feldspar and therefore little original Eu (see section 3.3). Y and Zr (where plotted) are generally consistent with the HREE and LREE, respectively. Th is not enriched with respect to La.

A plot of just the REE (Figure 3.26), normalized to chondrite values, shows relatively flat to slightly LREE

Table 3.4. Normalization factors for normal and extended REE diagrams. Typical tholeiitic MORB values from Pearce (1983), chondrite values from Wakita et al. (1971), and primitive mantle values taken from Hofmann (1988).

MORB		CHONDRITE				PRIMITIVE MANTLE			
Th	0.2	La	0.340			La	0.6139	Er	0.4167
Ta	0.18	Ce	0.910			Ce	1.6011	Tm	0.0643
Nb	3.5	Pr	0.121			Pr	0.2419	Yb	0.4144
Ce	10	Nd	0.640	Er	0.200	Nd	1.1892	Lu	0.0637
P2O5	0.12	Sm	0.195	Tm	0.032	Sm	0.3865	Hf	0.2676
Zr	90	Eu	0.073	Yb	0.220	Eu	0.1456	Zr	9.714
Hf	2.4	Gd	0.260	Lu	0.034	Gd	0.5128	Ta	0.0351
Sm	3.3	Tb	0.047			Tb	0.0940	Nb	0.6175
TiO2	1.5	Dy	0.300			Dy	0.6378	Th	0.0813
Y	30	Ho	0.078			Ho	0.1423	Y	3.940
Yb	3.4								
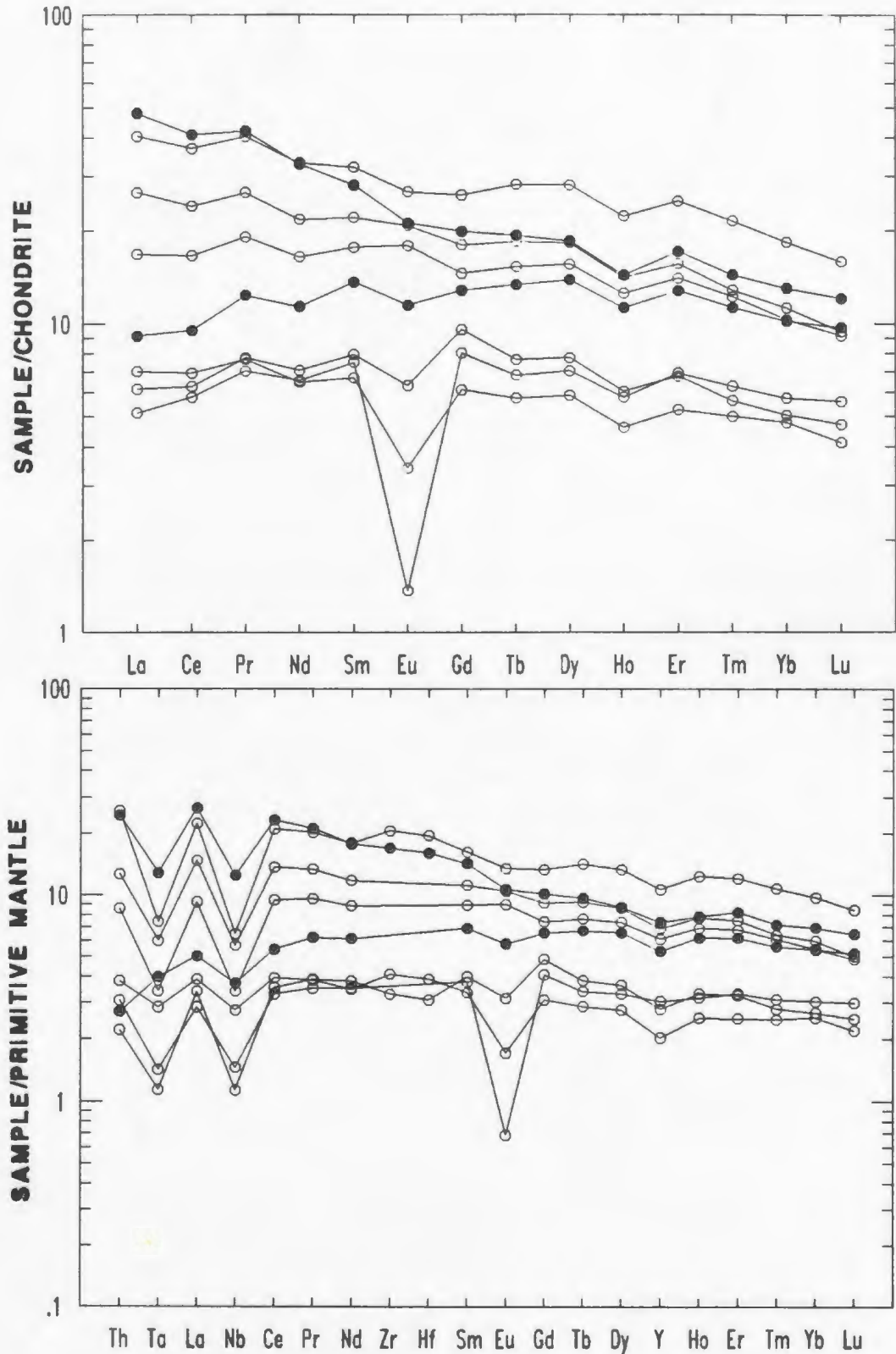
Figure 3.26. Chondrite-normalized REE and primitive mantle-normalized extended REE patterns for selected mafic to intermediate rock samples from the Tickle Pt. Fm. (open circles) and the Sam Head Fm. (filled circles).
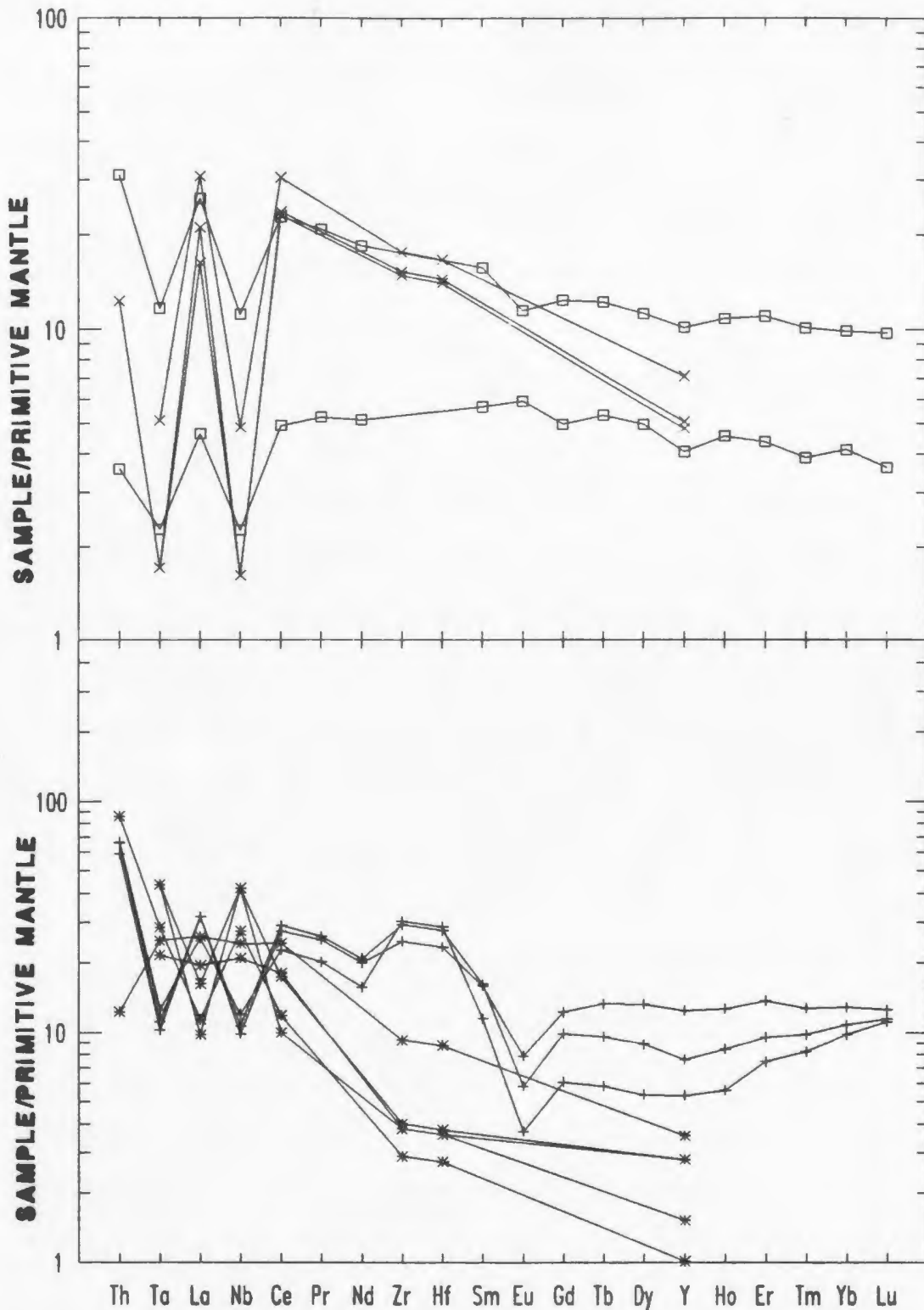
Figure 3.28. Extended REE profiles for mafic and felsic dykes cutting rocks of the Connaigre Bay Group. Upper diagram: open squares = older mafic dykes; X = younger mafic dykes. Lower diagram: + = older felsic dykes; * = younger felsic dykes.

enriched patterns. These patterns are typical of tholeiites (Graf, Jr., 1977).

3.2.2.2 Dacitic to Felsic Volcanic rocks

The 11 samples analysed are from the Tickle Point Formation. The extended REE patterns of the felsic rocks (Figure 3.27) are very similar in shape to the mafic rocks. There is a maximum of one order of magnitude between the upper and lower limits of any one element, also similar to the mafic rocks. All but one of the felsic rocks (i.e. sample 584083) have strong Nb and Ta depletions and slight Eu depletions. Th is enriched with respect to La, whereas Zr and Y are basically conformable with the LREE and HREE, respectively, except sample 584083 which has Zr enriched over the REE. Two samples, 584003 and SS88-208, have positive HREE slopes. These samples are slightly altered and contain minor pyrite. If F and CO-rich fluids were involved in the alteration, then they may complex the HREE (Taylor and Fryer, 1983) resulting in positive HREE enrichment.

The REE diagram (Figure 3.27) displays slightly LREE enriched patterns for the felsic rocks.

3.2.3 Mafic and Felsic Dykes

Five samples of the older dyke (two mafic, three felsic) and eight samples of the younger dykes (three mafic and five felsic) are plotted on extended REE diagrams (Figures 3.28).
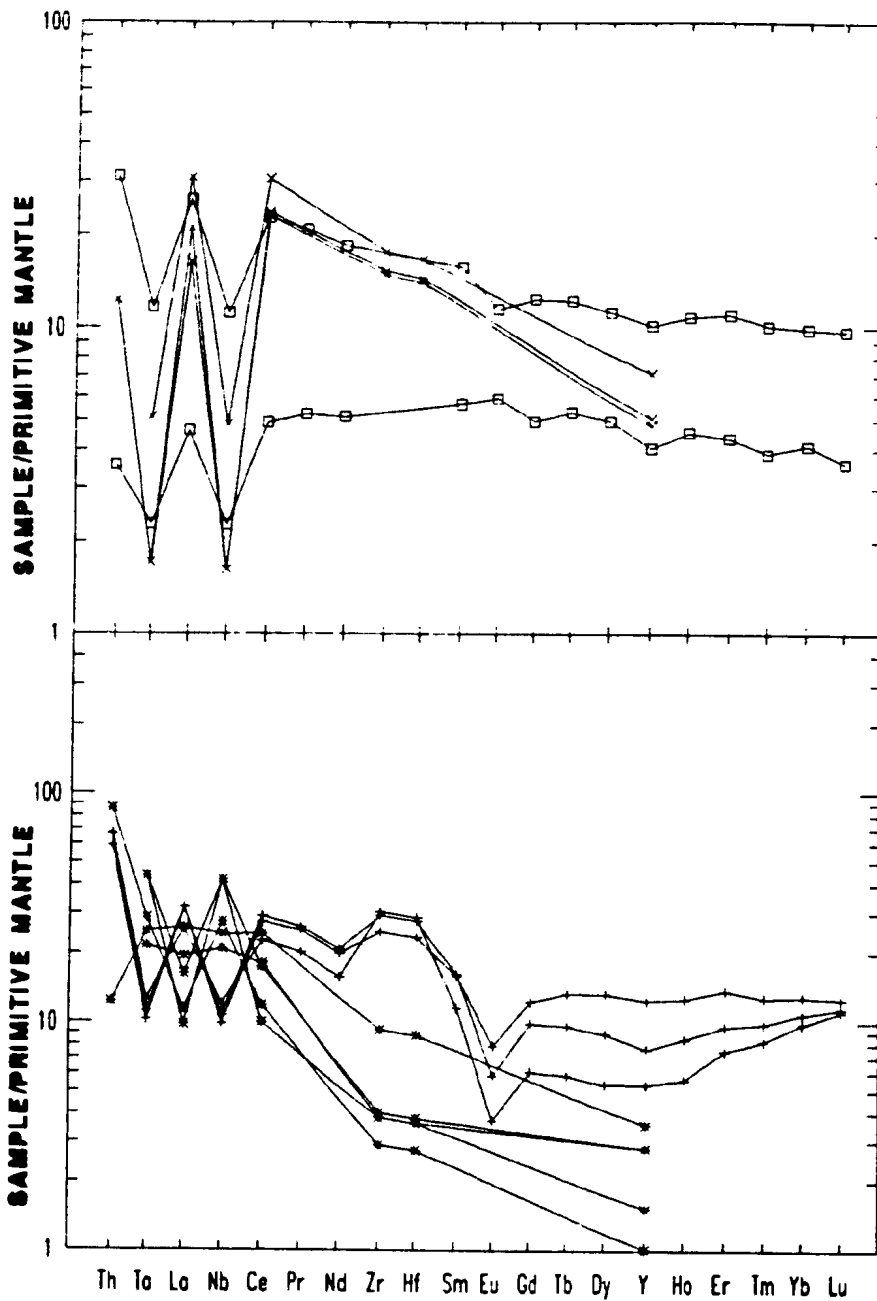
Figure 3.28. Extended REE profiles for mafic and felsic dykes cutting rocks of the Connaigre Bay Group. Upper diagram: open squares = older mafic dykes; X = younger mafic dykes. Lower diagram: + = older felsic dykes; * = younger felsic dykes.

The older mafic dyke samples have patterns similar to those of the mafic to intermediate volcanic rocks (i.e. Nb and Ta depletions, little or no Eu depletion, and flat REE patterns). Th is enriched over La in one dyke, but depleted in the other. Y behaves in a similar manner to the HREE. The felsic dyke analyses are very similar to the felsic volcanic rock analyses except for slightly higher Zr and Hf values for the dykes. With respect to the REE, the dykes also have slight LREE enrichments and minor Eu depletions.

The partial extended REE diagrams for the younger dykes display different shaped patterns than the older dyke set. The younger felsic dykes have lower Y, Zr, Hf, and La but higher Nb and Ta (both showing positive anomalies) than the older felsic dykes, giving the younger dykes a LREE-enriched pattern. The younger mafic dykes have large Nb and Ta depletions with a LREE-enrichment pattern, but overall are similar in shape to the older mafic dykes.

The major and trace element concentrations also show this large chemical distinction between the felsic dyke sets and the relatively smaller differences between the mafic dyke suites. The younger felsic dykes appear to have formed in alkaline setting whereas the younger mafic dykes have a definite arc signature.

The striking similarities between the volcanic rocks of the Connaigre Bay Group and the older dykes cutting them provides strong evidence that the dykes both cut and feed

these volcanic rocks.

3.3   Implications   for   Tectonic   and   Mineralization Environments

When using chemical discrimination diagrams to define tectonic origins, diagrams defined by immobile elements are preferred over plots which use mobile elements. Most tectonic diagrams have considerable overlap between their different tectonic fields, e.g. Pearce and Cann (1973, figure 3) wherein field B may contain samples of ocean floor basalt (OFB), low potassium tholeiites (LKT), and calcalkaline basalt (CAB). It will therefore be necessary to use a series of diagrams in order to eliminate certain tectonic environments during the process of selecting one which best fits the data.

The geochemical data suggests that the Connaigre Bay Group rocks are part of a volcanic arc, calcalkaline and tholeiitic in character, which underwent extension, resulting in the subsequent extrusion of island arc tholeiites.

The dacitic to felsic rocks are calcalkaline to tholeiitic (see Figures 3.14 and 3.15) whereas the mafic to intermediate rocks are tholeiitic (Figure 3.7 and 3.8). Since the general stratigraphy of the Connaigre Bay Group is a felsic to mafic succession from bottom to top, there is also a transition from calcalkaline to tholeiitic from bottom to top. This transition is opposite to the expected transition of early tholeiitic volcanism to calcalkaline volcanism as the arc matures

(Wilson, 1989). It should be noted that the Connaigre Bay Group covers approximately 200 km^2 which would represent only a small portion of a much larger and structurally complex arc. What underlies the calcalkaline felsic volcanic rocks is not known, so the felsic rocks may not represent the initial island arc volcanism.

There is strong evidence for suggesting an arc environment. Firstly, Wilson (1989) states that calcalkaline volcanism is totally restricted to subduction related processes, i.e. an arc setting. The abundance of tholeiitic rocks and the lack of abundant andesitic rocks suggest an arc setting in a collisional oceanic environment (island arc) over an oceanic-continental collisional environment (Andean-type volcanic arc) although the evidence for continental contamination suggests a proximity to a continental source. Secondly, when the mafic to intermediate volcanic rocks and dykes are plotted on a Th - Hf - Ta diagram (Figure 3.29), they fall into the field defined as destructive plate margin volcanism (Wood, 1980). The samples plot within the VAB field on both Pearce's (1980) Y vs. Cr diagram and Meschedes' (1986) Zr-Nb-Y plot but there is overlap into the within plate basalt (WPB) and mid-ocean ridge basalt (MORB) fields (Figures 3.30 and 3.31). The presence of fine-grained laminated sediments and carbonates interbedded with the volcanics implies that there were periods of quiescence in the island arc environment.
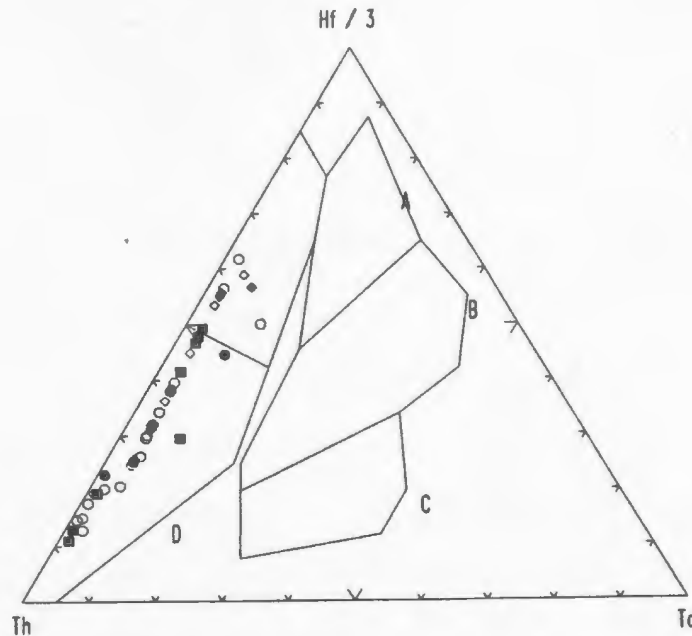
Figure 3.29. Th - Hf - Ta ternary diagram (from Wood, 1980).
The mafic to intermediate samples all plot in the
destructive plate margin field. A = N (normal)-type MORB; B
= E (enriched)-type MORB and tholeiitic within-plate basalts
and differentiates; C = alkaline within-plate basalts and
differentiates; D = destructive plate margin basalts and
differentiates. The arrowed line (_i.e._ where Hf/Th = 3)
within the D-field separates calcalkaline samples (below
line) from tholeiitic samples (above line). Symbols as in
Figures 3.1 and 3.18.
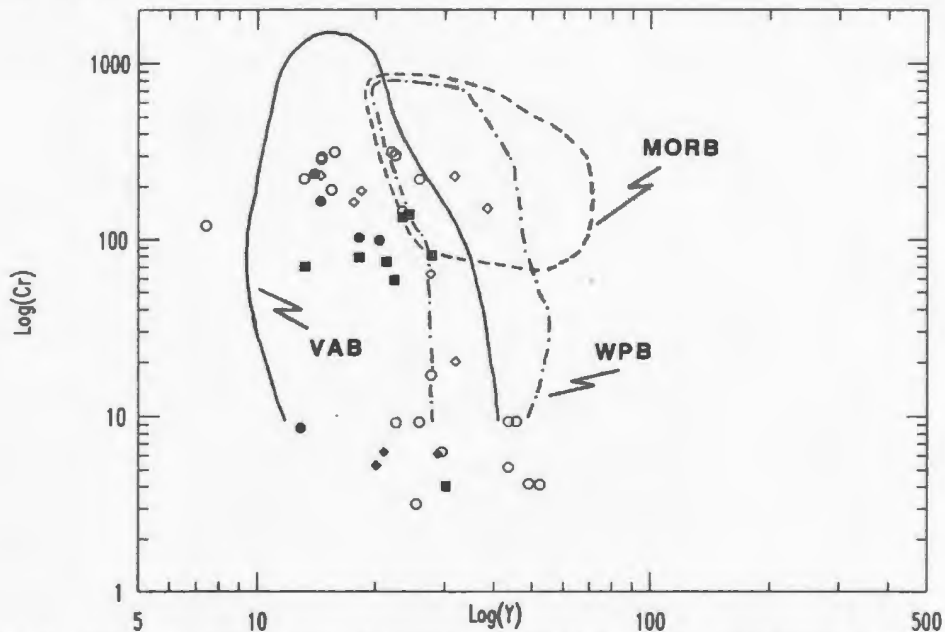
Figure 3.30. Y vs. Cr diagram with the respective tectonic
fields (from Pearce _et al._, 1981). The mafic to intermediate
rocks and the mafic dykes plot mainly in the VAB field but
some overlap into the WPB and MORB fields. VAB = volcanic
arc basalt, MORB = mid-ocean ridge basalt, and WPB = within-
plate basalt. Symbols as in Figures 3.1 and 3.18.

The extended REE patterns also display arc signatures. A typical island arc tholeiite signature contains a prominent Nb and Ta depletion with respect to La (Swinden et al., 1989; Wilson, 1989). Arc tholeiites also have relatively flat to slightly enriched LREE patterns (Henderson, 1984; Swinder et al., 1989), but back arc basin basalts (BABB) also display the same type of flat pattern (Taylor and Karner, 1983). The mafic to intermediate rocks display both the Nb and Ta depletions and the flat to slightly LREE enriched pattern. The mafic rocks, therefore, may represent the initial lavas that were extruded as the island arc rifted. The mafic rocks would have IAT characteristics, and may be of possible back-arc basin affinity.

It is not clear why there is a depletion in the high field strength (HFS) elements (i.e. Nb, Ta). It may be due to a previous depletion in the source area for the arc volcanics (Hickey and Frey, 1982; Sun and Nesbitt, 1978) or there may be residual phases in the arc source which retain the HFS elements (Green, 1980, 1981). Swinden et al. (1989) suggest a theory similar to Hickey and Frey (1982) and Sun and Nesbitt (1978); melting of a refractory source, which is capable of generating LREE depleted tholeiites.

Swinden et al. (1989) also suggest that the low field strength elements, represented by Th, should be enriched with respect to La in an island arc environment. This does not occur on the extended REE plots, where Th contents are equal

to or slightly lower than those of La. The REE and extended REE patterns for the felsic volcanic rocks have the strong Nb depletion and the Th enrichment. The stronger arc signature from the felsic rocks with respect to the mafic rocks may indicate that the felsic rocks represent true arc volcanism, originating from an arc source, whereas the mafic rocks represent the mixing of an arc source with a different non-arc tholeiitic source.

REE patterns may also be used to distinguish mineralized environments from barren environments. Campbell et al. (1982), while working in Archean felsic volcanic rocks, noted that mineralized horizons, regionally, have flat to slightly LREE enriched patterns with well developed negative Eu anomalies (Figure 3.32), while barren felsic volcanic horizons have steep REE patterns (strong LREE enrichment) and little or no negative Eu anomaly. Thurston (1981) suggests that the flat pattern is a result of the introduction of HREE by ore-bearing solutions. Campbell et al. (1982), stating that it is unlikely that ore-bearing fluids could enrich such a large volume of rock with HREE, imply that the patterns are a direct result of the partial melting processes in the crust or upper mantle and the subsequent fractional crystallization in a subvolcanic magma chamber. The latter theory also accounts for the negative Eu anomaly, i.e. extensive feldspar fractionation. Culler et al. (1973) believe that evidence from partitioning data suggests that REE are not concentrated in aqueous
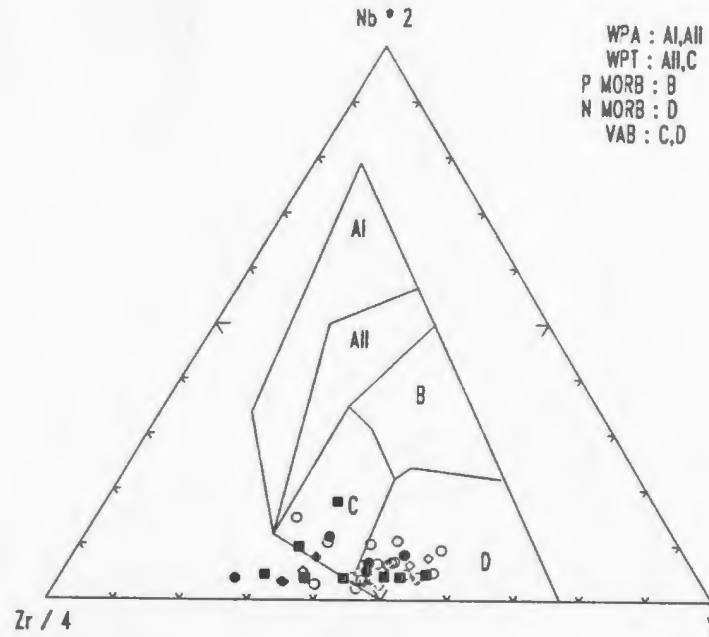
Figure 3.31. Zr - Nb - Y diagram taken from Meschede (1986)
Most samples plot in fields C and D, whereas some plot
outside the C-field toward the Zr axis. WPA = within-plate
alkali basalt, WPT = within-plate tholeiite, P-MORB = plume
influenced mid-ocean ridge basalt, N-MORB = normal mid-ocean
ridge basalt, and VAB = volcanic arc basalt. Symbols as in
Figures 3.1 and 3.18.
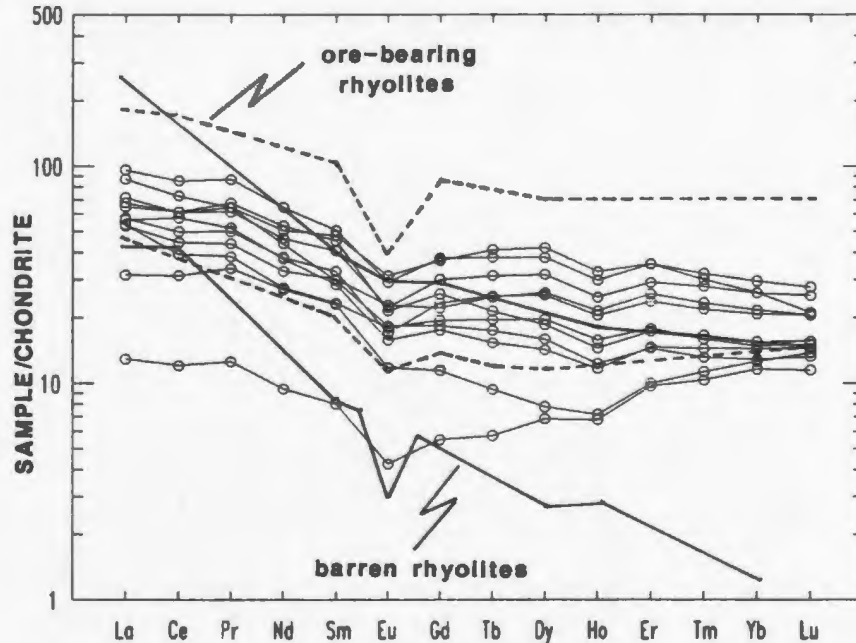
Figure 3.32. Chondrite-normalized REE profiles presenting
the patterns for dacitic to felsic rocks from the Tickle Pt.
Fm., and the superimposed ranges for ore-bearing and barren
rhyolites, as defined by Campbell et al. (1982).

solutions but prefer solid phases, therefore both of the above theories may be incomplete. The Campbell et al. (1982) theory would fit if the phases fractionating were LREE-enriched.

The Connaigre Bay Group felsic volcanics plot within the range for mineralized samples (Figure 3.32) inferring that the whole volcanic pile is a good locality for base-metal exploration. It is important to note, however, that even though REE are immobile at low grades of metamorphism, Taylor and Fryer (1982) and Graf (1977) suggest that REE mobility during hydrothermal alteration is real. Cl^- ions complex LREE while CO_3^{2-} and F^- complex HREE (Taylor and Fryer, 1984). The combination of HREE enrichment and the fact that there are numerous carbonate units throughout the Connaigre Bay Group hints that CO_3^{2-}-rich fluids were important for base-metal mineralization. F^- may have also been present in the mineralizing fluids but there is no fluorite present in the mineralized zones.

Figures 3.33 and 3.34 are diagrams which display the OFB character of the mafic rocks. Samples from the Sam Head Formation plot in the OFB field whereas Tickle Point and Doughball Point Formation samples plot mainly in the OFB field, but there is slight overlap with the arc environment. These Ti-based diagrams are also suggestive of a transition from arc to rifted-arc volcanism (i.e. IAT), but because the Sam Head Formation, with OFB characteristics, is stratigraphically between the Tickle Point and Doughball Point
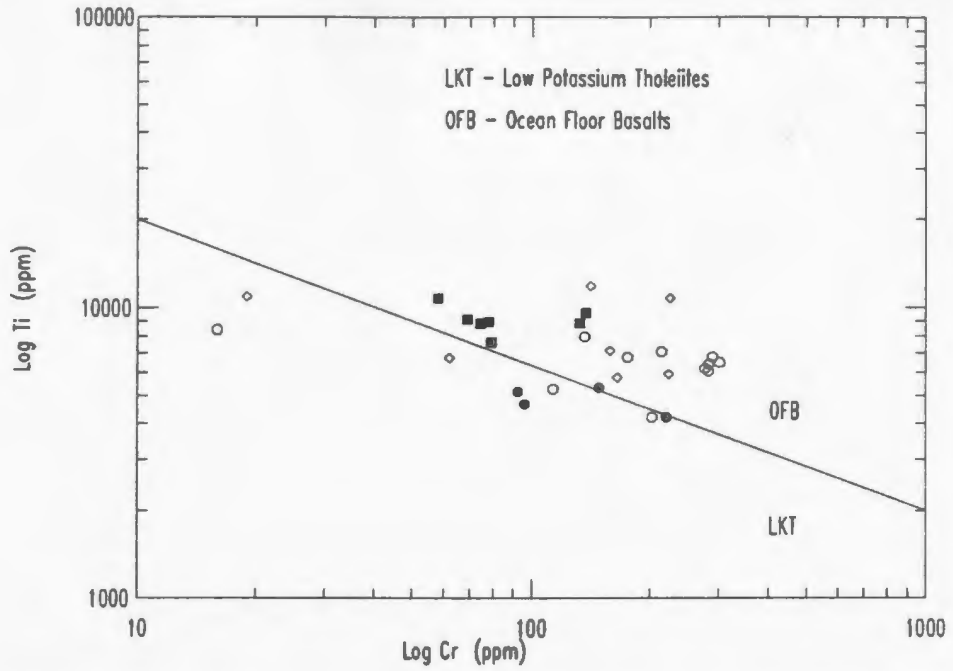
Figure 3.33. Cr vs. Ti plot defining LKT (low potassium tholeiite) and OFB (ocean floor basalt) fields, taken from Pearce (1975). Symbols as in Figures 3.1 and 3.18.
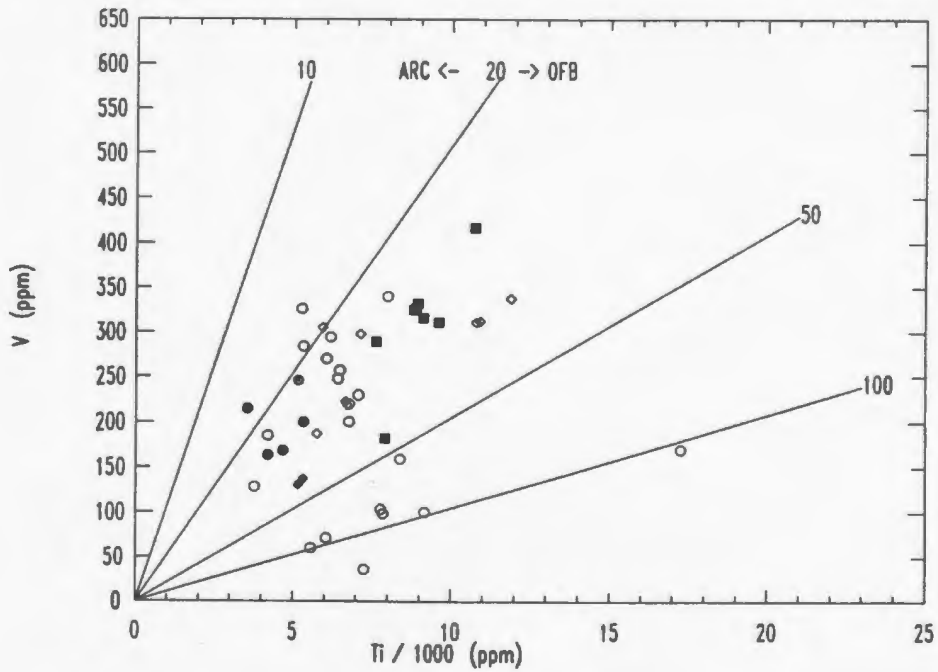
Figure 3.34. Plot of Ti vs. V displaying the volcanic arc (ARC) field and the ocean floor basalt (OFB) field, as defined by Shervais (1982). Symbols as in Figures 3.1 and 3.18.
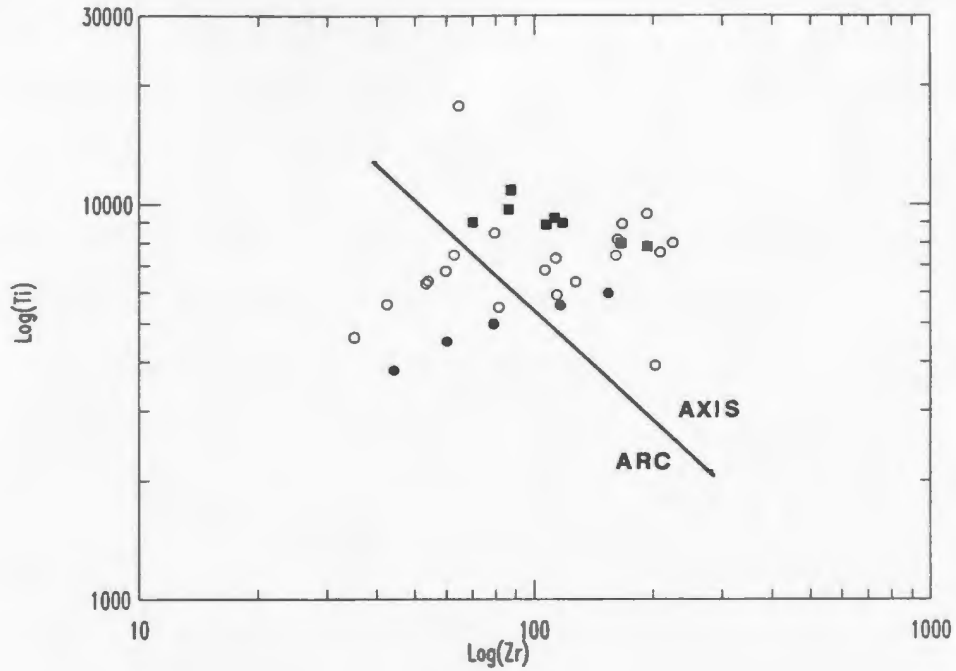
Figure 3.35. Zr vs. Ti diagram illustrating the arc/axis dividing line (after Pearce et al., 1981), and the transitional nature of the mafic rocks. Symbols as in Figures 3.1 and 3.18.
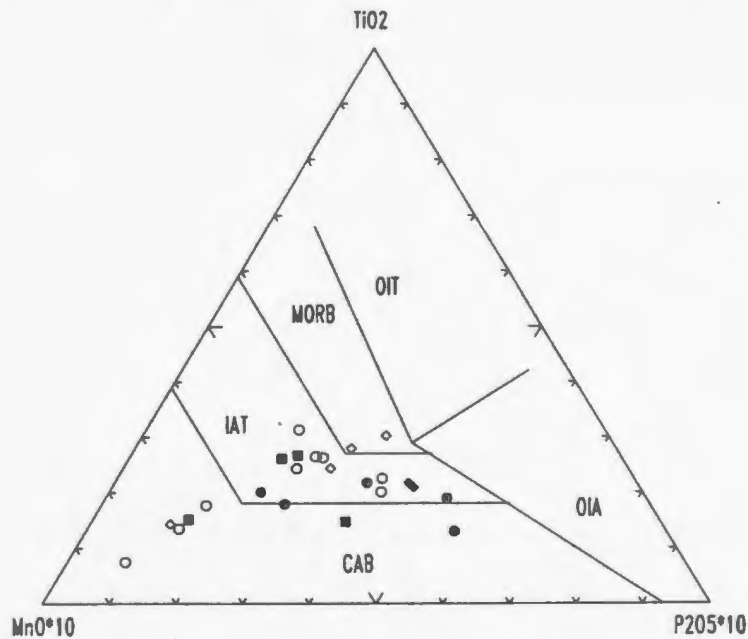
Figure 3.36. MnO − TiO_2 − P_2O_5 ternary plot for mafic samples containing between 45 and 54 wt.% SiO_2 (taken from Mullen, 1983). CAB = calcalkaline basalt, IAT = island arc tholeiite, MORB = mid-ocean ridge basalt, OIT = ocean island tholeiite, and OIA = ocean island alkali basalt. Symbols as in Figures 3.1 and 3.18.

Formations (both of which may be transitional to OFB), there are spatial and temporal difficulties.

A view of other discrimination diagrams (Figures 3.35 and 3.36) illustrates the transitional nature of the Connaigre Bay Group. Figure 3.35 shows a strong trend from arc to axis (spreading centre) activity (or vice versa). Figure 3.36 also displays a smooth trend between CAB and IAT.

Figure 3.35 was used by Pearce et al. (1981) to suggest that the Oman Ophiolite originated in an arc-basin complex. The geochemistry of the Connaigre Bay Group implies that, in this case, arc volcanism occurred first with the extrusion of calcalkaline-tholeiitic felsic volcanism with a later arc-rifting event with tholeiitic volcanism. A similar scenario is proposed by Swinden et al. (1989) for the formation of the Wild Bight Group. The Wild Bight Group displays a geochemical progression from early island arc volcanism, through an arc rifting stage, to the establishment of a back-arc basin containing volcanic rocks with a non-arc signature (Swinden et al., 1989).

A popular setting for massive sulphide deposition is an arc setting (Cathles et al., 1983; Franklin et al., 1981; Kirkham, 1987; Swinden et al., 1989). This type of setting creates certain features where deposition and preservation of VMS deposits can be attained. Island arcs can be areas of extension and high heat flow (Cathles et al., 1983) creating an environment where large quantities of fluids can convect

through the rocks, leaching metals, and becoming focussed to the surface along faults. The Kuroko deposits of Japan are classic examples of metal deposition in basins bounded by normal faults in a collapse-related graben (Franklin et al., 1981). The location of mineralized horizons within the Connaigre Bay Group illustrate that these zones parallel major faults, implying that the faults focussed metal-rich fluids to the surface where the metals were deposited in topographic depressions (see Chapter 4). Uyeda and Nisiwaki (1980) pointed out that most massive sulphide deposits occur in areas of extensional stress and Franklin et al. (1981) state that the presence of an extensional regime is essential for massive sulphide deposition.

Stephens et al. (1984) discuss the importance of the extensional tectonic regime for massive sulphide deposition, as seen in the postarc and post-early collision environments in the Appalachians and Caledonides, but they also stress that evidence for extension is lacking in other subduction related volcanic piles which host massive sulphides (e.g. early arc sequences of central Newfoundland).

Although the geochemical data supports an island arc environment, some of the trace element systematics present evidence that there is crustal contamination within the system. Figure 3.37 plots Zr vs. Zr/Y as modified by Pearce (1983) after Pearce and Norry (1979). Most of the mafic to intermediate samples plot in or near the continental arc

field, suggesting that in this island arc setting, there is contamination from a Zr-enriched source. This source could either be continental crust or within-plate material (Pearce, 1983), or possibly subducted, continentally derived, sediments.

A spidergram of the more immobile elements (Figure 3.38), adapted from Pearce (1983), demonstrates that the majority of the samples have enriched incompatible major and trace element concentrations with respect to a product that is the culmination of 80% basaltic magma and 20% melt derived by 50% partial melting of a graywacke source. The source contaminant in this study is generally more enriched than the graywacke source used by Pearce (1983).

O'Driscoll and Strong (1979) described the Connaigre Bay Group setting as one transitional from "orogenic" (e.g. Cascades) to "non-orogenic" (e.g. basin and range) because of the strong bimodal and calcalkaline character of the volcanic rocks. This present study defined a strong tholeiitic character (especially within the mafic volcanic rocks), and the trace element systematics describe an island arc setting with limited crustal contamination. These results are not unlike those of O'Driscoll and Strong (1979), only with a stronger "orogenic" (i.e. island arc setting) component and a limited "non-orogenic" (i.e. crustal contamination) component. The model for mid-Ordovician volcanism within the Central Mobile Belt (Figure 3.39) proposed by Swinden and Thorpe
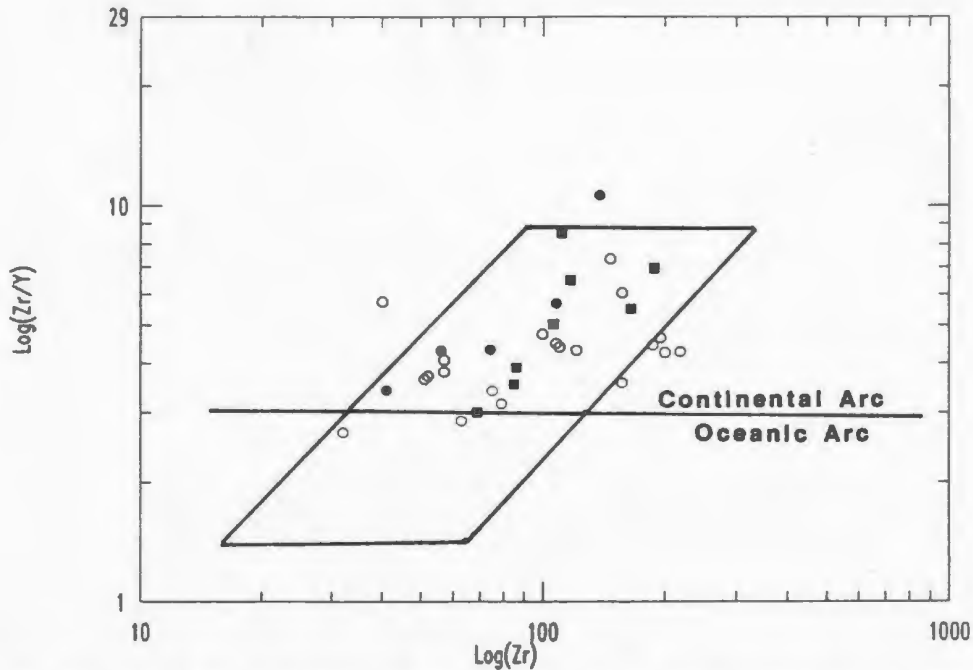
Figure 3.37. Plot of Zr vs. Zr/Y (from Pearce, 1983) displaying a dividing line between continental arc volcanic rocks and oceanic arc volcanic rocks. The field above the line represents average compositions for continental arc basalts and the field below the line represents average compositions for oceanic arc basalts. Symbols as in Figures 3.1 and 3.18.
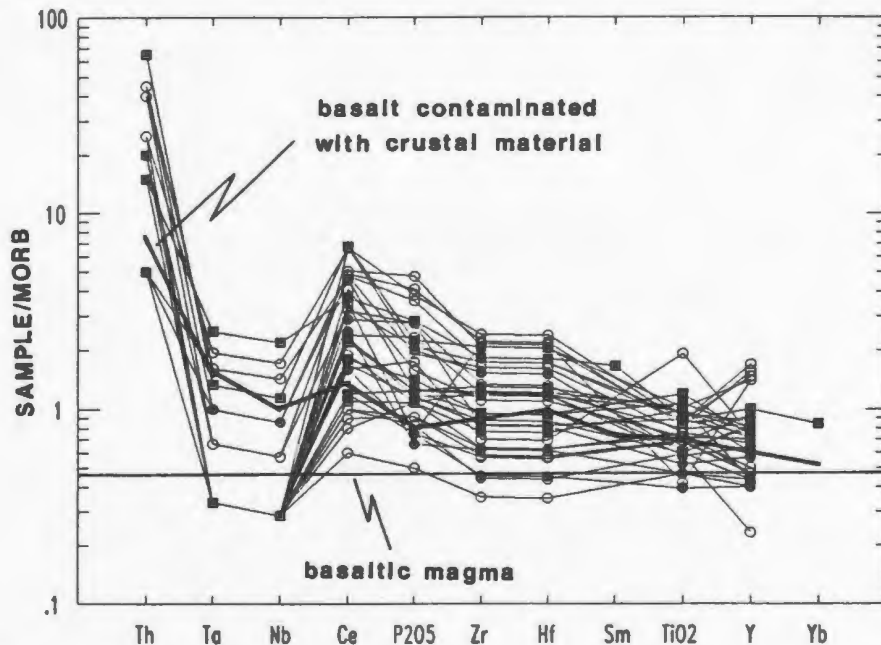
Figure 3.38. MORB-normalized spidergram adapted from Pearce (1983). The straight line (at approximately 0.5 MORB) represents a basalt magma and the above pattern represents a basalt contaminated by crustal material (*i.e.* graywacke). The Connaigre Bay Group mafic to intermediate rocks may have been contaminated by a highly enriched crustal source. Symbols as in Figure 3.1.
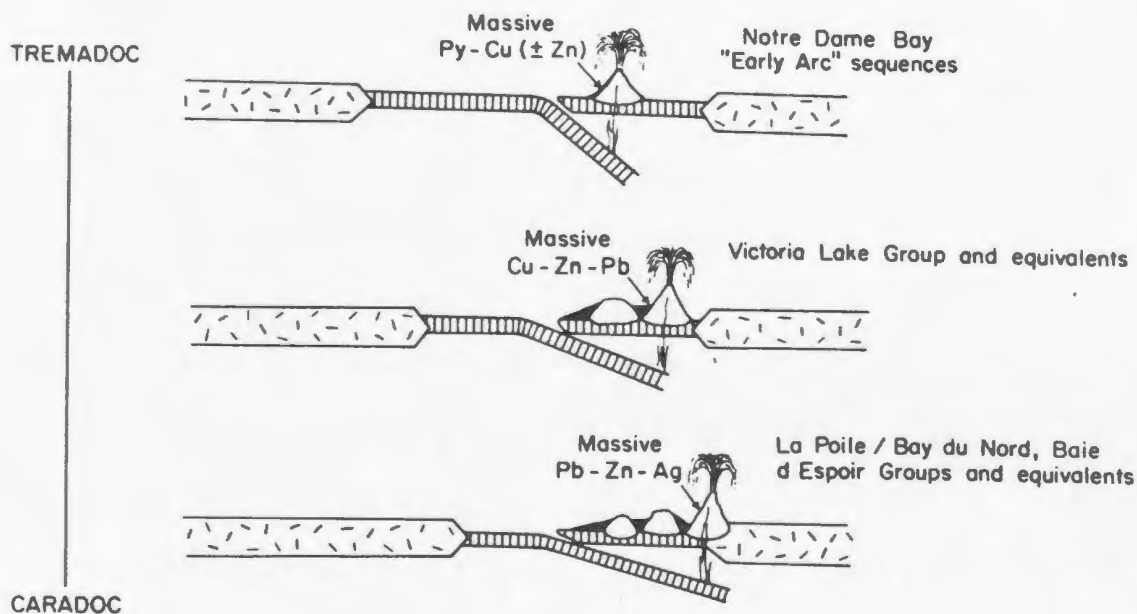
Figure 3.39. Schematic representation of diachronous
volcanism from the Tremadoc (initial volcanism in an oceanic
environment in the the Notre Dame Bay area) to the Caradoc
(volcanic sequences near the Hermitage Flexure near the
Avalon craton) within the Central Mobile Belt. This
illustrates that the Conaigre Bay Group volcanic rocks could
easily have been contaminated by possible underlying
continental crust. The diagram is taken from Swinden and
Thorpe (1984).

(1984) would probably represent a setting similar to that into which the Connaigre Bay Group was deposited.

Strong et al. (1978b) proposed that the Proterozoic rocks of the Burin Peninsula represent a sequence of continental bimodal volcanics which were rifted, resulting in the emplacement of oceanic tholeiites (Burin Group). This small ocean basin was then closed and bimodal volcanism returned (Marystown Group). The spatial (and temporal) closeness of the Connaigre Bay Group and the late Precambrian rocks of the Burin Peninsula suggest that the continental crust involved in the formation of the Burin Peninsula lithologies may have somehow been introduced into the island arc system, either as sediments or as melt fractions.

This then creates a problem of introducing continental material into an island arc setting. Wilson (1989) describes island arc environments as tectonically very complex, but theoretically island arc tholeiites should represent the products of the least complicated type of subduction-related magmatism; i.e. one in which no continental material is involved. Yet Wilson (1989) suggests that contamination may occur in two ways. The first, known as source contamination, occurs when subducted terriginous sediments are partially melted and lend their distinctive isotopic signature to the overlying wedge material. The second method, high level or crustal contamination, occurs when rising mantle-derived magmas incorporate sedimentary material which was intercalated

within the arc crust.

Tarney and Weaver (1987) suggest that the continental crust, as a whole, and of whatever age, is enriched in large ion lithophile (LIL) elements and has a distinct negative Nb anomaly. They state that it is very difficult to separate the effects of crustal contamination from those effects that may have been inherited from a mantle source which has gathered these characteristics through sediment subduction or contamination by subduction zone fluids.

Recent deep seismic studies undertaken across Newfoundland (Lithoprobe East Vibroseis, 1989) reveal that the Avalon Zone and the Gander Zone are separated by a near vertical fault (Dover - Hermitage Bay Fault system) which apparently extends through the crust to the mantle (Marillier et al., 1989). Marillier et al. (1989) also interpret that the Avalon Zone is floored by crustal (continental ?) material. This crustal material may somehow be involved in the island arc system, causing the above enrichments.

Swinden and Thorpe (1984) report on the style of volcanism and massive pyrite deposition in Early to Middle Ordovician island arc sequences within the Central Mobile Belt (Dunnage Zone). They state that sulphide deposits in proximity to the Hermitage Flexure have a more radiogenic lead isotope signature than those deposits in central and northern Newfoundland, suggesting crustal contamination within the subduction zone which was located at or near the Avalon craton

(Swinden and Thorpe, 1984). The lead isotope variations in the volcanic rocks may be explained as a diachronous event where there is initial island arc volcanism in the Tremadoc with subsequent migration of the volcanism toward a continental margin (Avalon craton) in the Caradoc (Figure 3.39), or volcanism occurred coevally from north to south within oceanic crust and at the Avalon margin (Swinden and Thorpe, 1984).

Lead isotope data from a galena separate from the Hermitage area ($^{208}Pb/^{204}Pb \approx 37.5$, $^{207}Pb/^{204}Pb \approx 15.54$, and $^{206}Pb/^{204}Pb \approx 17.81$; unpublished data from Noranda Exploration Co. Ltd.) is similar to values from deposits in the Eastern Townships, Quebec, but is less radiogenic than Pb isotope samples from massive sulphide deposits near the Hermitage Flexure (c.f. figure 10, Swinden and Thorpe, 1984). This suggests that the crustal contaminant within these deposits near the Hermitage Flexure is probably not Avalon Zone continental crust.

Pb isotope values from the Hermitage area plot on a trend defined by samples from the Ducktown District, Tennessee (c.f. figure 6, LeHuray, 1984). The Ducktown District deposits are within rocks that are apparently equivalent to Avalon Zone rocks, yet the thick sequences which host the deposits are generally thought to have formed in an intracratonic rift zone (LeHuray, 1984). It is possible that the Ducktown District and the Hermitage showings are a manifestation of similar hydrothermal processes originating from a homogeneous crustal

component at tectonically different areas.

CHAPTER 4

MINERALIZATION

4.1 Introduction

The bulk of the sulphide mineralization within the Connaigre Bay Group occurs through a limited stratigraphic thickness consisting of the felsic volcanic rocks of the uppermost Tickle Point Formation and the basal mafic tuffs with associated carbonates and cherts of the Sam Head Formation. The sulphide mineralization is stratabound. Outside of this interval there are a few minor occurrences of layered pyrite within the Tickle Point Formation. There are also numerous areas where quartz and/or carbonate veins contain small amounts of pyrite ± chalcopyrite, hematite, and barite, and cut all formations of the Connaigre Bay Group. For simplicity, the metallic mineralization in each formation (where applicable) will be described separately.

4.2 Connaigre Bay Group

4.2.1 Tickle Point Formation

4.2.1.1 Introduction

Many massive pyrite occurrences are known within the Tickle Point Formation but base-metal sulphides are only found at the Frenchman Head occurrence (Fig. 2.5, Appendix III). Due to the faulted stratigraphy within the Connaigre Bay Group,

determination of the general stratigraphic position of mineralized horizons can be difficult, but most mineralized zones occur near the apparent stratigraphic top of the Tickle Point Formation.

4.2.1.2 Frenchman Head

The Frenchman Head showing (Figure 4.1) was found in the early 1950's by personnel working for NALCO Ltd. and is now the property of Noranda Exploration Co. Ltd. The showing consists of three mineralized outcrops. These outcrops represent a single stratigraphic horizon, giving the discontinuous mineralized zone a strike length of at least 400 m with a width of between three and seven metres. The zone strikes approximately north-south at the northern extension and curves northeast-southwest at the southwest exposure, paralleling local stratigraphy. The mineralized horizon dips steeply to the east-southeast.

Mineralization at Frenchman Head is hosted in felsic volcanic rocks near a contact with an andesitic unit. In the vicinity of the mineralization, the felsic volcanic rocks are mainly recrystallized, occasionally spherulitic, flows and/or tuffs. The spherulites may be up to 0.5 cm in width and are filled with fine- to medium-grained quartz. Many of the spherulites are coated by a thin layer of fine-grained quartz. Between the spherulites is a very fine-grained dark matrix.

The non-spherulitic sections occur dominantly as large,
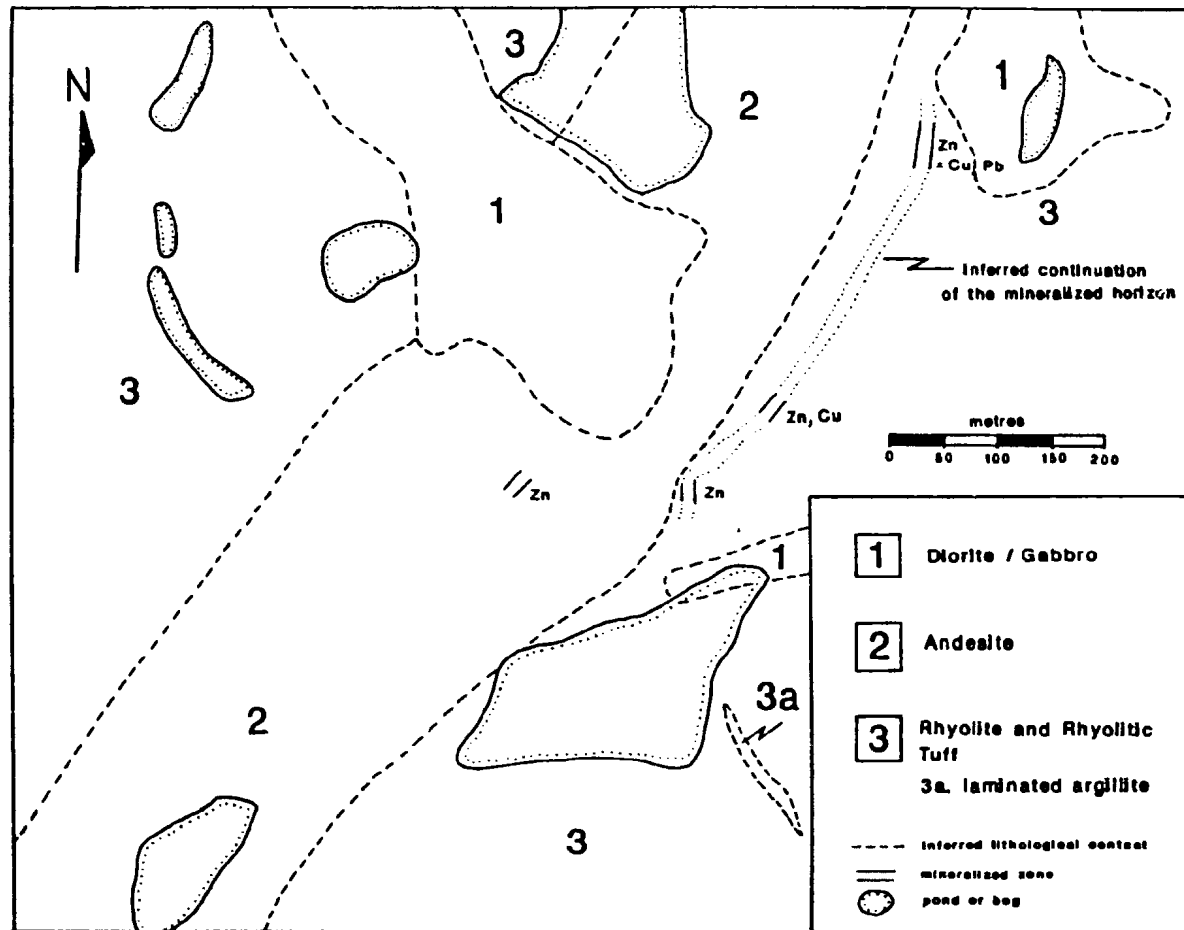
Figure 4.1. Geology of the Frenchman Head Showing.

composite, fine- to coarse-grained quartz grains with irregular boundaries displaying undulose extinction, indicating the rock was subject to strain. In the northeastern section of the zone, andalusite (Plate 4.1) and possible cordierite are present with the quartz indicating contact metamorphism.

The overlying andesitic rocks were not readily distinguishable from the underlying felsic tuffs and flows on an outcrop scale, but are separable by chemistry and the presence of zoned plagioclase (in the andesites), as viewed in thin section (Plate 4.2). The exact contact between the andesitic rocks and the felsic rocks around the mineralized zone is not known due to a thin interval of extensive carbonate ± chlorite alteration.

Rocks within this alteration zone react vigorously to HCl and are medium- to dark-green in color. Thin section analyses reveal the presence of relict spherulites (or possibly amygdules – Plate 4.3) composed mainly of fine-grained, dark impurities. The spherulites are slightly stretched with the long axis oriented parallel to the local stratigraphy. Carbonate and Ca-Mg-silicates are common matrix minerals between clusters of spherulites. The possibility of spherulites in this zone provides evidence that the rock mat have originally been a rhyolite or rhyolitic tuff.

The style of mineralization at Frenchman Head is dominantly stringer- and veinlet-type. Only a few thin (1-2
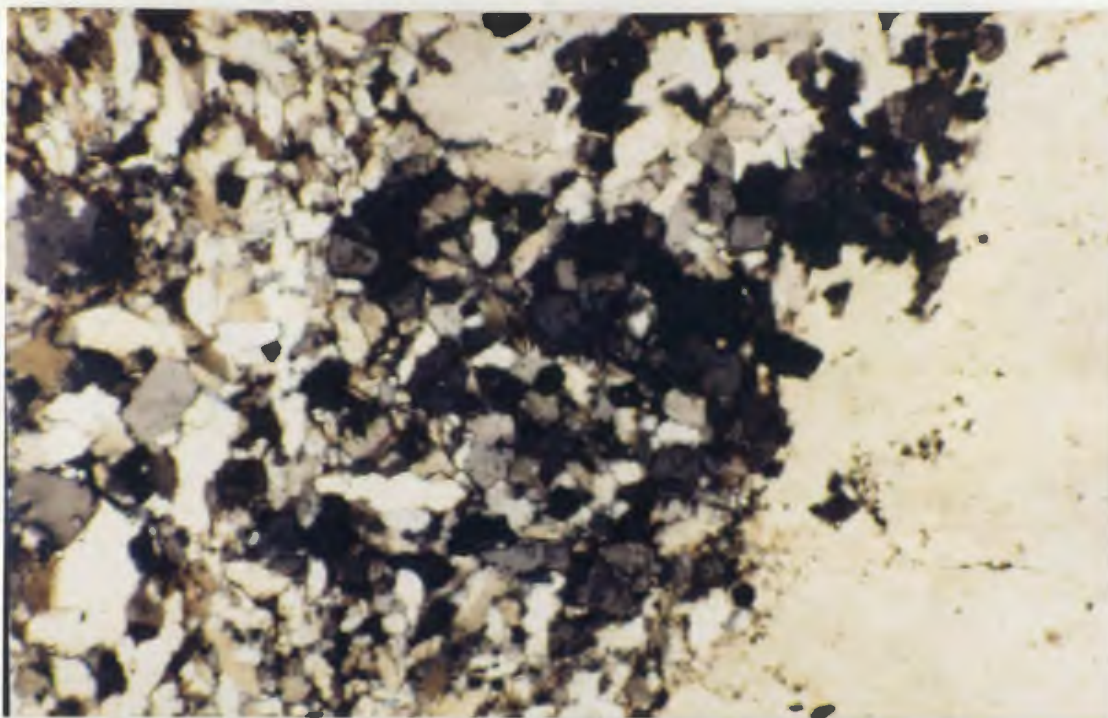
Plate 4.1. Small, dark gray, equant andalusite crystals (centre of photo) from a mineralized sample from Frenchman Head. Sample SS88-390 (584186), mag.= 32X, fov = 3.3 mm, X-nicols.

Plate 4.2. Oscillatory zoned plagioclase in andesitic rock from Frenchman head. Sample SS88-356 (584174), mag.= 22.5X, fov = 4.8 mm, X-nicols.
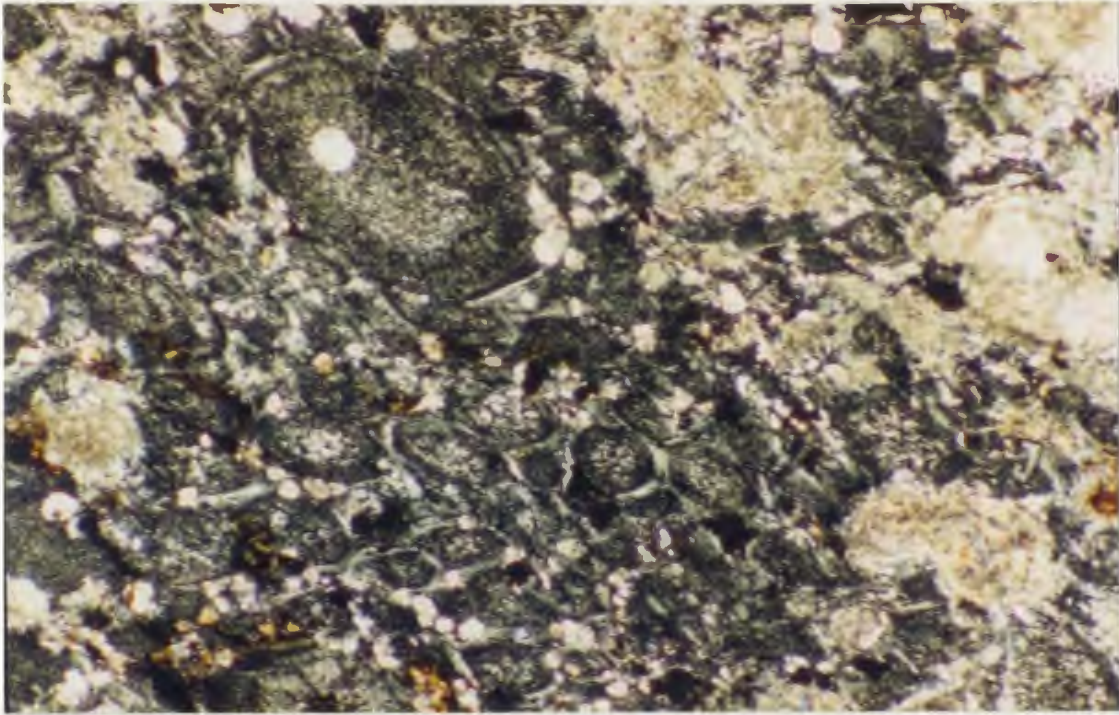
Plate 4.3. Relict spherulites (amygdules ?) in a carbonate-chlorite alteration zone at Frenchman Head. Sample SS88-407 (584193), mag.= 32X, fov = 3.3 mm, X-nicols.
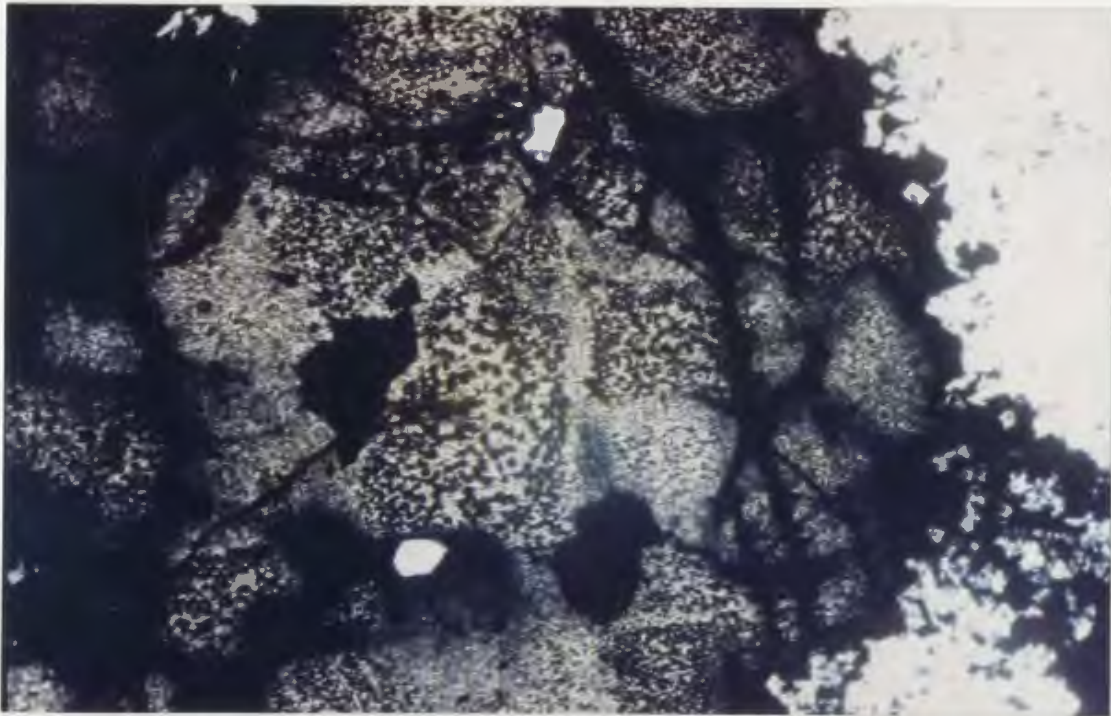
Plate 4.4. "Watermelon texture" consisting of dark, fine-grained chalcopyrite inclusions in a clear to light gray sphalerite crystal. sample SS88-414 (584196), mag.= 100X, fov = 1 mm, plane polarized light (PPL).

cm) discontinuous layers of sulphide (mostly pyrite) were found. The main stringer sulphide is pyrite, with lesser sphalerite, chalcopyrite, and rare galena.

Pyrite is subhedral to euhedral, commonly fractured and broken, and is frequently altered to hematite along fractures and crystal edges. Inclusions of sphalerite are common. Sphalerite is often filled with inclusions of chalcopyrite (Plate 4.4) in a style similar to Barton and Bethkes' (1987) "watermelon texture". This texture would indicate a solid-state replacement (due to rapid changes in the composition of the mineralizing fluid) of Fe-rich sphalerite by chalcopyrite, leaving Fe-poor sphalerite (Barton and Bethke, 1987). Very fine-grained chalcopyrite inclusions form elongate masses parallel to sphalerite crystal faces, similar to "orchard texture" also described by Barton and Bethke (1987) which also indicates a solid-state replacement process, or possible influx of Cu-rich fluid. Near the edges of the sphalerite crystals, where inclusions are rare, and in relatively inclusion-free crystals, the sphalerite ranges from colorless to greenish-yellow. Fe contents of these sphalerites are less than 1 wt.% (Table 4.1).

Chalcopyrite occurs as inclusions within sphalerite (as above) and rarely as free anhedral crystals. Galena was seen in only one slide as fine-grained crystals associated with sphalerite.

Along with the anomalous base-metal concentrations there

Table 4.1. Sphalerite compositions from Winter Hill and Frenchman Head.
PPL = plane polarized light.

LOCATION	SAMPLE NO.	COLOR (UNDER PPL)	WEIGHT % [ATOMIC %]				
			Zn	Fe	Cu	Mn	S
Winter Hill							
(lower zone)	5840016	dark orange-red	60.89	6.52	0.01	0.27	32.31
			[40.38]	[5.63]	[0.01]	[0.24]	[48.82]
	5840016	dark red	56.07	10.05	0.45	1.57	31.87
			[41.60]	[8.65]	[0.34]	[1.38]	[48.03]
(upper zone)	SS88-057	reddish-orange	57.69	8.89	0.31	1.24	31.88
			[42.88]	[7.67]	[0.23]	[1.09]	[48.13]
	5840042	dark red to black	58.02	9.60	0.16	1.25	30.97
			[43.39]	[8.34]	[0.12]	[1.10]	[47.05]
	5840042	dark red to black	56.34	10.21	0.09	1.26	32.10
			[41.74]	[8.78]	[0.07]	[1.11]	[48.30]
Frenchman Head	5840196	colorless	68.67	0.52	0.29	0.05	30.48
			[52.20]	[0.46]	[0.22]	[0.04]	[47.08]
	5840196	colorless	68.31	0.75	0.18	0.00	30.76
			[51.81]	[0.66]	[0.14]	[0.00]	[47.39]

are also anomalous Au values from the Frenchman Head showing. Background values within the Connaigre Bay Group are generally ≤5 ppb whereas the average Au content of the mineralized samples from Frenchman Head is 131 ppb with extremes of <5 and 350 ppb (Appendix III). The high Au values have corresponding anomalous Ag concentrations.

The Olive Cove showing (Noranda Exploration Co. Ltd.) is a small pyrite showing approximately 2.5 km east of Frenchman Head. This area is underlain by felsic volcanic rocks and minor tuffaceous sediments. The rocks here are variably silicified and chloritized. The felsic and tuffaceous rocks contain 1-3% disseminated pyrite but no base-metal sulphides. The mafic rocks also contain up to 2% pyrite and traces of chalcopyrite.

Complicating the geology are numerous mafic dykes and sills, some of which may actually be extrusive rocks.

4.2.1.3 Shoal Brook

The Shoal Brook showing (Figure 4.2) (Graves, 1986b) is located near a fault contact between the Tickle Point Formation and the Sam Head Formation. The showing consists of massive pyrite layers associated with felsic and intermediate tuffs and/or flows and minor mafic tuff with interbedded red and green argillite.

The intermediate to felsic rocks contain variable amounts of crystal and lithic fragments in a fine-grained quartz and
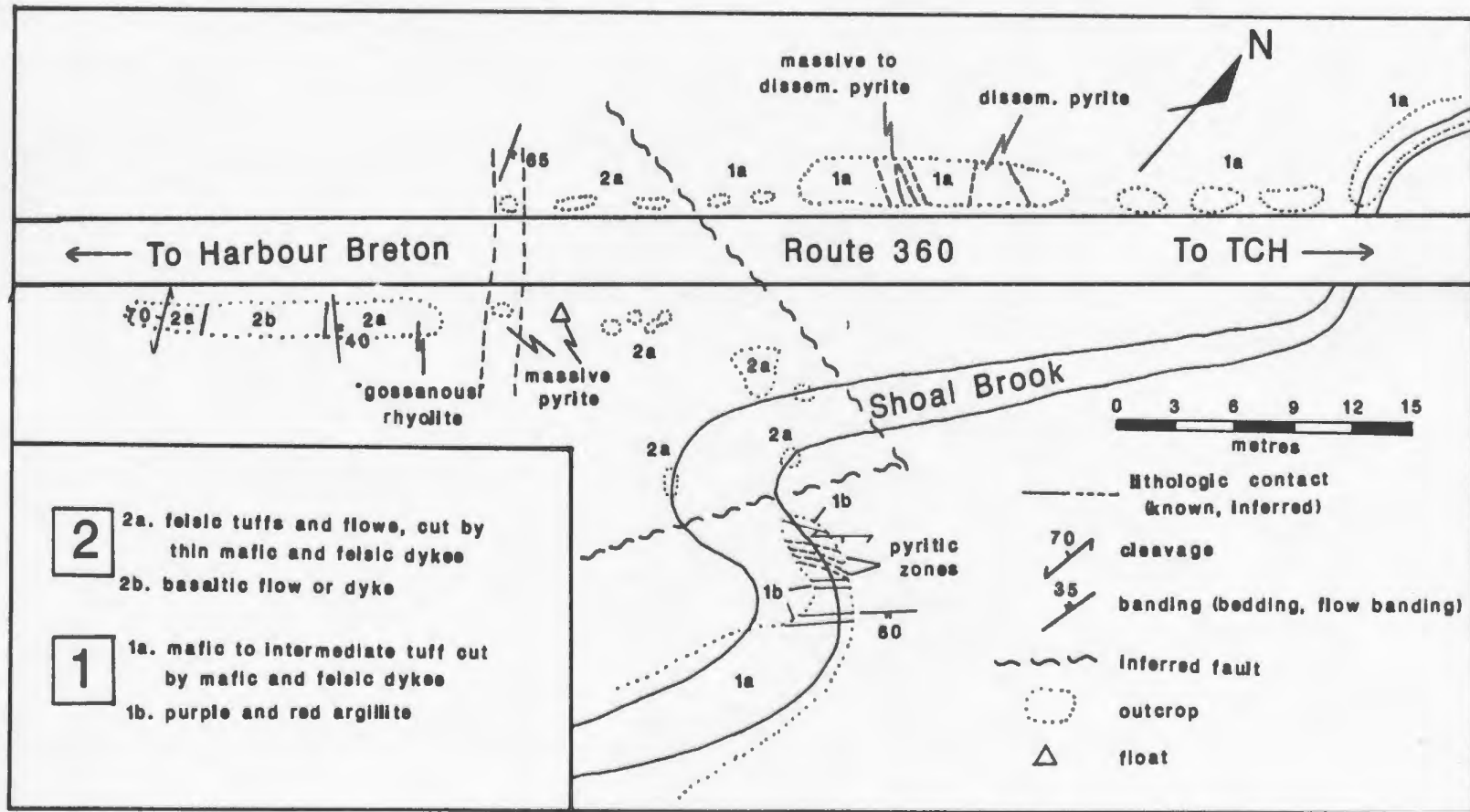
Figure 4.2. Detailed geology of the Shoal Brook Showing.

feldspar matrix. The crystals are anhedral to subhedral fragments of K-spar, quartz, and plagioclase with rare pyroxene crystals. The lithic fragments consist of small plagioclase laths in a glassy groundmass. Visually, the fragments are very similar to the matrix surrounding them.

The mafic rocks are chloritized and epidotized equivalents of the more felsic rocks. The argillites are very fine-grained, chloritized, and dominantly mafic in composition.

Sulphide mineralization consists of semi-massive to massive layered pyrite with no associated base-metal sulphides. Layering is defined in two ways: thin (2-5 mm) massive pyrite layers separated by thin (3-8 mm) layers of disseminated pyrite and; pyritic layers having a coarse massive base with pyrite becoming disseminated and finer grained toward the top. Pyrite is occasionally altered to hematite.

Directly underneath the massive pyrite is a rubbly, bleached zone. No sulphides occur in this two to three metre wide zone that appears to be conformable with the underlying rhyolite.

4.2.1.4 Selco Showings

The Selco showings (Figure 4.3) consist of massive, layered pyrite lenses located within fine-grained siliceous rocks near the head of Northeast Arm (Harbour Breton). Three
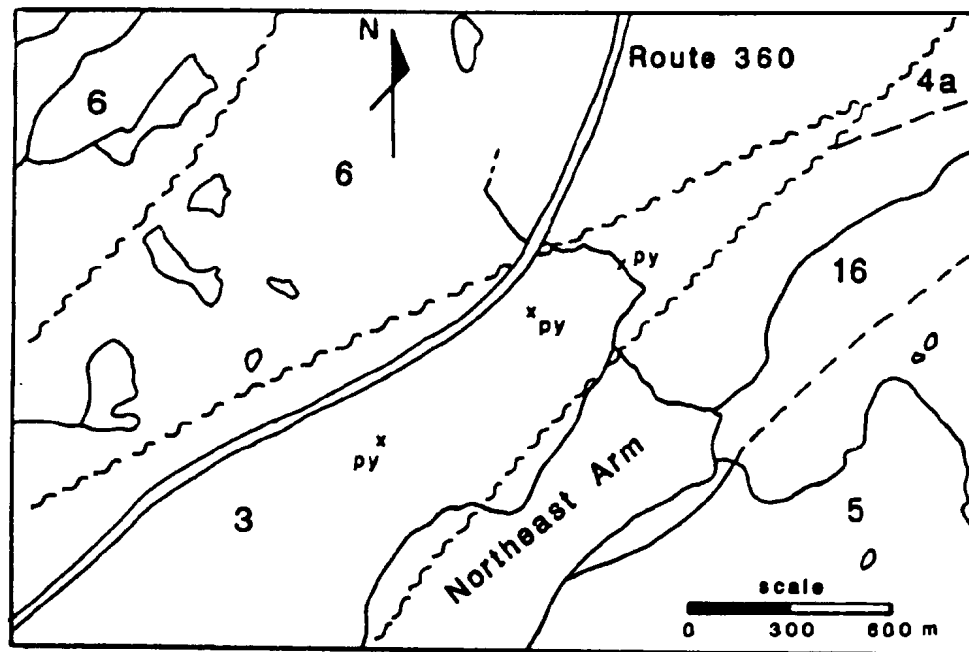
Figure 4.3. Location of the three massive pyrite outcrops constituting the Selco Showings. The map is redrawn from MacKenzie (1984) with geology from Greene and O'Driscoll (1976). The numbered lithological units are the same as in Figure 2.5. (Unit 4a = argillite)

pyrite outcrops are located over a length of approximately one kilometre. Due to the proximity to a faulted contact with other Connaigre Bay Group rocks, it is difficult to determine whether the lenses represent a single horizon or multiple en echelon lenses. Strike directions for the pyrite layers range from 090°N at the most southern outcrop, to 010°N at the middle exposure, to 050°N at the northern outcrop. The southern outcrop contains significant magnetite so the strike measurement may be inaccurate.

The strike directions of the layered pyrite may indicate an en echelon orientation whereas the local geology at each exposure suggests that they may be just one continuous or discontinuous unit. All three locations contain a sequence of layered massive pyrite (up to five metres thick) underlain by variably chloritized felsic rocks intruded by mafic dykes. The mineralization is overlain by thinly laminated to massive felsic tuff and/or chert.

The overlying fine-grained felsic rocks are composed of variable amounts of quartz, sericite, and plagioclase. The mineral assemblage is very fine to fine-grained and is often cut by thin quartz/carbonate veinlets.

The pyrite lenses contain no other opaque minerals except for the most southern outcrop where approximately 30-40% of the opaques are magnetite. The pyrite is layered, subhedral to euhedral, and fine grained. Occasionally stringers of slightly coarser grained pyrite cut the bedded pyrite. Magnetite occurs

as layers of bladed crystals intercalated with pyrite layers (Plate 4.5).

The gangue mineralogy within the massive pyrite layers consists of chlorite and quartz.

4.2.2 Sam Head Formation

4.2.2.1 Introduction

The Sam Head Formation at Winter Hill is host to the most abundant base-metal mineralization within the Connaigre Bay Group (see Appendix III). The mineralization is concentrated at one main showing, Winter Hill, with three smaller satellite occurrences, Winter Hill West, Winter Hill East, and Winter Hill North, containing the remainder of the mineralization. All showings were found and named by Noranda Exploration Co. Ltd. personnel in the mid-1980's (Graves, 1985 and 1986a).

The Winter Hill, Winter Hill West, and Winter Hill East occurrences lie within the relative stratigraphic horizon over approximately three km of strike length (Figure 2.5). Paralleling this strike direction is a fault which is the boundary between the Sam Head Formation and an elongate lens of the Simmons Brook Batholith. Winter Hill North is situated almost 500 m north from Winter Hill East and is 200-250 m higher in the stratigraphic column.

4.2.2.2 Winter Hill

The Winter Hill showing (Figure 4.4 and Plate 4.6)

Plate 4.5. Alternating layers of pyrite (whitish) and magnetite (dark gray) from the Selco Showings. Sample SS88-141 (584086), mag.= 32X, fov = 3.3 mm, reflected light.

Plate 4.6. Photo of Winter Hill with the Winter Hill Showing outlined (as in map - Figure 4.4). Large boulders at the base of the scree slope are 5-6 feet in height.
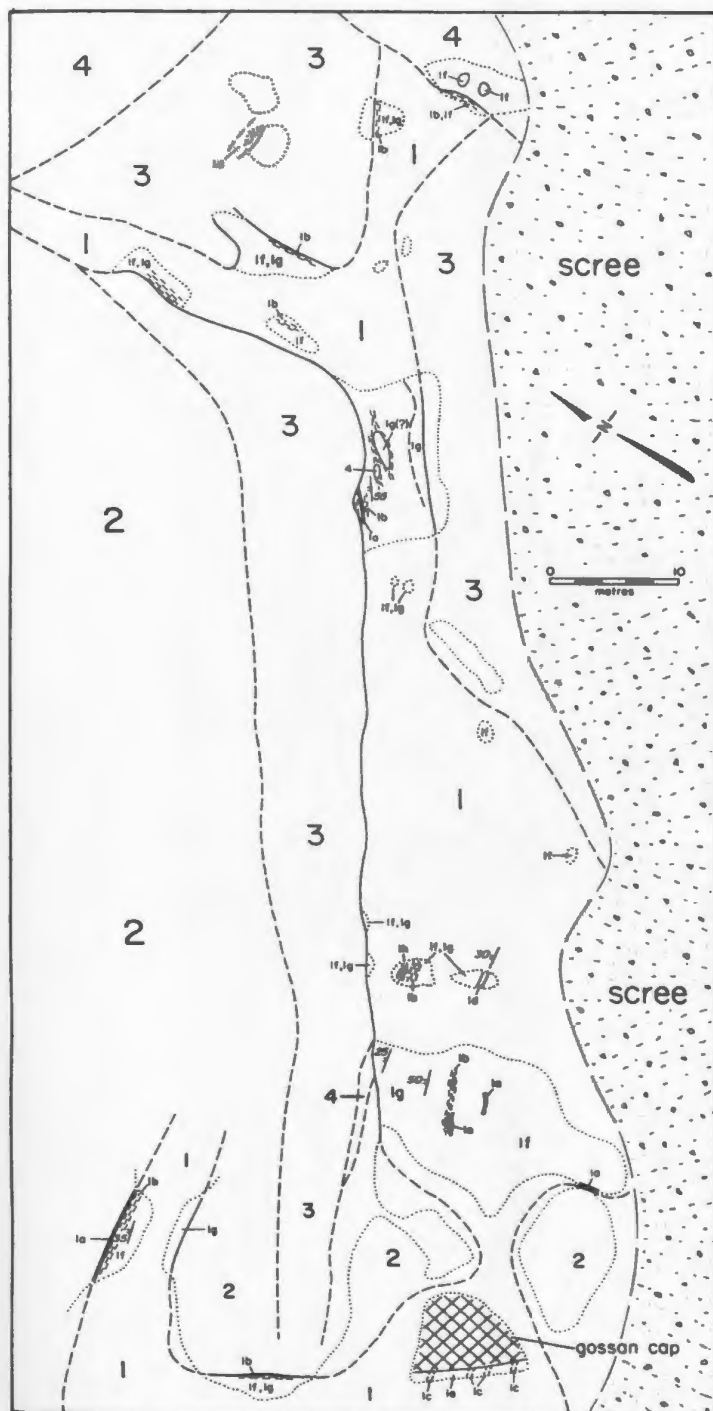
LEGEND

ORDOVICIAN OR OLDER

Hermitage Bay Complex

4 MAFIC DYKES/SILLS

3 FELSIC DYKES/SILLS

LATE PRECAMBRIAN

Sam Head Formation (Connaigre Bay Group)

2 MAFIC TUFF

1 CARBONATE/CALC-SILICATE LENS

    1a semi-massive to massive sphalerite

    1b thin sphalerite bands

    1c semi-massive to massive pyrite (± cpy, po, gn, sph)

    1d semi-massive to massive banded sulphides

    1e semi-massive to disseminated pyrite

    1f carbonate/marble

    1g calc-silicate

    1h breccia

Symbols

Geological boundary (known, approximate)..

Major outcrops...

Sulphide/Carbonate banding.........................

Figure 4.4. Detailed Geology of the Winter Hill Showing. Taken from Sears and O'Driscoll (1989).

contains pyrite, sphalerite, chalcopyrite, and galena mineralization (in decreasing order of abundance) hosted by a carbonate/Ca-Mg-silicate lens near the contact between the Tickle Point and the Sam Head Formations. On surface, the mineralized zone is approximately 120 m in length and ranges between 5 and 15 m in thickness (Figure 4.4). At an average dip of 40°, the true thickness of the zone would be 3 to 9 metres. Data from 4 diamond drill holes (Graves, 1985) indicate that the zone extends down dip at least 250 metres, while still maintaining its thickness but losing overall metal contents. Drill hole data also suggest that the zone either bifurcates near its apparent margins, or there is more than one mineralized horizon (Figure 4.5).

Footwall lithologies are only partially visible on the surface. The western edge of the mineralized zone is underlain by mafic tuffs, whereas the eastern portion is bounded by a felsic dyke. Drill hole data (Graves, 1985) indicate that the zone is underlain chiefly by fragmented felsic and silicified rocks with lesser mafic tuffs and flows (Figure 4.5). The structural hanging wall is dominated by mafic tuffs but the exposed upper contact is occupied by a felsic dyke similar to the dyke bounding the underside of the zone. The long dimension of the lens is open at the southwest end and is cut off by mafic dykes at the northeast end.

The Winter Hill showing can be divided into two subzones based upon base-metal contents and mineralogy: a structurally
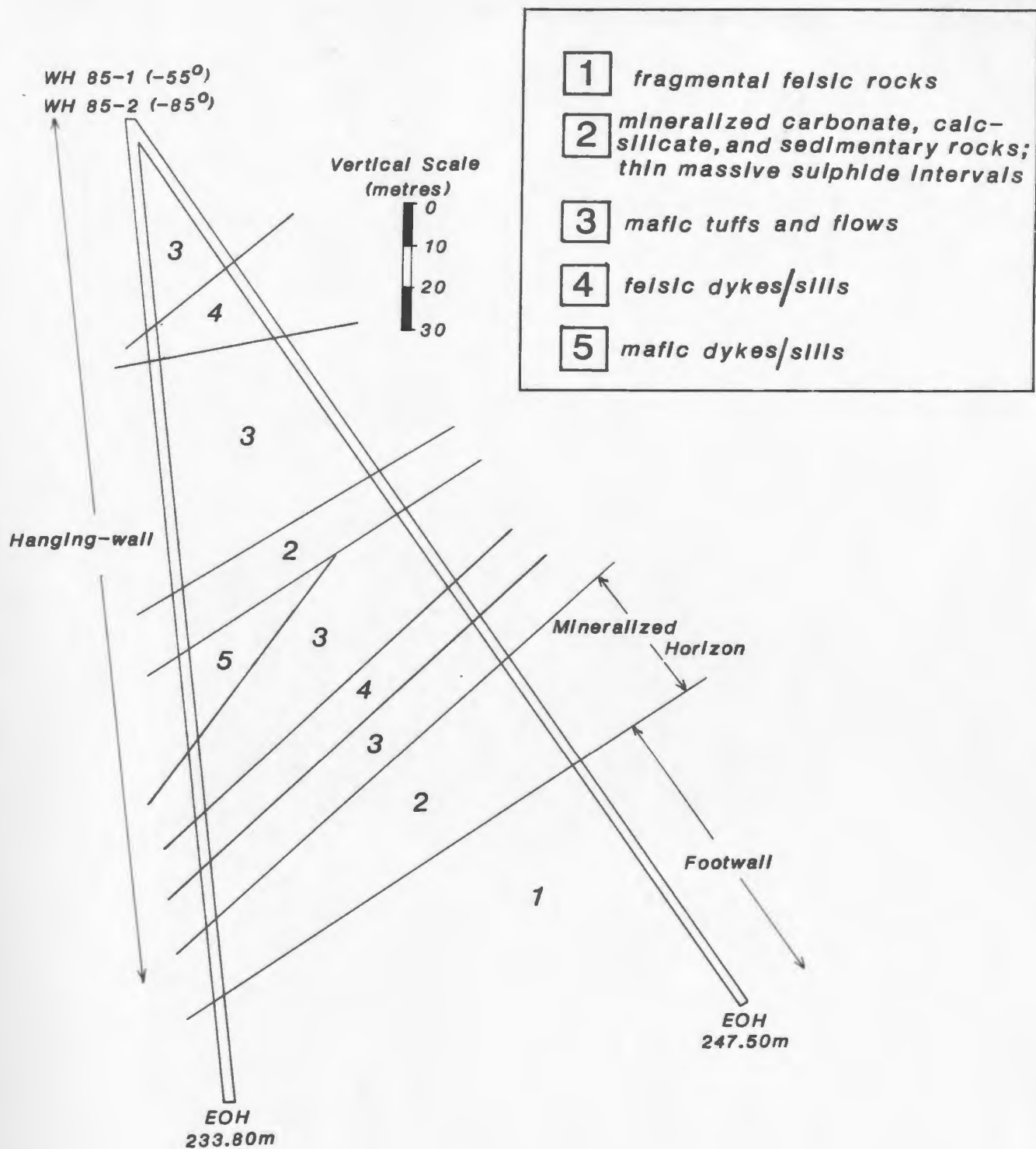
Figure 4.5. Gross stratigraphic correlation from diamond drill hole data from the Winter Hill Showing.
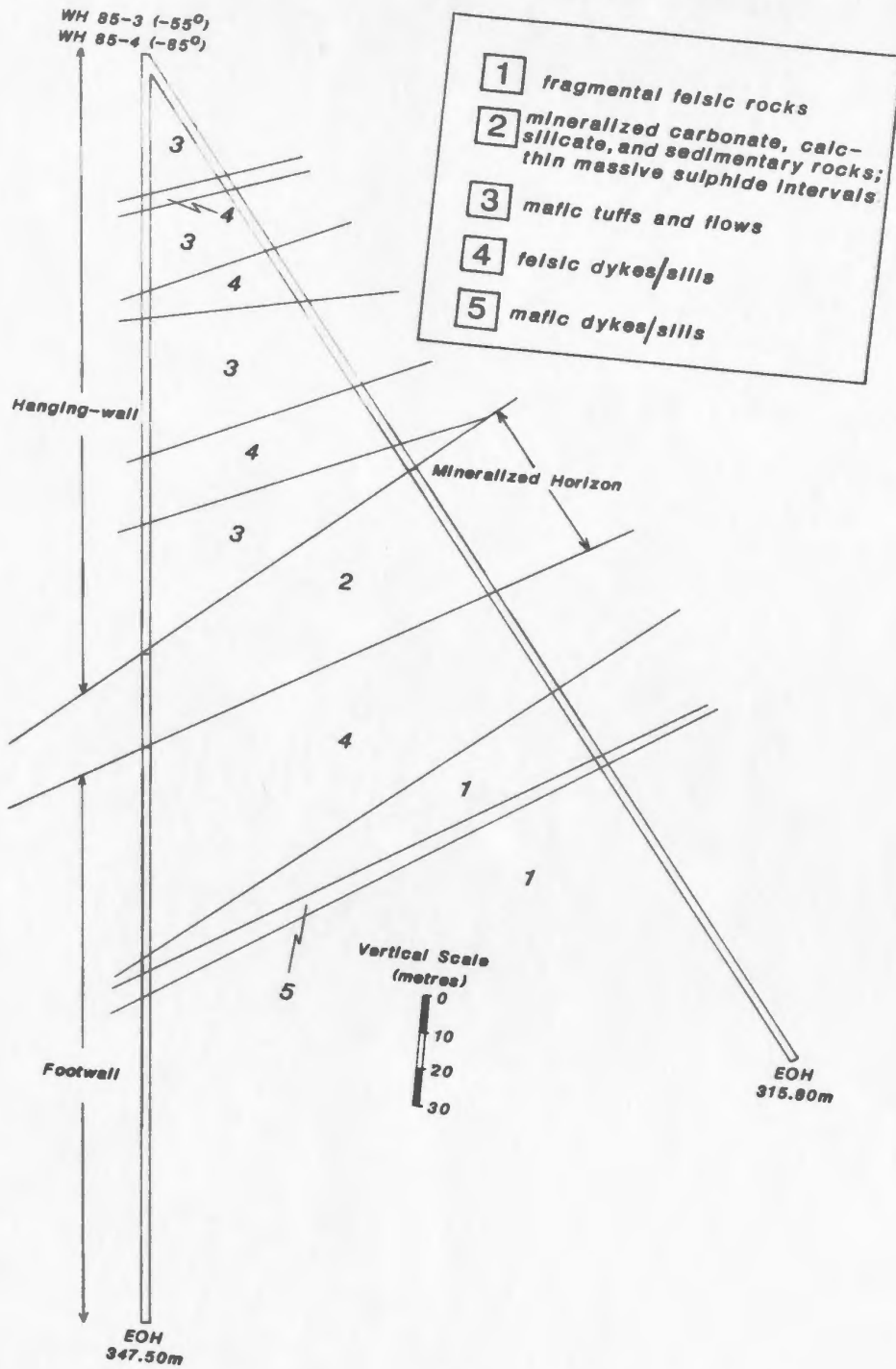
Figure 4.5. (continued)

(and presumably stratigraphically) lower Cu-rich zone and an upper Zn- + Pb-rich zone.

The lower zone consists primarily of thin ($\leq$ 0.5 m) lenses of massive pyrite separated by areas of disseminated and stringer pyrite and chalcopyrite ($\pm$ sphalerite) in a fine-grained quartz gangue (Plate 4.7). This zone is irregular in shape, approximately 10 m wide on surface at the lowest southwest exposure, pinching uphill to the northeast where the zone is roughly three metres wide (see Figure 4.4). The whole zone is capped by a weathered cover (gossan) up to 0.5 to 1 m thick.

Opaque mineralogy of the lower zone is dominated by pyrite with minor amounts of chalcopyrite and minor to trace abundances of sphalerite and pyrrhotite. Quartz is the most prominent gangue mineral with lesser cordierite, biotite, sericite, chlorite, and trace amounts of andalusite and Ca-Mg-silicates.

Pyrite occurs as fine- to coarse-grained, subhedral to euhedral crystals that frequently contain rounded inclusions of chalcopyrite and pyrrhotite (Plate 4.8). Some pyrite displays primary features such as colloform banding whereas other pyrite aggregates in stringers have an interlocking granular texture, possibly indicative of remobilization and/or recrystallization. Near the top of the lower zone, where sphalerite abundances increase, many pyrite crystals have semi-dendritic, fracture or breccia patterns (Plate 4.9). This

Plate 4.7. Thin lenses of massive pyrite (e.g. under small hammer handle) separated by intervals of disseminated pyrite in a siliceous host.
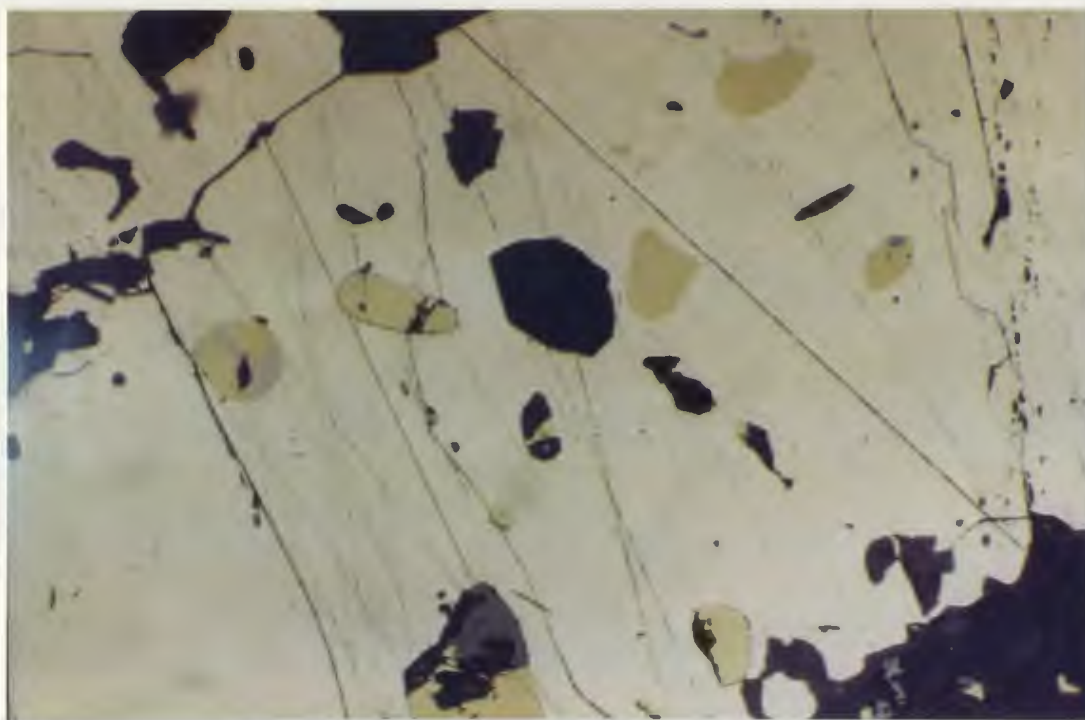
Plate 4.8. Large pyrite crystals with rounded inclusions of chalcopyrite (yellow) and pyrrhotite (light gray to light brown). Sample SS88-032 (584013), mag.= 200X, fov = 0.5 mm, reflected light.
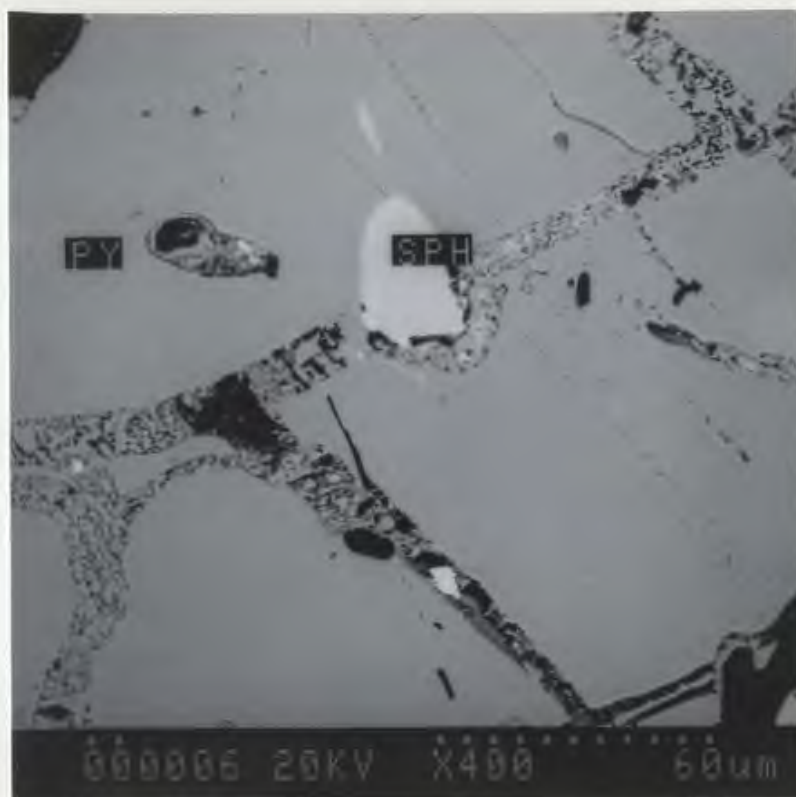
Plate 4.9. Scanning electron microscope (SEM) back scatter photograph of brecciated channels within pyrite grains. PY = pyrite, SPH = sphalerite. Sample SS88-039 (584016), mag.= 400X.
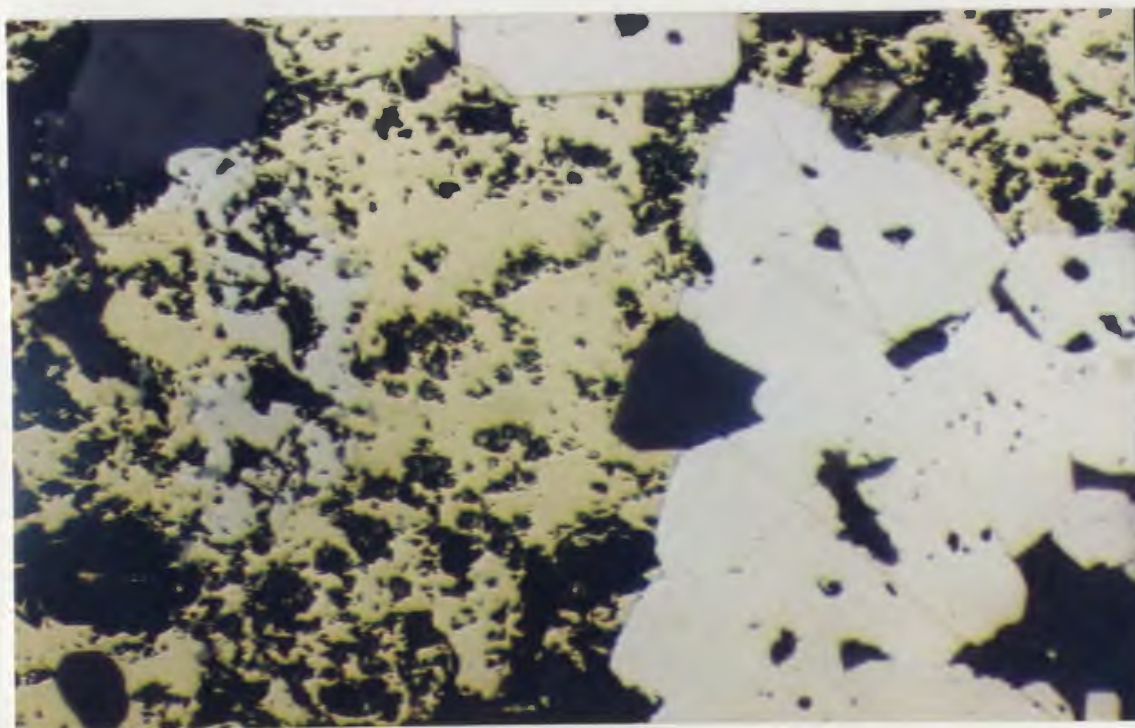
Plate 4.10. Crystals of chalcopyrite (yellow) associated with pyrite (white) in thin stringers from the lower zone at Winter Hill. Sample SS88-512, mag.= 100X, fov = 1 mm, reflected light.

fracture pattern is often difficult to follow into the surrounding gangue.

Chalcopyrite is present either as anhedral crystals associated with pyrite (Plate 4.10), typically as stringer mineralization, or as inclusions within pyrite grains. Towards the top of the zone, chalcopyrite increases in abundance and is often associated with sphalerite, i.e. it contains inclusions of sphalerite or it rims sphalerite crystals (Plate 4.11). Also in this zone, sphalerite often has inclusions of chalcopyrite.

Near the transition between the lower and upper zones, sphalerite constitutes approximately 50% of the opaques with pyrite and chalcopyrite making up the remainder. Under plane polarized light the sphalerite is deep red in color and is Fe-rich, ranging between 6.5 to 10.0 wt.% (Plate 4.12 and Table 4.1). Prominent malachite and smithsonite staining occur on the weathered surfaces in this area.

Pyrrhotite occurs generally as small subrounded inclusions within pyrite but infrequently is present as discrete grains. Rare hematite and/or magnetite are present as thin stringers, probably resulting from oxidization of pyrite stringers.

Fine- to medium-grained granular quartz is the most common gangue mineral (Plate 4.13). It occurs as interlocking polygonal crystals, which resulted from either the recrystallization of previous larger quartz crystals, or they
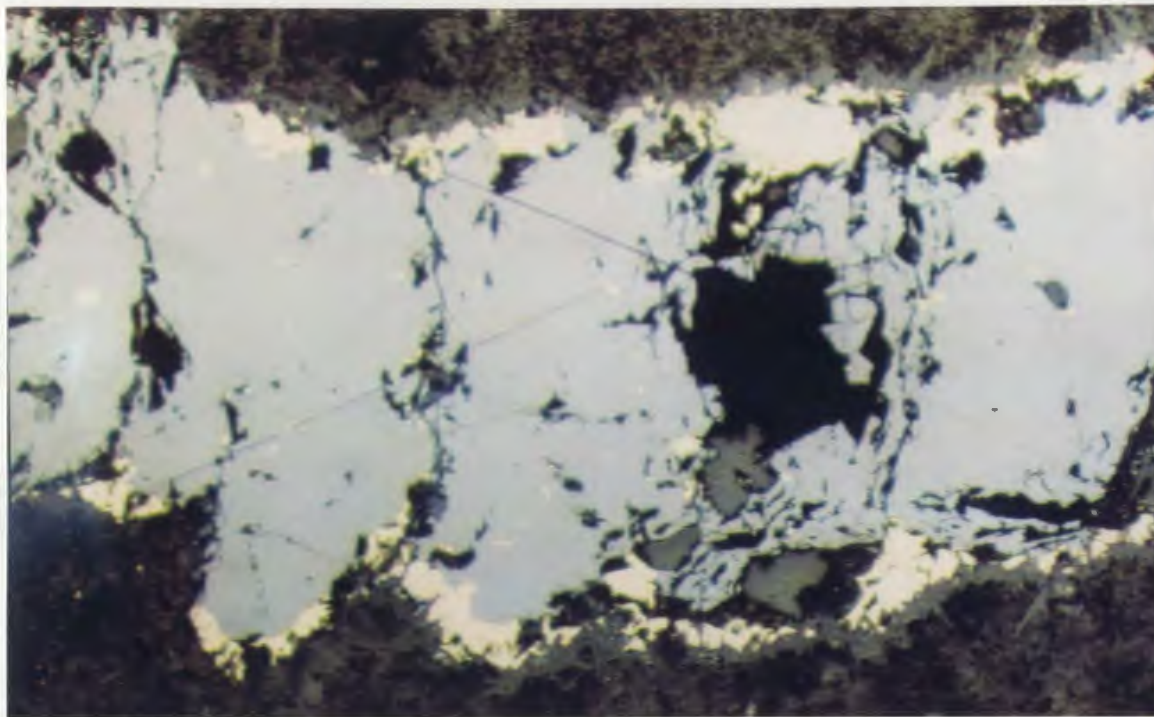
Plate 4.11. Large sphalerite crystal (gray) rimmed by chalcopyrite (whitish-yellow) near the lower zone – upper zone transition at Winter Hill. Sample SS88-039 (584016), mag.= 32X, fov = 3.3 mm, reflected light.
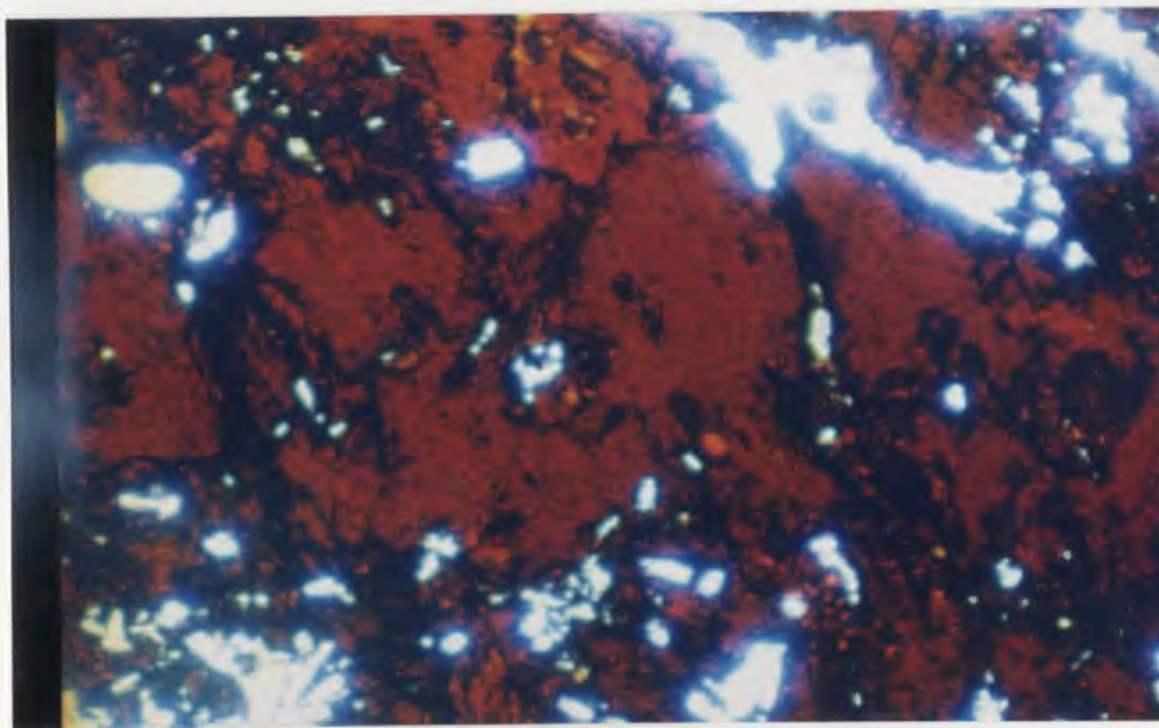
Plate 4.12. Fe-rich sphalerite from the upper zone at the Winter Hill Showing. Sample SS88-057, mag.= 32X, fov = 3.3 mm, PPL.
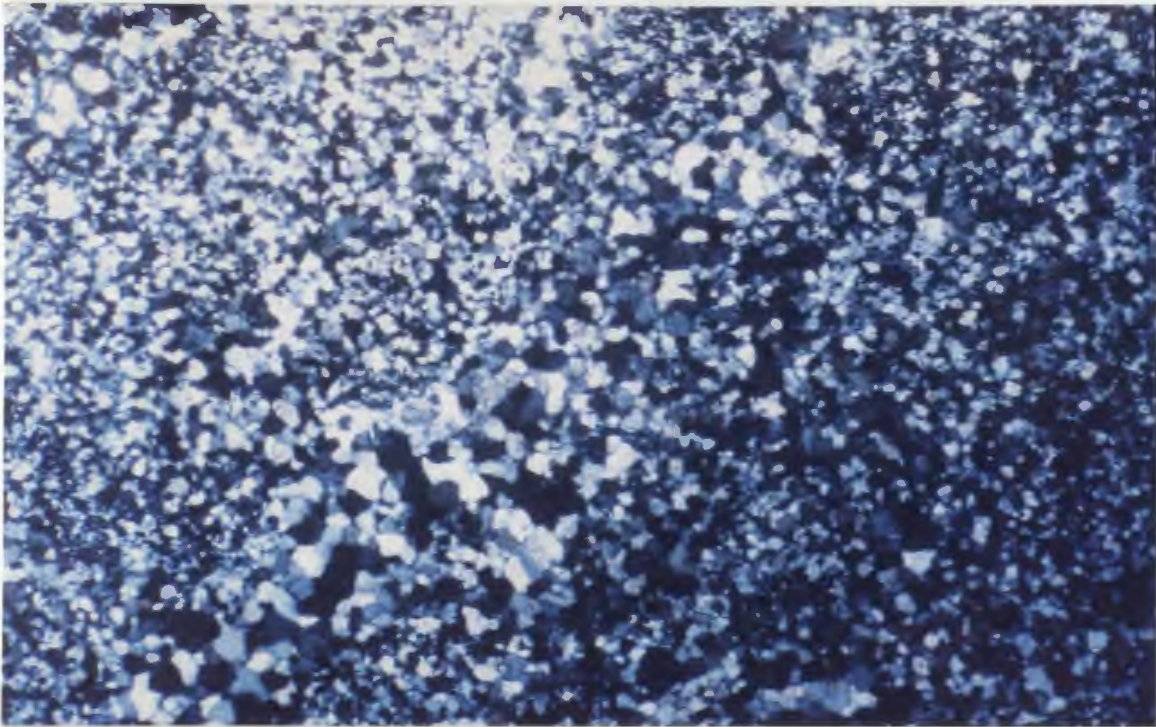
Plate 4.13. Fine-grained recrystallized quartz from the lower zone at the Winter Hill Showing. Sample SS88-103 (584066), mag.= 100X, fov = 1 mm, X-nicols.
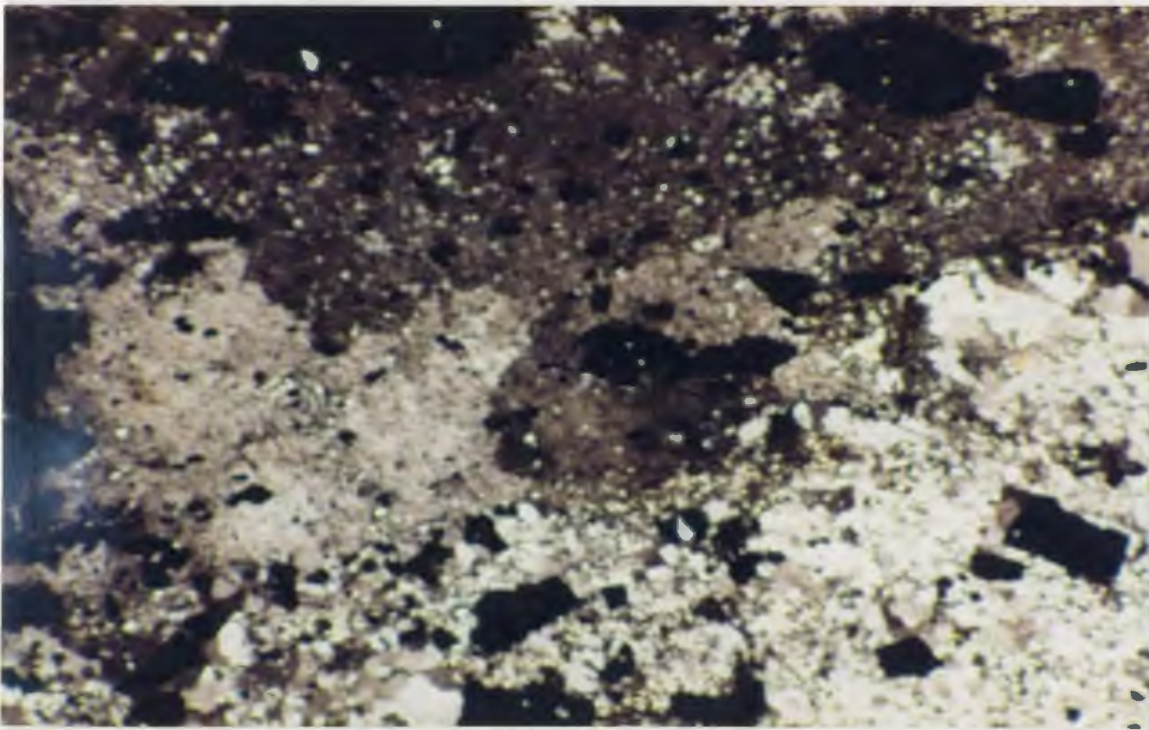
Plate 4.14. Cordierite (light gray to dark brown – near extinction) associated with fine-grained quartz (whitish, small, polygonal crystals). Sample SS88-037, mag.= 32X, fov = 3.3 mm, X-nicols.

crystallized from the mineralizing solutions. Associated with the quartz are cordierite, biotite and rare andalusite. In some sections cordierite may be half as abundant as quartz whereas biotite is uncommon. Cordierite occurs as large crystals displaying a wavy extinction pattern commonly containing small quartz inclusions (Plate 4.14). There is also one instance where a cordierite crystal is crudely sector zoned (i.e. a concentration of one or more components (e.g. MgO, Al_2O_3, etc...) along opposite crystal faces (Barker, 1983)). Minor sericite is present with cordierite and sometimes partially alters cordierite. Only one small mass of aluminosilicate (i.e. andalusite) has been identified and it is associated with cordierite. One section contains crudely aligned sericite which parallels the direction of the stringer mineralization. Chlorite and Ca-Mg-silicates (diopside ± tremolite) are present but not abundantly.

The Zn-rich upper zone can be divided into several discontinuous facies. Because of the thinness (3-7 m) of the upper zone and the discontinuous nature of the facies within the zone, the stratigraphic locations of separate facies are sometimes unclear as some facies may be vertically and/or laterally conformable.

The apparent basal facies is a chaoticly banded, impure dolomite marble with lesser calcite and ferroan dolomite marble (Plate 4.15). In an alteration zone along the lower contact with the mafic tuffs, fractured olivine crystals

Plate 4.15. Contorted banding in the carbonate unit (subunit 1f) at the Winter Hill Showing.
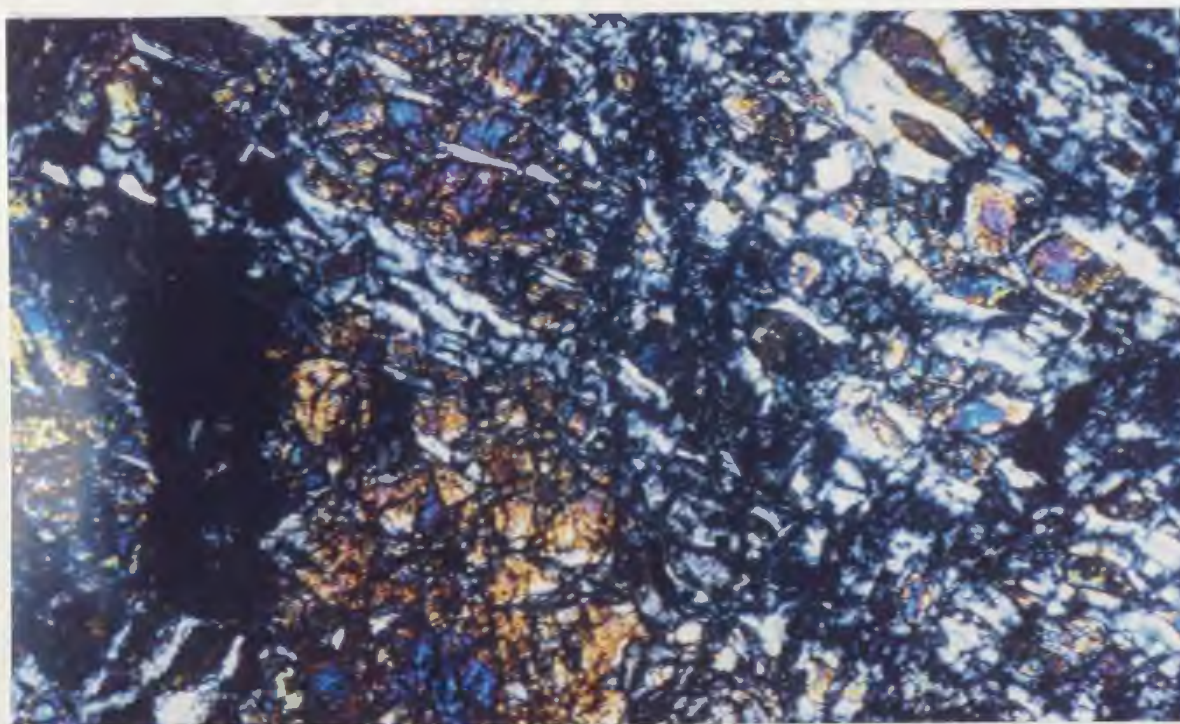
Plate 4.16. Serpentinized olivines in an alteration zone at the base of the carbonate/calc-silicate lens at Winter Hill. Sample SS88-048 (584024), mag.= 100X, fov = 1 mm, X-nicols.

(serpentinized) are common (Plate 4.16) along with lesser talc and possible magnesite. This alteration assemblage grades up into the marble unit. The marbles contain mainly small, equigranular, twinned and untwinned carbonate crystals. There are local concentrations of Ca-Mg-silicates (tremolite and diopside), serpentine, brucite, quartz, epidote, and possible fine-grained feldspar.

Ca-Mg-silicates dominate the mineralogy above the carbonate unit. Tremolite and diopside are the main minerals with minor local amounts of epidote. Quartz, talc, and carbonate are present as primary minerals whereas chlorite is an alteration product. Plagioclase and rutile are rare.

The Ca-Mg-silicates commonly occur either as masses of feathery, fine-grained, lath-like crystals (tremolite) or as fine grained subhedral crystals (diopside). They sometimes display layering with local concentrations of carbonate, or they may be layered due to changes in crystal size (Plate 4.17).

Discontinuous mineralized horizons occur above the Ca-Mg-silicate horizon. The horizons consist of lightly disseminated to massive layered sphalerite, pyrrhotite, pyrite, galena, and rare chalcopyrite (Plate 4.18 and 4.19). This mineralized package is approximately two to five metres thick and contains a discontinuous carbonate breccia horizon (Plate 4.20). The upper contact with the hanging is sharp.

Both disseminated and massive sulphides are almost

Plate 4.17. Layering in tremolite due to changes in crystal size. From the calc-silicate horizon (subunit 1g) at Winter Hill. Sample SS88-072 (584044), mag.= 20X, X-nicols.

Plate 4.18. Layered massive sphalerite (subunit 1a) from the Winter Hill Showing.
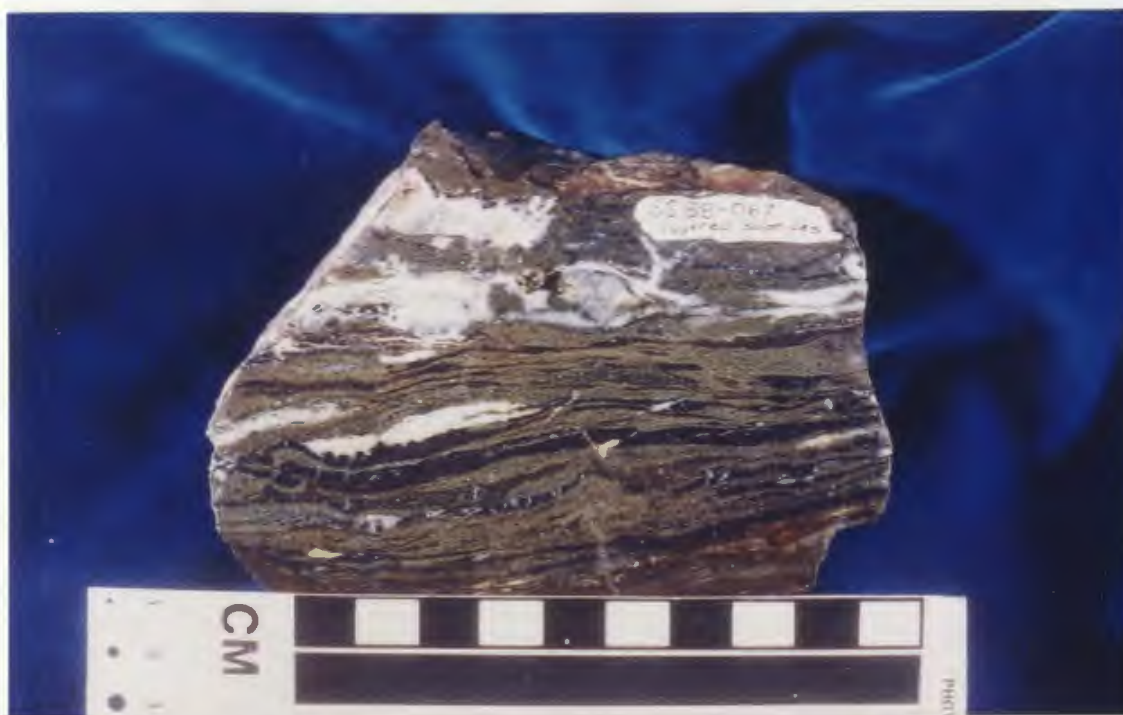
Plate 4.19. Layered pyrite (yellow-brown), sphalerite (dark brown), and lesser galena (bluish gray - below sample caption) with a quartz-carbonate gangue from the Winter Hill Showing. Sample SS88-067.

Plate 4.20. Discontinuous carbonate breccia horizon (subunit 1h) from the Winter Hill Showing.

ubiquitously anhedral and intimately (i.e. syngenetic) intergrown with the gangue mineralogy. Pyrite occurs occasionally as euhedral cubes usually in disseminated form.

Overall, sphalerite is the coarsest-grained sulphide sometimes up to five to seven mm in length (see Plate 4.12). It can occur as inclusion-free crystals in apparent equilibrium with the surrounding sulphides but it more frequently contains inclusions of one or more of the other sulphides and/or gangue minerals. The inclusions are generally rounded blebs that are monomineralic or a composite of two or more sulphides (i.e. pyrrhotite and chalcopyrite). Some chalcopyrite inclusions are exceptions to this as they occur mainly as elongate crystals parallel to the crystal boundaries of the sphalerite (Plate 4.21), similar to the "orchard texture" of Barton and Bethke (1987). This configuration of chalcopyrite in sphalerite may either be a replacement texture (Barton and Bethke, 1987; Sugaki et al., 1987) or the saturation of chalcopyrite along growing sphalerite crystal boundaries. Sphalerite, under plane polarized light, ranges from orange-red to black in color which reflects an increase in the wt.% Fe in the sphalerite (Table 4.1).

Galena is the next most common ore sulphide and occurs mostly with sphalerite and pyrrhotite (Plate 4.22). Galena is fine-grained, anhedral, and in all instances appears to be in equilibrium with the other sulphides although its association with pyrite is much less common than its association with
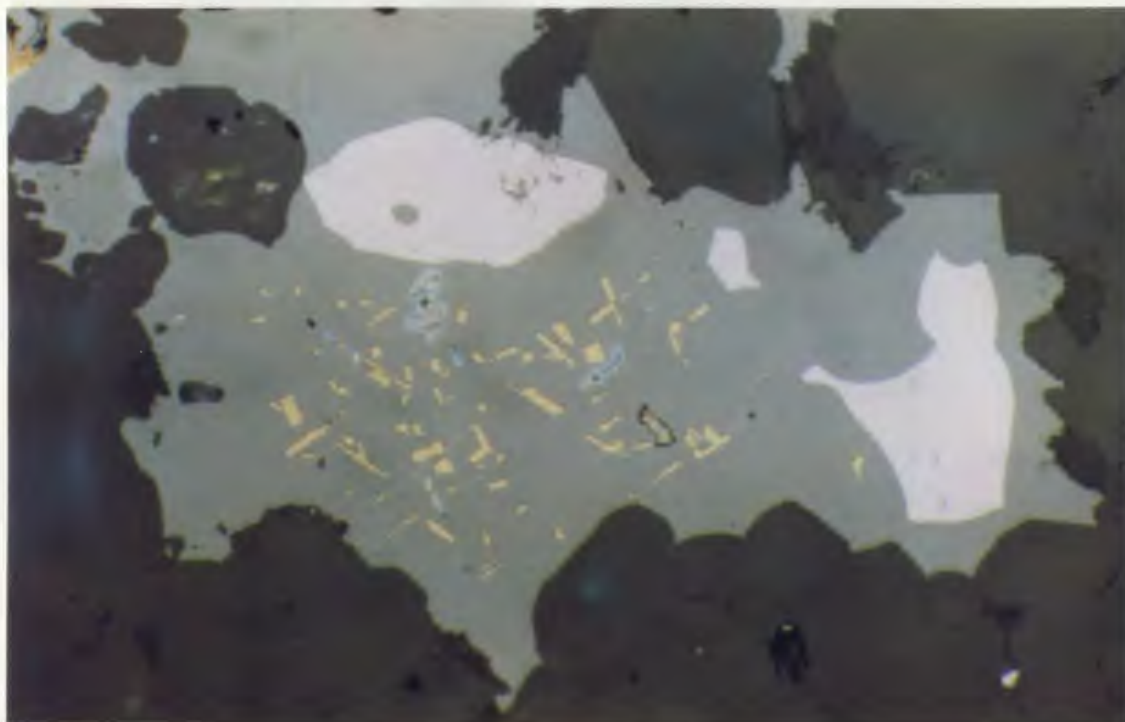
Plate 4.21. Elongate chalcopyrite crystals (yellow) along crystal boundaries in sphalerite (medium to dark gray). White crystals are galena. Sample SS88-101 (584065), mag.= 200X, fov = 0.5 mm, reflected light.
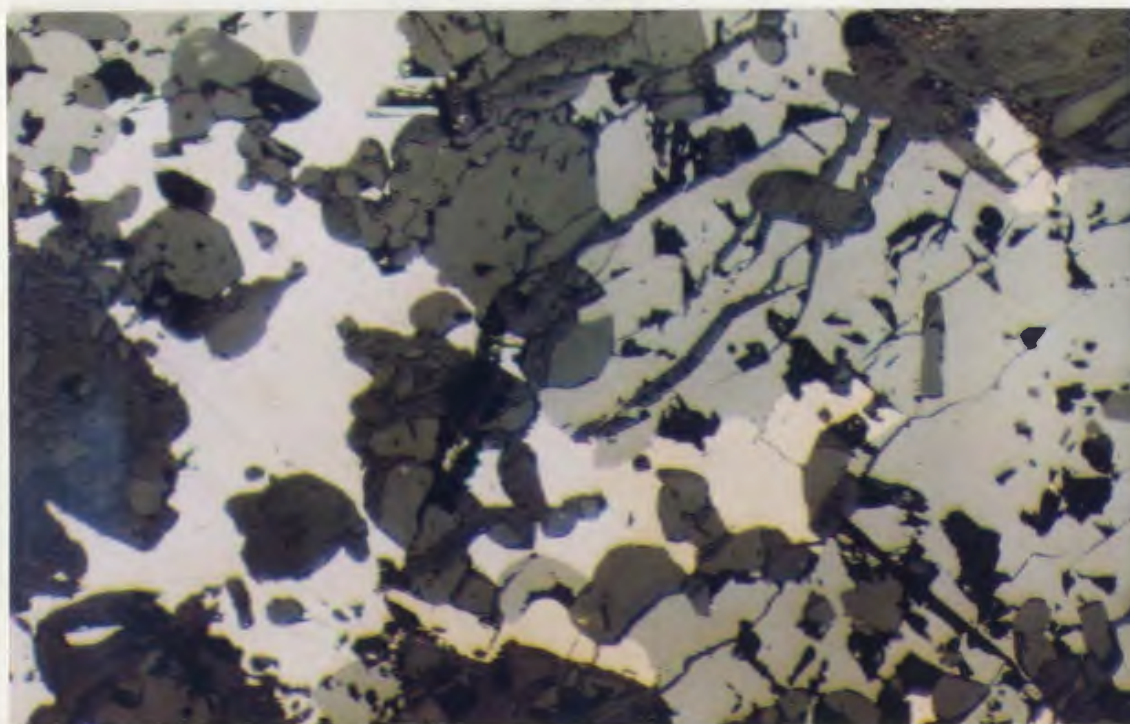
Plate 4.22. Sphalerite (medium gray), galena (white), and pyrrhotite (creamy brown) mineralization within the Winter Hill Showing. Sample SS88-089 (584055), mag.= 100X, fov = 1 mm, reflected light.

pyrrhotite.

Chalcopyrite is the least common sulphide, present locally in only minor to trace amounts usually as inclusions in sphalerite but sometimes as inclusions in pyrrhotite and pyrite and occasionally as free crystals. As mentioned previously, chalcopyrite occurs as elongate crystals parallel to crystal faces within sphalerite, but it also occurs as small rounded blebs in sphalerite which may not be a product of supersaturation along crystal faces, but a replacement phenomena. In the lower section of the upper zone, chalcopyrite sometimes occurs as mantles or coatings along sphalerite crystals (see Plate 4.11).

Pyrrhotite is the more common Fe-sulphide and is second in abundance to sphalerite. It is present as small anhedral crystals or groups of crystals displaying a characteristic anisotropic behaviour, as small roundish inclusions in pyrite and occasionally in other sulphides, and as larger crystals that are apparently pseudomorphed or altered by pyrite (Plate 4.23). Pyrrhotite is associated with most of the sphalerite and galena mineralization in the middle and top sections of the upper zone whereas pyrite dominates in the lower part of the upper zone.

Pyrite is present as fine-grained anhedral to euhedral crystals. It occurs in minor amounts (but locally abundant) in most of the upper Zn-rich zone. Some crystals of pyrite have a colloform texture (Plate 4.24), but these crystals contain
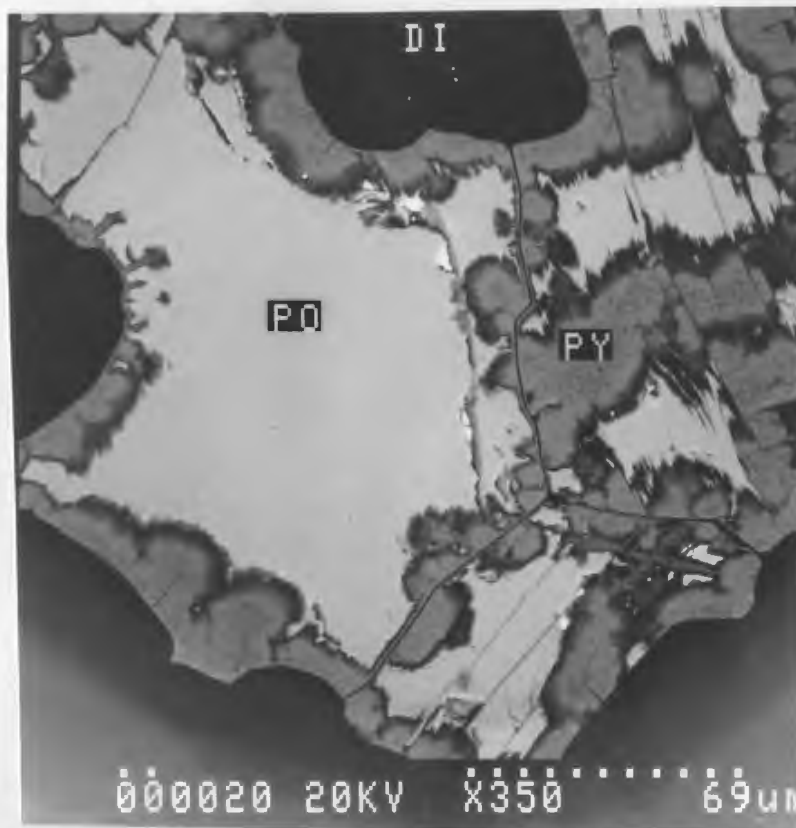
Plate 4.23. SEM back scatter photograph of a pyrrhotite (PO) crystal being replaced by pyrite (PY). Also present is a diopside (DI) inclusion. SS88-082 (584052), mag.= 350X.

Plate 4.24. SEM back scatter photograph of a pyrite (PY) crystal exhibiting colloform texture, and intergrown with sphalerite (ZN) and calcite (CC). Sample SS88-082 (584052), mag.= 600X.

a lot of impurities and may instead be marcasite and not pyrite (see Clemson, 1986), in which case the "colloform" texture is actually a supergene effect (A. Sangster, pers. comm.). Pyrite is also found as an alteration mineral along fractures in pyrrhotite.

Other less frequent sulphide mineral present include chalcocite, digenite, and possible cubanite. They are associated with chalcopyrite.

Magnetite and hematite are minor opaque oxide phases. Hematite occurs due to the oxidation of Fe-sulphides whereas magnetite is present as a primary mineral commonly found along the upper contact with the hanging wall. A few minute oriented crystals of ilmenite were located by SEM within some chalcopyrite grains.

4.2.2.3 Winter Hill West

The Winter Hill West showing (Figure 4.6) is located approximately 1.2 km southwest along strike from the Winter Hill showing and consists of two trenches ≈100 m apart. Minor to trace amounts of base-metal sulphides are hosted in fine- to locally medium-grained tuffaceous sediments. Pyrite, the most common sulphide in the main trench, is present as a massive lens with little to no associated base-metal sulphides. Below the massive pyrite is a thin layer of black, fine-grained argillite containing very few sulphides, but which has a noticeable pocked (or hollowed) weathered surface.
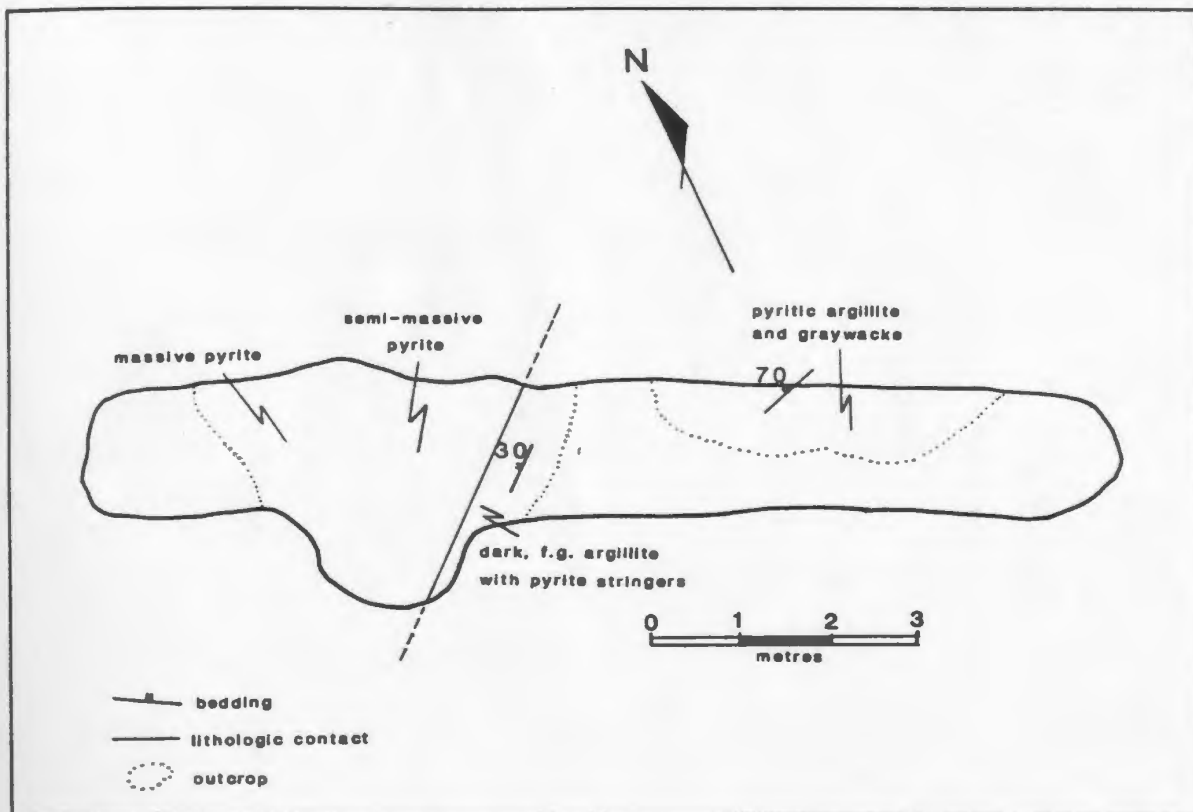
Figure 4.6. Geology of the main trench at Winter Hill West.
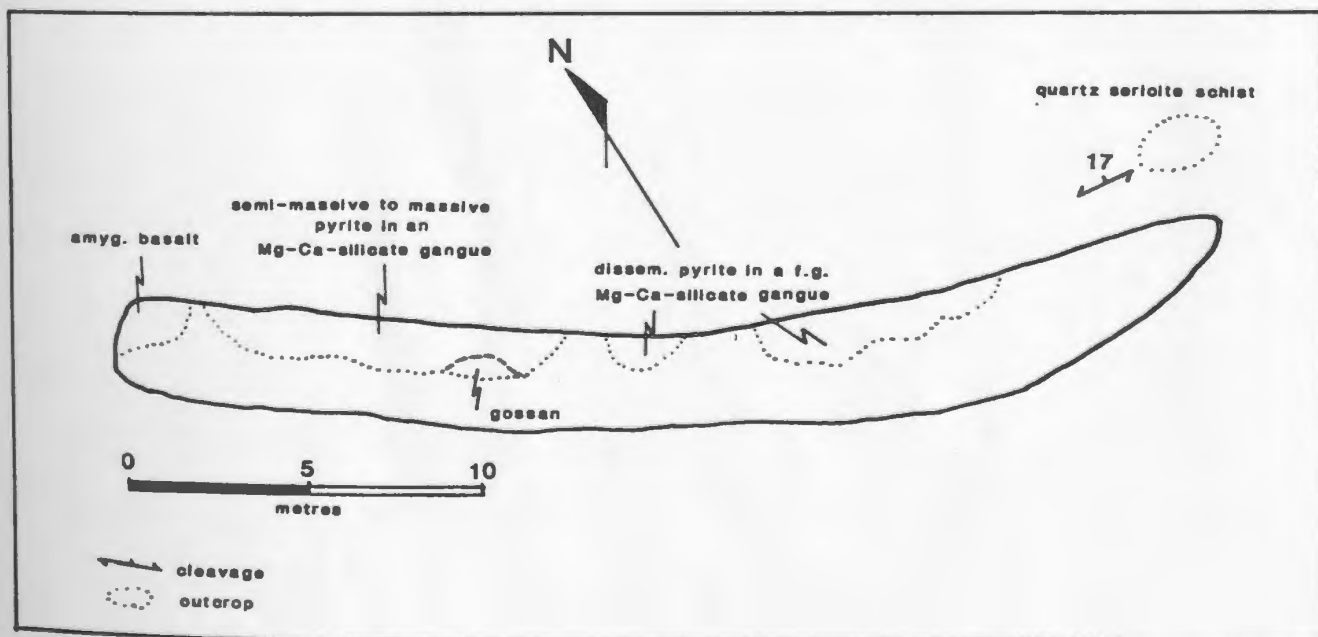
Figure 4.7. Trench geology at Winter Hill East.

The contact between the massive pyrite and the black argillite is very sharp. Stratigraphically below the argillite is a slightly coarser grained, layered tuffaceous sediment containing up to 20-30% pyrite, as layers and disseminations, and up to 2-5%, locally, combined sphalerite, galena, and chalcopyrite. Local layering ranges in strike from 40°N to 60°N, whereas the dip decreases from 70°N in the layered tuffaceous sediments to 30°N in the black argillite.

The opaque minerals are dominated by pyrite with much lesser amounts of sphalerite, galena, chalcopyrite, magnetite, and pyrrhotite. Pyrite is fine-grained, euhedral, and where base-metal sulphides are present, contains inclusions of these sulphides and pyrrhotite. Pyritic laminae contain up to 80% pyrite and are separated by intervals containing ≤ 20% pyrite. Chalcopyrite and sphalerite are more visible toward the eastern end of the trench where the total sulphide content is ≤ 10% and combined chalcopyrite and sphalerite is ≤ 2-3%. Pyrrhotite, if not present as inclusions in pyrite, will often display a colloform-like texture. Differential alteration within magnetite indicates possible crystal zoning.

The gangue mineralogy is mostly fine- to medium-grained quartz with subordinate sericite and chlorite. The silicates are intimately intergrown with the opaques and no definite paragenetic sequence can be determined. Thin veins of fine- to medium-grained recrystallized quartz, and minor sericite, are present in a few thin sections.

Drill holes from Winter Hill West intersected laminated volcanic sediments with pervasive disseminated pyrite and four intervals of massive pyrite, each approximately 1 m thick (Graves, 1986a). Mafic rocks above this horizon are silicified (Graves, 1986a).

4.2.2.4 Winter Hill East

Mineralization at the Winter Hill East trench (Figure 4.7) is located approximately 1.75 km northeast of the Winter Hill showing. This trench is very similar to the Winter Hill West showing. Semi-massive to disseminated pyrite, with lesser abundances of base-metal sulphides, is hosted in a fine-grained Ca-Mg-silicate-rich rock. The western edge of the mineralization is bounded by a silicified amygdaloidal basalt, whereas, the eastern end contains slightly pyritic and locally sheared mafic tuffaceous(?) sediments. The bulk of the sulphide mineralization is pyrite with local base-metal sulphide concentrations up to 5%. The metal concentrations (Pb ± Zn) occur in the semi-massive to massive pyrite. Boulders of weathered host rock contain the same pocked weathered surface as the dark argillites at Winter Hill West.

In thin section, pyrite is the most abundant sulphide followed closely by pyrrhotite with lesser galena, sphalerite, and chalcopyrite. Pyrite is present as fine- to coarse-grained, anhedral to subhedral crystals containing numerous Ca-Mg-silicate inclusions (Plate 4.25). Pyrrhotite occurs with

144
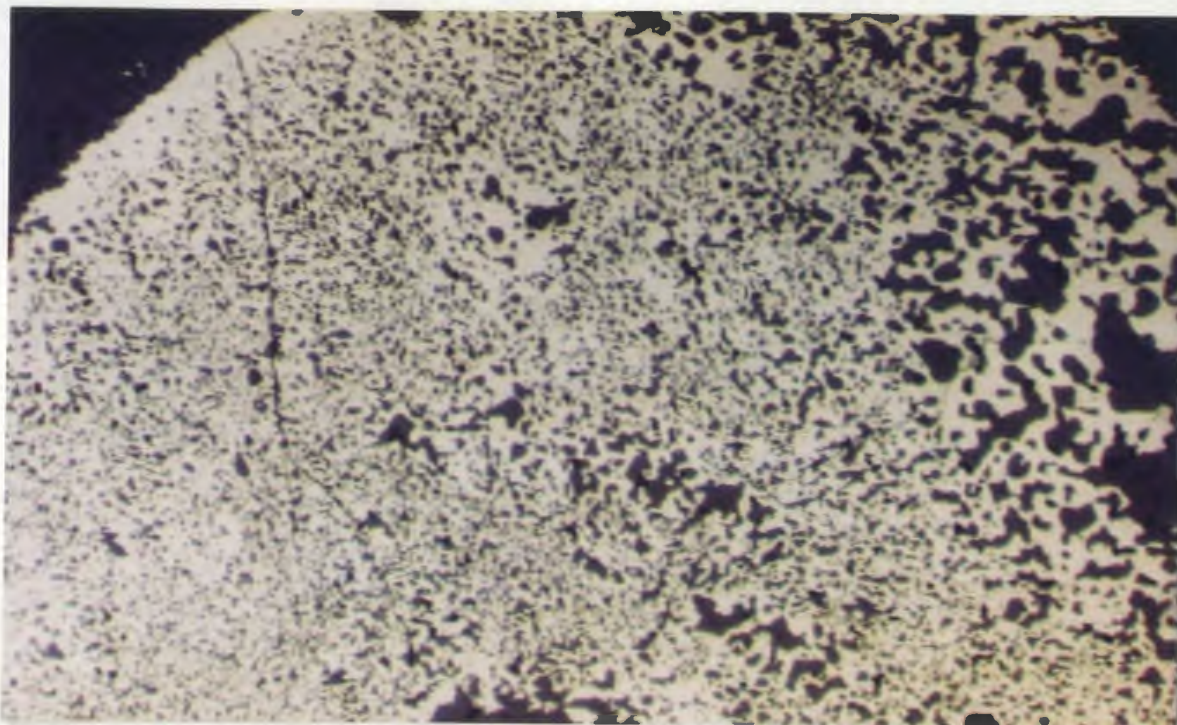
Plate 4.25. Large pyrite crystal from Winter Hill East containing numerous, rounded, calc-silicate inclusions. Sample SS88-121 (584076), mag.= 32X, fov = 3.3.mm, reflected light.
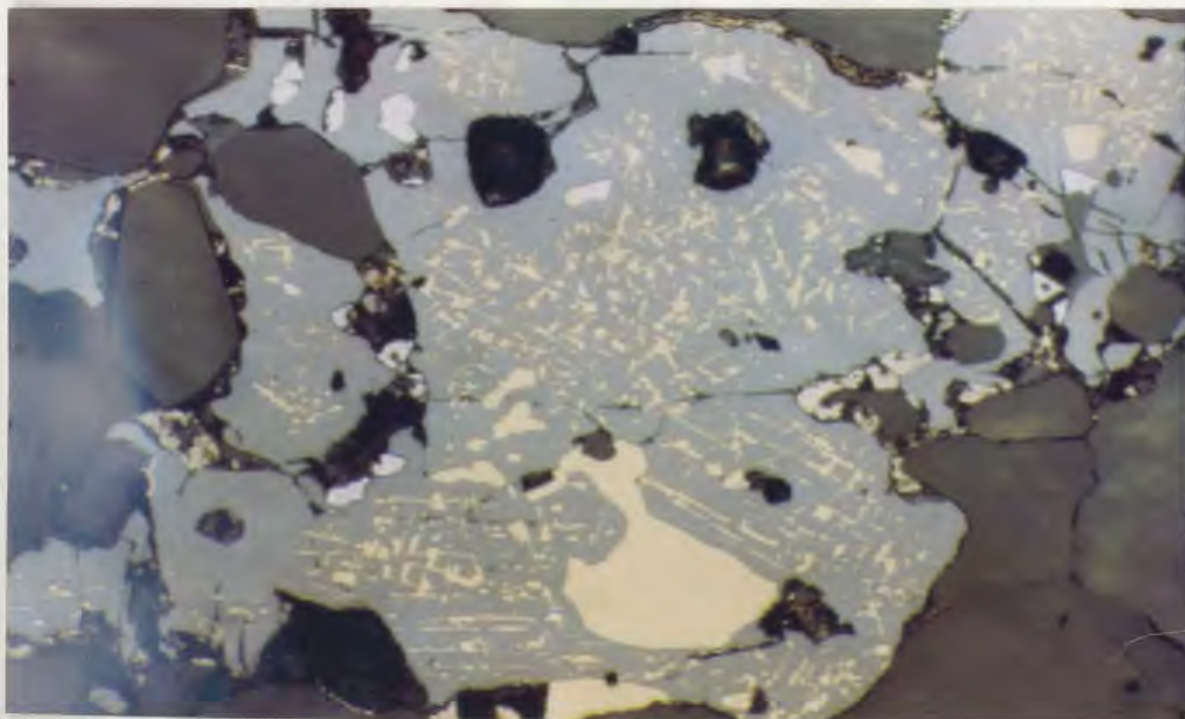
Plate 4.26. Chalcopyrite lamellae (?) and blebs (yellow) in a sphalerite crystal (medium gray) from the Winter Hill East Showing. Sample SS88-121 (584076), mag.= 200X, fov = 0.5 mm, reflected light.

pyrite and their exact relationship is difficult to determine but pyrrhotite appears to be an alteration product of pyrite. Galena is the prominent base-metal sulphide with only minor occurrences of sphalerite and chalcopyrite. Galena occurs in the form of anhedral blebs. Sphalerite and chalcopyrite also occur as anhedral grains with sphalerite occasionally containing chalcopyrite (Plate 4.26), either as inclusions (*i.e.* chalcopyrite growth along crystal boundaries) or as a exsolution lamellae.

The gangue mineralogy is made up mostly of diopside, actinolite, serpentine, chlorite, ± sericite and quartz. Textures range from a diopside-dominated, slightly foliated granular assemblage to an unoriented texture consisting mainly of fibrous tremolite ± actinolite. The granular texture contains interlocking diopside crystals which are progressively finer grained towards sulphide-rich sections. There are subordinate amounts of serpentine (colorless and yellow-orange pleochroic), chlorite, and probable sericite in the slightly foliated lithologies. Elongate masses of yellow-orange serpentine define a weak foliation. The tremolite-rich zone is fine-grained and may contain a significant amount of sericite and minor quartz.

The foliated rock bounding the eastern end of the trench is primarily an assemblage of fine-grained, fibrous Mg-silicates (actinolite and chlorite) ± sericite and quartz. The few opaques present are slightly stretched parallel to the

foliation. The amygdaloidal basalt at the western end of the trench is unmineralized and silicified. The contact between the basalt and the mineralized host is obscured by till cover.

Drill hole data (Graves, 1986a) indicate the presence of numerous tuffaceous units stratigraphically lower than the mineralization. At least one unit is over 30 m thick while most layers are 10 m or less. Pyrite is the major sulphide present with traces of bands containing disseminated sphalerite. The tuffaceous units are siliceous, which along with the presence of the mafic hornfels, indicate that silicification may have taken place. Mafic and felsic dykes are common and the felsic dykes may be responsible for part of the silicification and the hornfelsing of the mafic rocks.

4.2.2.5 Winter Hill North

Winter Hill North is located 500-600 m north-northwest of Winter Hill East. The mineralization is situated in Ca-Mg-silicate-rich boulders found beside an outcrop of apparently silicified Ca-Mg-silicate rock. The mineralized boulder mainly contains layered magnetite with lesser sphalerite and pyrite. The Ca-Mg-silicate rocks are light coloured and hard. Felsic fragments are visible within the unit (Plate 4.27). This horizon is approximately 200-250 m stratigraphically above the Winter Hill horizon and strikes at 55°N with a variable dip (70°-40°) to the north.

In the mineralized boulder, approximately 90% of the

Plate 4.27. Felsic fragment in a calc-silicate layer at Winter Hill North (≈ 500 m north of Winter Hill East).
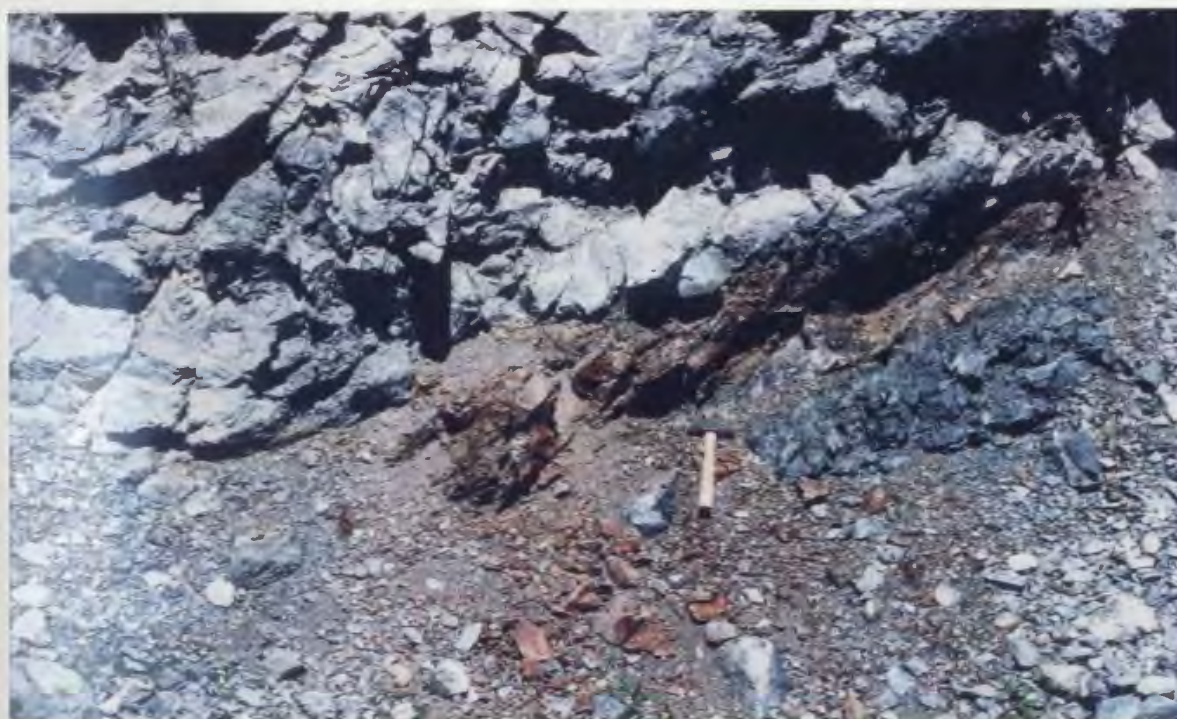
Plate 4.28. Rusty contact zone between a sliver of the Simmons Brook Batholith (upper left) and a mafic portion of the Tickle Point Formation (lower right).

opaque mineralogy is magnetite, the rest being sphalerite, pyrite, and a trace of chalcopyrite. The sulphides occur as thin, contorted layers intimately associated with fine- to medium-grained diopside, fine-grained serpentine, ± amphibole (actinolite?) and sericite. The contorted layering is probably a result of soft sediment deformation. Nonmineralized samples consist of a very fine-grained assemblage (probably mostly quartz, Mg-Ca-silicates, and sericite) with some small quartz crystal fragments(?).

A diamond drill hole (WHN-86-6, Graves, 1986a) located immediately north of the showing, intersected basalt and a package of mostly felsic and mafic intrusives, with a Ca-Mg-silicate layer between them. No mineralization, however, was found. Approximately 350 m to the east, DDH WHN-86-5 (Graves, 1986a) cut through several thin pyritic units in volcanic sedimentary and Ca-Mg-silicate rocks. Unfortunately no base-metal sulphides were associated with the pyrite.

4.2.2.6 Other Mineral Occurrences

There is only one other occurrence where base-metal sulphide concentrations are in excess of 1% within the Sam Head Formation. The occurrence, named Prospect #5 by Noranda Exploration Co. (Graves, 1986a), contains fine-grained disseminated pyrite and sphalerite in a carbonate host. This mineralized area is approximately 2.2 km north of the Winter Hill East showing.

Thin section analysis, and geochemistry, reveal that the carbonate crystals are dolomite. There is also a significant amount of unidentifiable dark, fine-grained material, which is probably a mixture of fine opaques and Ca-Mg-silicates. One section contains garnet. Sulphides are fine-grained with sphalerite and pyrite comprising all the identifiable opaques. The carbonates are cut by a network of quartz/carbonate veins.

Within the lower Sam Head Formation there are a number of mineralized horizons, usually within fine-grained argillite or near cherty sediments. These horizons are almost exclusively semi-massive to massive pyrite units up to 1 m thick with no base-metal sulphide accumulations. These pyrite units are generally layered parallel to bedding.

Within the Winter Hill area there are Ag and Au anomalies. The background values for Ag and Au in the Connaigre Bay Group outside of Winter Hill (excluding Frenchman Head) are approximately 0.1 ppm and <5 ppb respectively (Appendix III). From the mineralized samples taken from Winter Hill area, Ag and Au values averaged 47.3 ppm and 95 ppb respectively with extremes of 0.5 and 695 ppm and <5 and 400 ppb respectively. The highest Ag value came from a sample of the lower zone composed predominantly of fine-grained recrystallized quartz with minor sericite and approximately 5-8% sulphides. The other large values (i.e. 61.4, 76.5, 76.5, 151, 197 ppm) came from banded sulphide samples of the upper zone whereas two other anomalous values

(66.7, 66.2 ppm) were collected from semi-massive sulphides at Winter Hill East.

The highest Au value is coincident with the highest Ag assay, whereas the other high Au values (200, 245, 270, 270, 370 ppb) came from the upper zone samples containing mostly disseminated sulphides. Above average Ag and Au values are compatible but the higher Ag values do not necessarily correspond to the higher Au values.

There is one significant Au anomaly outside of the Winter Hill area. A sample of a pyritic quartz-carbonate vein taken from a roadside outcrop about 1.5 km northeast of Fish Cove (Figure 2.5) contains 1100 ppb Au. The host volcanic rocks are chloritized and sericitized and contain only background Au levels. Some carbonate crystals in the vein are zoned. One crystal was probed and it was found that towards the core there is a general increase in Mg and decrease in Fe with relatively constant Ca.

4.2.3 Doughball Point Formation

Mineralization within the Doughball Point Formation is restricted to very small occurrences of chalcopyrite and one or more occurrences of carbonate-hematite veins.

The chalcopyrite occurrences consist of sparsely disseminated grains associated with pyrite in thin quartz/carbonate veins. There is also some minor chalcopyrite in epidotized haloes around intrusive diabase dykes.

A semi-massive hematite vein, with a carbonate gangue, cuts mafic tuffs on the southeastern shore of Great Harbour Bight. The hematite occurs as elongate bladed crystals in a medium- to coarse-grained carbonate matrix. Minor barite is also found in some quartz-carbonate veins.

4.3 Intrusive Rocks

The intrusive bodies are generally barren of anomalous sulphide accumulations. The more mafic intrusions can have thin "gossanous" contacts with the country rock (Plate 4.28) but pyrite abundances in these zones rarely exceeds 2-3% with little or no associated base-metals. Occasionally there are magnetite- ± chalcopyrite-rich patches in diorite and gabbro associated with amphibole-rich pegmatitic areas, but these are small, generally only a few tens of cm in diameter.

No significant mineralization was located in the local granitoids.

4.4 Discussion

Lacking fluid inclusion and stable isotope data, other means must be utilized in order to define the general physio-chemical characteristics of the mineralizing fluids, and to explain certain problematic mineral assemblages present within the mineralized zones (i.e. Winter Hill). To do this, primary mineralizing processes must be separated from prograde or retrograde, secondary metamorphic processes (i.e. skarn(?)

mineralogies at Winter Hill). The possibility of metamorphic effects is essentially restricted to the carbonate/Ca-Mg-silicate lens at Winter Hill. This is not to infer that other areas are exempt from younger events, only that the effects are minimal and probably indistinguishable from effects of the primary mineralizing fluids.

The Winter Hill showing exhibits many of the classical characteristics of volcanogenic massive sulphide (VMS) deposits (Figure 4.8) as defined by Lydon (1984, 1988) and Franklin et al. (1981), including:

1. the stratabound configuration of the showing: a discordant lower stringer zone and a concordant upper layered zone;

2. the typical Cu and Zn zonation: a pyrite- and chalcopyrite-rich lower stringer zone and a more massive sphalerite-, pyrite-, pyrrhotite-, and galena-rich, upper zone;

3. strong silica alteration in the upper section of the lower zone;

4. chlorite alteration in the lower zone;

5. possible relict sedimentary structures (i.e. colloform(?) banding) in some of the sulphides;

6. a sharp contact with the relatively unaltered hanging-wall lithologies;

7. a discontinuous breccia within the carbonate/Ca-Mg-silicate lens containing massive sphalerite fragments, indicative of subaqueous mineralization and subsequent slumping;

8. the showing is underlain by fragmental rhyolitic rocks at
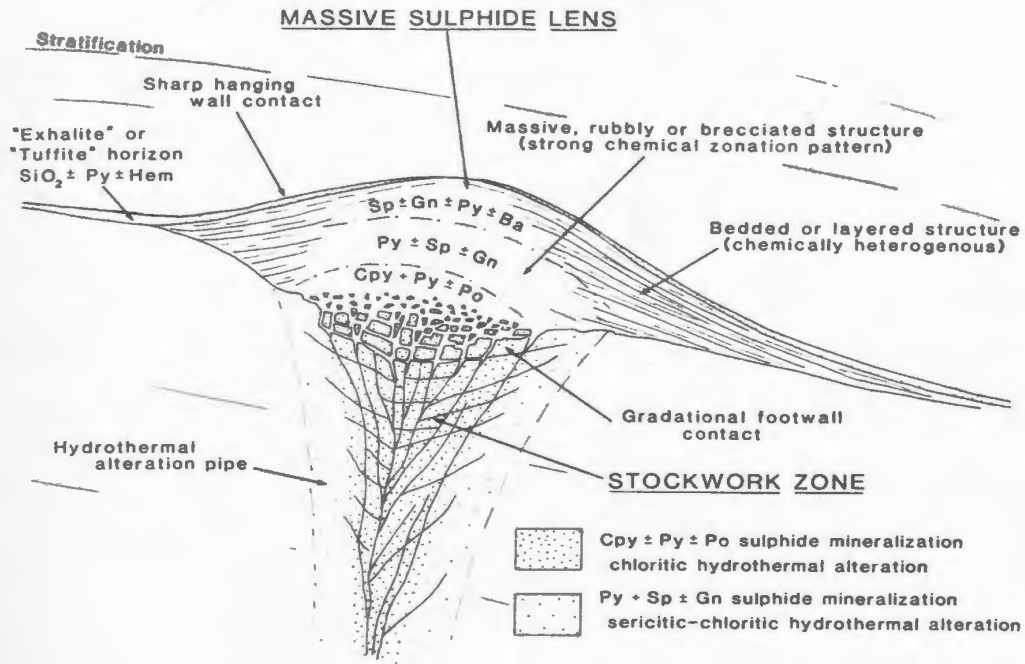
Figure 4.8. Schematic cross-section through an idealized volcanogenic massive sulphide deposit illustrating the more important lithological and mineralogical associations. Taken from Lydon (1984).
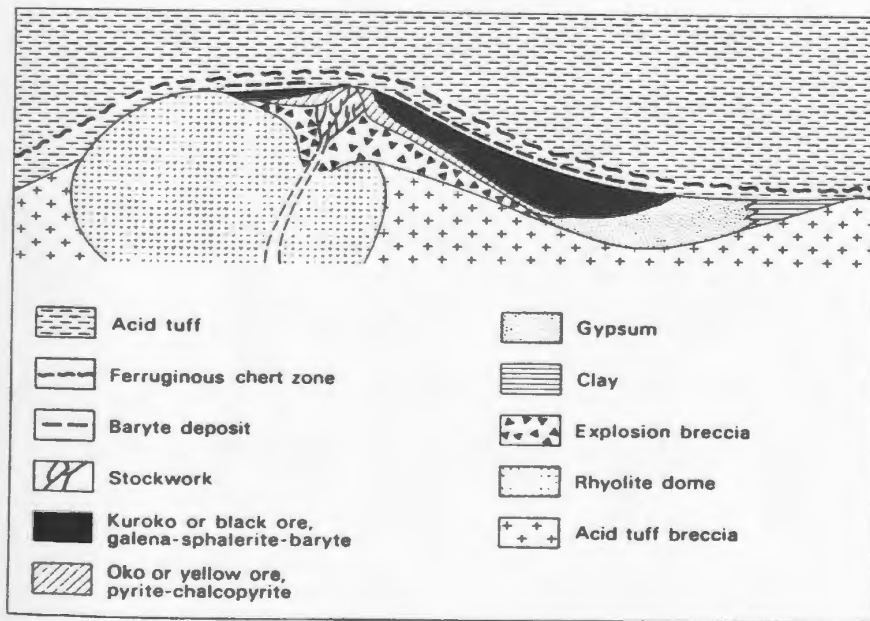
Figure 4.9. Schematic cross-section through an idealized Kuroko deposit. Taken from Evans (1980) after Sato (1977).

a transition from felsic dominated volcanism to mafic volcanism and;

9. Winter Hill and the majority of the other showings and occurrences are located within a limited stratigraphic interval indicating short-lived hydrothermal mineralization during a hiatus or change in volcanism (Graf, 1977).

These criteria suggest a Kuroko-type genesis over the other VMS deposit types (i.e. Cyprus-type, Besshi-type) mainly because of the dominantly felsic footwall rocks. Figure 4.9 illustrates an ideal Kuroko deposit, many features of which are not present at the Winter Hill Showing.

Mineralization within the Connaigre Bay Group can also be compared to other late Precambrian or Phanerozoic VMS deposits because of its richness in Zn (whereas Archean deposits are generally Cu-rich) and its location near the top of the first thick accumulation of felsic rocks (e.g., Tickle Point Formation).

These criteria provide strong evidence that the Winter Hill showing was formed in a volcanically active submarine environment. From this evidence certain characteristics of the paleoenvironment and the mineralizing fluids may be postulated.

The sulphide ore minerals at Winter Hill display a crude paragenetic sequence. It is well known that chalcopyrite precipitates at a higher temperature than either sphalerite or galena within VMS deposits (Ohmoto and Skinner, 1983) whereas

pyrite precipitates throughout the duration of the mineralizing activity (see fig. 7, Lydon, 1988). At Winter Hill chalcopyrite rims sphalerite in the transition area between the lower and upper zones. This texture probably represents the growth of higher temperature lower zone minerals over sphalerite-rich bands of the upper zone as the hydrothermal system grows (Lydon, 1988). Discontinuous hydrothermal activity may have resulted in complex chalcopyrite and sphalerite intergrowths (replacement, exsolution, saturation of chalcopyrite along sphalerite crystal boundaries) due to rapidly fluctuating temperature conditions.

A typical temperature range for VMS deposits is 300° ± 50°C (Franklin et al., 1981; Lydon, 1988), but temperatures may range anywhere from 150°C to 350°C (Ohmoto and Skinner, 1983). By determining the bulk sulphide assemblage, the temperature, sulphur activity (a_{S2}), and oxygen activity (a_{O2}) (indirectly) can be ascertained using log a_{S2} vs. temperature and log a_{O2} vs. a_{S2} diagrams. Sphalerite compositions, taken from Barton and Toumlin (1966), in equilibrium with pyrite and pyrrhotite are added for various sulphidation reactions taken from Barton and Skinner (1979). From Figure 4.10 the temperature range for Winter Hill would fall between approximately 300°-390°C and the log a_{S2} ranges from ≈-11.2 to ≈-6.2. Since pyrite, sphalerite, and pyrrhotite are the main sulphide phases present, the temperature is probably ≤350°C
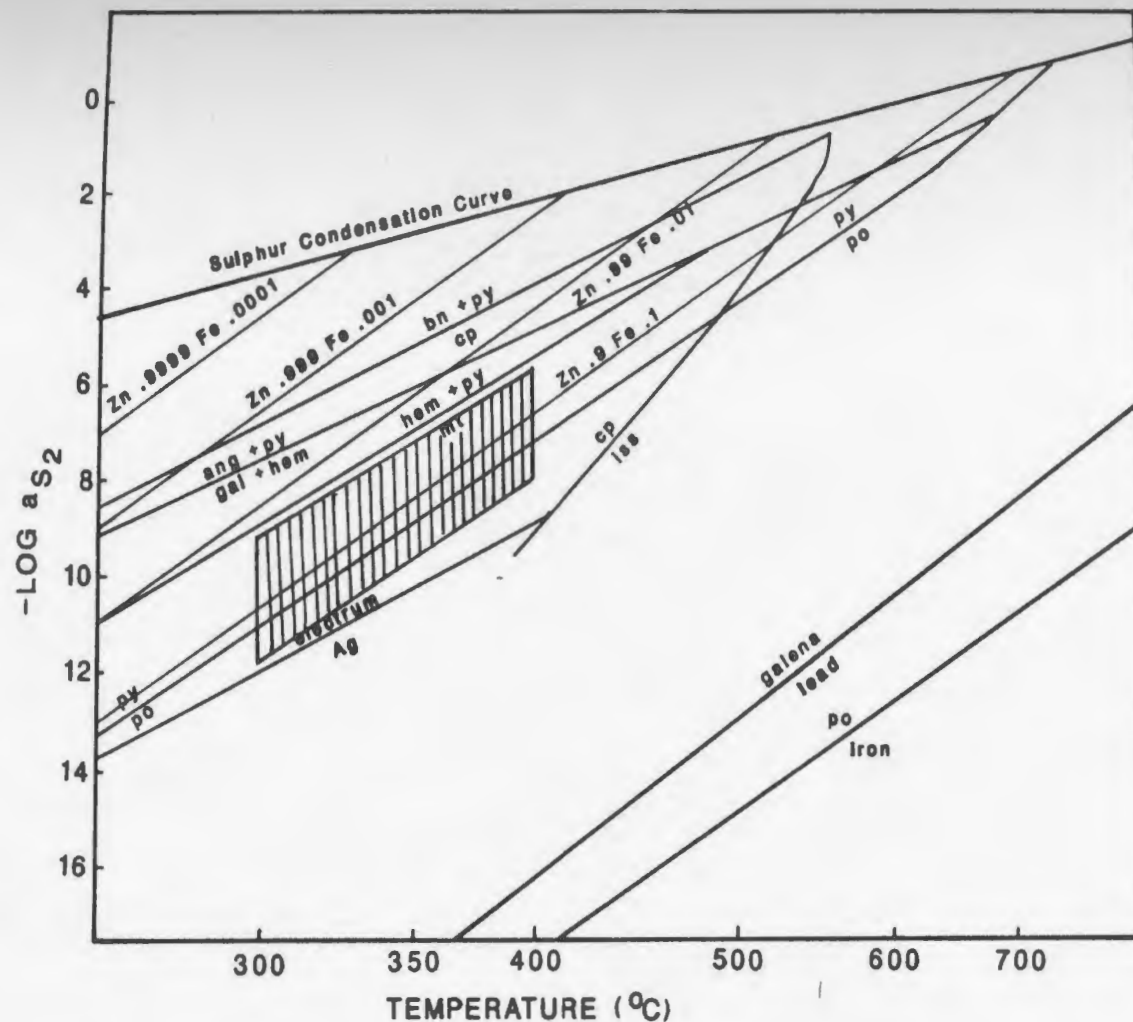
Figure 4.10. Temperature vs. -log a_{S_2} for various sulphidation reactions from Barton and Skinner (1979), with added sphalerite compositions in equilibrium with pyrite and pyrrhotite (from Barton and Toumlin, 1966).Ruled box outlines the probable conditions during mineralization at Winter Hill based upon mineral assemblages and sphalerite compositions.

where the pyrite-pyrrhotite univariant curve is close to the Zn_9Fe_1 (mol %) sphalerite composition (and common Winter Hill sphalerite composition) line. Temperatures at Frenchman Head were probably slightly lower than temperatures at Winter Hill due to the low Fe wt.% in the sphalerites and the absence of pyrrhotite.

Figure 4.11, taken from Urabe and Scott (1983), with data from Robie et al. (1978), shows that the a_{S2} range is more tightly constrained as the range is reduced to $\approx$-7.3 to -11. The a_{O2} lies somewhere between -30 and -34.

The Selco showings and Winter Hill North are the only mineralized zones with known primary magnetite associated with pyrite. This assemblage is restricted to a very small range in a_{S2} (-9.6 to -11) and a_{O2} (-33 to -31) (Figure 4.11).

The sphalerite composition may also put constraints on the temperature of mineralization. Sphalerite containing 9 to 12 mol% FeS (some Winter Hill sphalerite samples fall in this range - see Table 4.1) are characteristic of re-equilibrated sphalerite-(monoclinic) pyrrhotite-pyrite assemblages at temperatures below 250°-300°C (Scott and Kissen, 1973; Hutchinson and Scott, 1980). Therefore the hydrothermal fluids were at least 250°-300°C and probably higher.

Figure 4.10 may also explain why pyrrhotite is absent at Frenchman Head. Fe contents in sphalerite from Frenchman Head are $\leq$1 wt.% and therefore the sphalerite is completely within the pyrite stability field. This also indicates that a higher
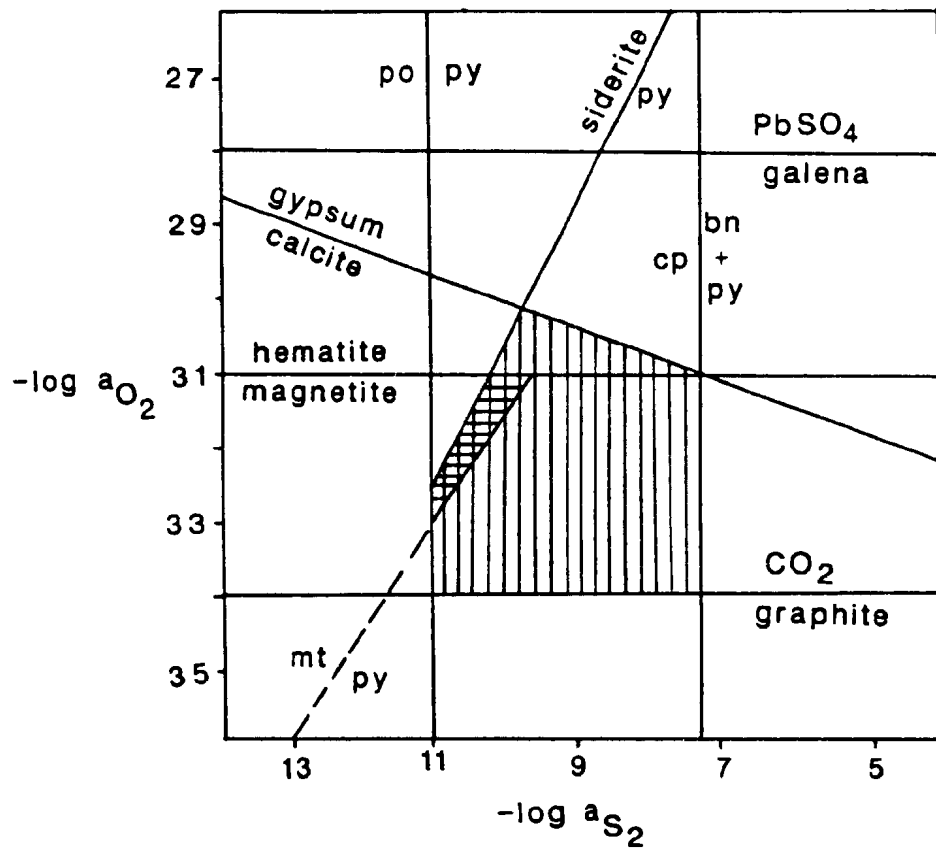
Figure 4.11. -Log a_{O_2} vs. -log a_{S_2} diagram at 300°C and CO_2 activity = 0.001 (adapted from Urabe and Scott (1983) with data from Robie et al. (1978)). The ruled box represents the conditions during mineralization at Winter Hill, whereas the small hatched rectangle represents the mineralization conditions during deposition of the Selco Showings and Winter Hill North.

a_{S2} was present at Frenchman Head with respect to Winter Hill. The absence of pyrrhotite at Frenchman Head adheres to the findings of Craig et al. (1984). They found that sphalerites with large Fe contents (i.e. $\approx$ 10 wt.%) occur with pyrrhotite $\pm$ pyrite, whereas sphalerite mineralization accompanied by pyrite and no pyrrhotite, contains very low Fe values (0.1 to 0.4 wt.%).

This difference in sphalerite compositions from Winter Hill to Frenchman Head is probably a reflection of the underlying lithologies. The Frenchman Head showing is underlain by rhyolites and rhyolitic tuffs and these rocks are traditionally Zn-rich and Fe-poor (Graf, 1977). Winter Hill is underlain by felsic rocks also, but there are some minor interbedded mafic flows, flow breccias, and tuffs which, when leached, would contribute Fe to the mineralizing solution.

There are a few indicators of the possible paleotopography at Winter Hill. The discontinuous carbonate breccia, the contorted banded carbonate, and the skewed configuration of the lower and upper zones together, all suggest that the sulphides accumulated on an unstable slope. The stringer zone (zone of hydrothermal fluid discharge) probably occupied a topographic high whereas the contemporaneous carbonate and sulphide deposition occurred on a slope which possibly graded into a small depression or basin.

The physio-chemical characteristics of the mineralizing

fluid, according to the classification of Sato (1972) (Figure 4.12), may be estimated by examining the size and shape of the different showings (Lydon, 1988). Type 3 fluids can be ruled out because for sulphides to accumulate they must be deposited from either type 1 (highly saline fluids whose densities are greater than seawater at all degrees of mixing (fig. 1, Lydon, 1988)) or type 2 fluids (initially less dense than seawater, then as it mixes with seawater, passes through a density maximum making it more dense than cold seawater (fig. 1, Lydon, 1988)). Type 1 solutions generally create flat, tabular, aerially extensive ore deposits whereas type 2 fluids generate lens shaped deposits of limited extent (Lydon, 1988). The Winter Hill area showings cover a strike length of approximately 3 km, but mineralization between them is discontinuous, possibly reflecting separate discharge vents for the mineralizing fluids, and therefore more characteristic of type 2 fluids. The lozenge shape of the Winter Hill showing also indicates proximal deposition of sulphides from type 2 fluids.

Microprobe analyses of chlorite and actinolite (Table 4.2) from the Winter Hill Showing reveal that there are Mg-rich chlorites in the upper zone, and Fe-rich chlorites and Fe-Mg-bearing actinolites in the lower zone. According to Mottl (1983), Mg-rich minerals are indicative of hydrothermal environments where the fluid is dominated by seawater. Guilbert and Park (1985) state that convecting hydrothermal
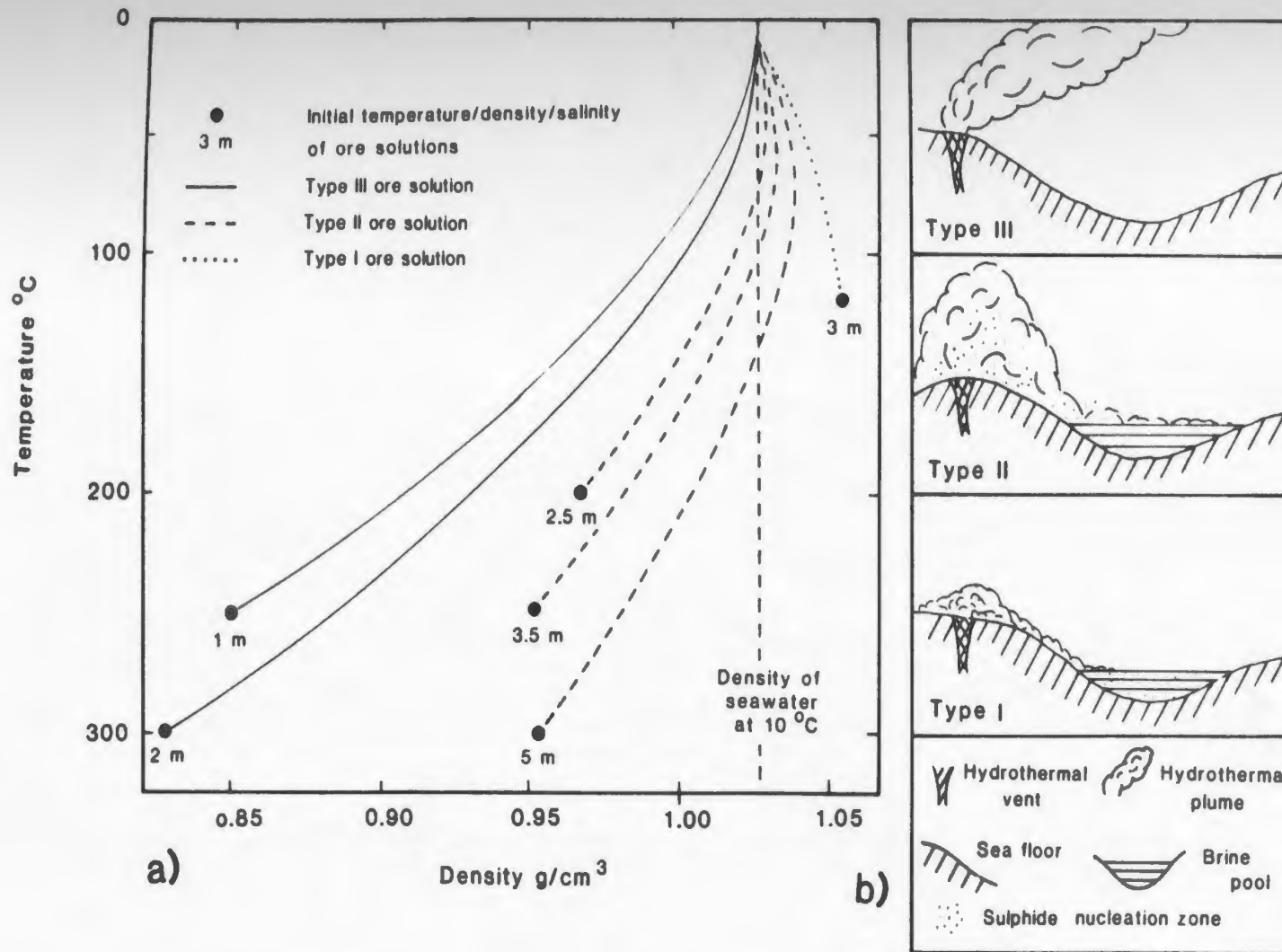
Figure 4.12 a) Density - temperature diagram illustrating the cooling trends of the three types of hydrothermal fluids when hot saline solutions mix with seawater at 10°C (after Sato (1972)). **b)** Schematic diagrams displaying the buoyancy of precipitating sulphides from Sato's (1972) different types of hydrothermal solutions.

Table 4.2. Microprobe analyses for chlorites, actinolites, and cordierites from Winter Hill.

CHLORITES

Sample #	Si	Ti	Al	Fe(tot)	Mn	Mg	Ca	Na	K	Cr	Ni	Total
SS88-039a	32.88	0.05	17.28	0.97	0.06	34.54	0.02	tr	0.02	tr	tr	85.82
SS88-039b	32.87	0.06	17.13	1.11	0.14	33.79	0.01	0.02	0.01	0.02	tr	85.16
SS88-032a	31.3	0.06	16.78	27.89	2.1	11.31	1.48	0.02	0.03	tr	tr	90.97
SS88-032b	26.31	0.05	17.79	40.77	0.93	4.26	0.05	0.01	0.05	0.03	0.03	90.28
SS88-109a	32.75	0.09	17.01	0.5	0.16	34.01	tr	0.02	tr	tr	0.05	84.59
SS88-109b	32.87	0.13	17.2	0.55	0.29	33.76	0.02	0.03	0.01	tr	0.04	84.9

ACTINOLITES

Sample #	Si	Ti	Al	Fe(tot)	Mn	Mg	Ca	Na	K	Cr	Ni	Total
SS88-032	54.25	0.05	2.25	9.68	1.68	16.96	11.73	0.07	tr	tr	0.02	96.69
SS88-032	55.2	0.08	1.87	10.3	2.05	16.93	11.79	0.03	0.02	0.03	tr	98.3

CORDIERITES

Sample #	Si	Ti	Al	Fe(tot)	Mn	Mg	Ca	Na	K	Cr	Ni	Total
SS88-037	49.61	0.03	31.01	7.63	1.36	7.89	0.05	0.29	0.01	0.01	0.01	97.9
SS88-512	48.59	0.03	31.89	4.29	0.83	9.63	0.07	0.39	0.84	0.01	0.05	96.62
SS88-512	48.48	0.03	32.2	5.11	0.86	9.75	0.05	0.21	tr	tr	tr	96.69
SS88-512	49.48	tr	32.45	4.9	0.79	10.41	0.04	0.17	0.02	0.01	tr	98.27
*DHZ	47.69	tr	32.52	8.67	0.04	7.56	0.52	0.53	0.42	tr	tr	97.95

*cordierite from argillaceous hornfels (taken from Deer et al., (1962))

fluids are basically seawater that have percolated through underlying mafic rocks (as at Winter Hill), therefore leaching much greater abundances of Mg^{2+} over the alkalis. The lack of Mg-chlorites (or any chlorites) at Frenchman head may indicate that hydrothermal fluids circulated through dominantly, if not wholly, felsic rocks.

When the probed chlorites from Winter Hill are plotted on an AFM diagram (Figure 4.13), four samples plot along the Al_2O_3 -MgO tie line due to the very low Fe concentrations. Of the two Fe-rich samples, one plots in, and the other just slightly outside, a box defined by Kean and Evans (1988) as the field of chlorite compositions for mineralized chlorite-schist zones from VMS deposits located in central Newfoundland. Mottl (1983) suggests that the Fe-rich chlorites (like Mg-rich chlorites and actinolites) are a characteristic of upwelling hydrothermal fluids.

Winter Hill is also host to some atypical mineral assemblages which would not be expected to occur at the temperatures expected for VMS deposits.

The lower zone contains abundant recrystallized quartz, along with cordierite, biotite, and ± andalusite. From Winkler (1976), the reaction chlorite + muscovite + quartz ↔ cordierite + biotite + andalusite + H_2O could account for this assemblage and could also be the cause for the lack of muscovite which is a common mineral in the stringer zones of VMS deposits (Lydon, 1988). The problem with this reaction is
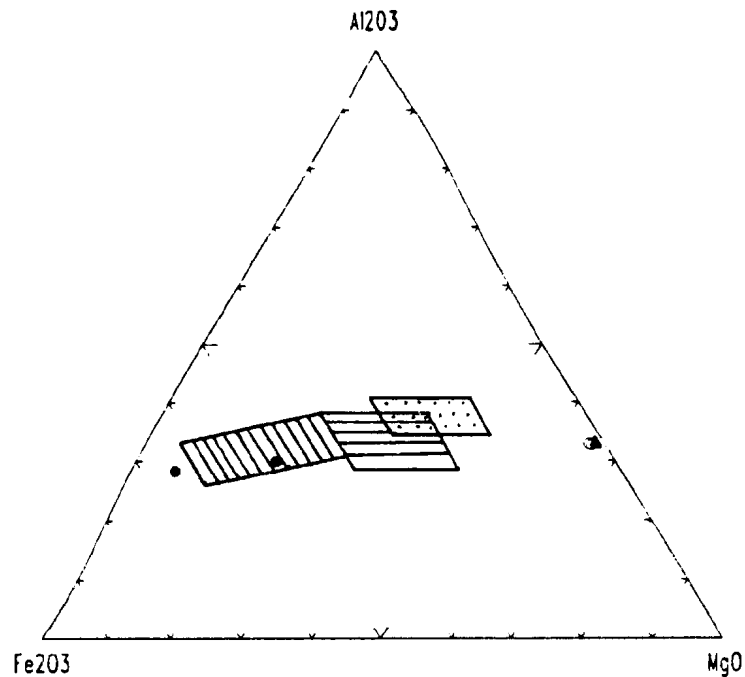
Figure 4.13. $Fe_2O_{3\,total}$ $-$ Al_2O_3 $-$ MgO ternary diagram of chlorite compositions. Filled circles are chlorites from the lower zone at Winter Hill whereas the filled triangles and the open circles are chlorites from the upper zone. 1 = field of chlorite compositions for mineralized chlorite schist zones (includes Little Bay, Whalesback, Colchester, Miles Cove, and Rendell-Jackman), 2 = field of chlorite compositions for host metabasalts, and 3 = field of chlorite compositions for hydrothermal chlorites in felsic rock sequences, Victoria Lake Group. Fields are taken from Kean and Evans (1988).

that it takes place at $\approx$ 505° $\pm$ 10°C at 500 bars H_2O pressure (Winkler, 1976). In deposits metamorphosed above the stability of chlorite, the mineralogy is reflected by a cordierite-anthophyllite assemblage (Franklin et al., 1980, p. 549; Guilbert and Park, 1985; Lydon, 1988), but this assemblage is generally restricted to metamorphosed deposits in regional high grade terranes whereas Winter Hill contains only localized cordierite-biotite-andalusite assemblages and the surrounding rocks contain only lower greenschist facies minerals (O'Driscoll and Strong, 1979). Guilbert and Park (1985) also suggest that a cordierite-anthopyllite assemblage can be produced due to contact metamorphic processes. From microprobe analysis (Table 4.2), the cordierite from Winter Hill is similar in composition to cordierite from argillaceous hornfels (Deer et al., 1962).

The upper zone at Winter Hill also contains a mineral assemblage that is characteristic of higher temperature metamorphism, viz.: diopside-tremolite-carbonate-forsterite-talc-brucite. These minerals may be a manifestation of contact metamorphism superimposed upon a range of low temperatures minerals. If the carbonate/Ca-Mg-silicate lens was initially a siliceous dolomite (which seems valid from the above mineralogy) then the following reactions from Turner (1981) are applicable to the lower temperature minerals:

$$3CaMg(CO_3)_2 + 4SiO_2 + H_2O \leftrightarrow Mg_3Si_4O_{10}(OH)_2 + 3CaCO_3 + 3CO_2$$

(dolomite)   (qtz)   (talc)   (calcite) $\approx$ 185°C

$$5CaMg(CO_3)_2 + 8SiO_2 + H_2O \leftrightarrow Ca_2Mg_5Si_8O_{22}(OH)_2 + 3CaCO_3 + 7CO_2 \quad \approx$$

190°C   (tremolite)
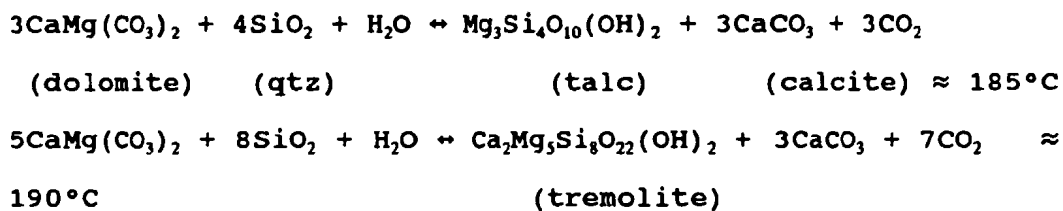
As temperature increases (i.e. closer to the thermal source), and depending on the amount of silica in the system, one or both of these reactions may apply for the formation of higher temperature minerals:

$$Ca_2Mg_5Si_8O_{22}(OH)_2 + 3CaCO_3 + 2SiO_2 \leftrightarrow 5CaMgSi_2O_6 + 3CO_2 + H_2O$$

$\approx$ 240°C   (diopside)

$$Ca_2Mg_5Si_8O_{22}(OH)_2 + 3CaCO_3 \leftrightarrow 4CaMgSi_2O_6 + CaMg(CO_3)_2 + CO_2 + H_2O$$

$\approx$280°C
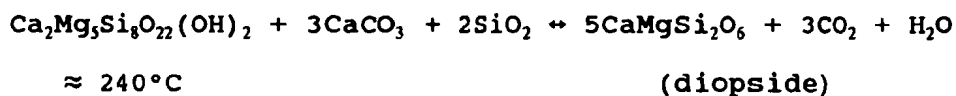
Closest to the thermal source the highest temperature reactions occur:

$$Ca_2Mg_5Si_8O_{22}(OH)_2 + 11CaMg(CO_3)_2 \leftrightarrow 8Mg_2SiO_4 + 13CaCO_3 + 9CO_2$$

$+ H_2O$ $\approx$305°C   (forsterite)
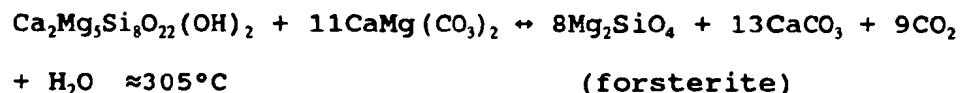
The temperatures for these reactions are quite low for thermal metamorphism and all these phases occur over a very small area which tends to suggest a small localized heat source with the potential to have only a small contact metamorphic aureole with a sharply decreasing thermal gradient away from the source. A likely source would be the felsic

and/or mafic dykes bounding most of the carbonate lens. Since mineral zoning (i.e. higher temperature minerals near the lens' boundary with progressively lower temperature minerals toward the centre of the lens) is present at both the upper and lower contacts of the lens, then this also lends support to the dykes being the heat source.

The presence of talc and brucite are strong indicators of the mole fraction of CO_2 (X_{CO2}) and H_2O (X_{H2O}). If X_{CO2} is close to zero then dolomite and water will react to form brucite ($Mg(OH_2)$), calcite, and CO_2 (Winkler, 1976). The brucite may also be altered periclase which could have formed with calcite and CO_2 due to the breakdown of dolomite (Winkler, 1976), but temperatures > 600°C would appear to be too high for the Winter Hill area.

The presence of Au associated with base-metal mineralization at Winter Hill and Frenchman Head provides evidence that the Au (and Ag) was probably precipitated from solution in conjunction with the base-metals. Like the base-metals, Au is chalcophile in character (Strong, 1981) and therefore it is not surprising that Au is present in anomalous amounts. Past and present VMS producers such as Buchans, Newfoundland (1.3 g/t) and Aznalcollor, Iberian Pyrite Belt (1 g/t), and non-producers such as Errington and Vermillion deposits in the Sudbury Basin (5.2 g/t) have known Au associated with syngenetic base-metal deposition (Franklin et al., 1983). Non massive-sulphide related anomalous Au values

(1100 ppb in a quartz-carbonate vein) are located proximal to fault zones. It is interesting that this high Au anomaly is coincident with a high lake sediment Au value reported by the Newfoundland Department of Mines (Davenport et al., 1989). Other above background analyses reported by Davenport et al. (1989) are almost always associated with faults or other structural lineaments, possibly suggesting a structural control and possible epigenetic origin for the Au mineralization.

Also, if the faults present throughout the Connaigre Bay Group were initiated or activated during volcanism (and associated mineralization) then Au from the probably structurally controlled base-metal horizon and fault related epigenetic Au are most likely contemporaneous and possibly have the same source; the underlying volcanic pile. Large scale sedimentary structures, such as bedding, which parallel the faults suggests that the faults were probably active during, and had some control over, sedimentation.

CHAPTER 5

GEOCHEMISTRY OF THE MINERALIZED ROCKS

5.1 Introduction

This section discusses the systematics and distribution of the base-metals and their associated elements (Appendix III). Little emphasis will be placed on the major elements except where there is a concentration of one or more related rock types (e.g. carbonate/Ca-Mg-silicate facies). There is also a section on REE (Appendix IV). REE and extended REE patterns are compared with those profiles of the unaltered host rocks and with patterns for mineralized occurrences from recent literature.

5.2 Connaigre Bay Group

5.2.1 Tickle Point Formation

5.2.1.1 Introduction

Twenty mineralized samples of the Tickle Point Formation were analysed (Appendix III and Table 5.1). There are seven samples each from the Frenchman Head and Selco Showings, and four samples from the Shoal Brook Showing. The two remaining samples are from minor isolated occurrences. The seven Frenchman Head samples are dominantly partially silicified mafic to intermediate volcanic rocks containing disseminated to near semi-massive pyrite and base-metal sulphide

Table 5.1. Average compositions for samples from Frenchman Head (1), the Selco Showings (2), Shoal Brook (3), and other minor pyritic occurrences (4). (-1 = less than one)

Sample #	1	2	3	4
SiO2 (wt.%)	55.92	33.27	47.84	46.57
TiO2	1.01	0.17	0.33	0.38
Al2O3	10.8	5.71	7.77	7.34
Fe2O3(total)	11.05	35.97	23.12	23.99
MnO	0.99	0.18	0.09	0.08
MgO	4.01	3.93	1.08	0.97
CaO	2.18	1.28	1.46	3.17
Na2O	0.21	0.27	1.93	0.69
K2O	3.36	0.7	1.12	1.54
P2O5	0.25	0.04	0.06	0.08
LOI	7.04	17.15	13.14	12.51
Total	96.82	98.67	97.93	97.32
Cr(ppm)	48	5	7	17
Ni	11	-1	2	-1
Co	15	1	4	5
V	126	7	29	58
Cu	1365	22	50	44
Pb	1386	133	171	34
Zn	25641	124	67	39
Cd	92.7	0.5	0.6	-0.1
Mo	14	11	19	5
Rb	43	11	16	54
Ba	2786	173	230	220
Sr	86	53	87	68
Ga	18	39	32	31
Li	8	8	7	27
Nb	-1	1	-1	-1
Zr	97	137	150	115
Y	22	26	31	11
Th	-1	-1	4	2
La	9	11	13	7
Ce	25	57	48	34
F	443	265	529	180
Be	1	0.8	0.9	1.3
Ag	8.34	1.03	4.7	5.87
Au(ppb)	111	-5	-5	553

mineralization. Six of the Selco Showing samples contain massive to massive layered pyrite with one of these six samples also containing thin (mm scale) magnetite layers. The seventh specimen is a silicious rock with disseminated pyrite. Two of the four samples from the Shoal Brook area are massive to massive layered pyrite whereas the other two examples consist of disseminated pyrite in an intermediate to silicious matrix. One sample from Tilt Point is massive pyrite and the final sample, from Fish Cove, is possible vein material within a semi-massive to massive pyrite layer.

Due to the limited number of samples, the formation is examined as a whole, when discussing base-metals and trace elements, instead of as distinct mineralized areas. For REE data, the mineralized areas will be examined both separately and on a formation-wide basis.

5.2.1.2 Base-metals and Trace Elements

Mineralized samples range from relatively barren massive pyrite (i.e. 46.58 wt.% Fe_2O_{3total} and 125 ppm total base-metals) to sphalerite-rich, Fe-poor mineralization (13.0 wt.% Zn and 4.76 wt.% Fe_2O_{3total}). Frenchman Head is the only occurrence containing high base-metal values (i.e. 0.5 wt.%) whereas the other areas contain only barren massive pyrite. Due to the large variations in concentrations, it is necessary to use log scales for most of the variation diagrams.

There are strong correlations between the base-metals.

Figure 5.1 illustrates Cu and Pb both increasing with increasing Zn, and Cu increases with increasing Pb. A Pb-Cu-Zn ternary diagram (Figure 5.2) is modelled after Lydon (1983). Lydon defines fields where the bulk base-metal contents of sedimentary exhalative (SEDEX) and volcanogenic massive sulphide (VMS) deposits commonly plot. Samples from the Tickle Point Formation are generally Zn-rich but some samples are Cu- and/or Pb-rich. Overall, the samples cannot be confidently put into either field although the trend towards increasing Cu over Zn and Pb implies the metals have a VMS origin. Swinden et al. (1988) use the same ternary diagram and define fields for mineralization for host rocks of dominantly mafic, felsic, or mixed composition. Mafic host rocks contain Cu-Zn-rich deposits, whereas felsic hosts contain Zn-Pb-rich deposits. The Tickle Point Formation samples overly the area where mixed mafic and felsic host rocks occur. This result agrees with the positioning of the mineralized zones; i.e. very close to the transition from felsic to mafic dominated volcanism.

The base-metals show a weak negative correlation with Fe (i.e. Fe_2O_{3total}) which is probably indicative of a decrease in pyrite with increasing base-metal sulphides. Histograms of Zn, Pb, and Cu (Figure 5.3) all display one population, which is skewed to the right, toward higher concentrations. This is likely an effect of local, small scale mineralization overprinting low background base-metal values.

Cadmium has an extremely strong affinity for sphalerite,
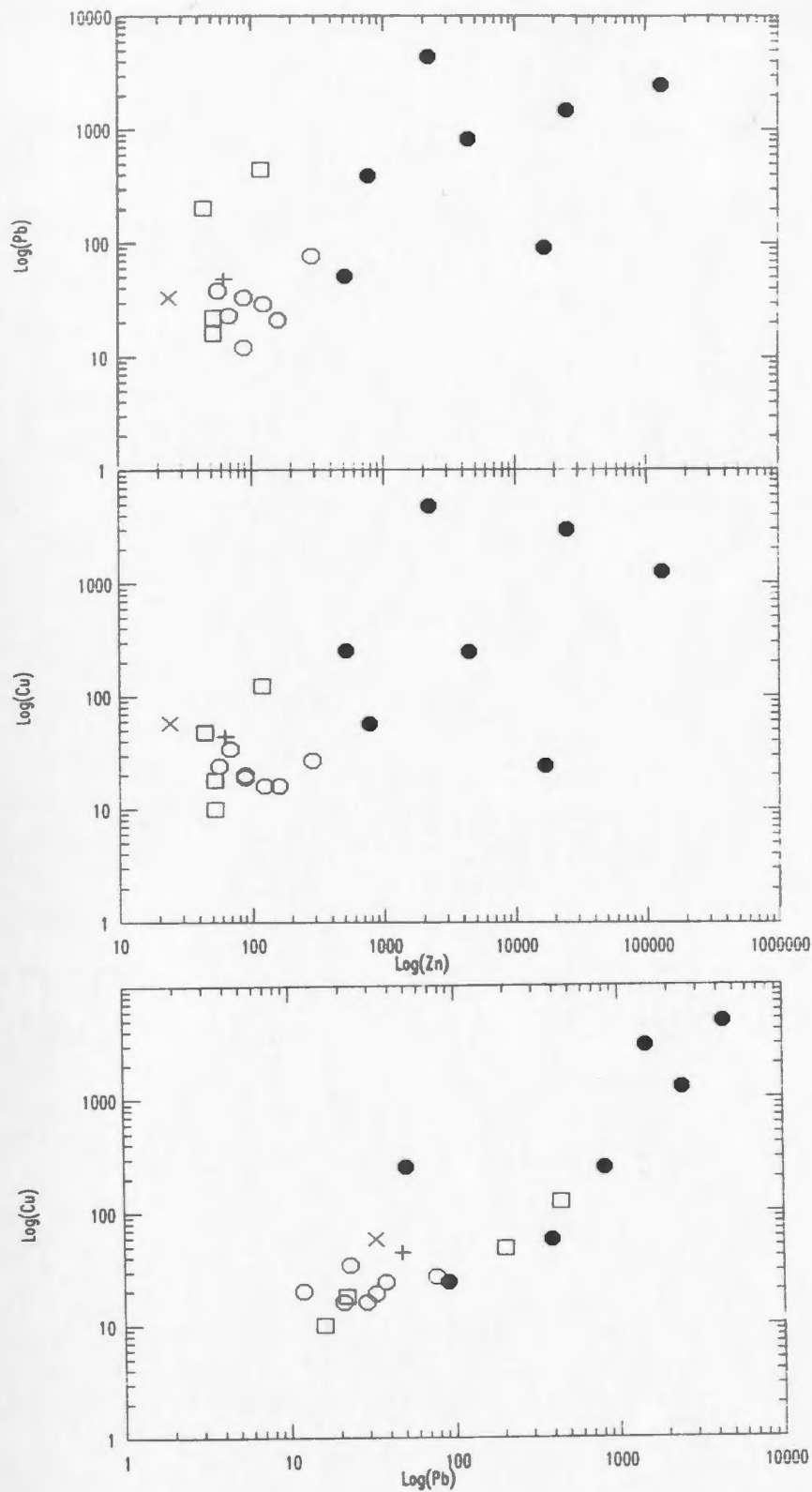
Figure 5.1. Base-metal variation diagrams for samples from the Tickle Point Formation. Closed circles = Frenchman Head Showing, open circles = Selco Showings, open squares = Shoal Brook Showing, X = Tilt Point, and cross = Fish Cove (Au occurrence).
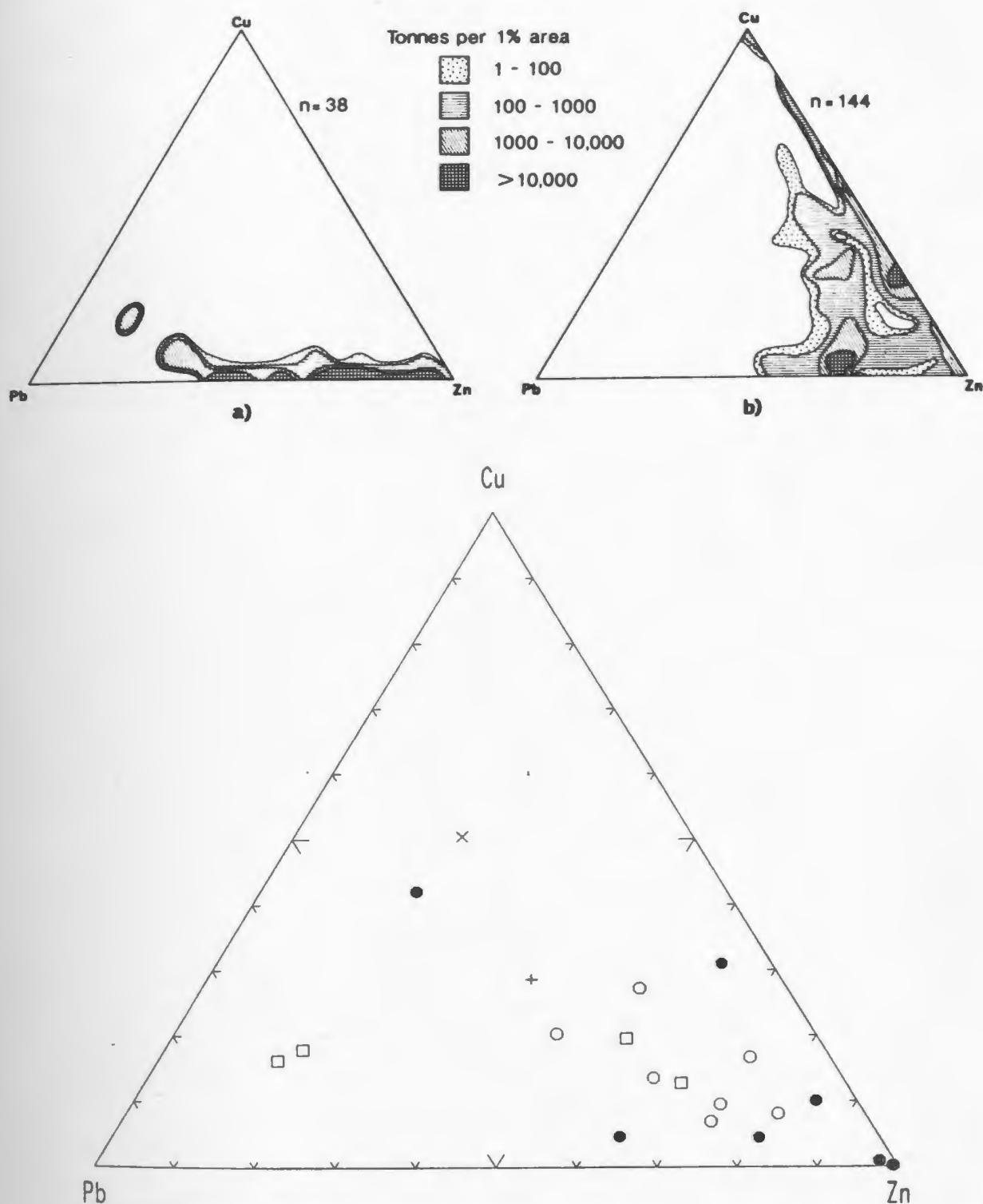
Figure 5.2. Pb-Cu-Zn ternary diagram for mineralized samples from the Tickle Point Formation. Ternary diagrams (a) and (b) represent bulk compositions for sediment-hosted stratiform Pb-Zn deposits (a) and VMS deposits of the Abitibi Belt, the New Brunswick area, Norwegian Caledonides, and the Green Tuff Belt of Japan (b) (taken from Lydon, 1983). Contours are total tonnes of ore metals per 1% area of the diagram. Symbols as in Figure 5.1.
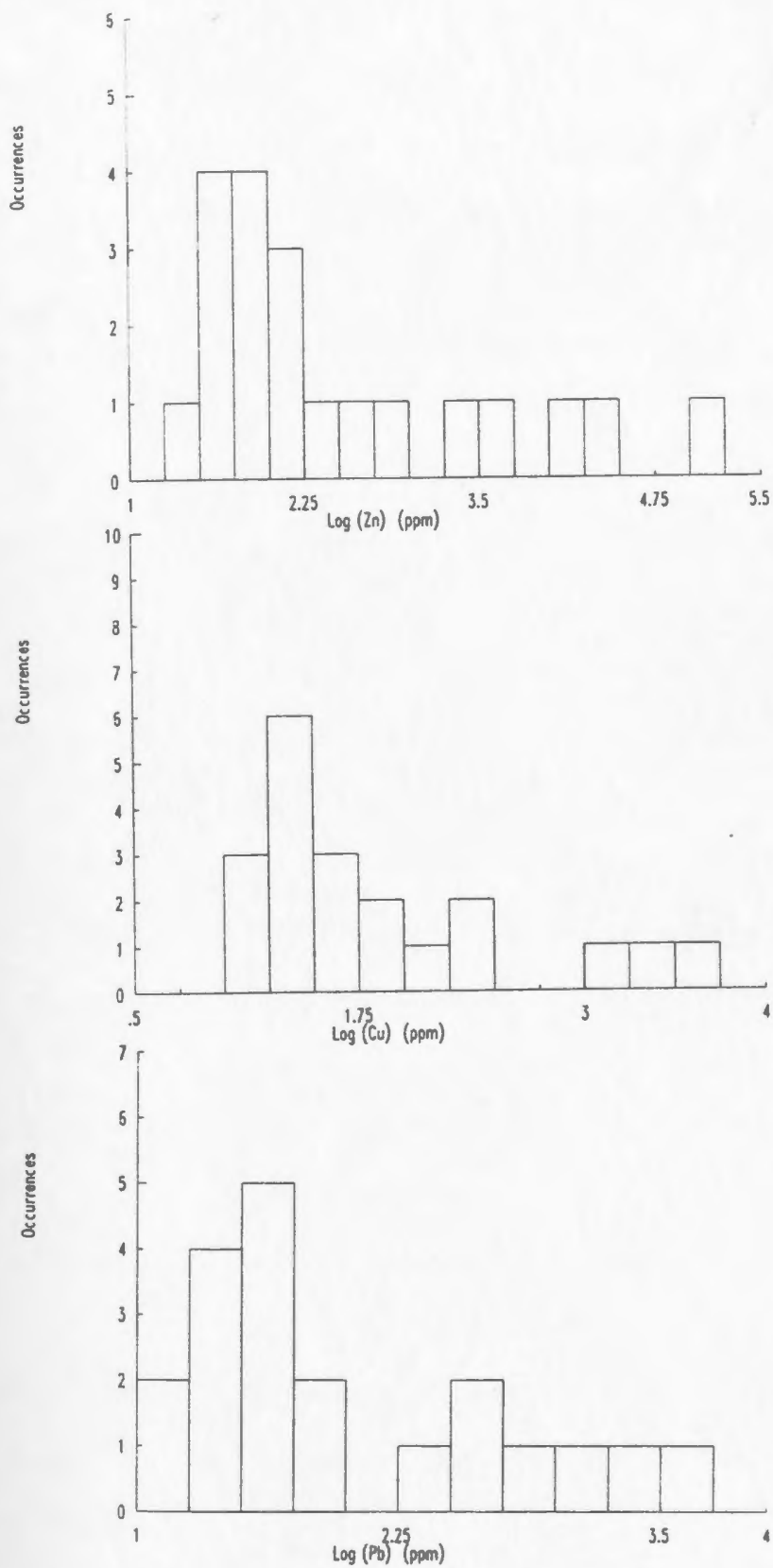
Figure 5.3. Histograms of Zn, Cu, and Pb for mineralized Tickle Point Fm. samples. Each histogram has a total of 20 samples.

as illustrated in Figure 5.4. There is a strong linear relationship between Cd and Zn in the Frenchman Head samples, whereas the other mineralized localities exhibit a scatter of points. The linear relationship occurs only above 1 ppm Cd and 200 ppm Zn (i.e. background values), and therefore the Frenchman Head samples are the only ones that exhibit the relationship. Cd also has a weak positive association with both Cu and Pb. This association may be due to the positive relationships between Cu, Pb, and Zn.

The only measurable Au values (>5 ppb) come from the Frenchman Head samples (up to 350 ppb), the sample representing Tilt Point (550 ppb), and the sample from Fish Cove (1100 ppb). There is no correlation between Au and Cu or Pb (Figure 5.5), but there is a negative correlation with Zn. Ag has a positive trend (possibly exponential) with Pb, a possible weak positive trend with Cu, and no trend with Zn. The weak trends are flat up until 5-10 ppm Ag and ≈ 50-100 ppm Cu or Pb, then the slopes increase sharply. The flat pattern is probably defining a background value whereas the steep slope is a mineralization effect. The Fish Cove and Tilt Point samples are anomalous (with respect to the other localities) because they contain high Au and Ag but low base-metal concentrations.

Swinden et al. (1988) used an Ag vs. Au plot to help define the original host rock lithologies. The diagram is designed to distinguish ophiolite-hosted Au-Ag mineralization
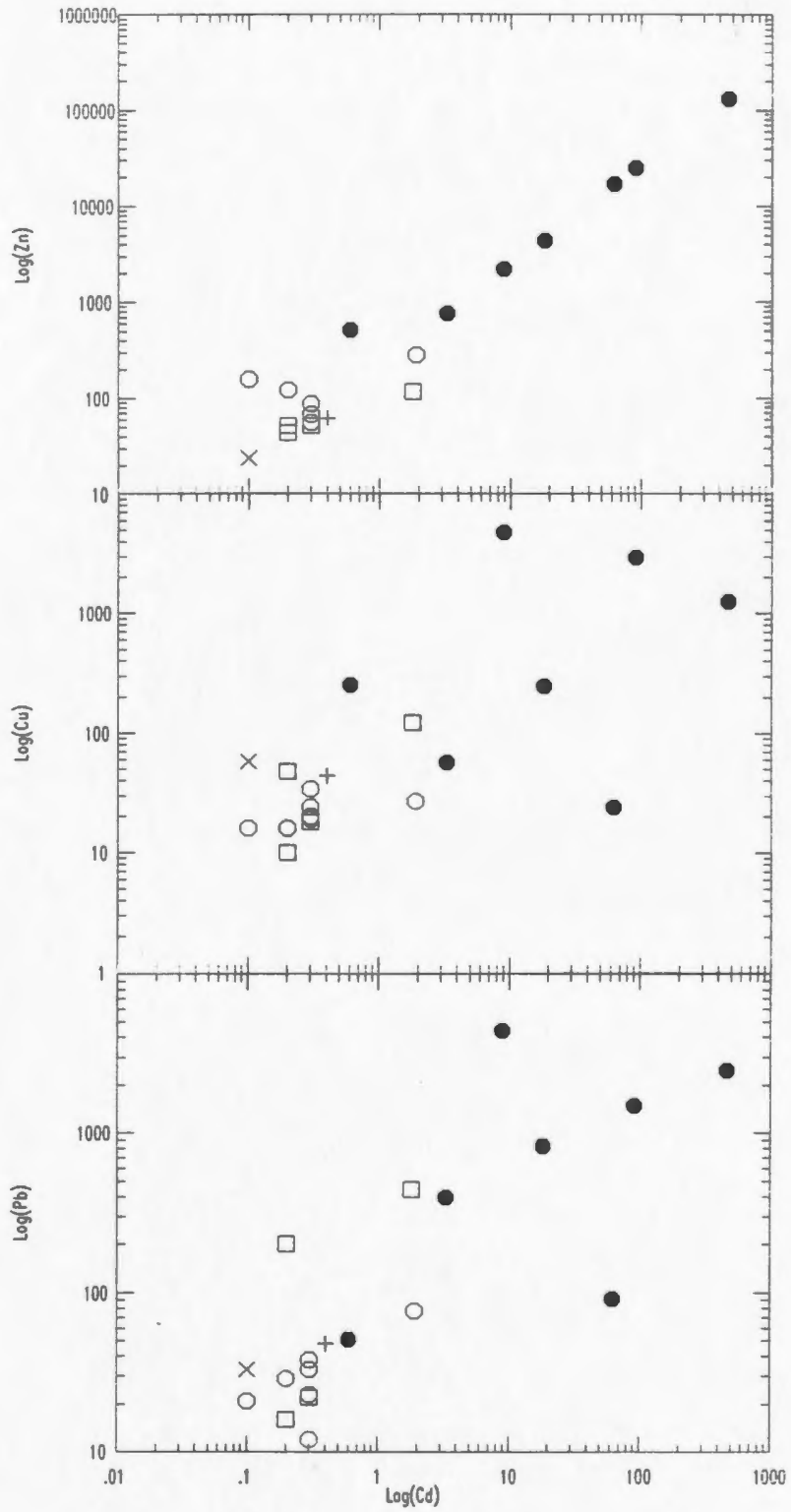
Figure 5.4. Variation diagram of Cd vs. the base-metals. Symbols as in Figure 5.1.
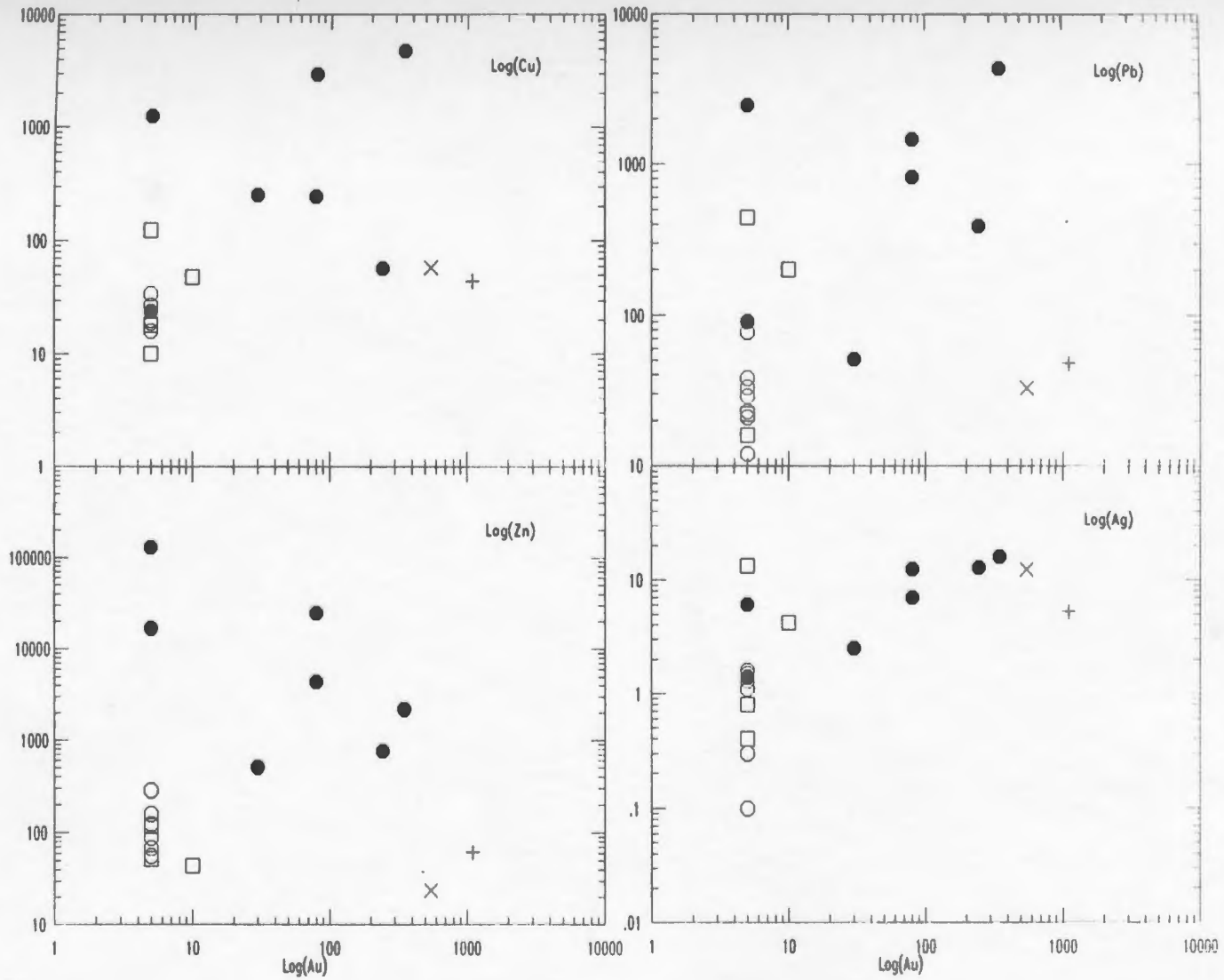
Figure 5.5. Variation diagrams involving Au (ppb) and Ag vs. the base-metals. Symbols as in Figure 5.1.
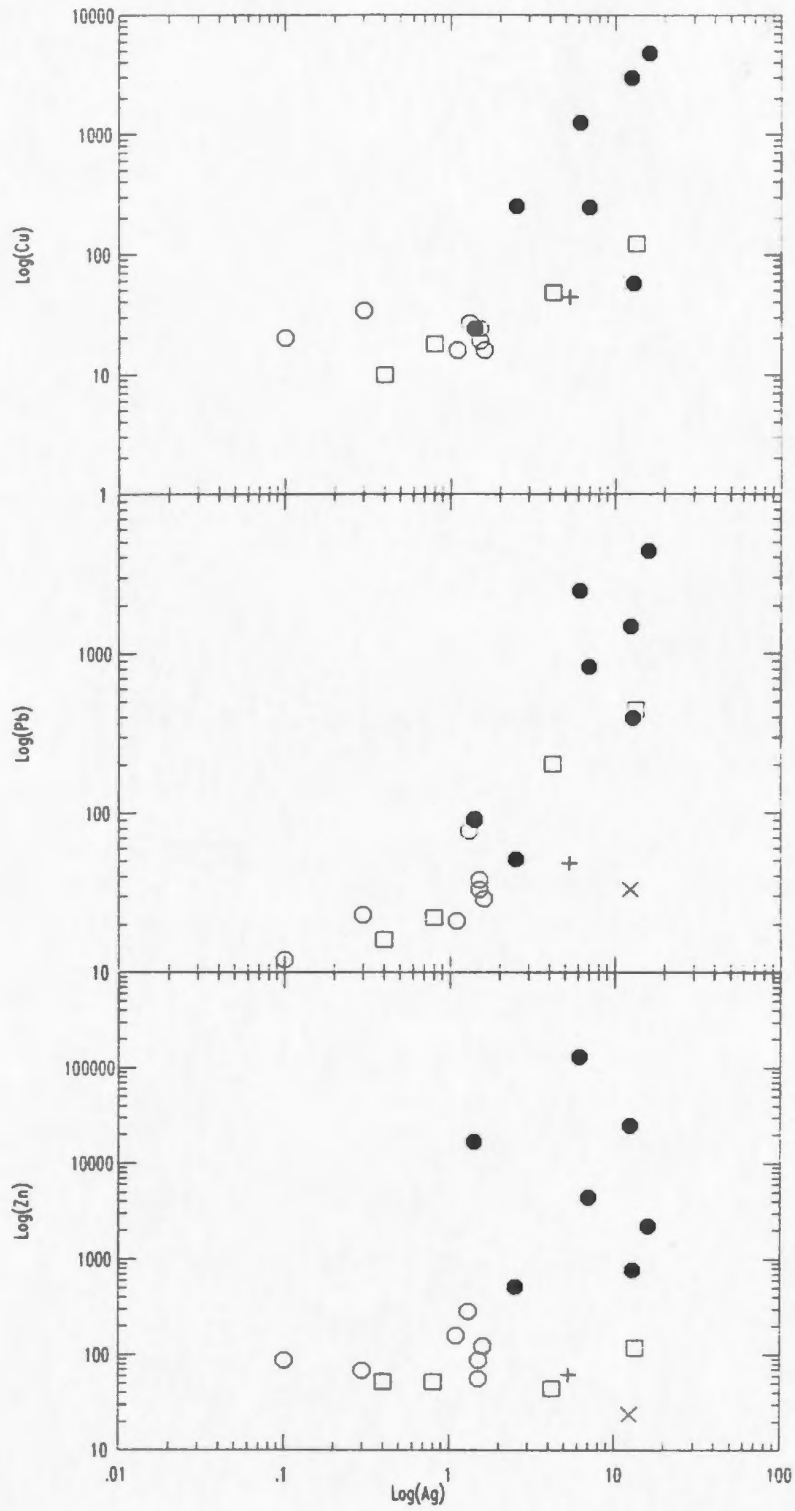
Figure 5.5. (continued)

from mafic-dominant and felsic-dominant Au-Ag mineralization. This diagram works better when the Ag and Au values are above $\approx$ 30 ppm and 500 ppb, respectively. At lower values, as in the Tickle Point Formation, there is almost complete overlap of all the host regions. Swinden et al. (1988) also use a plot of Zn/Pb vs. Au/Ag to delineate host rock lithologies (Figure 5.6). The Shoal Brook Showing samples plot entirely within the felsic dominated field, while the Frenchman Head and Selco Showing specimens plot in both the felsic-dominant and mixed mafic-felsic fields. The two samples from Fish Cove and Tilt Point plot in or near the "Fox Neck" type field, which is indicative of metal-poor deposits with low Zn/Pb and high Au/Ag ratios (Swinden et al., 1988).

The mafic transition elements (Cr, Co, Ni) generally have low abundances, with the highest concentrations occurring at Frenchman Head where the mineralization is hosted in andesitic rather than felsic rocks. The elements are correlative with each other. They show no association with Au, but Co and Ni both have a weak positive correlation with Ag (Figure 5.7). Above background Ni values display a weak correlation with Zn, Pb, and Cu, whereas neither Cr nor Co show any visible trends with the base-metals.

The mobile trace elements have large variations in concentrations implying a high degree of mobility. Nevertheless, Ba exhibits a strong positive correlation with Rb and a weaker correlation with Sr. Ba vs. Zr shows little
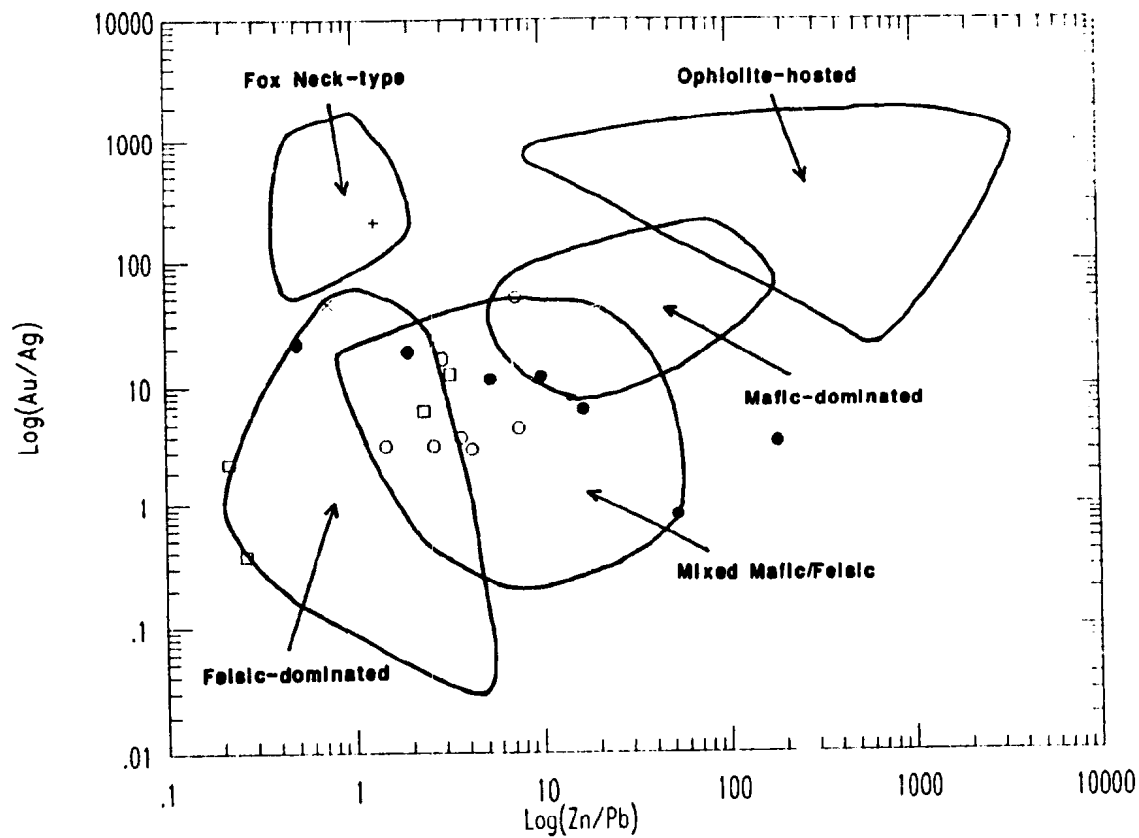
Figure 5.6. Zn/Pb vs. Au/Ag diagram taken from Swinden and
Kean (1988). The plot displays the increasing Zn/Pb and
Au/Ag ratios as the host rocks become more basic. The Tickle
Point Fm. samples plot mainly in the felsic-dominated and
mixed mafic-felsic fields. Symbols as in Figure 5.1.
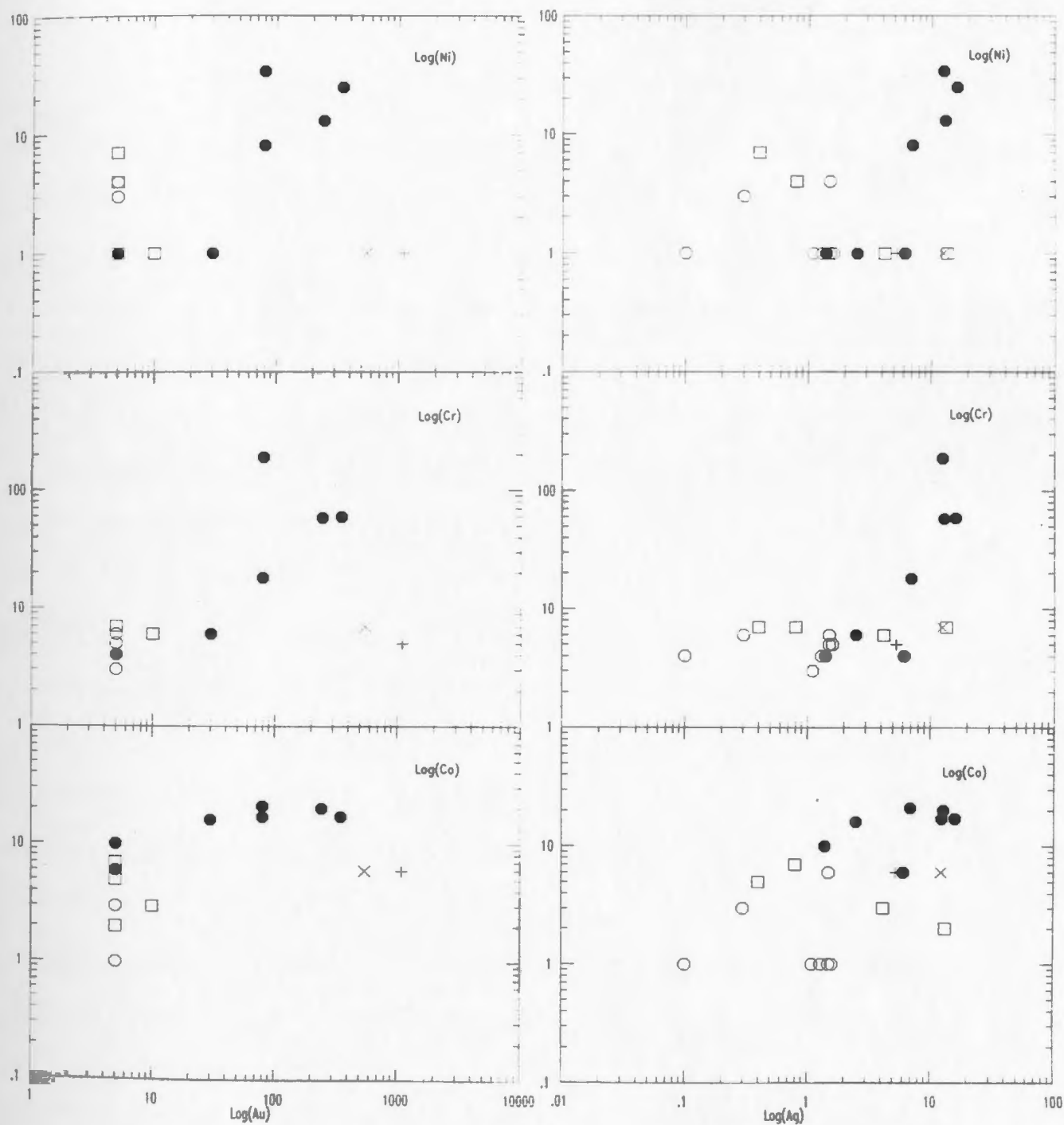
Figure 5.7. Variation diagrams of Au (ppb) and Ag plotted against Co, Ni, and Cr. Symbols as in Figure 5.1.

183

variations (*i.e.* parallel to Zr), suggesting that Zr remained fairly constant while Ba was mobile.

Zr vs. Y, Ce, and La (Figure 5.8) illustrates moderately strong positive relationships between the immobile elements and the REE (where Y represents the HREE). Zr vs. Zn (Figure 5.8) displays a wide scatter of data points, although there is a very weak positive trend of increasing Zn with increasing Zr within the Frenchman Head samples. Zr vs. Pb and Cu (Figure 5.8) display no visual trends but on the Zr vs. Pb plot, the Frenchman Head samples display a weak negative correlation of decreasing Pb with increasing Zr.

Figure 5.9 is a plot of F vs. Zn and illustrates a wide scatter of data points. There is a weak positive correlation between Zn and F within the Frenchman Head samples. This may possibly indicate that F was a constituent within the metal-bearing mineralizing fluids at Frenchman Head. F-bearing solutions are thought to complex HREE (Taylor and Fryer, 1983) and when F is plotted against Y (*i.e.* HREE) there is a weak, steep, positive correlation within the Frenchman Head samples, and a very weak, shallow positive trend within the Selco Showing samples.

5.2.1.3 REE and Associated Trace Elements

Eight samples from the Tickle Point Formation were analyzed for REE and selected trace elements (Appendix IV and Table 3.3). Four samples are from the Selco Showings, two are
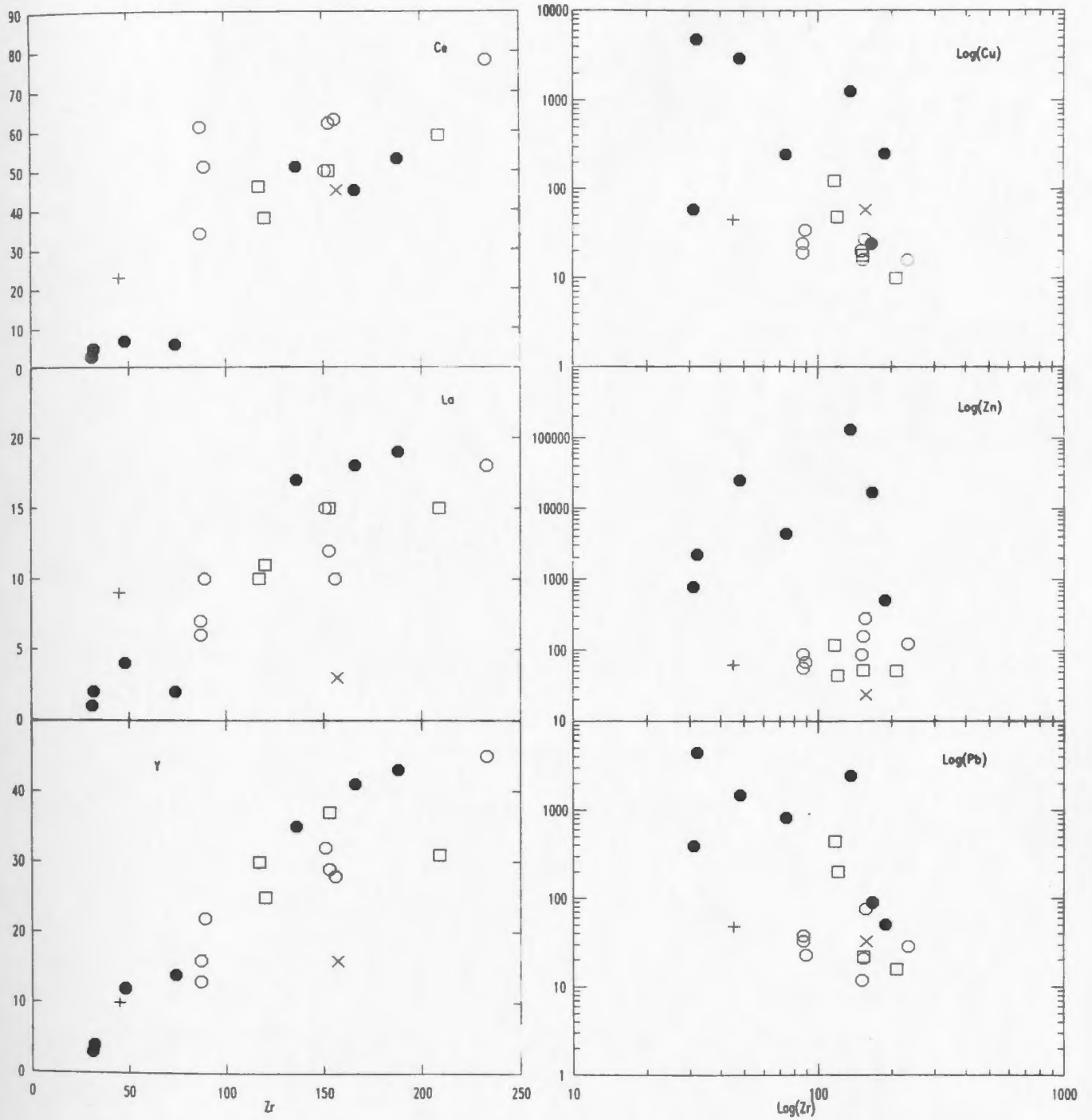
Figure 5.8. Zr vs. selected trace elements and the base-metals. Symbols as in Figure 5.1.
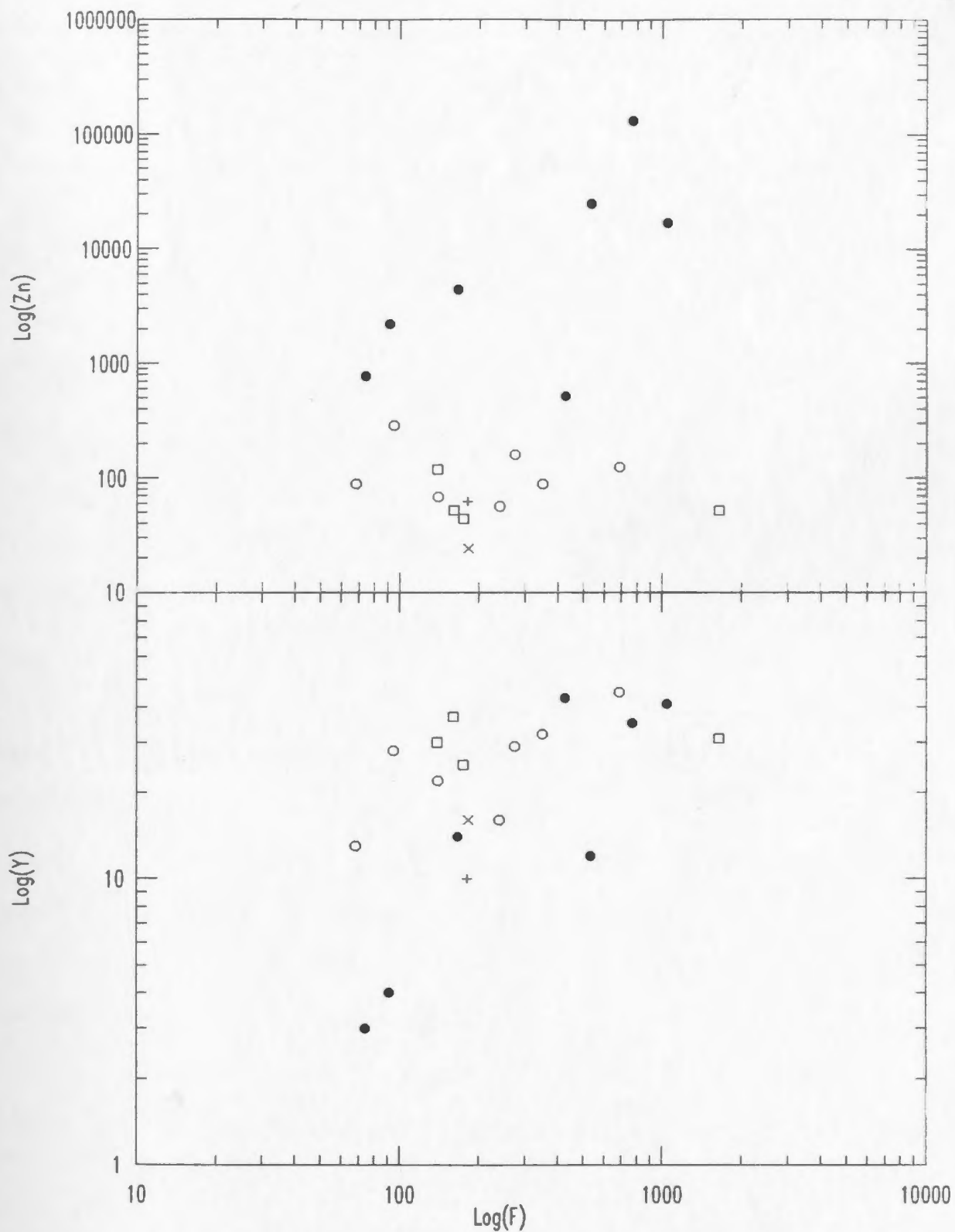
Figure 5.9. F vs. Zn and Y for samples from the Tickle Point Fm. Symbols as in Figure 5.1.

from Shoal Brook, and one each from Frenchman Head and Tilt Point.

The four Selco Showing samples display identical REE and extended REE patterns (Figure 5.10). The profiles display LREE enrichment, flat MREE and HREE patterns, and small negative Eu anomalies. The extended REE profiles have a Nb (and Ta) depletion and Th enrichment, all with respect to La. The extended patterns also exhibit slight Zr (and Hf) enrichment and a small negative Y anomaly.

The REE and extended REE profiles are almost identical to the patterns defined for the dacitic to felsic volcanic rocks (Chapter 3); consistent with their setting within the felsic units of the Tickle Point Formation. The overall REE abundances are lower in the mineralized rocks, probably because of the addition of the sulphide minerals. REE abundances are much lower in sulphide minerals than in silicate minerals (Henderson, 1984).

REE and extended REE diagrams from the other areas display more varied patterns (Figure 5.11). The Shoal Brook samples have Nb (and Ta) depletions, Th enrichments, and overall slight LREE enriched profiles. One sample (SS88-012) has a slight negative Eu depletion, whereas the other sample has a small positive Eu pattern. The Tilt Point sample also has a slight Nb (and Ta) depletion, a large Th enrichment, a large Zr (and Hf) enrichment, a negative Eu spike, and an overall U-snaped REE profile. The U-shaped plot is similar to
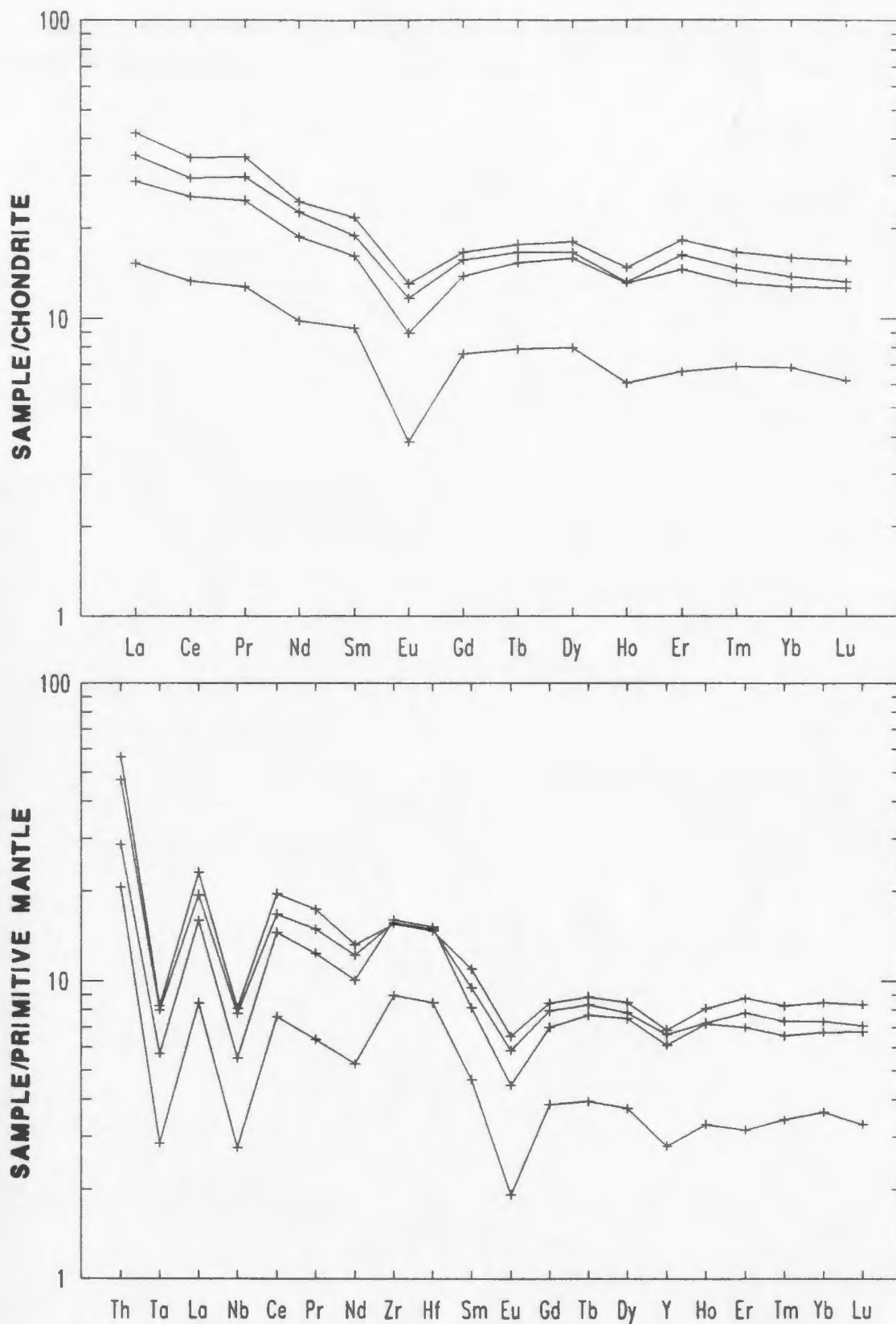
Figure 5.10. Chondrite-normalized REE and primitive mantle-normalized extended REE profiles for mineralized samples from the Selco Showings.
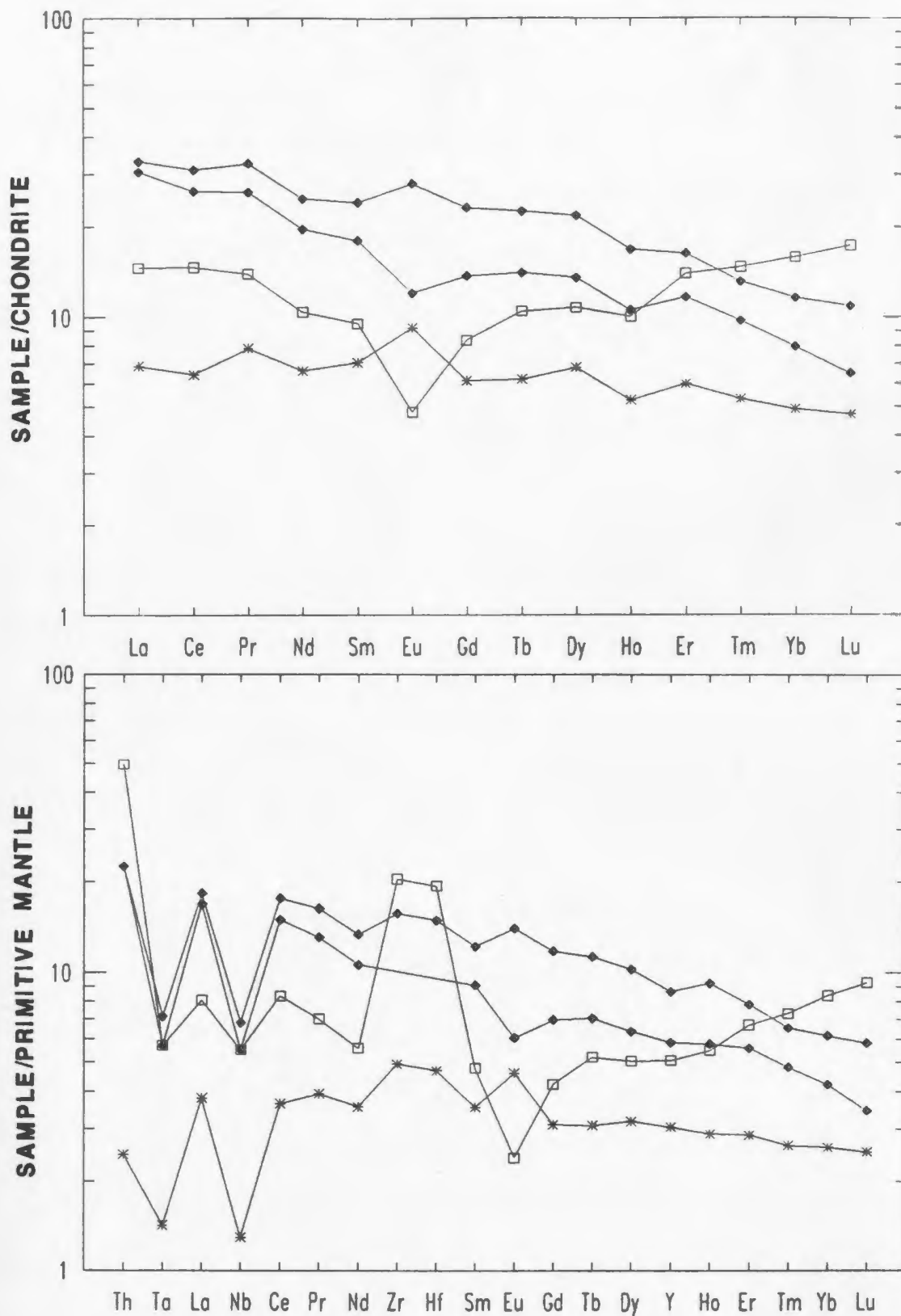
Figure 5.11. REE and extended REE patterns for samples from Shoal Brook (filled diamonds), Frenchman Head (asterisk), and Tilt Point (open squares).

the "near birdwing" profile described by Schade et al. (1989)
for the sillimanite-cordierite host rocks that are proximal to
the massive sulphide mineralization at Prieska, South Africa.
(The birdwing pattern is defined by Baker and Hellingwerf
(1986) as profiles having negative LREE slopes, large negative
Eu depletions, and positive HREE slopes.) The HREE enrichment
is probably due to HREE deposition as opposed to LREE and MREE
extraction. The HREE were likely transported in solution as
CO_3^{2-} or F complexes (Taylor and Fryer, 1983). The Eu depletion
is probably a function of feldspar destruction; the more
complete the destruction, the greater the negative Eu anomaly.
The other MREE are apparently uneffected by plagioclase
feldspar destruction as the sample/chondrite values for Sm and
Gd are that of an unaltered feldspar (see Fig. 1.5, Henderson,
1984).

The birdwing profiles for the Prieska samples appear to
be characteristic of the alteration zone around the
mineralized section and not the mineralized zone itself (see
figures 7 and 10 of Schade et al., 1989). Graf (1977) also
illustrated a birdwing pattern for a Cu-rich sulphide sample
from the Wedge deposit, in the Bathurst mining camp. The Kidd
Creek deposit also exhibits birdwing profiles in both the
stringer zone rhyolites and the chlorite schists from the
chlorite zone (Campbell et al., 1984). These patterns from the
Kidd Creek deposit may be a result of LREE and MREE
mobilization during intense hydrothermal alteration (Campbell

et al., 1984). Within the sillimanite-cordierite rock surrounding the Prieska deposit, only samples taken from the Smouspan Member within ≈ 56 m of the mineralized section exhibit birdwing profiles (Schade et al., 1989). This zone probably represents a metamorphosed hydrothermal alteration zone which would have originally underlain the massive sulphide mineralization.

The Frenchman Head profile has a very slight LREE enrichment, a flat MREE and HREE profile, and small Eu, Zr, and Hf enrichments. The extended patterns have small Nb (and Ta) depletions and Th is depleted with respect to La but is enriched with respect to Nb. This sample is very similar in shape and overall REE concentration to the mafic REE patterns exhibited by the relatively unaltered Frenchman Head examples. It is also similar in shape and REE concentration to non-arc tholeiite patterns present within the Wild Bight Group of central Newfoundland (Swinden, 1988).

5.2.2 Sam Head Formation

5.2.2.1 Introduction

Thirty nine samples were analysed from the Sam Head Formation (Appendix III and Table 5.2). Thirty samples are from the Winter Hill Showing, three each from Winter Hill East and West, two from Prospect #5, and one from Winter Hill North.

The thirty samples from the Winter Hill Showing can be

Table 5.2. Average compositions for mineralized samples from Winter Hill (1), Winter Hill West (2), Winter Hill East (3), Winter Hill North and Prospect #5 (4), and relatively unmineralized carbonate/calc-silicate samples from Winter Hill (5), (-1 = less than one).

Sample #	1	2	3	4	5
SiO2 (wt.%)	32.66	53.01	34.63	31.27	38.48
TiO2	0.11	0.16	0.3	0.08	0.36
Al2O3	2.76	5.9	5.17	2.29	7.17
Fe2O3(total)	12.48	22.23	16.54	20.25	3.59
MnO	0.68	0.09	1.3	0.82	0.57
MgO	14.83	1.67	17.39	14.72	21.44
CaO	10.6	0.5	8.28	7.83	12.63
Na2O	0.05	0.14	0.09	0.8	0.53
K2O	0.05	1.69	0.08	0.22	0.36
P2O5	0.08	0.03	0.08	0.04	0.08
LOI	11.12	11.17	11.75	15.25	12.7
Total	83.75	97.18	95.56	93.56	97.65
Cr(ppm)	9	6	31	5	11
Ni	1	-1	2	-1	2
Co	7	19	4	2	5
V	15	8	71	6	52
Cu	10513	637	920	1204	62
Pb	10688	446	15027	842	655
Zn	58834	6414	7113	11106	1844
Cd	272	27.9	25	42.6	7.9
Mo	13	5	21	4	5
Rb	2	46	3	4	14
Ba	34	360	151	63	149
Sr	19	8	9	44	77
Ga	19	31	24	17	12
Li	7	10	10	3	34
Nb	-1	-1	-1	-1	5
Zr	35	140	24	67	117
Y	6	14	7	12	22
Th	1	2	2	-1	4
La	2	10	3	6	12
Ce	9	40	20	28	26
F	1081	425	1916	1829	1841
Be	1.1	0.9	3.6	2.3	1.8
Ag	55	0.93	47.17	6.97	1.93
Au(ppb)	55.94	17	120	10	-5

divided into seven lower (stringer) zone samples and 23 upper zone disseminated to massive layered sulphide) samples. The lower zone samples are rocks composed mainly of recrystallized quartz containing disseminations and stringers of pyrite and chalcopyrite. The upper zone samples are composed of a variety of carbonate and/or Ca-Mg-silicate rocks containing disseminated to massive sulphide (dominantly Zn-Pb) mineralization. Two of the Winter Hill West samples (584072 and 584073) are semi-massive pyrite with minor chalcopyrite. The other sample (584075) is a fine-grained, siliceous, layered rock containing minor pyrite, sphalerite, and galena. Of the three samples from Winter Hill East, one (584076) is a Ca-Mg-silicate-rich sample containing pyrite, galena, and sphalerite; another (584077) is massive pyrite with minor sphalerite and galena; and the third sample is a sheared host rock containing pyrite ± sphalerite and galena. The Winter Hill North sample (584079) contains layered magnetite with minor sphalerite ± chalcopyrite and galena in a Mg-silicate-rich host. Of the final two samples from Prospect #5, one specimen (584097) contains semi-massive pyrite in a siliceous gangue, and the second sample (584099) is a Ca-Mg-silicate-rich rock containing minor visible sphalerite, from a marble outcrop ≈ 200 metres north of the semi-massive pyrite outcrop.

Base-metal, trace, and REE systematics will be approached in the same method as was used for the Tickle Point Formation.

5.2.2.2 Base-metals and Trace Elements

Unlike samples from the Tickle Point Formation, there are no strong correlations between the base-metals (Figure 5.12). Some elevated Zn values have a positive association with elevated Pb values, whereas all the low and some elevated Zn values display a flat trend (i.e. parallel to the Zn axis) with low Pb values. Cu vs. Pb may also display two separate trends. There is one trend that is parallel to the Cu axis at an average value of $\approx$ 50 ppm Pb and Cu values ranging from 10 to 140000 ppm. The other possible trend is a very weak one at average Pb values of $\approx$ 10000 ppm and Cu values of $\approx$ 500 ppm. Zn vs. Cu gives a wide scatter of data points resulting in no inherent trend. Histograms of the three base-metals (Figure 5.13) illustrate that Pb has two populations, Zn may have two populations, and Cu has basically one population. Since the mineralization is regionally underlain by the felsic Tickle Point Formation, which should originally be enriched in Zn-Pb over Cu, then the two populations for Zn and Pb may represent background and mineralization trends. The one Cu population may be a mineralization trend with the background values becoming lost within this population.

A Pb-Cu-Zn ternary diagram (Figure 5.14) displays the VMS nature of the Winter Hill area showings, and it also illustrates the typical VMS Cu and Zn-Pb zonation within the Winter Hill Showing. The Winter Hill East Showing has higher Pb/Zn ratios than the Winter Hill Showing while samples from
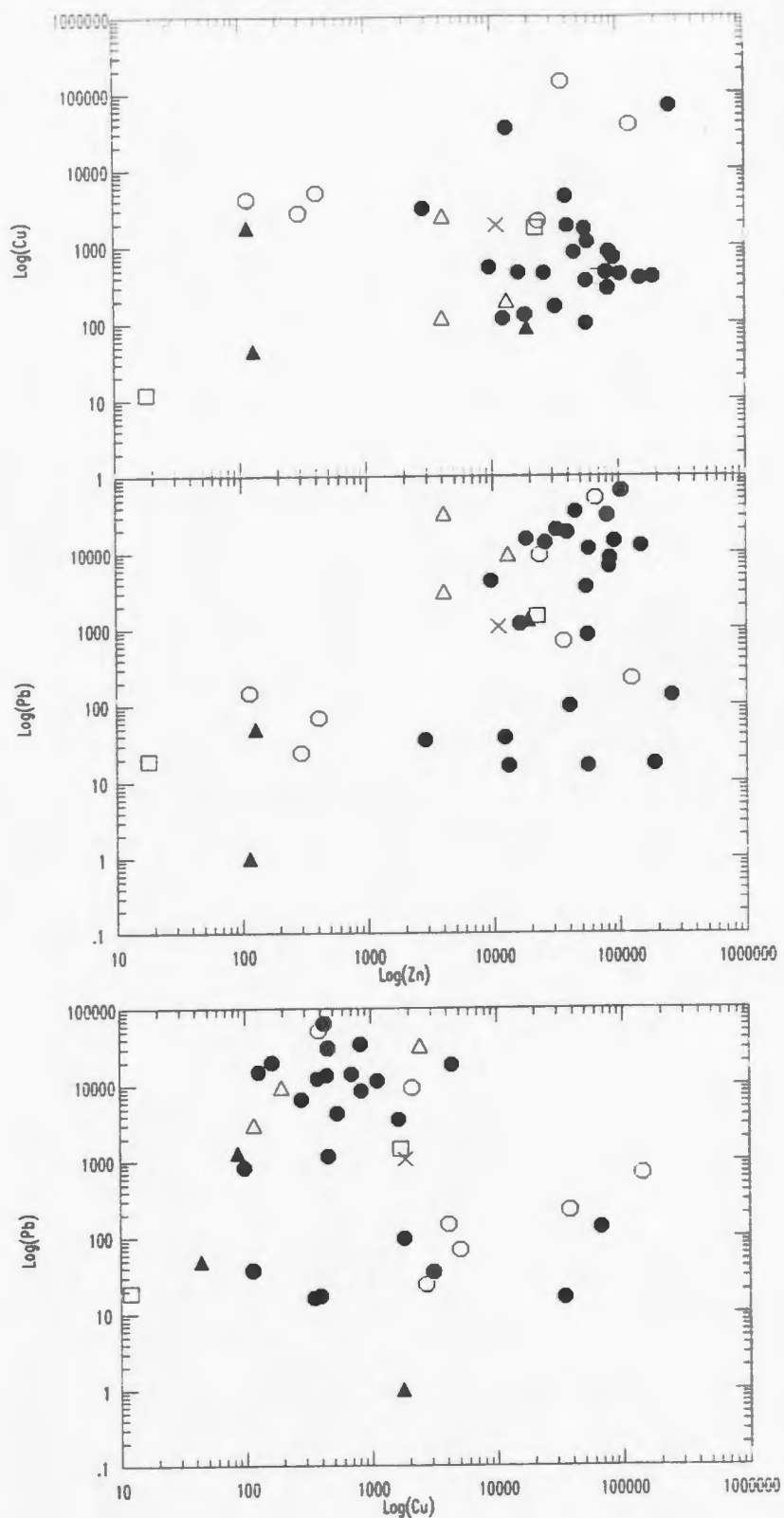
Figure 5.12. Base-metal variation plots for samples from the Sam Head Fm. Open circles = Winter Hill (lower zone), filled circles = Winter Hill (upper zone), open triangles = Winter Hill East, filled triangles = Winter Hill West, X = Winter Hill North, and open squares = Prospect #5.
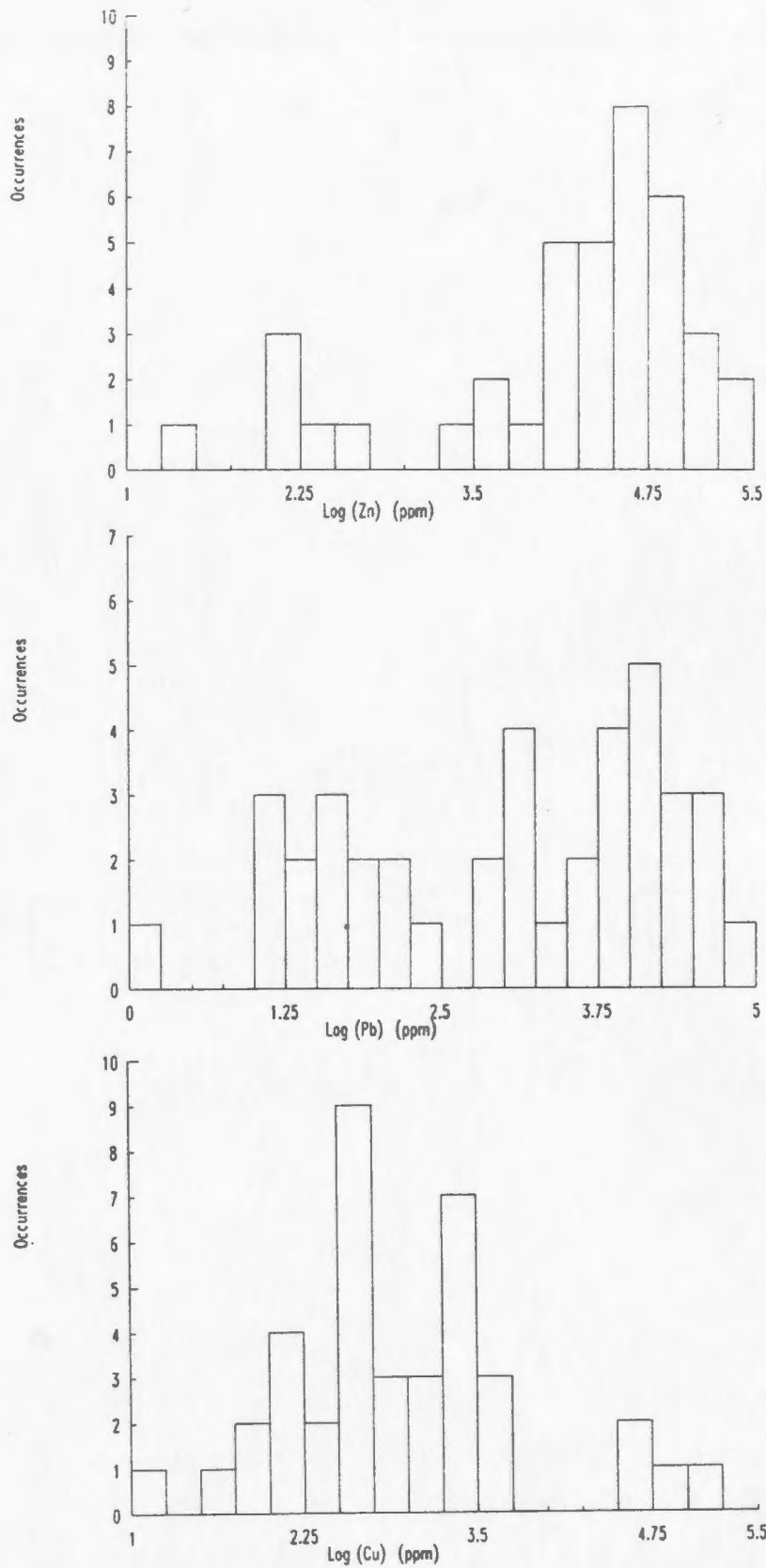
Figure 5.13. Histograms of Zn, Cu, and Pb for mineralized samples from the Sam Head Fm. Each histogram has a total of 39 samples.
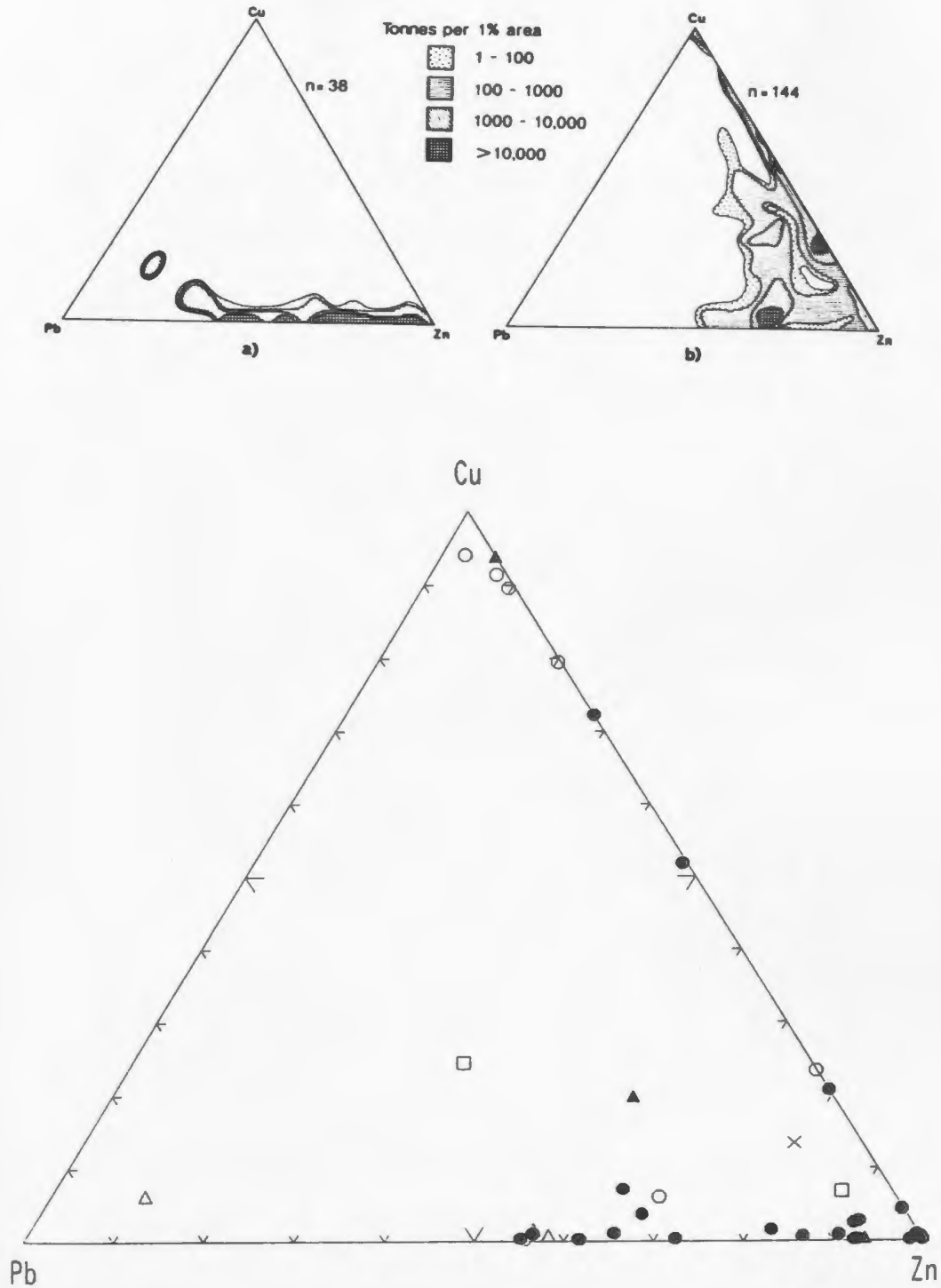
Figure 5.14. Pb-Cu-Zn ternary diagram for mineralized Sam Head Fm. samples. Ternary diagrams (a) and (b) represent bulk compositions for sediment-hosted stratiform Pb-Zn deposits (a) and VMS deposits of the Abitibi Belt, the New Brunswick area, Norwegian Caledonides, and the Green Tuff Belt of Japan (b) (taken from Lydon, 1983). Contours are total tonnes of ore metals per 1% area of the diagram. Symbols as in Figure 5.12.

Winter Hill West have variable Pb, Zn, and Cu contents.

Cadmium distribution is reflected in the partitioning of the base-metals. Cd has a strong positive trend with Zn but is not associated with either Cu or Pb (Figure 5.15). With respect to Au and Ag, Cd has no correlation with either, but there may be a weak trend of Ag with Cd values from the lower zone at the Winter Hill Showing.

Au has no association with either Zn or Cu and may possibly have a very weak positive trend with Pb (Figure 5.16). Ag has weak to moderate positive relationships with Pb and Zn but creates a scatter of data points when plotted against Cu. Au vs. Ag displays a weak positive correlation. The weak association between Au and Ag, and the weak relationship between Ag and Zn and Pb suggests that the precious metals are more closely related to the massive sulphide mineralization of the upper zone than with the Cu-rich stringer type mineralization of the lower zone at the Winter Hill Showing.

The mafic transition elements are very low in abundance in the Winter Hill area. Concentrations for each element rarely exceed 10 ppm with overall Cr + Co + Ni contents (for each sample) generally below 20 ppm. Since the lens is situated within mafic tuffs, higher concentrations of Cr, Co, and Ni might be expected. The low concentrations may imply that the mineralizing fluids passed mainly through felsic rocks (i.e. Tickle Point Formation) which stratigraphically
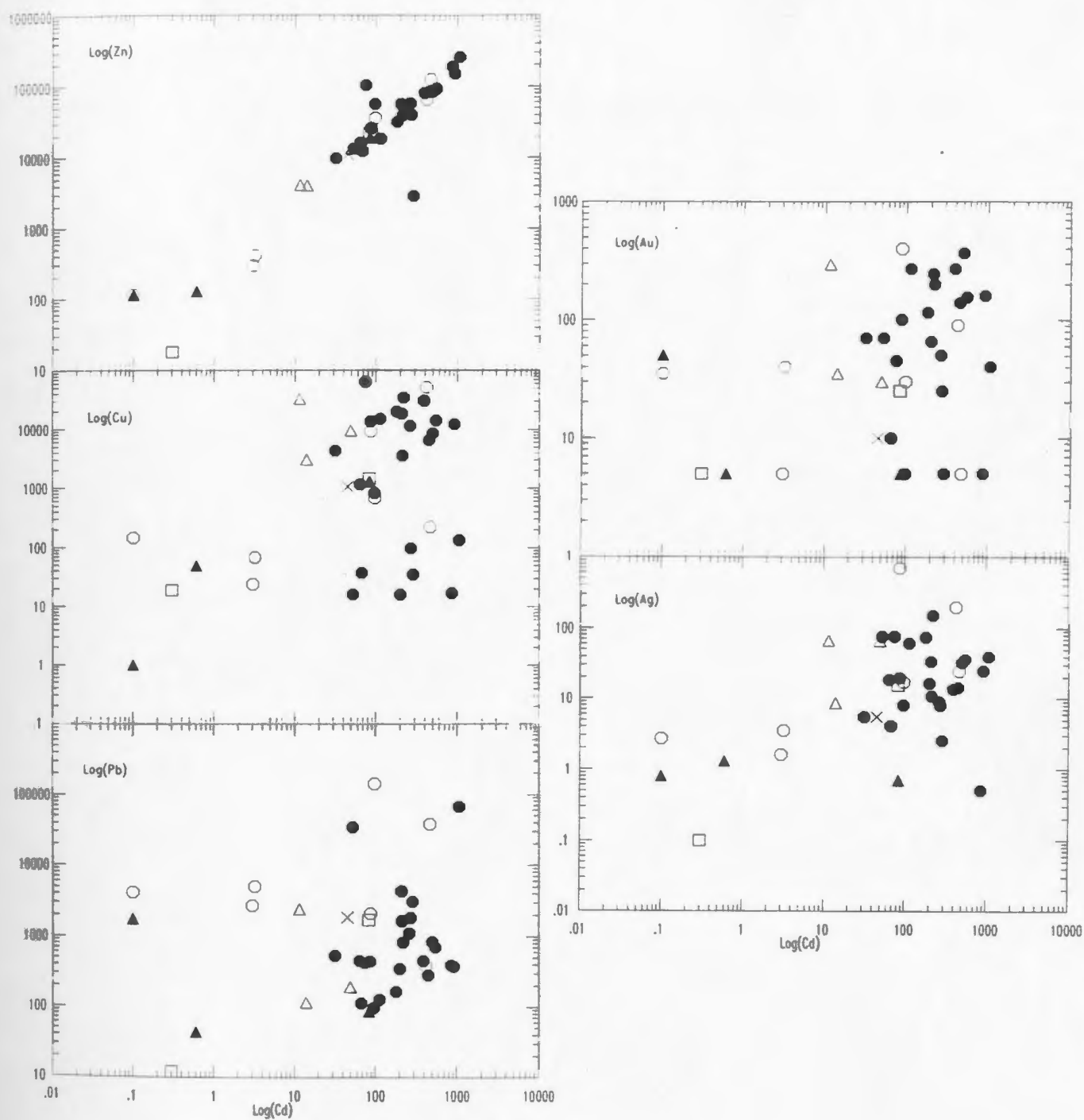
Figure 5.15. Variation diagrams of Cd vs. Au (ppb), Ag, and the base-metals. Symbols as in Figure 5.12.
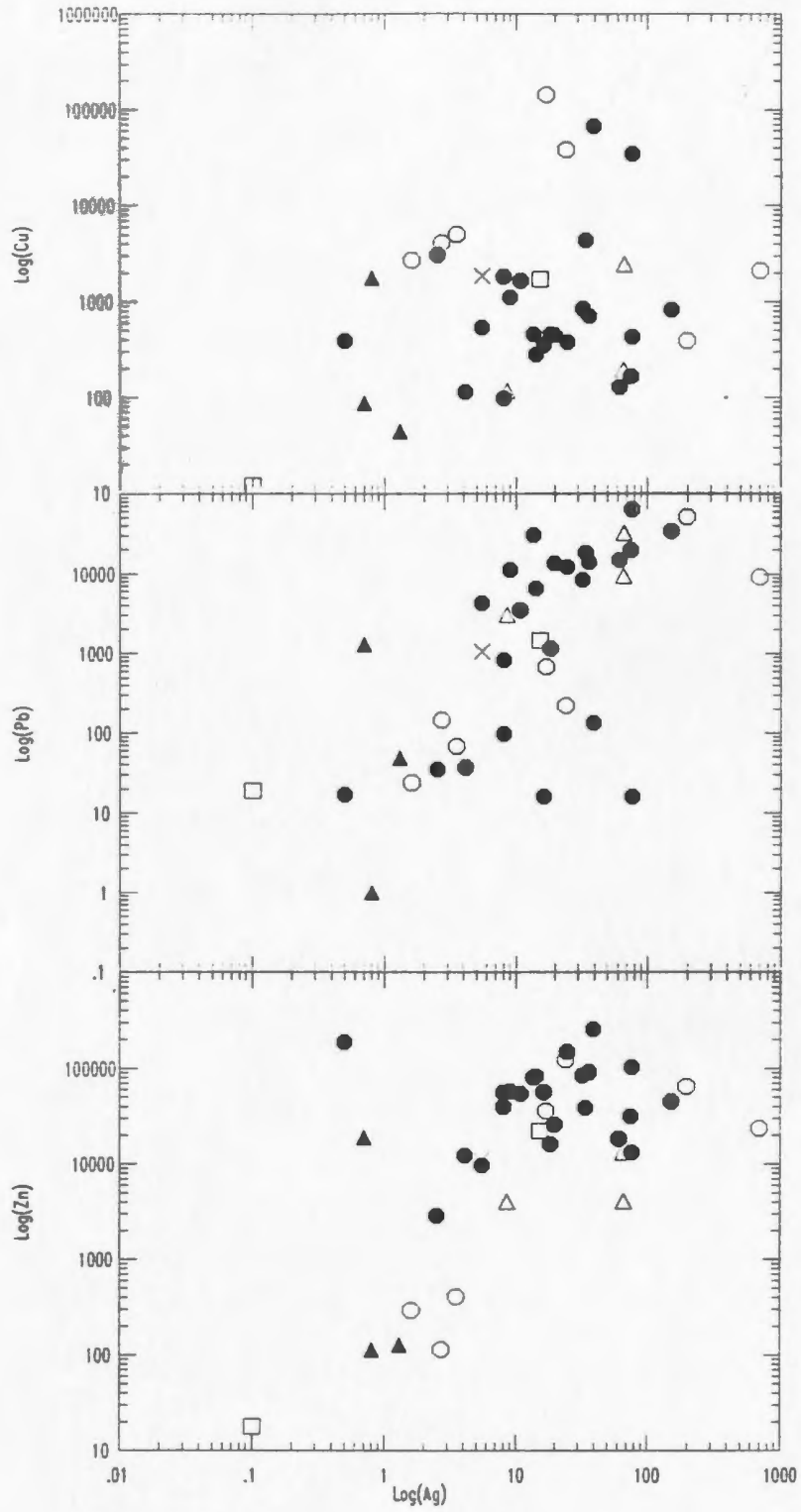
Figure 5.16. (continued)
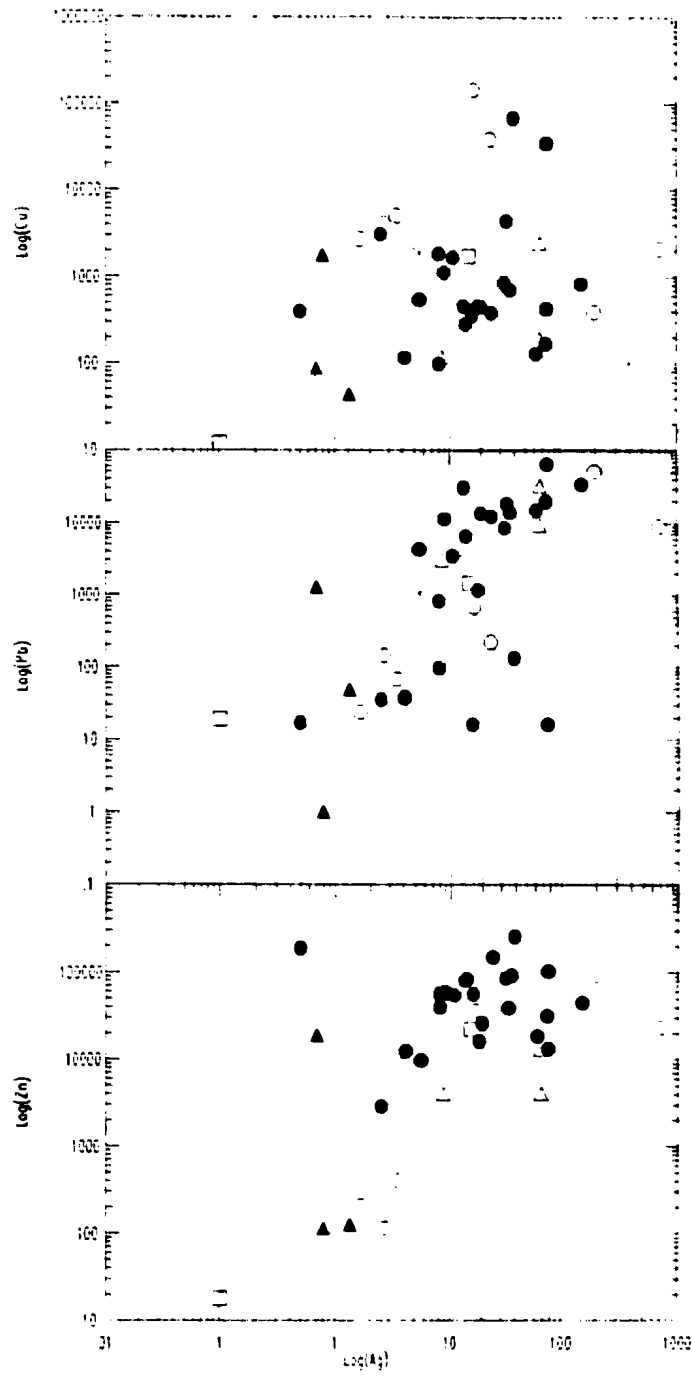
Figure 5.16. (continued)

underlie the mafic rocks.

Zr exhibits positive trends with Ce and Y but there is a large scatter in the data points at low Zr, Ce, and Y values (Figure 5.17). Figure 5.17 is also a plot of Zn vs. F to aid in determining whether F may have been a component of the mineralizing fluids. Elevated Zn and F values are related but within the large data cluster there is no discernable trend.

5.2.2.3 REE and Associated Trace Elements

Ten mineralized samples were analyzed for REE and selected trace elements (Appendix IV and Table 3.3). Four samples are from the Winter Hill Showing, four are from Winter Hill East, and two are from the Winter Hill West Showing.

REE and extended REE diagrams for mineralized Winter Hill samples are displayed in Figure 5.18. The REE profiles are all very similar as they have slight LREE enrichment, flat HREE patterns, and very slight positive Eu anomalies. The extended REE profiles are also similar except for a few differences. Two samples (584037 and 584067) have elevated Zr (and Hf) values, whereas sample 584046 has a large negative Zr anomaly. All the samples have Nb and Ta depletions, and all but one sample have a Th enrichment, all with respect to La. The patterns indicate that mineralization occurs in subduction-related volcanic rocks (Swinden et al., 1989).

Figure 5.19 illustrates REE and extended REE plots for samples from Winter Hill East. The REE diagram displays
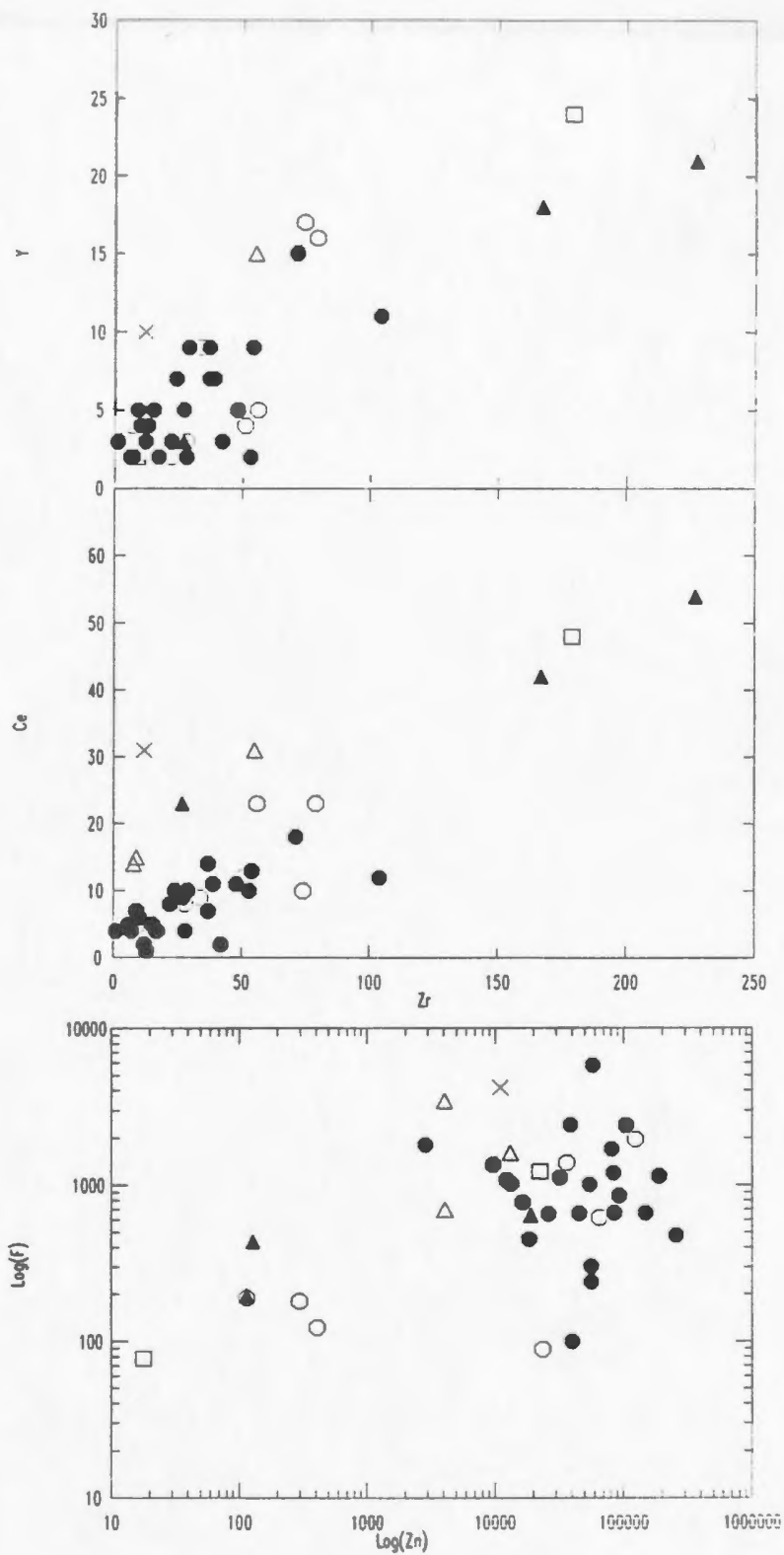
Figure 5.17. Zr vs. Y, Ce, and F for mineralized samples from the Sam Head Fm. Symbols as in Figure 5.12.
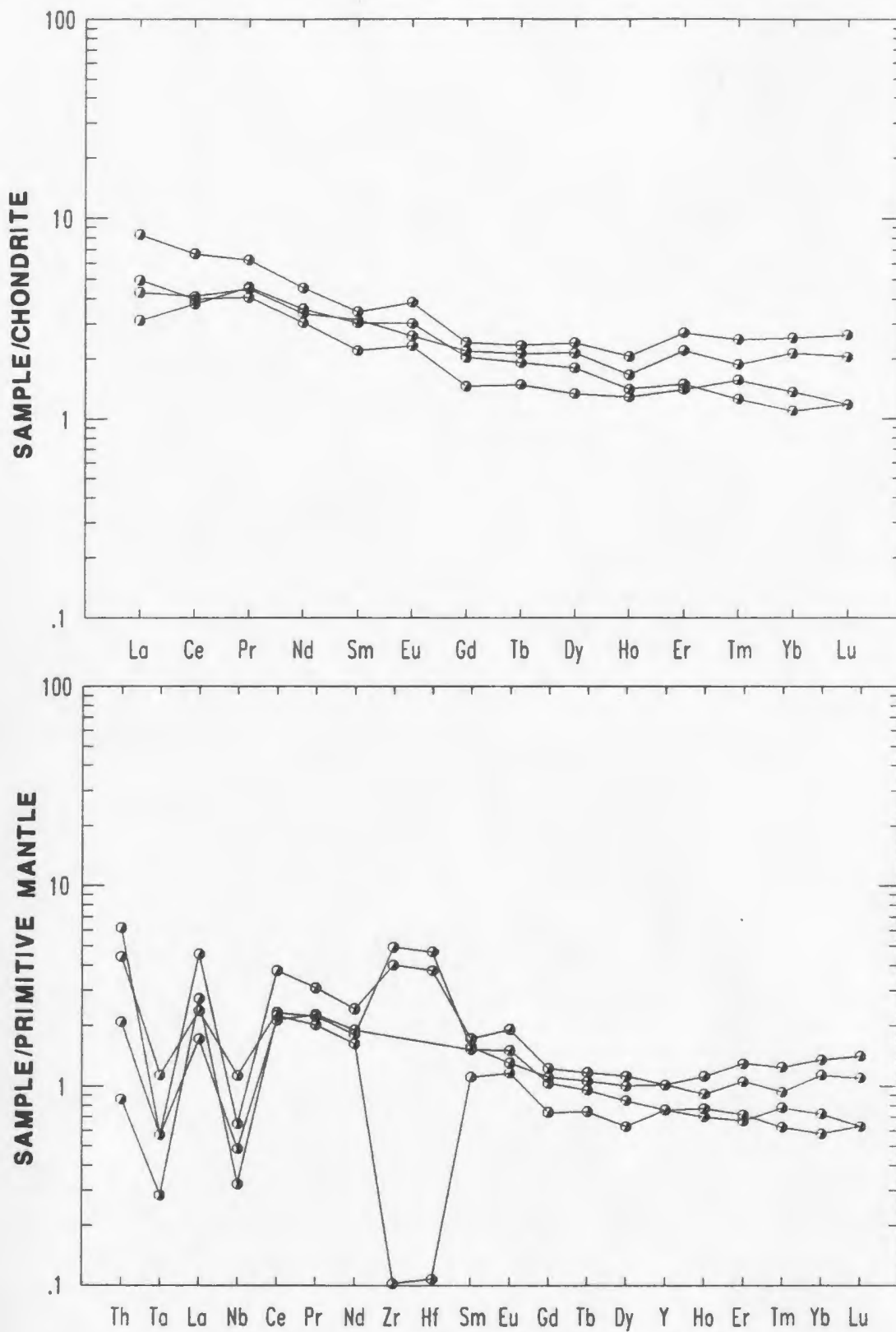
Figure 5.18. Chondrite-normalized REE and primitive mantle-normalized extended REE patterns for mineralized samples from the Winter Hill Showing.
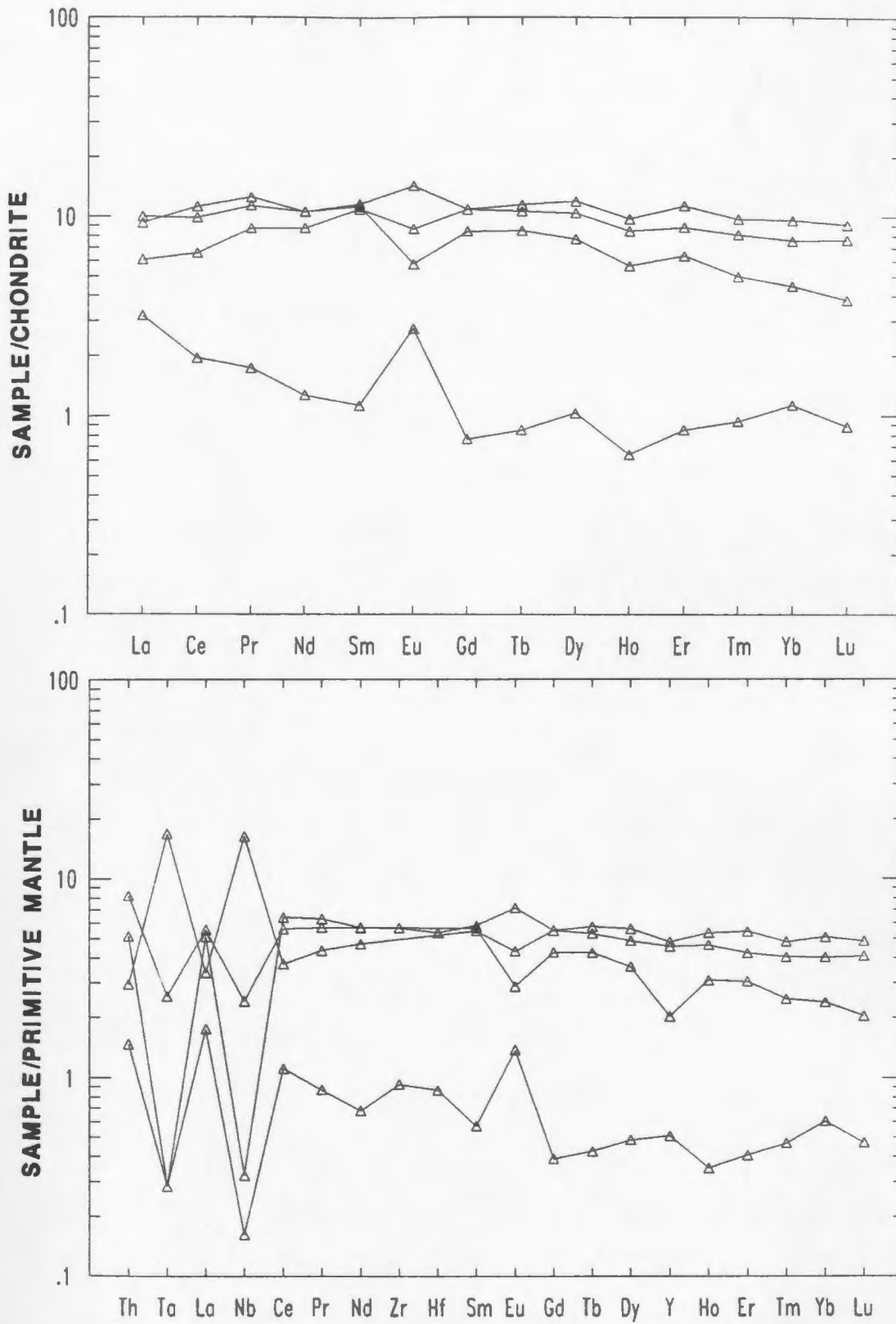
Figure 5.19. REE and extended REE profiles for mineralized samples from the Winter Hill East Showing.

relatively flat patterns at ≈ 10X chondrite, whereas sample 584076 has a negative LREE slope (i.e. LREE enriched), a positive Eu anomaly, a flat MREE and HREE pattern, and overall lower REE concentrations. Sample 584076 is a sample of semi-massive pyrite, galena, and minor sphalerite and chalcopyrite, while the other three samples basically contain disseminated pyrite in a siliceous host rock. Therefore the higher percentage of the sulphide minerals will account for the lower REE abundances. The positive Eu anomaly is probably due to the high Pb concentrations. Pb in VMS deposits is generally thought to have been leached from feldspars as fluids circulate through a volcanic pile. The positive Eu anomaly also indicates that feldspars were being leached since Eu is strongly enriched over the other REE in the feldspar lattice. (In addition, when the REE profile for sample 584076 is compared to that of a plagioclase crystal extracted from the Palisades Sill, New Jersey, (figure 3 of MacRae and Metson, 1985), the profiles are very similar while the feldspar crystal has a slightly larger Eu anomaly.) Graf (1977, figure 10) described Pb-rich samples from the Brunswick No. Six deposit that have large positive Eu anomalies. The large Eu spikes are associated only with galena and do not correlate with the major element chemistry, so therefore it was probably not fractionated by any of the precipitating phases (Graf, 1977). But Graf (1977) also has REE profiles for feldspar crystals, which if leached, could easily account for the shape

of the profile exhibited by sample 584076.

The extended REE profiles for two samples (SS88-124 and 534076) exhibit large Nb (and Ta) depletions, whereas one sample has a small Nb depletion (584078), and one sample (SS88-123) with a suspect positive Nb anomaly (see Appendix V for explanation). Th values are slightly enriched in two of the samples (SS88-124 and 584078) and slightly depleted, with respect to La, in a third sample.

Winter Hill West samples (Figure 5.20) have identical REE and extended REE patterns with only approximately 2X difference in overall REE concentrations. The profiles have negative LREE slopes, small negative Eu anomalies, positive HREE slopes, but an overall LREE enrichment. The extended patterns have identical Nb depletions and Th enrichments. The HREE enriched patterns are similar to the "near birdwing" REE profile from Tilt Point, although the Tilt Point sample has a slight overall HREE enriched pattern. The two Winter Hill West samples are also similar to the Selco Showing samples not only in shape, but also in overall REE abundances. The Selco Showing examples have flat HREE patterns, in contrast to the HREE enriched pattern from the Winter Hill West samples.

5.2.2.4 Carbonate/Ca-Mg-silicate Rocks

Carbonate/Ca-Mg-silicate rocks are an inherent part of the mineralized package of the Winter Hill Showing, yet they are generally free of any appreciable sulphide concent..ations
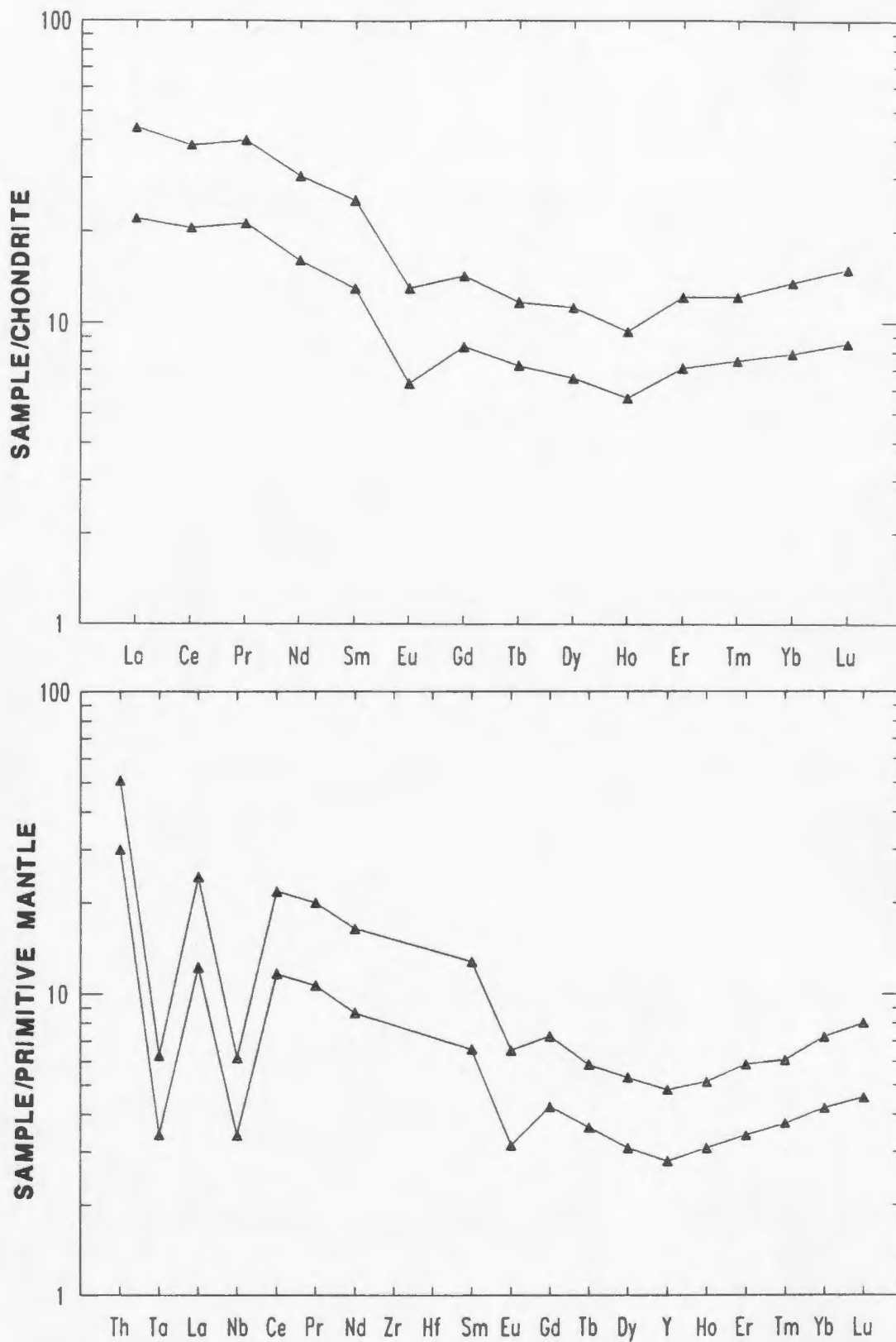
Figure 5.20. REE and extended REE patterns for samples from the Winter Hill West Showing.

(*i.e.* most have less than 1 wt.% total base-metals - *c.f.* Appendix III).

The sixteen rocks analyzed have large variations in most of their major elements due to the range in mineralogy within the rock types. The thirteen samples from Winter Hill have an SiO_2 range between 3.60 and 61.60 wt.%, MgO between 4.87 and 40.93 wt.%, and CaO from 0.29 to 35.89 wt.%. These numbers reflect the changes from carbonate to Ca- and Mg-rich silicates.

Variation diagrams involving SiO_2 and MgO (Figures 5.21 and 5.22) exhibit most of the variations between the rocks. TiO_2, Al_2O_3, P_2O_5, and the alkalis all display a wide data point scatter when plotted vs. SiO_2. Due to low TiO_2 and alkali values, most samples plot along or near the SiO_2 axis, whereas the larger Al_2O_3 and P_2O_5 values plot in the high SiO_2 range. CaO, MgO, and MnO display very weak negative trends with SiO_2 while LOI has a moderate negative association with silica. High MgO, CaO, and LOI values at low SiO_2 are representative of dolomitic compositions $((Ca,Mg)CO_3)$, whereas variable MgO and CaO at higher SiO_2 values are indicating the presence of forsterite, serpentine, tremolite, diopside, and other Ca-Mg-silicates. Only Fe_2O_{3total} has a weak to moderate positive relationship with increasing SiO_2. One sample containing 10.50 wt.% Fe_2O_{3total} is located within a diabase dyke so there may be possible contamination from the dyke.

MgO vs. CaO, TiO_2, MnO, P_2O_5, and the alkalis, illustrate
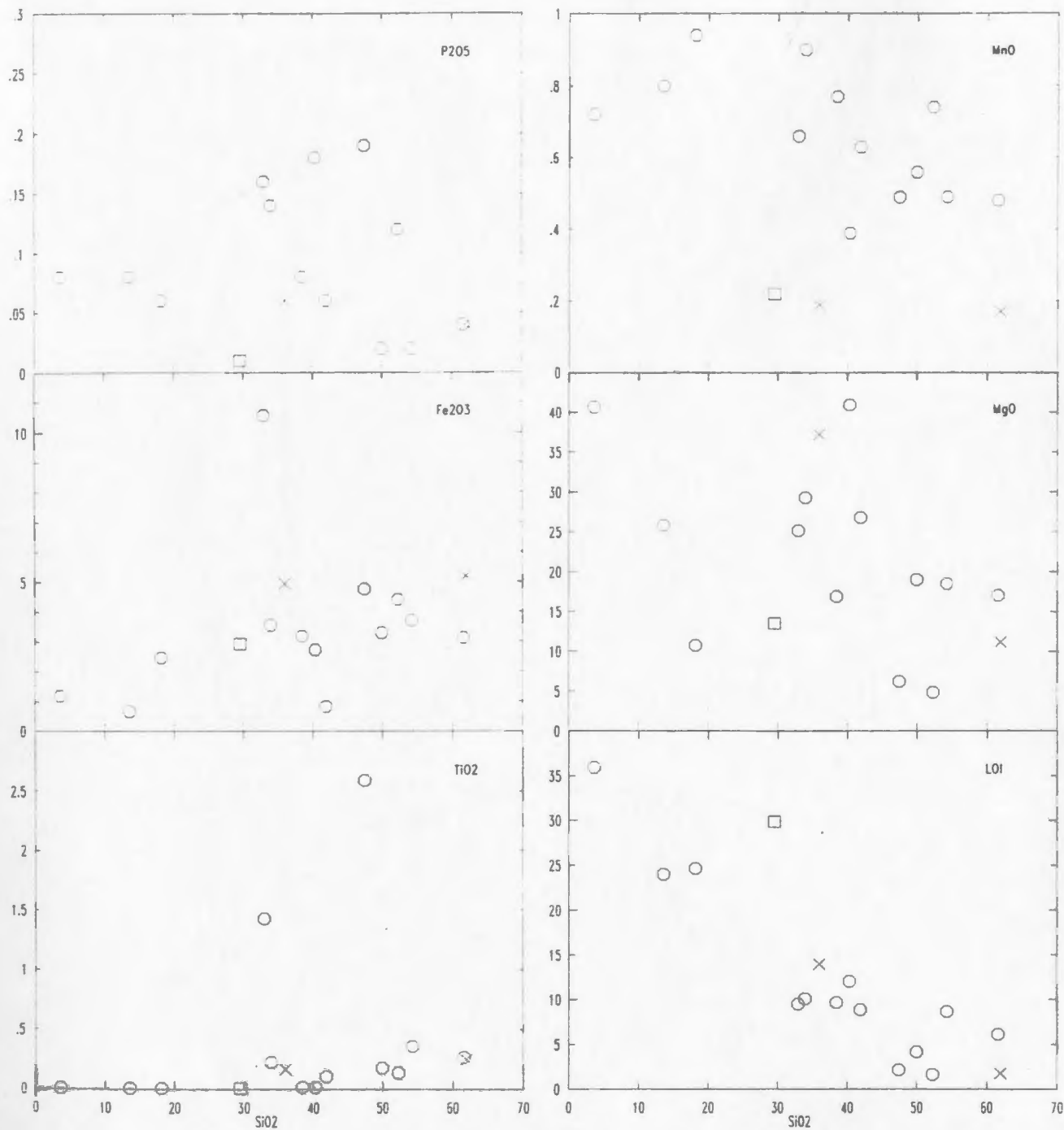
Figure 5.21. Variation diagrams involving SiO$_2$ vs. other major elements for the carbonate/Ca-Mg-silicate samples from the Winter Hill area. Open circles = Winter Hill, X = Winter Hill North, and open squares = Prospect #5.
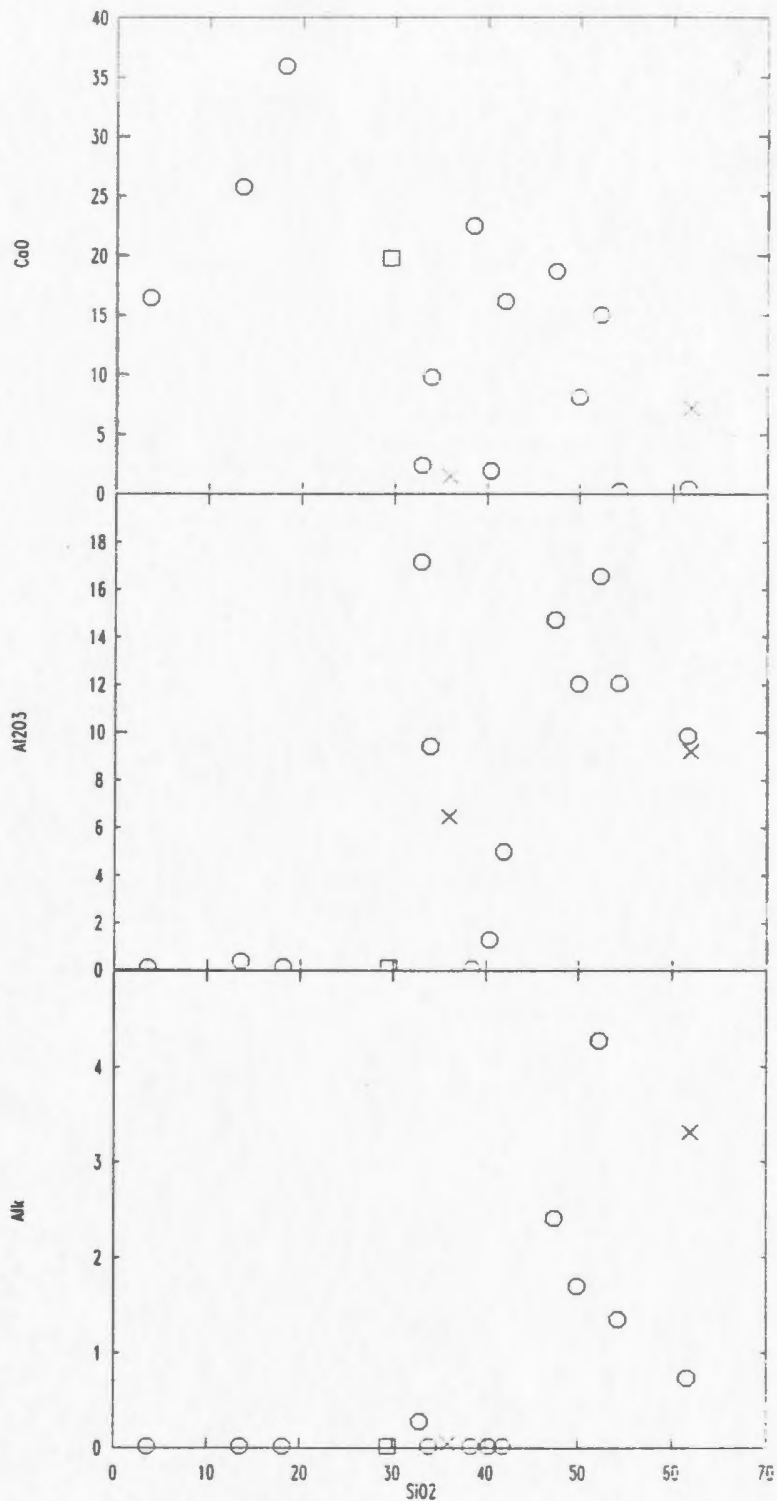
Figure 5.21. (continued)
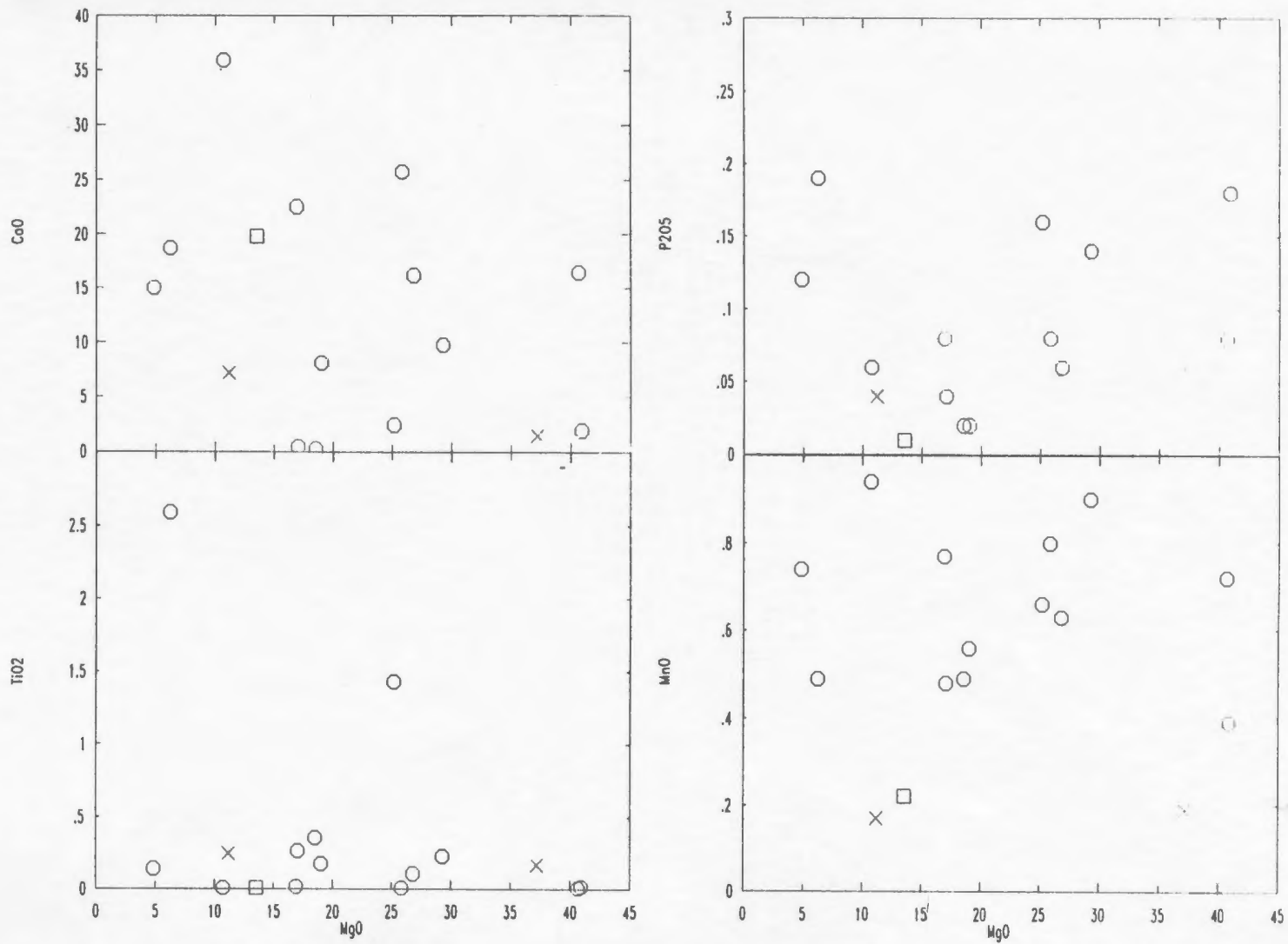
Figure 5.22. MgO vs. other major elements for the carbonate/Ca-Mg-silicate samples from the Winter Hill area. Symbols as in Figure 5.21.
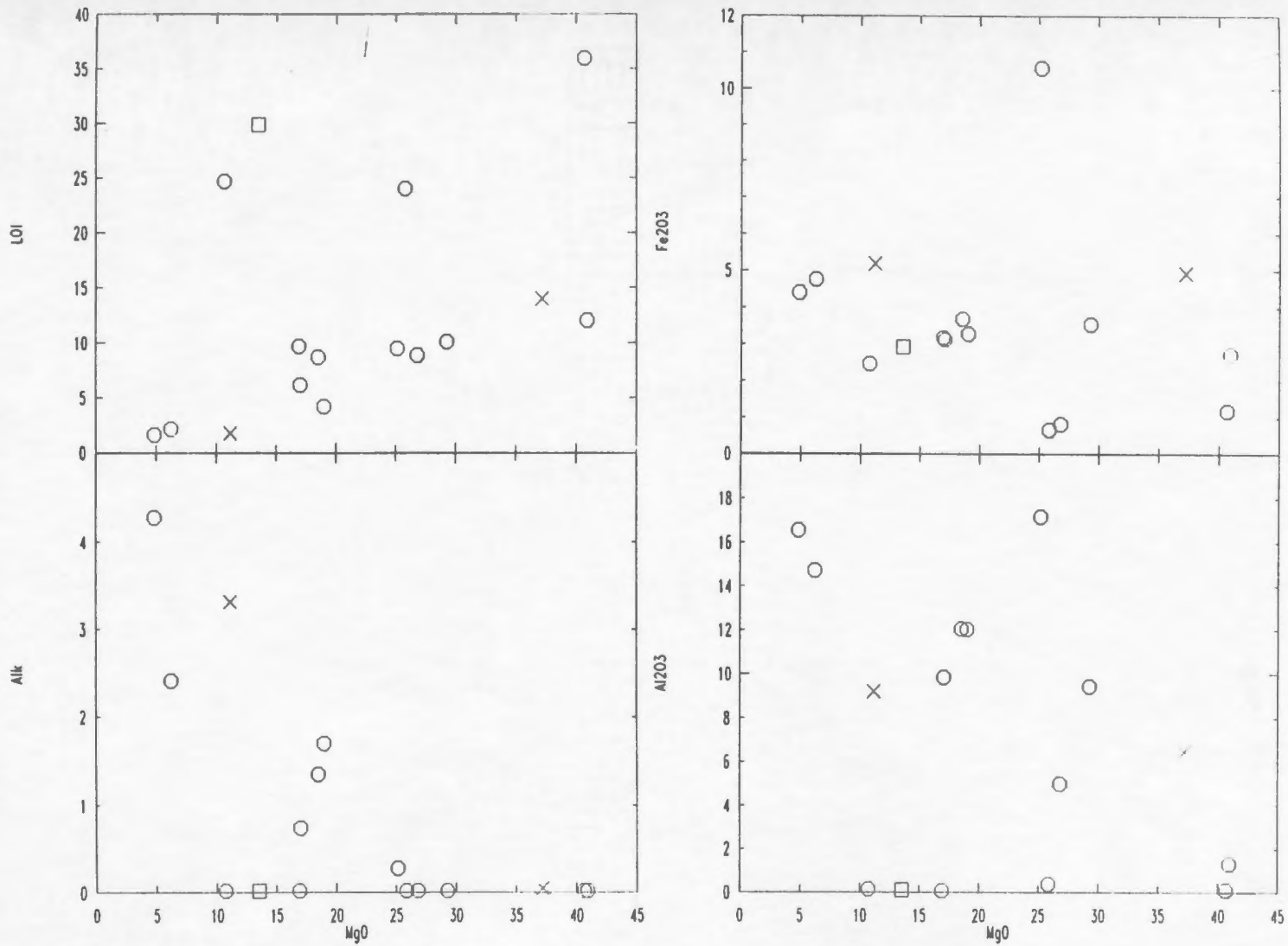
Figure 5.22. (continued)

no visible trends although at lower MgO values ($\underline{i.e.}$ < 20 wt.%), the alkalis display a negative trend with increasing MgO. Also, if the two lowest and two highest MgO values are eliminated, then MnO and P_2O_5 would show weak positive trends with MgO. Al_2O_3 and Fe_2O_{3total} vs. MgO display very weak negative associations as MgO increases, and LOI shows a weak positive correlation with mgO, especially if the four largest LOI values are disregarded.

With respect to the trace elements, there are large ranges for all elements, including the immobile elements. Yet some igneous trends ($\underline{e.g.}$ Zr-Y) can still be found in these chemical sediments (Figure 5.23). A Pb-Cu-Zn ternary plot (Figure 5.24) illustrates how Zn is enriched over Pb and Cu even though base-metal concentrations are very low. Franklin $\underline{et}$ $\underline{al.}$ (1981, figure 83) display Pb-Cu-Zn ternary plots for rocks which are basement to the Kuroko deposits of Japan. They exhibit the same Zn-Pb-rich character as the deposits although they contain only small amounts of base-metals.

5.3 Discussion

The previous chapters provided evidence for the regional tectonic setting (island arc - rifted arc regime), mineral deposit type (VMS), and have also described some of the more important physical and physio-chemical characteristics of the deposits ($\underline{i.e.}$ alteration assemblages and zonations, fluid chemistry and temperature, temporal and spatial relationships
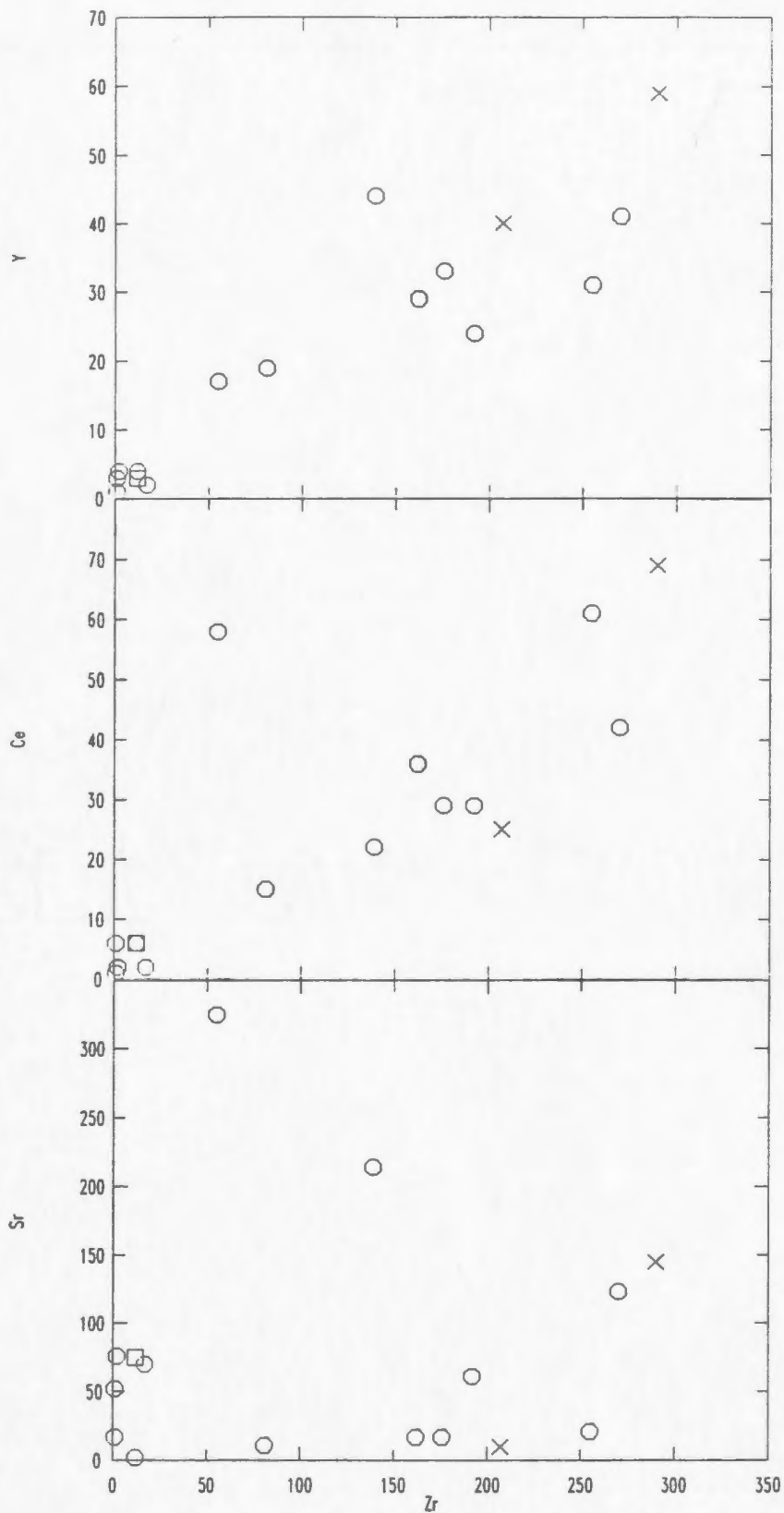
Figure 5.23. Zr vs. selected trace elements. Symbols as in Figure 5.21.
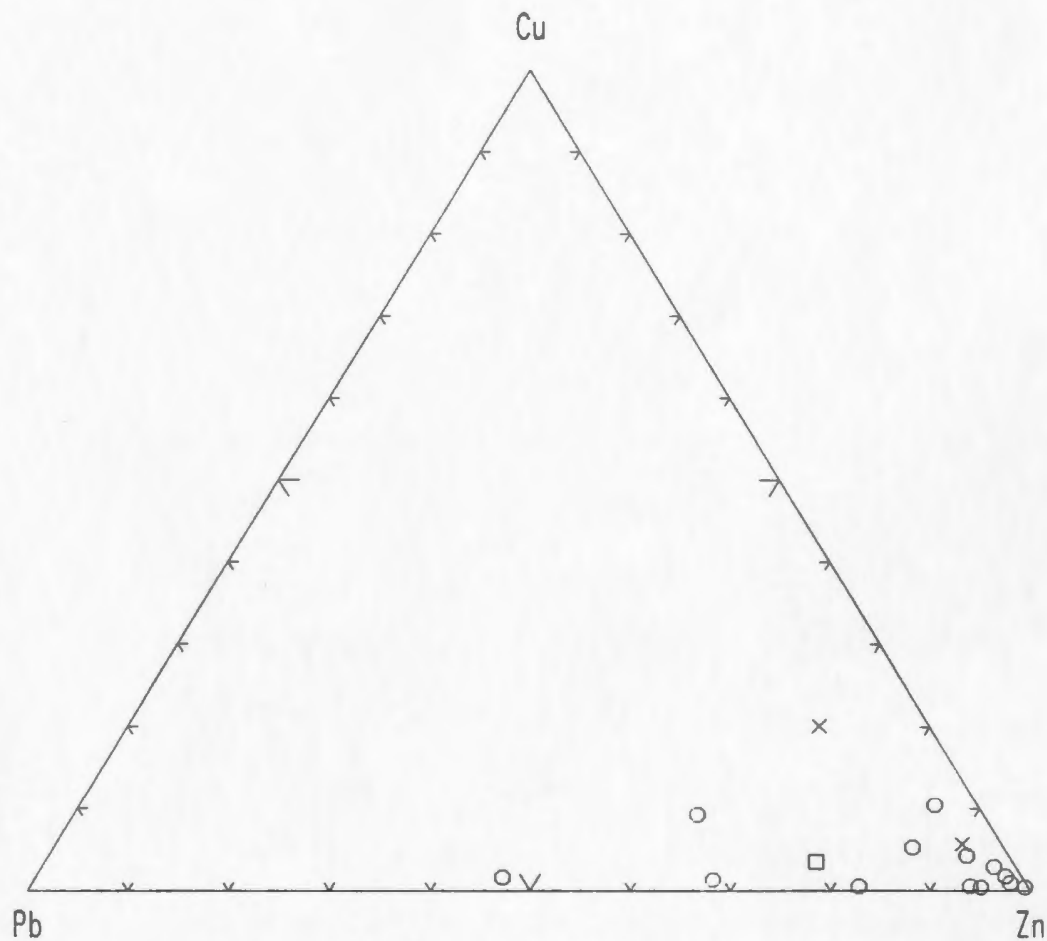
Figure 5.24. Pb-Cu-Zn ternary diagram for the relatively unmineralized carbonate/Ca-Mg-silicate samples from the Winter Hill area. Symbols as in Figure 5.21.

of the base-metal sulphides, paleotopographic features, etc...). Trace and REE characteristics of the mineralized rocks, as described previously, are used to reinforce these ideas.

The proposed VMS model is enhanced by the spatial zonation exhibited by the base-metal sulphides at Winter Hill. The distinction between chalcopyrite-pyrite and sphalerite-galena-pyrrhotite(pyrite) mineralization is very similar to the zonation within many massive sulphide deposits (Franklin et al., 1981; Lydon, 1988). The relative abundances of the base-metal sulphides in these occurrences share characteristics with VMS deposits of the Abitibi Belt and the New Brunswick area, as described by Lydon (1983), and to Canadian and Japanese Phanerozoic massive sulphide deposits in volcanic and volcano-sedimentary rocks (Sangster and Scott, 1976, figure 26).

The volumetrically dominant Zn-Pb mineralization is indicative of the underlying, dominantly felsic volcanic, footwall lithologies. Solomon (1976) noted that 70% of the Zn-Pb-(Cu) ores are exclusively within felsic volcanic rocks, while 92% have abundant felsic rocks in their footwalls. Divi et al. (1980), using a Canadian deposits data set, agreed with the generalization that Zn-Pb-(Cu) ores overlie mainly felsic volcanic rocks and Cu-Zn ores are underlain by basically mafic volcanic rocks, but he also added that the trend is far from perfect.

The REE patterns for some of the mineralized samples infer that the metals could have been carried in CO_3^{2-} and F^--bearing solutions. Within the Tickle Point Formation, one sample each from Shoal Brook and Tilt Point have positive HREE slopes, whereas both samples from the Winter Hill West Showing have positive HREE slopes. Taylor and Fryer (1983) suggest that within granitoid mineral deposits, HREE are complexed and transported by CO_3^{2-}-and F^--rich solutions. If the mineralizing fluids were CO_3^{2-}-bearing, then the carbonate lens at Winter Hill may either be a result of chemical sedimentation from a seawater source, or it may be a precipitate from the mineralizing solution. It is important to note that the only significant base-metal accumulations occur where there is a substantial thickness of carbonate-rich rock. Therefore the carbonate acted as a chemical trap or the carbonate was precipitated from solution with the sulphides.

The extended REE patterns mimic the arc signature as found in the unaltered volcanic rocks. The Nb depletion within the volcanic rocks is probably a direct result of processes occurring within or above the subducting slab. The mineral deposits located within these volcanic rocks would be expected to display some similar chemical characteristics, especially with regards to the immobile elements. The REE patterns should be almost wholly influenced by REE concentrations derived from magmatic waters or by REE concentrations which were possibly leached from the volcanic pile due to convecting seawater.

This will occur if REE concentrations from seawater are so low (on the order of 10^{-5} to 10^{-6}X chondrite, (Humphris, 1984)) that even with a minute amount of mixing or contamination from a magmatic solution, the REE profile of the contaminated seawater should reflect the REE composition of that juvenile fluid. Therefore, a significant seawater role in base-metal mineralization can be easily masked.

CHAPTER 6

SUMMARY AND CONCLUSIONS

The Winter Hill, Frenchman Head, and other sulphide showings and occurrences are examples of volcanogenic massive sulphide deposition. Many features present within these mineralized areas (i.e. mainly Winter Hill) are characteristic of VMS deposits, including:

(i) the base-metal zonation within the carbonate lens at Winter Hill (i.e. a Cu-rich lower discordant stringer zone and a Zn- and Pb-rich upper concordant semi-massive to massive sulphide zone);

(ii) silica and chlorite (± sericite) alteration zones present mainly within the stringer zone;

(iii) a relatively unaltered hanging-wall;

(iv) mineral textures (e.g. possible colloform texture in pyrite) indicative of open space filling within the sulphide mound; and,

(v) internal sedimentary textures (banded carbonates/calc-silicates, carbonate breccias) which suggest deposition on an unstable slope or topographic high.

There are also regional stratigraphic features which suggest that a VMS genesis is valid. The mineralized horizons are restricted to the uppermost portions of the felsic Tickle Point Formation and the lowermost sections of the mafic Sam

Head Formation. The change in volcanism from felsic-dominated to mafic-dominated probably resulted in a period of quiescence during which hydrothermal fluids could convect through the volcanic pile to the surface where sulphide minerals would be deposited. Rapid volcanism and sedimentation then covered the mineralized sections, preserving them.

Another regional feature is the alignment of the mineralized zones (e.g. Winter Hill area; Selco Showings) parallel to major faults (Figure 6.1 and 4.3). The parallelism suggests that the faults were active during volcanism, sedimentation, and mineralization creating aligned stratigraphic features into which the mineralization was trapped and preserved. It is also probable that the faults acted as conduits along which the fluids were channelled to the seafloor.

There is little hard data in reference to the mineralizing fluid chemistry, but much can be inferred from indirect observations. According to Sato's (1972) classification of mineralizing fluids (see Figure 4.12), the mineralized zones within the Connaigre Bay Group probably resulted from sulphide deposition from type 2 solutions (i.e. solutions initially less dense than seawater, but which become more dense than the cold seawater through mixing with cold seawater). Type 3 fluids result in only disseminated mineralization, type 1 solutions create aerially extensive deposits, whereas type 2 produce laterally limited lens-shaped
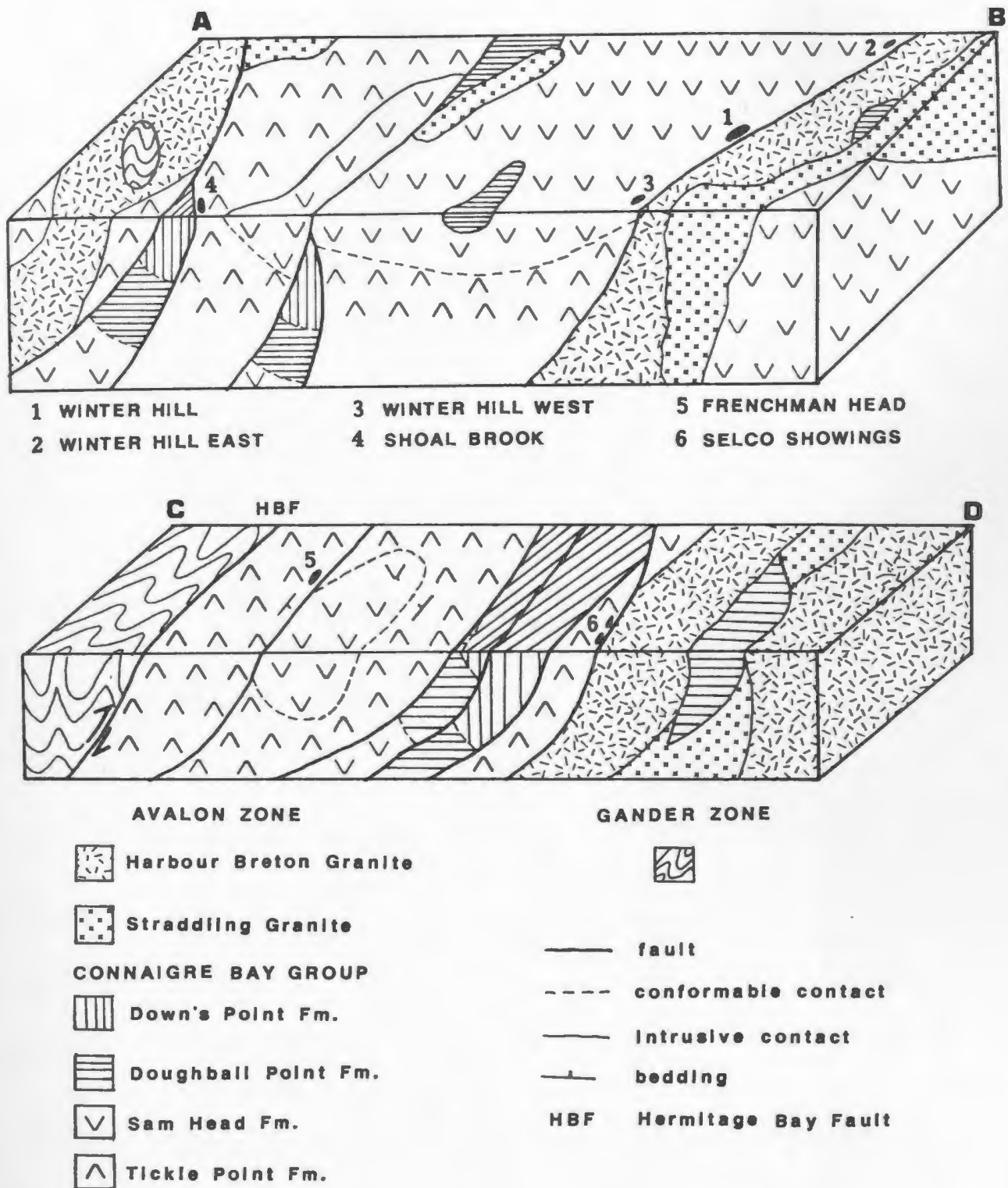
Figure 6.1. Schematic cross-section through the Connaigre Bay Group. The sketches illustrate the similar stratigraphic position of the more important mineralized zones and their close proximity to major faults. See Figure 2.5 for the location of the cross-sections and lithologic ages.

bodies. The Winter Hill Showing (proper) is of limited extent ($\approx$ 120 metres) and is lens-shaped. The Winter Hill area showings extend $\approx$ 3 kilometres but it is not known whether the mineralization is continuous between the showings.

Fluid temperatures, estimated by sulphide mineral assemblages, are between 300°C and 400°C, but the high Fe contents within the sphalerite from Winter Hill indicate that temperatures were probably closer to 300°C (Scott and Kissen, 1973; Hutchinson and Scott, 1980). Lower Fe wt.% in the sphalerites from Frenchman Head suggest that the fluids were slightly cooler than those at Winter Hill. Log a_{S2} values were between -11 and -7.3 and log a_{O2} values between -34 and -30 for the Winter Hill Showing. Other small occurrences also fall within this range (see Figure 4.9).

REE patterns suggest that the fluids contained F⁻ and/or CO_3^{2-} because some mineralized samples have HREE-enriched profiles. HREE are complexed by F- and CO_3^{2-}-bearing solutions (Taylor and Fryer, 1983), and the common association of carbonate with mineralization (i.e. carbonate-rich lens at Winter Hill and carbonate alteration directly beneath the Frenchman Head Showing) implies that CO_3^{2-} was an important fluid constituent.

The volcanic rock chemistry is one that is transitional from calcalkaline-tholeiitic to tholeiitic. The earlier calcalkaline-tholeiitic, mainly felsic volcanism (Tickle Point Formation) is followed by tholeiitic, mafic volcanism (Sam

Head Formation). The volcanic rock chemistry, along with the distinctive REE (i.e. LREE-enriched) and extended REE (positive Nb anomalies) profiles, are characteristic of island arc environments. The calcalkaline-tholeiitic stage was a one of arc building probably during the initiation of subduction. This was followed by a time of arc-rifting and the subsequent extrusion and deposition of tholeiitic mafic flows and tuffs. The association of fine-grained terriginous and chemical sediments, and VMS deposition, suggests this rifting stage was closely followed by a period of volcanic inactivity. This was followed by more rifting and the deposition of the mafic tuffs, agglomerates, and flows (and minor siliceous volcanics) of the Doughball Point Formation. The uppermost sequence (Down's Point Formation) consists of sandstones and conglomerates containing felsic, mafic, and granitic clasts, implying the arc was built up or slightly uplifted and then subjected to subaerial (fluvial ?) to shallow subaqueous sediment deposition.

There is evidence for crustal contamination within the arc system. Figures 3.37 and 3.38 (both from Pearce, 1983) illustrate a continental influence with respect to the more incompatible elements. Swinden and Thorpe (1984) state that VMS deposits and occurrences in the southern part of the Dunnage Zone, near the Avalon craton, have been contaminated by continental crust (see Figure 3.39). This same scenario may be applied in the Hermitage area with the Connaigre Bay Group

representing island arc volcanism near a continental source.

The occurrence of volcanogenic massive sulphides within the Avalon Zone has some important impacts. The first being that they are the only known VMS showings within the Avalon Zone of Newfoundland (Taylor et al., 1979). There are other base-metal occurrences within the Newfoundland Avalon Zone, but they are either epigenetic in origin (polymetallic veins of limited extent) or consist of stratiform Cu mineralization within subaerial basalts (Taylor et al., 1979). There are also other massive sulphide deposits within rocks that are correlative with the Avalon Zone rocks (i.e. the Ducktown District within the late Proterozoic Great Smoky Group (Carolina Slate Belt)) but these deposits are located generally in thick sequences of sedimentary or metasedimentary rocks interpreted to have formed in an intracratonic rift (LeHuray, 1984), although the Gossan Leads Deposits within the Ashe Formation (in Virginia) contain significant quantities of interlayered amphibolite (i.e. metamorphosed mafic material) within the hanging-wall sequence (Gair and Slack, 1984). The felsic- to mafic-dominated volcanism now becomes a prime target for massive sulphide exploration, especially along the western margin of the Avalon Zone.

The second impact with finding island arc related massive sulphide deposits is that it alters the tectonic history of the Avalon Zone. O'Driscoll and Strong (1979) suggested that the tectonic setting for the Connaigre Bay Group is one that

is transitional between orogenic and non-orogenic due to the strong bimodal and calcalkaline character. This present study discovered that tholeiitic rocks are abundant (especially in the mafic suites) and trace element signatures suggest an island arc environment with some crustal contamination. This implies a much stronger "orogenic" component and a limited "non-orogenic" effect than that found by O'Driscoll and Strong (1979).

Two genetic models for sulphide deposition within the Connaigre Bay Group have been suggested by Noranda Exploration Company Limited personnel (1985). The first model involves sedimentary-exhalative (SEDEX) deposition (similar to Mt. Isa, Australia) and the second model centres around a skarn-type replacement origin.

The first model is appropriate with respect to the hydrothermal system that occurs beneath the mineralized zone and the style of deposition (i.e. syngenetic), but this model breaks down with respect to the lithologies present in and around the showings. SEDEX deposits are situated within thick piles of sedimentary rocks (or their metamorphic equivalents) that generally form in an intracratonic basin (Gustafson and Williams, 1981). The Winter Hill and Frenchman Head showings are situated almost exclusively within volcanic rocks of island arc affinity, and the deposits themselves display VMS characteristics (see beginning of chapter). It is noted, however, that even though the Ducktown Deposit is situated in

sedimentary rocks, they have characteristics of VMS deposits (*i.e.* mineralogy) (LeHuray, 1984).

The VMS characteristics of the showings also rule out a skarn-type replacement origin for the sulphides. Contact metamorphic minerals present within the Winter Hill Showing do suggest that there were some secondary effects due to local intrusive activity, but this activity was apparently limited to local recrystallization of previous minerals (forming Ca-Mg-silicates and minor cordierite and andalusite) with no visible remobilization of the sulphides.

The Winter Hill and Frenchman Head showings are the only areas containing appreciable quantities of base-metals, but it is encouraging to note that VMS deposits tend to occur in clusters (Lydon, 1984) that are calculated to cover an average area of approximately 850 km^2 (Sangster, 1980). Campbell *et al.* (1984) suggest that REE mobility within a deposit may be an indicator of its size. Greater REE mobility occurs in larger deposits whereas there is limited or no mobility in small VMS deposits. These two points may be useful to explorationists looking for base-metal deposits within the Connaigre Bay Group.

REFERENCES

Baker, J.H., and Hellingwerf, R.H., 1986. Rare earth elements in lithochemical prospecting for W–Mo–Au mineralized granites and related high- and low-temperature skarns. Institute of Geology and Mineral Exploration and Association of Exploration Geologists International. South European Symposium on Exploration Geochemistry, November, 1986, Athens, Program with Abstracts, p. 15.

Barker, D.S., 1983. Igneous rocks. Prentice-Hall, New Jersey, 417 p.

Barr, S.M. and Raeside, R.P., 1989. Tectono-stratigraphic terranes in Cape Breton, Nova Scotia: Implications for the configuration of the northern Appalachian orogen. Geology, vol. 17, pp. 822-825.

Barton, P.B., Jr., and Bethke, P.M., 1987. Chalcopyrite disease in sphalerite: pathology and epidemiology. American Mineralogist, vol. 22, pp. 451-467.

Barton, P.B., Jr., and Skinner, B.J., 1979. Sulphide mineral stabilities. In Barnes, H.L., (ed.), Geochemistry of hydrothermal ore deposits, 2nd ed. Wiley, New York, pp. 278-403.

Barton, P.B., Jr., and Toumlin, P., 1966. Phase relations involving sphalerite in the Fe-Zn-S system. Economic Geology, vol. 61, pp. 815-849.

Blackwood, R.F., 1975. The Hermitage Fault and adjacent rocks: northeast corner of the Gaultois map-sheet. Unpublished report, Newfoundland Department of Mines and Energy, Mineral Development Division, Open File (1M/147), 9 p.

Blackwood, R.F. and Kennedy, M.J., 1975. The Dover Fault: western boundary of the Avalon Zone in northeastern Newfoundland. Canadian Journal of Earth Sciences, vol. 12, pp. 320-325.

Blackwood, R.F. and O'Driscoll, C.F., 1976. The Gander-Avalon Zone boundary in southeastern Newfoundland. Canadian Journal of Earth Sciences, vol. 13, pp. 1155-1159.

Butler, A.J. and Davenport, P.H., 1978. A lake sediment

geochemical survey of the Meelpaeg Lake area, central Newfoundland. Newfoundland Department of Mines and Energy, Mineral Development Division, Open File No. 986.

Campbell, I.H., Coad, P., Franklin, J.M., Gorton, M.P., Scott, S.D., Sowa, J., and Thurston, P.C., 1982. Rare earth elements in volcanic rocks associated with Cu-Zn massive sulphide mineralization: a preliminary report. Canadian Journal of Earth Sciences, vol. 19, pp. 619-623.

Campbell, I.H., Lesher, C.M., Coad, P., Franklin, J.M., Gorton, M.P., and Thurston, P.C., 1984. Rare earth element mobility in alteration pipes below massive Cu-Zn sulphide deposits. Chemical Geology, vol. 45, pp. 181-202.

Cathles, L.M., Guber, A.L., Lenagh, T.C., and Dudas, F.O., 1983. Kuroko-type massive sulphide deposits of Japan: products of an aborted island arc rift. Economic Geology, Monograph #5, pp. 96-114.

Chayes, F., 1964. Variable-covariance relations in Harker diagrams of volcanic suites. Journal of Petrology, vol. 5, pp. 219-237.

Clemson, J.E., 1986. Mineralogy of samples from the Winter Hill prospects, Hermitage area, Newfoundland. Unpublished Noranda Exploration Co. Ltd. report, 42 p.

Colman-Sadd, S.P., Greene, B.A., and O'Driscoll, C.F., 1979. Gaultois, Newfoundland. Newfoundland Department of Mines and Energy, Mineral Development Division, Map 79-104, scale 1:50,000.

Cox, K.G., Bell, J.D., and Pankhurst, R.J., 1979. The interpretation of igneous rocks. Allan and Unwin, London, 450 p.

Craig, J.R., Ljokjell, P., and Vokes, F.M., 1984. Sphalerite compositional variations in sulphide ores of the Norwegian Caledonides. Economic Geology, vol. 79, pp. 1727-1735.

Cullers, R.L., Medaris, L.G., and Haskin, L.A., 1973. Experimental studies of the distribution of rare earths as trace elements among silicate minerals and liquids and waters. Geochimica et Cosmochimica Acta, vol. 37, pp. 1499-1512.

Davenport, P.H., Nolan, L.W., and Hayes, J.P., 1989. Gold and associated elements in lake sediment from regional survey in the northwestern part of the Belleoram map area

(1M/5, 11- 16). Newfoundland Department of Mines, Open File 1M/276.

Deer, W.A., Howie, R.A., and Zussman, J., 1962. Rock-forming minerals, vol. 1. Longman, London, 333 p.

Divi, S.R., Thorpe, R.I., and Franklin, J.M., 1980. Use of discriminant analysis to evaluate compositional controls of stratiform massive sulphide deposits in Canada. Geological Survey of Canada, Paper 79-20, 23 p.

Dunning, G.R., Barr, S.M., Raeside, R.P., and Jamieson, R.A., 1989. U-Pb zircon, titanite, and monazite ages in the Bras d'Or and Aspy terranes of Cape Breton Island, Nova Scotia: implications for magmatic and metamorphic history. Geological Society of America Bulletin, vol. 102, pp. 322-330.

Ehlers, E.G., and Blatt, H., 1982. Petrology: igneous, sedimentary, and metamorphic. Freeman and Company, San Francisco, 732 p.

Elias, P., and Strong, D.F., 1982. Paleozoic granitoid plutonism of southern Newfoundland: contrasts in timing, tectonic setting, and level of emplacement. Transactions of the Royal Society of Edinburgh: Earth Sciences, vol. 73, pp. 43-57.

Floyd, P.A., and Winchester, J.A., 1975. Magma type and tectonic setting discrimination using immobile elements. Earth and Planetary Science Letters, vol. 27, pp. 211-218.

Franklin, J.M., Lydon, J.W., and Sangster, D.F., 1981. Volcanic- associated massive sulphide deposits. Economic Geology, 75th Anniversary Volume, pp. 485-627.

Gair, L.E., and Slack, J.F., 1984. Deformation, geochemistry, and origin of massive sulphide deposits, Gossan Lead District, Virginia. Economic Geology, vol. 79, pp. 1483-1520.

Graf, J.L., Jr., 1977. Rare earth elements as hydrothermal tracers during the formation of massive sulphide deposits in volcanic rocks. Economic Geology, vol. 72, pp. 527-548.

Graves, G., 1985. Second year assessment report, Licence 2474, on diamond drilling at Winter Hill, NTS 1M/12. Unpublished Noranda Exploration Co. Ltd. report, 63 p.

Graves, G., 1986a. Report on diamond drilling, Licence 2474 and 2539, Hermitage and Frenchman Head claim groups, NTS 1M/12, Project No. 4A81. Unpublished Noranda Exploration Co. Ltd report, 42 p.

Graves, G., 1986b. Hermitage, Project 4A81 summary report, NTS 1M/12. Unpublished Noranda Exploration Co. Ltd. report, 20 p.

Greene, B.A., 1975. Harbour Breton map area. Report of Activities, 1974. Newfoundland Department of Mines and Energy, Mineral Development Division, Report75-1,pp. 3-9.

Greene, B.A. and O'Driscoll, C.F., 1976. Gaultois map area. Report of Activities, 1975, Newfoundland Department of Mines and Energy, Mineral Development Division, Report 76-1, pp. 56-63.

Green, T.H., 1980. Island arc and continental-building magmatism – A review of petrogenetic models based on experimental petrology and geochemistry. Tectonophysics, vol. 63, pp. 367-385.

Green, T.H., 1981. Experimental evidence for the role of accessory phases in magma genesis. Journal of Volcanological Geothermal Research, vol. 10, pp. 405-422.

Guilbert, J.M., and Park, C.F., Jr., 1985. The geology of ore deposits. W.H. Freeman and Company, New York, 985 p.

Gustafson, L.B., and Williams, N., 1981. Sediment-hosted stratiform deposits of copper, lead, and zinc. Economic Geology, 75th Anniversary Volume, pp. 139-178.

Henderson, P., 1984. General geochemical properties and abundances of the rare earth elements. In Henderson, P., (ed.), Rare earth element geochemistry. Elsevier, Amsterdam, pp. 1-32.

Hickey, R.L., and Frey, F.A., 1982. Geochemical characteristics of boninite series volcanics: implications for their source. Geochimica et Cosmochimica Acta, vol. 46, pp. 2099-2115.

Hillebrand, W.F., Lundell, C.E.F., Bright, H.A., and Kofman, J.I., 1953. Applied inorganic analysis, 2nd edition. John Wiley and Sons, New York.

Hofmann, A.W., 1988. Chemical differentiation of the earth: the relationship between mantle, continental crust, and oceanic crust. Earth and Planetary Science Letters, vol.

90, pp. 297-314.

Hughes, C.J., 1972. Geology of the Avalon Peninsula, Newfoundland, and its possible correspondence with Morocco. Notes et Memoires du Service Geologique de Maroc, no. 236, pp. 265-275.

Hughes, C.J., 1973. Spillites, keratophyres, and the igneous spectrum. Geological Magazine, vol. 109, no. 6, pp. 513-527.

Humpris, S.E., 1984. The mobility of the rare earth elements in the crust. In Henderson P., (ed.), Rare earth element geochemistry. Elsevier, Amsterdam, pp. 343-374.

Hutchinson, M.N., and Scott, S.D., 1980. Sphalerite geobarometry applied to metamorphosed sulphide ores of the Swedish Caledonides and U.S. Appalachians. Norges geologiske undersokelse, vol. 360, pp. 59-71.

Irvine, T.N., and Baragar, W.R.A., 1971. A guide to the chemical classification of the common igneous rocks. Canadian Journal of Earth Sciences, vol. 8, pp. 523-548.

Jamieson, R.A., van Breeman, O., Sullivan, R.W., and Currie, K.L., 1986. The age of igneous and metamorphic events in the western Cape Breton Highlands, Nova Scotia. Canadian Journal of Earth Sciences, vol. 23, pp. 1891-1901.

Jensen, L.S., 1976. A new cation plot for classifying subalkaline volcanic rocks. Ontario Ministry of Natural Resources, Miscellaneous Paper No. 66, 22 p.

Jochum, K.P., Seufert, H.M., Spettel, B., and Palme, H., 1986. The Solar System abundances of Nb, Ta, and Y and the relative abundances of refractory lithophile elements in differentiated planetary bodies. Geochimica et Cosmochimica Acta, vol. 50, pp. 1173-1183.

Kean B.F., and Evans, D.T.W., 1988. Mineral deposits of the Lushs Bight Group. In Swinden, H.S., and Kean, B.F., (eds.), The volcanogenic sulphide districts of central Newfoundland. Mineral Deposits Division, Geological Association of Canada, pp. 80-90.

Keen, C.E., Keen, M.J., Nichols, B., Reid, I., Stockmal, G.S., Colman-Sadd, S.P., O'Brien, S.J., Miller, H., Quinlan, G., Williams, H., and Wright, J., 1986. Deep seismic reflection profile across the northern Appalachians. Geology, vol. 14, pp. 141-145.

Keppie, J.D., 1979. Geological map of the Province of Nova

Scotia. Nova Scotia Department of Mines and Energy, scale 1:500,000.

Kontak, D.J., Tuach, J., Strong, D.F., Archibald, D.A., and Farrar, E., 1988. Plutonic and hydrothermal events in the Ackley Granite, southeast Newfoundland, as indicated by total-fusion $^{40}Ar/^{39}Ar$ geochronology. Canadian Journal of Earth Sciences, vol. 25, pp. 1151-1160.

Kirkham, R.V., 1987. Tectonic setting of the Buchans Group. In Kirkham, R.V., (ed.), Buchans Geology, Newfoundland. Geological Survey of Canada, Paper 86-24, pp. 23-34.

Krauskopf, K.B., 1967. Introduction to geochemistry. McGraw-Hill, New York, 721 p.

LeHuray, A.P., 1984. Lead and sulphur isotopes and a model for the origin of the Ducktown Deposit, Tennessee. Economic Geology, vol. 79, pp. 1561-1573.

Lithoprobe East Vibroseis Route, 1989. Report of transect meeting, G.M. Quinlan (ed.), 107 p.

Lydon, J.W., 1983. Chemical parameters controlling the origin and deposition of sediment-hosted stratiform lead-zinc deposits. In Sangster, D.F., (ed.), Short course in sediment-hosted stratiform lead-zinc deposits. Mineralogical Association of Canada, pp. 175-250.

Lydon, J.W., 1984. Volcanogenic massive sulphide deposits. Part 1: a descriptive model. Geoscience Canada, vol. 11, no. 4, pp. 195-202.

Lydon, J.W., 1988. Volcanogenic massive sulphide deposits. Part 2: genetic models. Geoscience Canada, vol. 15, no. 1, pp. 43-65.

MacRae, N.D., and Metson, J.B., 1985. In situ rare earth element analysis of coexisting pyroxene and plagioclase by secondary ion mass spectrometry. Chemical Geology, vol. 53, pp. 325-333.

Marillier, F., Keen, C.E., Stockmal, G.S., Quinlan, G., Williams, H., Colman-Sadd, S.P., and O'Brien, S.J., 1989. Crustal structure and surface zonation of the Canadian Appalachians: implications of deep seismic reflection data. Canadian Journal of Earth Sciences, vol. 26, pp. 305-321.

McKenkie, C.B., 1984. Report on geology, geochemistry, and geophysics, Licence 2365, Connaigre Bay, Newfoundland,

NTS 1M/12. Unpublished Selco-BP Resources Canada Ltd. report, 39 p.

Meschede, M., 1986. A method of discriminating between different types of mid-ocean ridge basalts and continental tholeiites with the Nb-Zr-Y diagram. Chemical Geology, vol. 56, pp. 207-218.

Morton, C., 1984. A geological, geochemical, and structural analyses of the lower Ordovician Tulks Hill Cu-Zn-(Pb) volcanogenic massive sulphide deposit, central Newfoundland, Canada. Unpublished M.Sc. dissertation, Memorial University of Newfoundland, St. John's, Newfoundland, 323 p.

Mottl, M.S., 1983. Metabasalts, axial hot springs and the structure of hydrothermal systems at mid-ocean ridges. Geological Society of America Bulletin, vol. 94, pp. 161-186.

Myers, K.E., and Breitkopf, J.H., 1989. Basalt geochemistry and tectonic settings: a new approach to relate tectonic and magmatic processes. In Gorbatshev, R., (ed.), Proterozoic Geochemistry. Lithos, vol. 23, pp. 53-62.

Noranda Exploration Company Limited, 1984. Unpublished geology survey of the Frenchman Head area. Scale 1:2500.

Noranda Exploration Company Limited, 1985. Internal memorandum.

O'Brien, S.J., Wardle, R.J., and King, A.F., 1983. The Avalon Zone: a Pan-African terrane in the Appalachian Orogen of Canada. Geological Journal, vol. 18, pp. 195-222.

O'Driscoll, C.F., 1977. Geology, petrology, and geochemistry of the Hermitage Peninsula, southern Newfoundland. Unpublished M.Sc. dissertation, Memorial University of Newfoundland, St. John's, Newfoundland, Canada, 144 p.

O'Driscoll, C.F. and Strong, D.F., 1979. Geology and geochemistry of late Precambrian volcanic and intrusive rocks of southwestern Avalon Zone in Newfoundland. Precambrian Research, vol. 8, pp. 19-48.

Ohmoto, H., and Skinner, B.J., 1983. The Kuroko and related volcanogenic massive sulphide deposits: introduction and summary of new findings. In Ohmoto, H., and Skinner, B.J., (eds.), Kuroko and related volcanogenic massive sulphide deposits. Economic Geology, Monograph #5, pp. 1-

8.

Papezik, V.S., 1972. Late Precambrian ignimbrites in eastern Newfoundland and their tectonic significance. In Proceedings of the 24th International Geological Congress, Montreal, Section 1, pp. 147-152.

Pearce, J.A., 1975. Basalt geochemistry used to investigate past tectonic environment on Cyprus. Tectonophysics, vol. 25, pp. 41-68.

Pearce, J.A., 1980. Geochemical evidence for the genesis and eruptive setting of lavas from Tethyan ophiolites. In Panayictou, A., (ed.), Ophiolites, Proceedings International Ophiolite Symposium, Cyprus, 1979. The Geological Survey of Cyprus, Nicosia, pp. 261-272.

Pearce, J.A., 1983. Role of the sub-continental lithosphere in magma genesis at active continental margins. In Hawkesworth, C.J., and Norry, M.J., (eds.), Shiva Publishing, Nantwich, pp. 230-249.

Pearce, J.A., Alabaster, T., Shelton, A.W., and Searle, M.P., 1981. The Oman Ophiolite as a Cretaceous arc-basin complex: evidence and implications. Philosophical Transactions of the Royal Society of London, vol. 300, pp. 299-317.

Pearce, J.A., and Cann, J.R., 1973. Tectonic setting of basic volcanic rocks determined using trace element analyses. Earth and Planetary Science Letters, vol. 19, pp. 290-300.

Pearce, J.A., Harris, N.B.W., and Tindle, A.G., 1984. Trace element discrimination diagrams for the tectonic interpretation of granitic rocks. Journal of Petrology, vol. 25, part 4, pp. 956-983.

Pearce, J.A., and Norry, M.J., 1979. Petrogenetic implications of Ti, Zr, Y, and Nb variations in volcanic rocks. Contributions to Mineralogy and Petrology, vol. 69, pp. 33-47.

Rast, N., O'Brien B.H., and Wardle, R.J., 1976. Relationships between Precambrian and lower Paleozoic rocks of the Avalon Platform in New Brunswick, the northeast Appalachians, and the British Isles. Tectonophysics, vol. 30, pp. 315-338.

Robie, R.A., Hemingway, B.S., and Fisher, J.R., 1978. Thermodynamic properties of minerals and related

substances at 298.15K and 1 bar (10^5 pascals) pressure and at higher temperatures. United States Geological Survey, Bulletin 1452, 456 p.

Rose, A.W., and Burt, D.M., 1979. Hydrothermal alteration. In Barnes, H.L., (ed.), Geochemistry of hydrothermal ore deposits, 2nd ed. Wiley, New York, pp. 173-235.

Roser, B.P., and Korsch, R.J., 1986. Determination of the tectonic setting of sandstone-mudstone suites using SiO_2 contents and K_2O/Na_2O ratio. Journal of Geology, vol. 94, pp. 635-650.

Sangster, D.F., 1980. Quantitative characteristics of volcanogenic massive sulphide deposits: 1. Metal content and size distribution of massive sulphide deposits in volcanic centres. Canadian Institute of Mining and Metallurgy, vol. 73, pp. 74-81.

Sangster, D.F., and Scott, S.D., 1976. Precambrian strata-bound, massive Cu-Zn-Pb sulphide ores of North America. In Wolf, K.H., (ed.), Handbook of strata-bound and stratiform ore deposits, vol. 6. Elsevier, New York, pp. 129-222.

Sato, T., 1972. Behaviours of ore-forming solutions in seawater. Mining Geology, vol. 22, pp. 31-42.

Schenk, P.E., 1971. Southeastern Atlantic Canada, northwestern Africa, and continental drift. Canadian Journal of Earth Sciences, vol. 8, pp. 1218-1251.

Schade, J., Cornell, D.H., and Theart, H.F.J., 1989. Rare earth element and isotopic evidence for the genesis of the Prieska massive sulphide deposit, South Africa. Economic Geology, vol. 84, pp. 49-63.

Scott, S.D., and Barnes, H.L., 1971. Sphalerite geothermometry and geobarometry. Economic Geology, vol. 61, pp. 815-849.

Scott, S.D., and Kissen, S.A., 1973. Sphalerite composition in the Zn-Fe-S system below 300°C. Economic Geology, vol. 68, pp. 475-479.

Sears, W.A., and O'Driscoll, C.F., 1989. Metallogeny of the Connaigre Bay Group, southern Newfoundland. Current Research, Newfoundland Department of Mines and Energy, Mineral Development Division, Report 89-1, pp. 193-199.

Solomon, M., 1976. "Volcanic" massive sulphide deposits and

their host rocks - a review and an explanation. In Wolf, K.H., (ed.), Handbook of stratabound and stratiform ore deposits, vol 2. Elsevier, Amsterdam, pp. 21-50.

Stephens, M.B., Swinden, H.S., and Slack, J.F., 1984. Correlation of massive sulphide deposits in the Appalachian-Caledonian Orogen on the basis of paleotectonic setting. Economic Geology, vol. 79, pp. 1442-1478.

Strong, D.F., 1981. A model for granophile mineral deposits. Geoscience Canada, vol. 8, No. 4, pp. 155-161.

Strong, D.F., O'Brien, S.J., Taylor, S.W., Strong, P.G., and Wilton, D.H., 1978a. Geology of the Marystown (1M/13) and the St. Lawrence map sheets, Newfoundland. Newfoundland Department of Mines and Energy, Mineral Development Division, Report 77-7, 38 p.

Strong, D.F., O'Brien, S.J., Taylor, S.W., Strong, P.G., and Wilton, D.H., 1978b. Late Proterozoic rifting in eastern Newfoundland. Canadian Journal of Earth Sciences, vol. 15, pp. 117-131.

Sugaki, A., Kitakaze, A., and Kolima, S., 1987. Bulk composition of intimate intergrowths of chalcopyrite and sphalerite and their genetic implications. Mineralium Deposita, vol. 22, pp. 26-32.

Sun, S.S., and Nesbitt, R.W., 1978. Geochemical regularities and genetic significance of ophiolitic basalts. Geology, vol. 6, pp. 689-693.

Swinden, H.S, 1988. Volcanogenic sulphide deposits of the Wild Bight Group, Notre Dame Bay. In Swinden, H.S., and Kean, B.F., (eds.), The volcanogenic sulphide districts of central Newfoundland. Mineral Deposits Division, Geological Association of Canada, pp. 179-192.

Swinden, H.S., Jenner, G.A., Kean, B.F., and Evans, D.T.W., 1989. Volcanic rock geochemistry as a guide for massive sulphide exploration in central Newfoundland. Current Research, Newfoundland Department of Mines and Energy, Mineral Deposits Section, Report 89-1, pp. 201-219.

Swinden, H.S., Kean, B.F., and Dunning, G.R., 1988. Geological and paleotectonic settings of volcanogenic sulphide mineralization in central Newfoundland. In Swinden, H.S., and Kean, B.F., (eds.), The volcanogenic sulphide districts of central Newfoundland. Mineral Deposits Division, Geological Association of Canada, pp. 5-26.

Swinden, H.S., and Thorpe, R.I., 1984. Variations in style of volcanism and massive sulphide deposition in Early to Middle Ordovician island-arc sequences of the Newfoundland Central Mobile Belt. Economic Geology, vol. 79, pp. 1596-1619.

Tarney, J., and Weaver, P.L., 1987. Geochemistry and petrogenesis of early Proterozoic dyke swarms. In Halls, H.C., and Fahrig, W.F., (eds.), Mafic Dyke Swarms. Geological Association of Canada Special Paper 34, pp. 81-94.

Taylor, B., and Karner, G.D., 1983. On the evolution of marginal basins. Review of Geophysics and Space Physics, vol. 21, no. 8, pp. 1727-1741.

Taylor, R.P., and Fryer, B.J., 1982. Rare earth element geochemistry as an aid to interpreting hydrothermal ore deposits. In Metallization associated with acid magmatism, vol. 6, Wiley, London, pp. 357- 365.

Taylor, R.P., and Fryer, B.J., 1983. Rare earth element lithogeochemistry of granitoid mineral deposits. Canadian Institute of Mining and Metallurgy Bulletin, vol. 76, no. 860, pp. 74-84.

Taylor, S.W., O'Brien, S.J., and Swinden, H.S., 1979. Geology and mineral potential of the Avalon Zone and granitoid rocks of eastern Newfoundland. Newfoundland Department of Mines and Energy, Mineral Development Division, Report 79-3, 52 p.

Thurston, P.C., 1981. Economic evaluation of Archean felsic volcanic rocks using REE geochemistry. In Glover, J.E., and Groves, D.I., (eds.), Archean Geology. Second International Archean Symposium. Geological Society of Australia Special Publication 7, pp. 439-450.

Turner, F.J., 1981. Reactions in siliceous dolomitic limestones. In Metamorphic petrology: mineralogical, field, and tectonic aspects, 2nd ed. McGraw-Hill, New York, pp. 161-169.

Urabe, T., and Scott, S.D., 1983. Geology and footwall alteration of the South Bay massive sulphide deposit, northwestern Ontario, Canada. Canadian Journal of Earth Sciences, vol. 20, pp. 1862-1879.

Uyeda, S., and Nisiwaki, C., 1980. Stress field, metallogenesis and mode of subduction. Geological Association of Canada, Special Paper 20, pp. 323-340.

Wagenbauer, H.A., 1988. Report of the geochemical laboratory for 1988. Report of Activities 1988, Newfoundland Department of Mines and Energy, Geochemistry and Geophysics Section, pp. 123-124.

Wagenbauer, H.A., 1989. Report of the geochemical laboratory for 1989. Report of Activities 1989, Newfoundland Department of Mines and Energy, Geochemistry and Geophysics Section, pp. 101.

Wagenbauer, H.A., Riley, C.A., and Dawe, G., 1983. Geochemical laboratory. Current Research, Newfoundland Department of Mines and Energy, Geochemistry Section, Report 83-1, pp. 133-137.

Wakita, H., Rey, P., and Schmitt, R.A., 1971. Abundances of the 14 rare-earth elements and 12 other trace elements in Apollo 12 samples: five igneous and one breccia rocks and four soils. Proceedings of the 2nd Lunar Science Conference, pp. 1319-1329.

Widmer, K., 1950. Geology of the Hermitage Bay area, Newfoundland. Unpublished Ph.D. dissertation, Princeton University, Princeton, New Jersey, 439 p.

Williams, H., 1971. Geology of the Belleoram map area, Newfoundland (1M/11). Geological Survey of Canada, Paper 70-65, 39 p.

Williams, H., Kennedy, M.J., and Neale, E.R.W., 1972. The Appalachian Structural Province. In Price, R.A. and Douglas, R.J.W., (eds.), Variations in tectonic styles in Canada. Geological Association of Canada, Special Paper No. 11, pp. 181-261.

Williams, H. (compiler), 1978a. Tectonic lithofacies map of the Appalachian Orogen. Memorial University of Newfoundland Map No. 1, scale 1:1,000,000.

Williams, H., 1978b. Geological development of the northern Appalachians: its bearing on the evolution of the British Isles. In Bowes, D.R., and Leake, B.E., (eds.), Crustal evolution in northwestern Britain and adjacent regions. Geological Journal, Special Issue No. 10, pp. 1-22.

Williams, H., 1979. Appalachian orogen in Canada. Canadian Journal of Earth Sciences, vol. 16, pp. 792-807.

Williams, H., 1982. Geology of the Canadian Appalachians. In Palmer, A.R., (ed.), Perspectives in Regional Geological Synthesis. D-NAG Special Publication No. 1, pp. 57-66.

Williams, H., Colman-Sadd, S.P., and Swinden, H.S., 1988. Tectonic-stratigraphic subdivisions of central Newfoundland. Current Research, Part B, Geological Survey of Canada, Paper 88-1B, pp. 91-98.

Wilson, M., 1989. Igneous petrogenesis. Unwin-Hyman, London, 466 p.

Winchester, J.A., and Floyd, P.A., 1977. Geochemical discrimination of different magma series and their differentiation products using immobile elements. Chemical Geology, vol. 20, pp. 325-343.

Winkler, H.G.F., 1976. Petrogenesis of metamorphic rocks, 4[a] ed. Springer-Verlag, New York, 334 p.

Wood, D.A., 1980. The application of a Th-Hf-Ta diagram to problems of tectonomagmatic classification and to establishing the nature of crustal contamination of basaltic lavas of the British Tertiary volcanic province. Earth and Planetary Science Letters, vol. 50, pp. 11-30.

Appendix I. Chemical analyses for relatively unaltered volcanic and sedimentary rocks from the Connaigre Bay Group. Hf and Ta are recalculated from Zr and Nb respectively. (na = not analysed, -1 = less than one)

Mafic to Intermediate Volcanic Rocks

Sample #	584216	584228	584192	584136	584139	584151	584152
SiO2 (wt.%)	56.25	54.10	65.80	48.35	45.65	47.90	47.55
TiO2	1.52	1.47	0.88	1.33	1.98	1.18	1.01
Al2O3	16.13	15.66	12.76	15.59	14.90	16.24	15.68
Fe2O3(total)	10.74	11.71	5.39	11.86	10.21	10.44	11.24
MnO	0.12	0.12	0.22	0.23	0.58	0.20	0.38
MgO	7.91	7.65	0.72	6.92	9.55	7.58	8.89
CaO	2.29	4.51	0.52	5.26	9.44	9.46	4.79
Na2O	2.06	3.09	0.17	2.90	1.76	2.34	1.93
K2O	1.14	0.41	7.74	1.58	2.15	1.35	4.39
P2O5	0.15	0.14	0.10	0.14	0.11	0.13	0.09
LOI	1.50	0.78	4.26	5.88	4.62	3.15	4.09
Total	99.81	99.64	98.56	100.04	100.05	99.97	100.04
Cr(ppm)	69	74	113	136	301	214	282
Ni	23	21	15	41	90	73	75
Co	31	31	24	36	30	35	42
V	316	325	326	340	257	230	270
Cu	76	35	30	90	11	64	57
Pb	3	5	49	2	19	1	3
Zn	178	136	39	85	139	89	95
Cd	0.20	0.40	0.10	0.10	0.10	0.20	-0.10
Mo	3.00	3.00	3.00	4.00	4.00	4.00	3.00
Rb	16	10	123	34	26	33	71
Ba	152	101	4078	355	684	158	1188
Sr	81	109	49	211	194	174	203
Ga	24	18	17	26	22	26	21
Li	100.00	74.00	6.00	15.00	9.00	10.00	11.00
Nb	-1.0	-1.0	-1.0	-1.0	-1.0	-1.0	-1.0
Ta	0.06	0.06	0.06	0.06	0.06	0.06	0.06
Zr	111	106	40	75	57	110	51
Hf	3.00	2.86	1.08	2.03	1.54	2.97	1.38
Y	13	21	7	22	15	25	14
Th	-1.00	-1.00	-1.00	-1.00	-1.00	-1.00	-1.00
La	8.00	8.00	3.00	5.00	3.00	7.00	4.00
Ce	22.00	23.00	10.00	17.00	10.00	19.00	12.00
F	299.00	365.00	266.00	193.00	396.00	187.00	215.00
Be	1.20	1.00	1.00	0.80	1.30	0.80	0.60
Ag	-0.1	0.1	3.6	-0.1	-0.1	-0.1	-0.1
Au(ppb)	na	na	10.0	na	-5.0	na	-5.0

Appendix I. (continued)

Mafic to Intermediate Volcanic Rocks

Sample #	584156	584188	584193	584233	584209	584017	584018
SiO2 (wt.%)	46.90	46.05	41.25	47.35	51.80	48.35	46.75
TiO2	2.88	1.03	0.70	1.13	0.59	1.48	1.60
Al2O3	13.44	16.35	10.26	12.69	13.44	15.46	15.76
Fe2O3(total)	19.55	11.67	8.45	15.49	7.55	13.03	13.64
MnO	0.42	0.21	1.09	1.25	0.18	0.29	0.29
MgO	4.48	9.04	15.97	9.15	0.15	6.85	6.90
CaO	5.99	9.11	12.08	1.51	19.25	8.86	9.67
Na2O	2.47	1.86	0.15	0.10	0.03	3.45	3.20
K2O	1.18	0.96	1.15	2.01	0.02	0.51	0.55
P2O5	0.21	0.11	0.06	0.13	0.09	0.13	0.15
LOI	2.61	3.67	7.51	8.33	5.29	1.12	0.89
Total	100.13	100.06	98.67	99.14	98.39	99.53	99.40
Cr(ppm)	9	276	202	175	8	132	137
Ni	4	78	47	48	-1	23	24
Co	43	44	25	52	1	40	40
V	170	294	185	220	215	327	311
Cu	86	126	56	47	2990	95	20
Pb	3	15	7	20	53	10	8
Zn	157	92	75	420	14	280	222
Cd	0.10	0.20	0.40	0.20	7.10	1.10	0.40
Mo	4.00	3.00	4.00	6.00	5.00	4.00	4.00
Rb	13	10	9	35	3	11	15
Ba	329	176	1145	1279	3015	182	230
Sr	192	122	53	19	1262	335	243
Ga	36	19	19	19	23	26	26
Li	7.00	11.00	12.00	19.00	2.00	14.00	16.00
Nb	-1.0	-1.0	-1.0	-1.0	-1.0	-1.0	-1.0
Ta	0.06	0.06	0.06	0.06	0.06	0.06	0.06
Zr	63	52	32	57	41	69	85
Hf	1.70	1.41	0.86	1.54	1.11	1.86	2.30
Y	22	14	12	14	12	23	24
Th	-1.00	-1.00	1.00	-1.00	-1.00	4.00	3.00
La	5.00	4.00	2.00	2.00	8.00	4.00	5.00
Ce	16.00	9.00	6.00	8.00	16.00	11.00	12.00
F	222.00	271.00	841.00	510.00	154.00	328.00	451.00
Be	0.80	0.80	0.90	0.70	1.00	0.70	1.20
Ag	0.1	0.1	-0.1	0.2	5.9	0.1	-0.1
Au(ppb)	-5.0	-5.0	-5.0	-5.0	10.0	-5.0	na

Mafic to Intermediate Volcanic Rocks

Sample #	584225	584008	584068	584084	584086	584095	584096
SiO2 (wt.%)	45.95	59.90	52.15	61.50	45.55	63.30	63.70
TiO2	1.79	1.31	1.32	1.21	1.07	0.63	0.89
Al2O3	17.24	13.03	18.01	13.89	15.14	11.87	11.50
Fe2O3(total)	13.30	8.03	11.04	6.07	9.45	8.89	8.83
MnO	0.83	0.28	0.42	0.18	0.18	0.12	0.14
MgO	9.82	4.26	4.31	1.92	7.13	1.62	1.66
CaO	7.07	7.14	7.01	5.07	11.57	5.45	9.48
Na2O	1.86	1.89	3.95	5.06	2.72	2.49	0.43
K2O	0.44	0.16	0.68	0.46	0.85	1.99	0.02
P2O5	0.17	0.43	0.34	0.49	0.19	0.09	0.14
LOI	1.21	2.96	0.92	3.37	4.14	2.83	2.36
Total	99.68	99.39	100.15	99.22	97.99	99.28	99.15
Cr(ppm)	58	9	4	4	283	9	9
Ni	21	1	5	-1	93	5	4
Co	33	9	25	4	33	43	28
V	417	98	182	36	248	128	284
Cu	42	7	18	5	20	54	45
Pb	39	128	161	3	4	27	32
Zn	597	346	360	78	75	57	69
Cd	0.40	2.30	-0.10	0.20	0.30	0.40	0.20
Mo	3.00	3.00	4.00	3.00	3.00	5.00	4.00
Rb	10	5	26	10	12	32	4
Ba	206	95	358	98	288	298	13
Sr	210	227	399	154	517	217	293
Ga	27	19	28	26	19	20	31
Li	55.00	10.00	17.00	7.00	11.00	5.00	7.00
Nb	-1.0	5.0	7.7	2.0	-1.0	-1.0	-1.0
Ta	0.06	0.29	0.45	0.12	0.06	0.06	0.06
Zr	86	157	165	200	100	195	79
Hf	2.32	4.24	4.46	5.41	2.70	5.27	2.14
Y	22	44	30	47	21	42	25
Th	-1.00	9.00	3.00	8.00	5.00	-1.00	-1.00
La	6.00	19.00	17.00	17.00	15.00	11.00	9.00
Ce	18.00	48.00	37.28	49.00	41.00	35.00	23.00
F	743.00	572.00	577.00	602.00	309.00	138.00	239.00
Be	1.30	1.40	1.50	1.40	1.10	0.70	0.90
Ag	0.1	-0.1	0.2	-0.1	-0.1	0.2	0.1
Au(ppb)	na	na	na	na	na	-5.0	-5.0

Appendix I. (continued)

Mafic to Intermediate Volcanic Rocks

Sample #	584108	584134	584143	584147	584173	584182	584185
SiO2 (wt.%)	48.90	66.10	49.20	48.05	60.50	61.10	76.10
TiO2	1.13	1.40	0.86	0.89	1.53	1.30	0.93
Al2O3	14.75	8.08	16.58	15.08	13.24	14.13	8.13
Fe2O3(total)	9.13	11.82	9.11	7.83	8.20	7.29	5.50
MnO	0.22	0.12	0.16	0.14	0.22	0.46	0.02
MgO	7.47	4.09	4.14	5.89	3.93	4.74	0.53
CaO	6.10	0.38	8.31	7.97	6.04	3.02	0.36
Na2O	2.13	0.61	2.61	2.21	2.14	3.08	0.11
K2O	1.19	1.09	1.81	1.42	0.26	1.67	2.57
P2O5	0.23	0.25	0.15	0.24	0.57	0.46	0.28
LOI	7.12	6.03	9.17	10.97	2.95	2.74	4.19
Total	98.37	99.97	102.10	100.69	99.58	99.99	98.72
Cr(ppm)	288	16	92	148	5	4	3
Ni	101	8	30	42	-1	-1	-1
Co	33	19	27	26	8	6	4
V	201	159	246	200	100	103	60
Cu	48	19	21	18	10	5	199
Pb	9	68	4	12	6	5	61
Zn	146	173	80	73	98	231	5540
Cd	0.10	0.20	0.20	0.20	0.10	0.10	2.30
Mo	4.00	12.00	4.00	3.00	3.00	4.00	26.00
Rb	16	16	51	33	2	43	71
Ba	267	442	473	400	1954	337	201
Sr	116	16	161	154	139	122	5
Ga	26	20	26	29	22	22	20
Li	18.00	10.00	23.00	19.00	9.00	16.00	4.00
Nb	5.0	-1.0	3.0	1.0	3.0	6.0	-1.0
Ta	0.29	0.06	0.18	0.06	0.18	0.35	0.06
Zr	147	157	108	138	187	218	108
Hf	3.97	4.24	2.92	3.73	5.05	5.89	2.92
Y	20	26	19	13	42	51	24
Th	-1.00	-1.00	-1.00	4.00	9.00	5.00	-1.00
La	16.00	8.00	18.00	25.00	19.00	25.00	7.00
Ce	48.00	33.00	46.00	67.00	51.00	67.00	24.00
F	30.00	409.00	308.00	461.00	559.00	654.00	519.00
Be	1.50	0.80	1.20	1.30	1.30	1.20	0.70
Ag	0.2	0.3	0.1	0.1	-0.1	-0.1	1.0
Au(ppb)	na	5.0	-5.0	na	na	-5.0	-5.0

Appendix I. (continued)

Mafic to Intermediate Volcanic Rocks

Sample #	584187	584203	584211	584212	584226
SiO_2 (wt.%)	70.85	41.00	48.25	46.75	54.25
TiO_2	1.01	1.27	0.78	0.70	1.49
Al_2O_3	8.84	17.48	15.28	15.76	15.88
Fe_2O_3(total)	7.01	13.77	10.20	11.43	11.25
MnO	0.45	0.22	0.19	0.20	0.15
MgO	4.23	5.43	5.38	5.60	9.52
CaO	0.60	16.53	8.64	9.90	3.83
Na_2O	0.08	0.42	4.23	2.20	1.73
K_2O	1.68	0.76	0.44	0.62	0.93
P_2O_5	0.33	0.27	0.33	0.08	0.15
LOI	4.83	2.28	5.96	6.37	1.02
Total	99.91	99.43	99.68	99.61	100.20
Cr(ppm)	6	79	96	220	78
Ni	-1	50	36	67	25
Co	5	34	33	41	36
V	71	289	168	163	332
Cu	35	44	87	189	83
Pb	653	2	-1	5	4
Zn	1250	82	86	77	148
Cd	5.60	0.40	0.50	0.50	0.20
Mo	3.00	4.00	4.00	4.00	3.00
Rb	37	18	6	11	18
Ba	150	1169	322	324	252
Sr	7	453	388	236	76
Ga	15	28	19	18	19
Li	12.00	10.00	11.00	9.00	78.00
Nb	2.0	4.0	1.0	-1.0	-1.0
Ta	0.12	0.24	0.06	0.06	0.06
Zr	121	188	74	56	117
Hf	3.27	5.08	2.00	1.51	3.16
Y	28	27	17	13	18
Th	4.00	13.00	1.00	-1.00	-1.00
La	9.00	25.00	13.00	11.00	8.00
Ce	32.00	68.00	29.00	25.00	23.00
F	681.00	289.00	377.00	195.00	282.00
Be	0.80	1.80	1.00	0.80	1.00
Ag	1.8	-0.1	-0.1	0.1	0.2
Au(ppb)	-5.0	na	na	na	na

Dacitic to Felsic Volcanic Rocks

Sample #	584183	584011	584003	584085	584107	584109	584111
SiO2 (wt.%)	57.85	64.70	79.50	74.65	72.40	74.35	72.90
TiO2	0.83	0.56	0.29	0.39	0.38	0.30	0.22
Al2O3	16.91	15.48	9.92	12.78	12.07	11.56	13.02
Fe2O3(total)	6.29	5.32	1.20	1.90	2.85	3.28	2.13
MnO	0.28	0.24	0.01	0.02	0.12	0.04	0.05
MgO	4.17	6.16	0.08	0.65	0.53	0.38	0.61
CaO	4.44	0.30	0.10	0.49	1.64	1.15	1.47
Na2O	3.70	0.26	4.35	5.09	5.69	4.67	6.46
K2O	1.70	3.65	1.87	1.33	0.49	0.95	0.31
P2O5	0.24	0.03	0.01	0.06	0.05	0.04	0.02
LOI	3.21	3.14	0.79	1.65	2.27	2.89	1.92
Total	99.62	99.84	98.12	99.01	98.49	99.61	99.11
Cr(ppm)	4	21	3	5	3	4	4
Ni	2	5	-1	-1	-1	-1	-1
Co	10	7	-1	-1	-1	2	1
V	80	26	4	5	2	3	4
Cu	22	4	2	6	8	4	6
Pb	17	5	16	3	11	12	14
Zn	120	116	10	20	108	32	34
Cd	0.10	-0.10	0.10	0.20	0.60	0.30	0.30
Mo	3.00	4.00	3.00	3.00	2.00	3.00	6.00
Rb	32	75	17	29	8	12	7
Ba	732	380	380	88	102	171	200
Sr	294	14	45	75	64	83	127
Ga	16	23	6	14	23	16	-1
Li	11.00	24.00	3.00	5.00	4.00	4.00	4.00
Nb	7.0	9.0	10.0	5.0	5.0	6.0	6.0
Ta	0.41	0.53	0.59	0.29	0.29	0.35	0.35
Zr	249	216	216	297	301	314	277
Hf	6.73	5.84	5.84	8.03	8.14	8.49	7.49
Y	33	23	17	50	51	33	59
Th	-1.00	11.00	7.00	9.00	2.00	4.00	6.00
La	19.00	20.00	4.00	20.00	21.00	18.00	25.00
Ce	53.00	66.00	21.00	69.00	70.00	63.00	77.00
F	396.00	1170.00	35.00	203.00	185.00	135.00	142.00
Be	1.50	2.60	0.90	1.40	1.40	1.30	2.00
Ag	-0.1	-0.1	0.2	-0.1	0.1	0.1	-0.1
Au(ppb)	na	-5.0	-5.0	-5.0	na	-5.0	na

Dacitic to Felsic Volcanic Rocks

Sample #	584113	584115	584124	584127	584135	584159	584165
SiO2 (wt.%)	69.90	76.80	74.40	76.40	74.50	70.95	72.05
TiO2	0.17	0.22	0.31	0.28	0.30	0.22	0.32
Al2O3	9.60	12.30	11.84	11.25	11.36	12.05	12.76
Fe2O3(total)	9.28	1.76	3.17	2.88	3.38	5.14	4.24
MnO	0.03	0.05	0.03	0.05	0.07	0.11	0.05
MgO	0.24	0.49	0.78	0.36	1.84	3.45	0.91
CaO	0.24	0.41	0.28	2.80	0.09	0.04	0.12
Na2O	4.31	5.76	4.97	4.59	4.04	0.87	1.55
K2O	0.57	1.07	0.98	0.25	2.10	3.02	3.40
P2O5	0.01	0.03	0.05	0.05	0.04	0.03	0.05
LOI	5.11	1.16	2.21	1.08	2.39	4.17	3.42
Total	99.46	100.05	99.02	99.99	100.11	100.05	98.87
Cr(ppm)	3	4	4	4	5	14	3
Ni	-1	-1	-1	-1	-1	1	-1
Co	1	-1	-1	2	1	-1	3
V	-1	1	1	13	7	6	43
Cu	9	5	6	12	7	7	10
Pb	31	6	13	8	12	33	5
Zn	19	24	77	19	60	102	33
Cd	0.60	0.10	0.50	0.10	0.10	0.20	0.40
Mo	3.00	3.00	2.00	5.00	4.00	6.00	4.00
Rb	8	10	14	6	34	77	102
Ba	327	299	194	92	405	8138	372
Sr	44	43	44	164	47	10	17
Ga	20	13	20	18	19	18	19
Li	3.00	3.00	4.00	3.00	6.00	10.00	6.00
Nb	2.0	5.0	8.0	6.0	8.0	8.0	7.0
Ta	0.12	0.29	0.47	0.35	0.47	0.47	0.41
Zr	199	270	390	266	330	271	265
Hf	5.38	7.30	10.54	7.19	8.92	7.32	7.16
Y	26	47	40	46	46	30	26
Th	2.00	2.00	-1.00	1.00	2.00	4.00	4.00
La	6.00	21.00	23.00	14.00	21.00	22.00	24.00
Ce	32.00	72.00	83.00	49.00	75.00	66.00	69.00
F	83.00	140.00	231.00	83.00	179.00	623.00	507.00
Be	1.20	1.30	1.70	1.10	1.70	1.70	1.30
Ag	0.5	0.2	0.1	-0.1	0.1	0.3	-0.1
Au(ppb)	-5.0	-5.0	10.0	10.0	-5.0	-5.0	-5.0

Dacitic to Felsic Volcanic Rocks

Sample #	584174	584184	584199	584001	584002	584006	584007
SiO2 (wt.%)	65.15	75.75	65.65	75.20	64.40	66.65	68.45
TiO2	0.48	0.24	0.48	0.33	0.60	0.56	0.72
Al2O3	15.91	12.88	15.79	11.33	14.49	12.84	11.49
Fe2O3(total)	4.13	1.97	4.27	2.23	4.75	5.86	4.85
MnO	0.15	0.07	0.14	0.07	0.07	0.13	0.17
MgO	1.18	1.24	1.15	1.49	1.37	2.02	2.39
CaO	3.36	0.21	3.22	0.24	0.77	3.35	2.67
Na2O	4.63	2.35	4.45	3.70	2.07	4.02	3.07
K2O	1.51	2.95	1.95	2.10	7.51	0.51	1.63
P2O5	0.18	0.02	0.17	0.04	0.07	0.09	0.22
LOI	1.57	2.17	1.64	1.67	0.79	2.43	2.43
Total	98.25	99.85	98.91	98.40	96.89	98.46	98.09
Cr(ppm)	4	3	5	5	6	16	8
Ni	-1	-1	1	-1	1	10	-1
Co	5	1	6	1	4	13	5
V	32	4	26	6	14	767	38
Cu	10	34	9	2	5	12	3
Pb	8	7	10	6	18	12	12
Zn	57	53	60	62	53	66	102
Cd	0.10	0.10	0.20	-0.10	-0.10	-0.10	-0.10
Mo	3.00	4.00	3.00	3.00	5.00	4.00	4.00
Rb	13	72	37	35	135	8	15
Ba	1326	408	1037	369	1435	147	771
Sr	318	18	306	83	74	228	104
Ga	12	21	15	10	17	22	17
Li	8.00	8.00	6.00	8.00	10.00	9.00	8.00
Nb	6.0	9.0	5.0	10.0	11.0	6.0	9.0
Ta	0.35	0.53	0.29	0.59	0.65	0.35	0.53
Zr	217	285	210	250	315	172	158
Hf	5.86	7.70	5.63	6.76	8.51	4.65	4.27
Y	27	39	26	37	79	39	42
Th	3.00	6.00	3.00	12.00	13.00	8.00	11.00
La	20.00	23.00	20.00	17.00	25.00	15.00	19.00
Ce	54.00	71.00	48.00	59.00	79.00	42.00	53.00
F	240.00	263.00	272.00	156.00	215.00	199.00	387.00
Be	1.50	1.70	1.60	1.70	1.40	1.00	1.30
Ag	0.1	-0.1	-0.1	-0.1	0.1	0.4	-0.1
Au(ppb)	-5.0	-5.0	na	-5.0	na	-5.0	-5.0

Dacitic to Felsic Volcanic Rocks

Sample #	584105	584117	584122	584123	584125	584126	584128
SiO2 (wt.%)	71.00	73.25	79.20	74.75	68.80	65.45	68.05
TiO2	0.28	0.30	0.20	0.28	0.35	0.58	0.41
Al2O3	9.09	13.63	8.71	10.79	13.81	15.07	10.39
Fe2O3(total)	8.22	1.36	4.75	2.67	4.20	6.52	8.48
MnO	0.04	0.03	0.12	0.10	0.13	0.18	0.08
MgO	0.77	0.67	2.11	2.63	2.18	2.57	0.89
CaO	0.72	1.41	0.08	1.02	1.06	0.21	3.73
Na2O	4.52	6.99	2.26	3.26	1.24	2.47	3.33
K2O	0.65	0.29	0.64	1.13	3.69	2.58	0.39
P2O5	0.06	0.04	0.03	0.03	0.06	0.10	0.07
LOI	4.85	1.46	1.89	2.82	3.43	3.82	3.93
Total	100.20	99.43	99.99	99.48	98.95	99.55	99.75
Cr(ppm)	3	3	4	3	3	8	8
Ni	-1	-1	-1	-1	-1	1	-1
Co	1	-1	2	-1	1	5	4
V	-1	11	2	-1	5	37	22
Cu	9	6	8	6	6	10	10
Pb	19	6	6	9	8	7	14
Zn	33	21	81	87	121	169	35
Cd	0.20	0.20	0.20	0.20	0.20	0.10	0.20
Mo	6.00	3.00	2.00	3.00	3.00	9.00	4.00
Rb	7	7	13	17	85	53	7
Ba	308	75	77	168	542	308	137
Sr	44	57	15	45	16	28	173
Ga	13	9	9	10	30	34	13
Li	3.00	5.00	9.00	9.00	8.00	11.00	3.00
Nb	3.0	6.0	2.0	8.0	9.0	7.0	4.0
Ta	0.18	0.35	0.12	0.47	0.53	0.41	0.24
Zr	159	329	244	326	449	284	197
Hf	4.30	8.89	6.59	8.81	12.14	7.68	5.32
Y	32	24	23	26	43	22	38
Th	-1.00	4.00	-1.00	-1.00	-1.00	-1.00	1.00
La	18.00	6.00	7.00	19.00	64.00	14.00	18.00
Ce	51.00	37.00	36.00	63.00	191.00	48.00	52.00
F	170.00	124.00	314.00	548.00	596.00	500.00	135.00
Be	1.60	1.10	0.70	1.60	2.00	2.40	1.20
Ag	0.2	-0.1	-0.1	-0.1	0.1	0.7	0.1
Au(ppb)	-5.0	na	na	na	na	15.0	15.0

Dacitic to Felsic Volcanic Rocks

Sample #	584157	584175	584179	584223	584207
SiO_2 (wt.%)	72.10	80.25	81.15	68.95	65.55
TiO_2	0.45	0.14	0.17	0.27	0.65
Al_2O_3	12.13	8.58	9.43	15.00	14.72
Fe_2O_3(total)	3.56	3.20	2.56	2.72	2.94
MnO	0.16	0.02	0.01	0.08	0.14
MgO	1.83	0.16	0.55	1.78	0.64
CaO	0.33	0.47	0.02	2.31	3.49
Na_2O	3.57	4.17	0.08	3.64	6.52
K_2O	3.07	0.20	3.36	2.42	0.80
P_2O_5	0.09	0.01	0.02	0.03	0.13
LOI	2.30	2.10	2.22	1.47	3.50
Total	99.59	99.30	99.57	98.67	99.08
Cr(ppm)	4	3	3	3	4
Ni	-1	-1	-1	1	2
Co	1	1	-1	1	1
V	14	9	3	36	10
Cu	14	10	3	15	15
Pb	113	16	301	5	16
Zn	96	173	72	54	76
Cd	0.10	0.70	0.40	0.10	0.10
Mo	2.00	4.00	4.00	5.00	4.00
Rb	47	1	85	63	14
Ba	795	1863	547	444	251
Sr	41	27	4	65	207
Ga	11	9	11	24	13
Li	5.00	2.00	4.00	26.00	8.00
Nb	7.0	4.0	5.0	6.0	7.0
Ta	0.41	0.24	0.29	0.35	0.41
Zr	232	169	209	345	242
Hf	6.27	4.57	5.65	9.32	6.54
Y	33	19	13	40	35
Th	2.00	3.00	2.00	7.00	5.00
La	16.00	10.00	4.00	24.00	26.00
Ce	45.00	33.00	20.00	71.00	71.00
F	277.00	72.00	138.00	334.00	297.00
Be	1.00	0.70	0.70	2.30	1.70
Ag	-0.1	0.1	0.5	-0.1	-0.1
Au(ppb)	-5.0	-5.0	-5.0	na	na

Appendix I. (continued)

Sedimentary Rocks

Sample #	584009	584074	584098	584112	584149	584154	584158
SiO2 (wt.%)	74.05	48.40	76.95	74.55	60.25	60.50	57.65
TiO2	0.22	1.20	0.34	0.28	1.01	0.71	1.32
Al2O3	12.20	15.89	12.02	12.86	11.46	15.17	13.68
Fe2O3(total)	2.88	10.77	1.08	1.97	12.26	6.40	10.52
MnO	0.09	0.37	0.01	0.06	0.32	0.12	0.33
MgO	2.35	8.44	1.00	0.77	4.59	2.24	4.27
CaO	0.37	8.34	0.63	0.72	3.36	4.52	6.39
Na2O	0.62	2.37	4.18	6.51	1.62	0.51	2.49
K2O	3.51	1.03	2.13	0.29	0.05	3.05	0.11
P2O5	0.12	0.20	0.04	0.03	0.07	0.18	0.15
LOI	2.19	3.08	1.10	1.25	4.00	6.46	3.24
Total	98.60	100.09	99.48	99.29	98.99	99.86	100.15
Cr(ppm)	8	284	7	6	12	51	17
Ni	2	117	2	-1	6	26	7
Co	2	40	-1	-1	19	14	24
V	15	221	5	1	202	67	290
Cu	4	79	5	7	39	23	31
Pb	4	51	11	9	10	10	9
Zn	39	227	16	37	185	81	122
Cd	-0.10	0.20	0.30	0.70	4.90	0.30	0.10
Mo	3.00	3.00	2.00	4.00	3.00	4.00	4.00
Rb	100	15	46	6	4	96	2
Ba	538	232	402	129	13	607	13
Dr	14	129	56	65	197	93	295
Ga	19	29	14	16	23	20	23
Li	25.00	12.00	10.00	4.00	12.00	29.00	8.00
Nb	6.0	1.0	10.0	6.0	-1.0	13.0	-1.0
Zr	144	129	347	302	110	272	160
Y	18	24	56	58	30	33	32
Th	6.00	3.00	1.00	2.00	-1.00	8.00	-1.00
La	16.00	13.00	64.00	20.00	11.00	38.00	14.00
Ce	46.00	34.00	173.00	70.00	34.00	99.00	38.00
F	901.00	656.00	280.00	198.00	326.00	416.00	393.00
Be	1.90	1.20	2.80	1.80	1.10	2.20	1.10
Ag	0.10	0.70	0.10	0.10	0.10	0.10	0.10
Au(ppb)	-5.0	-5.0	na	-5.0	-5.0	na	na

Appendix I. (continued)

Sedimentary Rocks

Sample #	584162	584163	584167	584206	584208	584213	584221
SiO2 (wt.%)	73.90	75.20	34.90	52.80	60.65	54.30	82.40
TiO2	0.25	0.19	0.36	1.16	0.90	0.79	0.20
Al2O3	9.99	7.79	9.11	15.20	17.21	9.83	7.38
Fe2O3(total)	3.16	4.11	5.15	8.73	7.95	16.58	1.99
MnO	0.17	0.13	0.48	0.18	0.15	0.18	0.16
MgO	5.74	5.71	1.76	1.61	1.75	2.99	3.63
CaO	0.84	0.43	23.91	6.89	2.50	4.51	0.21
Na2O	3.00	1.87	2.95	1.52	3.11	1.49	0.26
K2O	0.03	0.05	0.15	3.25	2.52	0.40	1.42
P2O5	0.02	0.01	0.20	0.35	0.19	0.08	0.01
LOI	2.81	3.06	19.42	7.47	2.88	8.21	2.06
Total	99.91	98.55	98.39	99.16	99.81	99.36	99.72
Cr(ppm)	7	4	22	14	12	16	4
Ni	5	-1	12	4	4	10	-1
Co	1	2	6	18	16	16	-1
V	15	9	29	140	106	136	8
Cu	6	5	17	45	15	88	5
Pb	4	2	21	5	12	761	18
Zn	73	75	101	101	107	2480	74
Cd	-0.10	0.10	0.20	0.20	0.10	13.90	-0.10
Mo	1.00	2.00	5.00	4.00	4.00	10.00	2.00
Rb	2	-1	-1	110	82	6	43
Ba	65	37	6688	568	591	191	666
Dr	65	45	237	145	276	219	16
Ga	12	12	12	19	23	18	4
Li	12.00	14.00	11.00	9.00	12.00	9.00	53.00
Nb	6.0	5.0	8.0	14.0	10.0	-1.0	4.0
Zr	240	220	157	230	189	160	159
Y	46	47	32	34	30	34	21
Th	-1.00	1.00	2.00	6.00	6.00	-1.00	4.00
La	20.00	17.00	27.00	35.00	36.00	13.00	13.00
Ce	56.00	52.00	66.00	85.00	84.00	37.00	40.00
F	374.00	376.00	257.00	503.00	438.00	323.00	393.00
Be	1.00	0.90	1.50	1.90	2.00	1.00	1.10
Ag	0.10	0.10	0.10	0.10	0.10	2.90	0.20
Au(ppb)	na	-5.0	na	na	na	na	na

Appendix I. (continued)

Sedimentary Rocks

Sample #	584222	584229	584232
SiO2 (wt.%)	77.60	78.25	68.80
TiO2	0.11	0.24	0.44
Al2O3	5.30	9.36	11.20
Fe2O3(total)	8.10	1.31	4.52
MnO	0.22	0.08	0.09
MgO	2.89	7.78	7.92
CaO	0.30	0.16	0.49
Na2O	0.12	0.09	0.43
K2O	0.85	1.25	2.07
P2O5	0.01	0.03	0.11
LOI	3.08	1.77	3.14
Total	98.58	100.32	99.21
Cr(ppm)	5	3	6
Ni	-1	1	-1
Co	2	-1	2
V	17	2	21
Cu	1640	6	18
Pb	7	2	5
Zn	120	88	57
Cd	0.30	0.10	0.20
Mo	43.00	3.00	3.00
Rb	27	37	55
Ba	117	113	429
Dr	8	45	20
Ga	17	13	13
Li	15.00	3.00	90.00
Nb	2.0	5.0	4.0
Zr	170	281	238
Y	13	37	24
Th	1.00	7.00	6.00
La	10.00	18.00	18.00
Ce	28.00	56.00	54.00
F	330.00	227.00	396.00
Be	1.00	0.50	1.10
Ag	0.70	0.10	0.10
Au(ppb)	-5.0	na	na

Appendix II. Chemical analyses for the intrusive rocks of the Hermitage Peninsula. Hf and Ta are
recalculated from Zr and Nb, respectively. (na = not analysed, -1 = less than one)

Grole Diorite, Simmons Brook Batholith, and Straddling Granite

Sample #	584138	584088	584089	584091	584132	584133	584205
SiO2 (wt.%)	47.30	46.60	41.10	47.55	47.60	47.30	45.25
TiO2	1.01	0.27	0.18	0.15	0.37	0.38	0.19
Al203	15.13	12.44	9.31	19.32	4.93	17.63	20.21
Fe2O3(total)	10.56	14.29	18.29	5.31	15.76	4.23	4.36
MnO	0.37	0.35	0.26	0.10	0.35	0.10	0.04
MgO	9.58	10.86	13.04	11.05	15.62	6.30	10.21
CaO	8.97	4.54	8.59	9.50	11.30	16.95	12.92
Na2O	2.01	2.99	0.30	2.34	0.31	2.31	0.88
K2O	1.84	0.43	0.16	0.82	0.05	0.19	2.08
P2O5	0.11	0.04	0.06	0.02	0.07	0.05	0.01
LOI	3.25	6.92	6.81	3.69	3.15	4.23	4.06
Total	100.13	99.73	98.10	99.85	99.51	99.67	100.21
Cr(ppm)	222	27	137	271	420	1259	816
Ni	98	8	318	136	699	50	106
Co	39	17	163	38	180	20	30
V	224	69	65	30	82	97	62
Cu	33	36	979	43	8300	11	135
Pb	8	3	-1	2	5	6	86
Zn	101	289	144	61	97	46	131
Cd	0.30	0.20	0.20	0.10	0.60	0.10	2.40
Mo	3.00	6.00	4.00	4.00	6.00	4.00	3.00
Rb	19	7	3	11	1	7	37
Ba	390	210	19	184	11	32	664
Sr	183	85	127	304	69	123	276
Ga	24	25	27	14	20	18	10
Li	13.00	9.00	6.00	20.00	2.00	9.00	30.00
Nb	-1.0	-1.0	-1.0	-1.0	-1.0	-1.0	-1.0
Zr	47	290	30	23	17	129	-1
Y	15	88	18	8	34	22	2
Th	-1.00	4.00	4.00	7.00	-1.00	-1.00	-1.00
La	3.00	52.00	11.00	6.00	9.00	5.00	1.00
Ce	12.00	125.00	33.00	-1.00	24.00	16.00	2.00
F	254.00	305.00	160.00	135.00	141.00	128.00	85.00
Be	0.60	1.10	0.60	0.40	0.50	0.90	0.50
Ag	0.1	-0.1	0.9	0.1	8.0	-0.1	0.1
Au(ppb)	na	-5.0	-5.0	na	25.0	na	na

Appendix II. (continued)

Grole Diorite, Simmons Brook Batholith, and Straddling Granite

Sample #	584214	584215	584092	584093	584131	584172	584178
SiO2 (wt.%)	60.30	48.15	25.10	49.20	41.90	45.75	50.85
TiO2	0.32	1.31	0.26	1.17	0.04	1.38	1.60
Al2O3	20.90	16.45	2.54	15.11	22.07	15.77	16.82
Fe2O3(total)	3.99	11.02	46.40	11.33	2.33	10.66	11.57
MnO	0.08	0.18	0.20	0.16	0.06	0.18	0.30
MgO	1.00	8.56	8.50	5.21	3.91	9.52	3.88
CaO	5.67	9.91	4.83	10.28	21.68	10.21	7.47
Na2O	5.89	2.61	0.18	2.41	0.74	2.39	3.14
K2O	0.89	0.52	0.03	0.18	0.32	0.46	1.61
P2O5	0.09	0.23	0.04	0.14	0.02	0.15	0.39
LOI	0.95	1.02	6.36	4.77	7.06	3.13	2.29
Total	100.08	99.96	94.44	99.96	100.13	99.60	99.92
Cr(ppm)	4	248	294	116	142	337	13
Ni	1	117	1090	28	60	137	15
Co	8	41	282	27	14	43	29
V	30	219	52	337	11	229	237
Cu	9	50	14400	28	11	64	70
Pb	6	-1	85	33	15	-1	9
Zn	46	80	85	82	58	72	142
Cd	0.10	0.40	0.50	0.20	-0.10	0.20	0.10
Mo	5.00	4.00	8.00	4.00	5.00	4.00	5.00
Rb	16	8	3	8	10	2	34
Ba	407	136	6	42	38	1442	2955
Sr	346	241	9	376	54	285	308
Ga	21	27	55	25	9	21	28
Li	10.00	10.00	5.00	13.00	14.00	9.00	8.00
Nb	-1.0	1.0	-1.0	-1.0	-1.0	-1.0	7.0
Zr	333	116	93	78	17	107	251
Y	7	23	13	26	3	22	47
Th	4.00	13.00	-1.00	3.00	-1.00	-1.00	4.00
La	12.00	10.00	5.00	8.00	1.00	7.00	26.00
Ce	26.00	28.00	53.00	27.00	3.00	22.00	71.00
F	90.00	229.00	96.00	275.00	149.00	183.00	605.00
Be	1.70	1.00	0.40	1.00	1.70	0.90	1.70
Ag	-0.1	-0.1	14.9	0.2	-0.1	-0.1	-0.1
Au(ppb)	na	na	50.0	-5.0	-5.0	na	-5.0

Appendix II. (continued)

Grole Diorite, Simmons Brook Batholith, and Straddling Granite

Sample #	584201	584012	584204
SiO2 (wt.%)	46.75	73.50	74.45
TiO2	1.60	0.35	0.24
Al2O3	16.00	12.73	12.17
Fe2O3(total)	10.86	2.66	2.54
MnO	0.18	0.04	0.04
MgO	9.12	0.64	1.94
CaO	9.83	1.94	0.09
Na2O	2.58	2.72	2.62
K2O	0.36	2.97	2.30
P2O5	0.16	0.04	0.01
LOI	2.75	1.02	2.42
Total	100.19	98.61	98.82
Cr(ppm)	283	10	9
Ni	141	3	1
Co	41	4	1
V	235	18	2
Cu	49	13	10
Pb	2	10	18
Zn	85	74	49
Cd	0.40	0.20	0.40
Mo	4.00	2.00	3.00
Rb	6	78	55
Ba	2054	313	416
Sr	229	45	19
Ga	21	19	13
Li	12.00	16.00	14.00
Nb	-1.0	10.0	2.0
Zr	210	304	223
Y	24	31	39
Th	1.00	9.00	8.00
La	5.00	17.00	28.00
Ce	18.00	41.00	79.00
F	164.00	163.00	533.00
Be	0.80	1.30	1.60
Ag	-0.1	-0.1	-0.1
Au(ppb)	na	na	na

Appendix II. (continued)

Felsic Dykes (older)

Sample #	584043	584048	584064	584069	584094	584034	584049
SiO2 (wt.%)	75.85	76.70	68.20	74.75	78.35	77.40	78.00
TiO2	0.19	0.21	0.19	0.21	0.08	0.24	0.18
Al2O3	11.55	12.40	11.65	11.74	11.32	12.04	11.21
Fe2O3(total)	1.65	0.72	4.05	2.39	0.81	1.14	1.22
MnO	0.18	0.06	0.69	0.12	0.01	0.07	0.06
MgO	3.34	0.67	8.21	3.34	0.07	0.58	0.48
CaO	0.42	0.45	2.17	0.68	1.15	0.57	1.17
Na2O	2.38	6.62	3.11	4.38	3.69	6.30	5.71
K2O	1.21	0.11	0.17	0.34	3.73	0.26	0.21
P2O5	0.00	0.02	0.02	0.02	0.01	0.03	0.02
LOI	1.28	0.77	1.59	1.01	0.48	0.80	0.71
Total	98.05	98.73	100.05	98.98	99.70	99.43	98.97
Cr(ppm)	3	9	4	4	4	3	5
Ni	-1	4	1	-1	1	2	2
Co	3	3	4	6	1	3	3
V	1	1	1	18	11	4	6
Cu	18	12	92	2	13	8	21
Pb	45	32	72	60	18	45	22
Zn	558	600	286	199	8	267	145
Cd	1.90	3.80	0.60	2.70	0.30	1.70	2.10
Mo	4.00	2.00	4.00	2.00	2.00	3.00	2.00
Rb	32	3	6	8	66	6	5
Ba	645	90	104	432	448	107	87
Sr	49	54	126	79	102	58	77
Ga	10	11	25	19	13	8	15
Li	68.00	9.00	36.00	34.00	3.00	9.00	7.00
Nb	7.0	10.0	1.0	7.0	8.0	8.0	8.0
Ta	0.41	0.59	0.06	0.41	0.47	0.47	0.47
Zr	266	284	256	294	102	222	241
Hf	7.19	7.68	6.92	7.95	2.76	6.00	6.51
Y	27	34	23	27	63	39	49
Th	12.00	12.00	-1.00	8.00	24.00	9.00	8.00
La	19.00	18.00	23.00	19.00	21.00	15.00	17.00
Ce	56.00	60.00	68.00	63.00	60.00	47.00	54.00
F	462.00	84.00	547.00	250.00	69.00	80.00	104.00
Be	1.70	1.30	1.60	1.20	1.70	1.20	1.30
Ag	3.0	0.1	0.7	0.1	-0.1	0.2	0.1
Au(ppb)	na	-5.0	-5.0	na	na	-5.0	na

Appendix II. (continued)

Felsic Dykes (older)

Sample #	584057	584062	584137	584176	584217
SiO2 (wt.%)	77.25	76.85	73.30	78.50	75.95
TiO2	0.17	0.17	0.44	0.52	0.23
Al2O3	11.48	12.08	10.84	7.95	11.97
Fe2O3(total)	1.39	0.73	3.12	3.95	1.80
MnO	0.14	0.54	0.37	0.23	0.06
MgO	1.88	0.72	3.10	1.01	0.41
CaO	0.54	0.52	2.42	0.58	1.26
Na2O	5.52	6.43	3.17	1.53	6.17
K2O	0.20	0.13	1.04	2.78	0.16
P2O5	0.02	0.02	0.07	0.16	0.03
LOI	0.91	0.74	2.25	2.05	0.49
Total	99.50	98.93	100.12	99.26	98.53
Cr(ppm)	5	4	3	5	3
Ni	1	1	-1	-1	1
Co	3	3	1	1	1
V	4	4	12	26	7
Cu	7	11	7	7	12
Pb	52	132	12	4	17
Zn	589	489	83	55	49
Cd	15.10	1.30	-0.10	0.20	0.30
Mo	2.00	2.00	2.00	6.00	3.00
Rb	7	5	11	31	1
Ba	125	58	288	776	69
Sr	69	57	83	29	75
Ga	12	12	13	7	10
Li	20.00	8.00	6.00	5.00	5.00
Nb	5.0	6.0	5.0	5.0	6.0
Ta	0.29	0.35	0.29	0.29	0.35
Zr	258	256	209	158	288
Hf	6.97	6.92	5.65	4.27	7.78
Y	26	44	47	25	48
Th	6.00	6.00	3.00	-1.00	1.00
La	19.00	18.00	19.00	14.00	20.00
Ce	60.00	58.00	58.00	40.00	26.00
F	171.00	94.00	328.00	205.00	93.00
Be	1.10	1.30	1.50	0.50	1.00
Ag	0.1	0.3	-0.1	-0.1	-0.1
Au(ppb)	na	na	na	-5.0	na

Appendix II. (continued)

Felsic Dykes (younger)

Sample #	584033	584142	584148	584219	584224
SiO2 (wt.%)	73.70	74.55	72.95	71.70	72.10
TiO2	0.03	0.03	0.04	0.02	0.08
Al2O3	14.47	14.56	15.31	15.52	14.75
Fe2O3(total)	0.96	0.72	0.87	1.00	1.17
MnO	0.05	0.06	0.09	0.05	0.12
MgO	0.78	0.20	0.21	0.29	0.50
CaO	0.62	1.19	1.55	0.91	1.21
Na2O	4.64	4.39	4.67	5.19	4.69
K2O	2.02	2.31	2.11	2.20	2.06
P2O5	0.09	0.10	0.08	0.10	0.07
LOI	1.35	1.92	2.38	1.05	1.21
Total	98.71	100.03	100.26	98.03	97.96
Cr(ppm)	6	3	4	3	4
Ni	4	-1	1	2	-1
Co	2	-1	1	1	-1
V	-1	-1	1	1	3
Cu	7	7	4	9	9
Pb	23	7	14	8	6
Zn	433	50	67	49	65
Cd	0.80	0.30	0.30	0.20	0.20
Mo	2.00	4.00	3.00	3.00	2.00
Rb	36	72	63	65	44
Ba	561	286	591	540	444
Sr	92	79	308	168	115
Ga	16	18	17	14	10
Li	19.00	4.00	4.00	13.00	13.00
Nb	17.0	26.0	26.0	13.0	15.0
Ta	1.00	1.53	1.53	0.76	0.88
Zr	28	37	39	37	90
Hf	0.76	1.00	1.05	1.00	2.43
Y	4	11	11	6	14
Th	7.00	-1.00	-1.00	-1.00	1.00
La	7.00	6.00	10.00	12.00	16.00
Ce	19.00	16.00	28.00	29.00	39.00
F	261.00	192.00	280.00	208.00	185.00
Be	1.70	2.40	2.70	2.10	1.60
Ag	0.1	-0.1	-0.1	-0.1	-0.1
Au(ppb)	na	na	na	na	na

Appendix II. (continued)

Mafic Dykes (older)

Sample #	584114	584141	584145	584155	584169	584171	584189
SiO2 (wt.%)	45.10	45.85	55.60	47.65	42.05	49.20	43.80
TiO2	1.98	1.19	1.12	1.80	0.96	1.82	0.99
Al2O3	15.20	15.25	15.83	15.05	15.38	11.24	16.64
Fe2O3(total)	13.73	11.14	8.67	12.21	8.69	12.12	12.37
MnO	0.28	0.61	0.20	0.33	0.15	0.20	1.11
MgO	8.07	7.21	5.18	7.37	8.66	2.59	10.67
CaO	6.68	11.34	8.23	8.77	9.42	16.38	6.24
Na2O	2.27	2.07	2.67	3.09	1.21	0.07	1.59
K2O	0.19	1.76	0.03	1.36	0.48	0.01	3.04
P2O5	0.23	0.10	0.18	0.23	0.06	0.22	0.11
LOI	6.07	3.39	4.22	2.47	11.94	5.08	3.16
Total	99.80	99.91	101.93	100.33	99.00	98.93	99.72
Cr(ppm)	141	158	62	225	165	19	223
Ni	59	49	33	63	99	6	62
Co	45	35	27	39	40	25	35
V	338	298	219	311	187	312	305
Cu	66	73	14	70	54	24	282
Pb	6	9	8	2	5	1	902
Zn	131	132	103	121	63	64	1600
Cd	0.20	0.10	0.10	0.20	0.10	0.20	3.90
Mc	4.00	4.00	3.00	4.00	3.00	4.00	4.00
Rb	6	17	5	31	5	3	43
Ba	138	814	566	292	48	778	436
Sr	147	271	434	266	137	568	117
Ga	31	25	25	28	20	33	23
Li	16.00	7.00	18.00	8.00	45.00	6.00	16.00
Nb	-1.0	-1.0	2.0	-1.0	-1.0	-1.0	-1.0
Ta	0.06	0.06	0.12	0.06	0.06	0.06	0.06
Zr	145	67	178	135	53	96	41
Hf	3.92	1.81	4.81	3.65	1.43	2.59	1.11
Y	36	17	27	31	16	30	14
Th	-1.00	-1.00	1.00	-1.00	-1.00	-1.00	-1.00
La	13.00	4.00	20.00	8.00	3.00	5.00	2.00
Ce	33.00	14.00	54.00	27.00	9.00	1.00	9.00
F	827.00	258.00	465.00	234.00	115.00	249.00	785.00
Be	1.40	0.90	1.30	1.00	0.60	0.70	0.90
Ag	-0.1	0.2	-0.1	0.1	0.2	-0.1	0.8
Au(ppb)	-5.0	-5.0	na	na	na	-5.0	-5.0

Appendix II. (continued)

Mafic Dykes (younger)

Sample #	584177	584118	584121
SiO2 (wt.%)	51.80	53.60	57.35
TiO2	1.11	0.8ᶜ	0.86
Al2O3	18.89	19.83	19.23
Fe2O3(total)	9.56	8.32	6.09
MnO	0.18	0.14	0.08
MgO	2.90	3.44	1.57
CaO	8.36	2.64	2.61
Na2O	2.91	4.52	4.23
K2O	1.29	1.50	2.35
P2O5	0.24	0.18	0.18
LOI	2.04	4.40	5.01
Total	99.28	99.46	99.56
Cr(ppm)	6	6.00	5.00
Ni	7	2.00	2.00
Co	24	20.00	12.00
V	223	137.00	130.00
Cu	64	19.00	16.00
Pb	5	11.00	16.00
Zn	92	103.00	105.00
Cd	0.10	0.10	0.10
Mo	6.00	4.00	5.00
Rb	26	74.00	168.00
Ba	598	374.00	330.00
Sr	390	318.00	143.00
Ga	16	25.00	19.00
Li	10.00	63.00	126.00
Nb	3.0	1.00	1.00
Ta	0.18	0.06	0.06
Zr	171	148.00	144.00
Hf	4.62	4.00	3.89
Y	28	20.00	19.00
Th	-1.00	-1.00	1.00
La	19.00	13.00	10.00
Ce	49.00	38.00	37.00
F	357.00	na	322.00
Be	1.40	1.50	1.20
Ag	-0.1	0.10	1.10
Au(ppb)	na	10.00	55.00

Appendix III. Chemical analyses for mineralized and carbonate/calc-silicate samples from the Connaigre Bay Group. (na = not analysed, -1 = less than one, COI = gain on ignition)

Mineralized Sam Head Formation samples

Winter Hill

Sample #	584013	584014	584015	584016	584019	584022	584023
SiO2 (wt.%)	68.70	47.00	32.00	18.65	17.40	22.75	9.15
TiO2	0.23	0.46	0.43	0.16	0.22	0.03	0.06
Al2O3	3.23	2.68	6.34	8.83	7.76	6.35	4.14
Fe2O3(total)	15.02	27.41	33.92	13.88	35.85	5.92	17.51
MnO	0.29	0.07	0.18	0.52	0.22	0.28	0.24
MgO	2.03	0.32	1.38	18.26	14.95	24.05	9.26
CaO	0.83	0.09	0.16	0.85	0.85	0.14	0.35
Na2O	0.02	0.11	0.25	0.03	0.05	0.01	0.01
K2O	0.12	0.31	0.32	0.01	0.01	0.01	0.01
P2O5	0.01	0.02	0.02	0.18	0.10	0.07	0.16
LOI	7.72	16.75	20.01	15.93	14.99	13.11	15.43
Total	98.20	95.22	95.01	77.30	92.40	72.72	56.32
Cr(ppm)	11	9	25	5	6	3	7
Ni	1	-1	1	-1	-1	-1	-1
Co	9	33	39	2	2	9	6
V	16	17	31	18	27	12	9
Cu	2730	5040	4120	37800	34400	393	67100
Pb	24	68	145	221	16	17	133
Zn	294	407	115	124000	13200	187000	257000
Cd	3.00	3.20	0.10	465.00	52.00	850.00	1050.00
Mo	58.00	113.00	55.00	4.00	12.00	1.00	5.00
Rb	4	7	11	7	2	1	4
Ba	14	90	121	5	23	11	16
Sr	15	4	10	2	1	1	2
Ga	24	33	49	30	49	22	31
Li	7.00	7.00	23.00	7.00	3.00	3.00	4.00
Nb	-1.0	-1.0	-1.0	-1.0	-1.0	1.0	1.0
Zr	79	51	56	74	71	12	42
Y	16	4	5	17	15	3	3
Th	4.00	1.00	-1.00	4.00	-1.00	8.00	2.00
La	9.00	1.00	2.00	2.00	1.00	1.00	-1.00
Ce	23.00	12.00	23.00	10.00	18.00	2.00	2.00
F	182.00	123.00	190.00	1960.00	1020.00	1140.00	478.00
Be	0.30	0.20	0.70	0.60	0.50	0.50	0.30
Ag	1.6	3.5	2.7	24.2	76.5	0.5	39.1
Au(ppb)	-5.0	40.0	35.0	5.0	70.0	-5.0	40.0

Appendix III. (continued)

Winter Hill

Sample #	584055	584058	584061	584063	584065	584066	584067
SiO2 (wt.%)	33.15	39.05	11.45	28.00	39.10	87.85	3c.65
TiO2	0.03	0.02	0.01	0.11	0.01	0.01	0.03
Al2O3	0.31	0.34	0.16	2.73	0.21	0.94	1.43
Fe2O3(total)	12.18	8.87	1.87	17.31	5.56	3.51	5.24
MnO	1.13	0.66	0.98	0.54	0.33	0.02	1.38
MgO	23.84	18.45	8.00	17.23	18.53	1.06	18.77
CaO	10.30	14.21	38.98	5.05	14.34	0.14	19.63
Na2O	0.01	0.01	0.02	0.11	0.01	0.13	0.01
K2O	0.01	0.01	0.01	0.02	0.01	0.09	0.01
P2O5	0.13	0.05	0.08	0.07	0.06	0.01	0.07
LOI	8.29	7.44	27.35	13.75	6.30	2.76	5.29
Total	89.38	89.11	88.91	84.92	84.46	96.51	89.11
Cr(ppm)	8	9	6	8	8	5	-
Ni	-1	3	-1	2	-1	-1	-1
Co	3	4	2	3	3	1	3
V	7	9	8	10	14	4	3
Cu	1120	829	128	455	387	2120	537
Pb	11290	34595	14963	30465	51775	9186	4251
Zn	57600	45100	18400	80300	65100	23600	7650
Cd	260.00	217.00	112.00	390.00	418.00	86.60	31.40
Mo	2.00	2.00	5.00	1.00	2.00	2.00	8.00
Rb	1	-1	1	3	2	4	1
Ba	7	10	44	9	6	74	16
Sr	3	4	81	3	3	3	21
Ga	19	14	13	24	9	12	4
Li	5.00	4.00	2.00	7.00	3.00	12.00	4.00
Nb	-1.0	-1.0	-1.0	-1.0	-1.0	-1.0	-1.0
Zr	22	53	13	54	28	22	39
Y	3	2	4	9	3	2	7
Th	1.00	-1.00	-1.00	-1.00	1.00	-1.00	-1.00
La	2.00	2.00	3.00	3.00	2.00	2.00	4.00
Ce	8.00	10.00	1.00	13.00	8.00	8.00	11.00
F	5810.00	660.00	451.00	1690.00	622.00	89.00	1350.00
Be	3.00	2.50	0.90	1.00	0.50	0.50	1.40
Ag	9.0	151.0	61.4	13.6	197.0	695.0	5.5
Au(ppb)	50.0	200.0	270.0	270.0	90.0	400.0	70.0

Appendix III. (continued)

Winter Hill

Sample #	584028	584029	584031	584032	584035	584036	584037
SiO2 (wt.%)	26.45	34.00	8.70	43.55	49.05	11.80	32.05
TiO2	0.27	0.07	0.02	0.03	0.03	0.08	0.03
Al2O3	14.96	1.87	0.22	0.29	0.95	0.81	0.75
Fe2O3(total)	14.42	18.17	6.55	10.31	4.47	5.34	16.94
MnO	0.46	0.43	0.70	0.79	0.60	1.11	1.03
MgO	26.45	17.50	20.86	15.43	21.79	7.01	16.25
CaO	0.15	8.42	20.95	19.48	8.13	24.56	9.07
Na2O	0.08	0.08	0.01	0.01	0.12	0.03	0.02
K2O	0.35	0.01	0.01	0.01	0.03	0.01	0.01
P2O5	0.14	0.06	0.07	0.08	0.03	0.06	0.07
LOI	15.42	12.75	17.27	1.42	5.57	GOI	12.40
Total	99.15	93.36	75.36	91.40	90.77		88.62
Cr(ppm)	7	10	6	6	5	7	9
Ni	-1	5	2	1	-1	1	1
Co	4	3	2	4	2	4	2
V	27	6	5	3	3	19	10
Cu	3110	164	445	98	348	376	1660
Pb	35	19745	13535	827	16	12235	3496
Zn	2860	31800	26000	56200	56200	148000	54500
Cd	285.00	179.00	85.40	96.00	199.00	913.00	211.00
Mo	5.00	7.00	4.00	3.00	2.00	20.00	7.00
Rb	7	2	1	1	1	1	1
Ba	138	7	73	13	6	21	4
Sr	4	6	79	3	6	62	3
Ga	34	18	8	9	4	11	17
Li	41.00	6.00	3.00	6.00	5.00	5.00	16.00
Nb	2.0	-1.0	1.0	-1.0	2.0	1.0	-1.0
Zr	104	37	17	7	9	10	48
Y	11	9	2	2	5	4	5
Th	4.00	4.00	4.00	3.00	5.00	4.00	2.00
La	1.00	4.00	1.00	1.00	2.00	2.00	2.00
Ce	12.00	14.00	4.00	4.00	7.00	6.00	11.00
F	1800.00	1120.00	653.00	303.00	241.00	667.00	1010.00
Be	0.70	0.90	0.30	0.60	2.80	1.20	2.60
Ag	2.5	74.5	19.7	8.0	16.4	24.7	10.8
Au(ppb)	-5.0	115.0	100.0	-5.0	65.0	160.0	245.0

Appendix III. (continued)

Winter Hill

Sample #	584038	584042	584044	584046	584051	584052	584053
SiO2 (wt.%)	20.20	41.15	49.05	47.95	22.60	11.50	42.30
TiO2	0.02	0.02	0.03	0.01	0.49	0.15	0.01
Al2O3	0.36	0.90	1.10	0.15	6.37	2.05	0.13
Fe2O3(total)	21.61	4.76	4.79	4.54	5.23	6.24	11.64
MnO	0.88	0.72	0.57	0.59	0.69	1.85	0.63
MgO	10.84	18.45	18.56	22.55	18.50	8.58	14.31
CaO	11.60	4.15	17.32	11.71	21.74	26.51	19.27
Na2O	0.04	0.15	0.03	0.04	0.07	0.01	0.01
K2O	0.05	0.01	0.01	0.01	0.01	0.11	0.01
P2O5	0.05	0.08	0.12	0.08	0.11	0.07	0.06
LOI	14.33	7.25	4.16	5.48	17.71	8.56	5.56
Total	79.98	77.64	95.74	93.11	93.52	65.63	93.93
Cr(ppm)	5	6	6	7	35	15	8
Ni	-1	2	2	1	9	3	1
Co	4	3	3	2	14	6	8
V	3	6	4	3	93	41	1
Cu	704	428	456	4390	113	839	1830
Pb	13993	64345	1161	18346	37	8452	97
Zn	92000	104000	16300	38800	12300	84700	40000
Cd	545.00	73.50	63.70	207.00	66.80	498.00	269.00
Mo	13.00	3.00	4.00	2.00	4.00	12.00	2.00
Rb	3	-1	-1	-1	-1	3	1
Ba	21	5	7	6	13	154	13
Sr	26	4	4	8	83	121	1
Ga	22	5	4	3	15	13	12
Li	7.00	11.00	28.00	17.00	3.00	4.00	5.00
Nb	-1.0	2.0	2.0	1.0	-1.0	-1.0	-1.0
Zr	28	37	24	1	29	15	6
Y	2	7	7	3	9	5	2
Th	-1.00	5.00	4.00	-1.00	-1.00	-1.00	-1.00
La	1.00	2.00	5.00	1.00	4.00	2.00	1.00
Ce	4.00	7.00	10.00	4.00	10.00	5.00	5.00
F	859.00	2410.00	777.00	2420.00	1070.00	663.00	100.00
Be	1.20	2.30	2.20	1.90	1.10	1.00	0.90
Ag	36.3	76.5	18.4	34.0	4.1	32.4	8.0
Au(ppb)	155.0	45.0	10.0	na	na	370.0	25.0

Appendix III. (continued)

Winter Hill

Sample #	584071	584202
SiO2 (wt.%)	25.25	23.40
TiO2	0.14	0.11
Al2O3	1.70	4.89
Fe2O3(total)	21.27	13.64
MnO	2.18	0.31
MgO	14.55	17.03
CaO	7.95	1.01
Na2O	0.02	0.07
K2O	0.01	0.01
P2O5	0.05	0.30
LOI	13.85	16.89
Total	86.97	77.66
Cr(ppm)	7	7
Ni	-1	-1
Co	5	11
V	26	11
Cu	280	143000
Pb	6504	681
Zn	83300	36300
Cd	447.00	96.40
Mo	21.00	8.00
Rb	1	1
Ba	14	64
Sr	3	3
Ga	30	18
Li	5.00	5.00
Nb	-1.0	-1.0
Zr	27	34
Y	5	9
Th	-1.00	-1.00
La	1.00	1.00
Ce	9.00	9.00
F	1190.00	1390.00
Be	0.60	0.90
Ag	14.2	17.0
Au(ppb)	140.0	30.0

Appendix III. (continued)

Winter Hill West and Winter Hill East

Sample #	584072	584073	584075	584076	584077	584078
SiO2 (wt.%)	42.80	42.70	73.50	43.20	22.30	38.40
TiO2	0.03	0.25	0.20	0.01	0.02	0.38
Al2O3	1.64	7.95	8.12	0.21	6.26	9.05
Fe2O3(total)	34.04	27.00	5.65	8.34	27.71	13.57
MnO	0.11	0.08	0.09	0.84	1.09	1.96
MgO	1.27	2.40	1.33	17.06	15.16	19.96
CaO	0.95	0.18	0.36	17.66	3.07	4.11
Na2O	0.09	0.18	0.14	0.01	0.09	0.18
K2O	0.01	2.34	2.73	0.01	0.03	0.20
P2O5	0.01	0.04	0.04	0.09	0.05	0.11
LOI	15.53	15.65	4.13	6.71	19.05	9.49
Total	96.48	98.77	96.29	94.14	94.83	97.91
Cr(ppm)	7	8	4	5	5	83
Ni	-1	3	-1	-1	-1	8
Co	50	6	1	-1	-1	13
V	-1	14	10	4	11	199
Cu	1780	44	87	2450	194	117
Pb	-1	49	1290	32575	9426	3082
Zn	114	128	19000	4100	13200	4040
Cd	-0.10	0.60	83.10	11.50	49.40	14.00
Mo	5.00	5.00	4.00	3.00	60.00	1.00
Rb	3	58	78	2	3	4
Ba	37	483	559	13	339	100
Sr	5	7	13	3	15	8
Ga	38	38	18	-1	41	31
Li	5.00	15.00	10.00	4.00	5.00	21.00
Nb	-1.0	-1.0	2.0	-1.0	-1.0	-1.0
Zr	27	227	167	9	8	55
Y	3	21	18	2	4	15
Th	-1.00	-1.00	7.00	3.00	1.00	1.00
La	3.00	16.00	12.00	4.00	1.00	5.00
Ce	23.00	54.00	42.00	15.00	14.00	31.00
F	196.00	435.00	645.00	699.00	1610.00	3440.00
Be	0.20	1.20	1.40	3.00	1.30	6.50
Ag	0.8	1.3	0.7	66.7	66.2	8.6
Au(ppb)	50.0	5.0	-5.0	295.0	30.0	35.0

Appendix III. (continued)

Winter Hill North and Prospect #5

Sample #	584079	584097	584099
SiO2 (wt.%)	27.60	52.65	13.55
TiO2	0.01	0.21	0.01
Al2O3	0.24	6.51	0.11
Fe2O3(total)	31.71	22.08	6.95
MnO	1.59	0.01	0.86
MgO	25.87	0.40	17.89
CaO	2.97	0.98	19.55
Na2O	0.01	2.37	0.01
K2O	0.01	0.65	0.01
P2O5	0.04	0.02	0.06
LOI	6.44	12.61	26.69
Total	96.49	98.49	85.69
Cr(ppm)	4	5	5
Ni	-1	-1	-1
Co	3	4	-1
V	10	5	3
Cu	1870	12	1730
Pb	1059	19	1449
Zn	11000	18	22300
Cd	45.10	0.30	82.40
Mo	2.00	5.00	6.00
Rb	1	12	-1
Ba	6	167	15
Sr	1	65	67
Ga	26	23	1
Li	1.00	5.00	2.00
Nb	-1.0	-1.0	-1.0
Zr	12	179	9
Y	10	24	2
Th	-1.00	-1.00	-1.00
La	4.00	12.00	1.00
Ce	31.00	48.00	5.00
F	4190.00	78.00	1220.00
Be	5.30	1.00	0.50
Ag	5.5	0.1	15.3
Au(ppb)	10.0	-5.0	25.0

Appendix III. (continued)

Mineralized Tickle Point Formation samples

Frenchman Head

Sample #	584186	584191	584194	584195	584196	584197	584198
SiO2 (wt.%)	59.10	46.90	78.20	71.70	61.35	50.30	23.30
TiO2	1.18	0.86	0.57	0.61	0.71	1.58	1.55
Al2O3	10.46	12.55	7.30	9.50	7.84	13.06	14.89
Fe2O3(total)	4.76	12.00	3.27	6.20	13.60	9.59	27.93
MnO	0.18	3.47	0.06	0.03	0.18	2.13	0.91
MgO	1.21	5.58	0.43	0.15	1.17	9.46	9.98
CaO	0.68	1.42	0.16	0.08	0.42	6.07	6.40
Na2O	0.22	0.50	0.25	0.16	0.30	0.02	0.13
K2O	3.05	3.99	4.70	7.23	4.47	0.03	0.08
P2O5	0.43	0.10	0.07	0.04	0.09	0.50	0.54
LOI	6.90	8.48	2.36	3.86	8.14	5.58	15.74
Total	88.17	95.85	97.37	99.56	98.27	98.32	100.15
Cr(ppm)	4	188	59	58	18	4	6
Ni	-1	34	25	13	8	-1	-1
Co	6	17	17	20	21	10	16
V	69	178	134	146	130	95	130
Cu	1250	2950	4780	57	245	24	252
Pb	2466	1483	4393	393	826	91	51
Zn	130000	24800	2200	767	4410	16800	511
Cd	464.00	91.30	8.90	3.30	18.30	62.60	0.60
Mo	13.00	6.00	18.00	28.00	15.00	3.00	15.00
Rb	79	40	51	75	45	3	5
Ba	275	7190	2886	4391	3736	33	991
Sr	16	41	30	30	37	144	301
Ga	19	14	-1	11	15	24	46
Li	7.00	11.00	3.00	3.00	4.00	11.00	18.00
Nb	1.0	-1.0	-1.0	-1.0	-1.0	2.0	-1.0
Zr	136	48	32	31	74	166	188
Y	35	12	4	3	14	41	43
Th	-1.00	-1.00	-1.00	-1.00	-1.00	2.00	1.00
La	17.00	4.00	2.00	1.00	2.00	18.00	19.00
Ce	51.00	7.00	5.00	3.00	6.00	45.00	53.00
F	769.00	536.00	91.00	74.00	166.00	1040.00	426.00
Be	1.30	1.20	0.50	0.70	0.50	1.70	1.10
Ag	6.1	12.5	16.0	12.9	7.0	1.4	2.5
Au(ppb)	-5.0	80.0	350.0	245.0	80.0	-5.0	30.0

Appendix III. (continued)

Mineralized Tickle Point Formation samples

Selco Showings

Sample #	584087	584102	584103	584104	584106	584161	584164
SiO2 (wt.%)	32.55	32.70	19.55	66.10	28.95	33.30	19.75
TiO2	0.26	0.14	0.11	0.21	0.21	0.12	0.11
Al2O3	7.67	4.71	3.29	9.39	6.65	4.68	3.58
Fe2O3(total)	35.19	39.01	47.72	11.00	35.82	36.44	46.58
MnO	0.28	0.23	0.17	0.07	0.25	0.10	0.16
MgO	5.57	2.21	1.34	3.07	7.03	3.66	4.65
CaO	0.32	1.10	0.09	0.49	0.25	2.13	4.56
Na2O	0.04	0.01	0.01	1.44	0.27	0.02	0.09
K2O	0.16	0.01	0.02	4.41	0.30	0.01	0.02
P2O5	0.08	0.03	0.07	0.04	0.02	0.02	0.02
LOI	16.14	17.43	23.20	6.64	19.94	18.35	18.35
Total	98.26	97.58	95.57	102.86	99.69	98.83	97.97
Cr(ppm)	5	4	5	4	3	6	6
Ni	-1	-1	-1	-1	-1	4	3
Co	1	1	-1	1	-1	6	3
V	-1	-1	-1	-1	-1	39	13
Cu	16	27	19	20	16	24	34
Pb	29	77	33	12	21	38	23
Zn	123	285	88	88	159	56	68
Cd	0.20	1.90	0.30	0.30	0.10	0.30	0.30
Mo	8.00	11.00	7.00	3.00	11.00	20.00	19.00
Rb	8	4	5	53	9	-1	1
Ba	22	5	7	1015	120	38	1
Sr	6	51	-1	47	9	153	107
Ga	47	41	47	22	28	42	49
Li	12.00	7.00	6.00	8.00	13.00	10.00	3.00
Nb	-1.0	-1.0	-1.0	12.0	-1.0	-1.0	-1.0
Zr	233	156	87	151	153	87	89
Y	45	28	13	32	29	16	22
Th	-1.00	-1.00	-1.00	5.00	-1.00	-1.00	-1.00
La	18.00	10.00	6.00	15.00	12.00	7.00	10.00
Ce	78.00	63.00	61.00	50.00	62.00	34.00	51.00
F	688.00	95.00	68.00	350.00	274.00	240.00	140.00
Be	0.70	0.50	0.70	1.20	0.50	0.50	1.60
Ag	1.6	1.3	1.5	-0.1	1.1	1.5	0.3
Au(ppb)	-5.0	-5.0	-5.0	-5.0	-5.0	-5.0	-5.0

Appendix III. (continued)

Mineralized Tickle Point Formation samples

Shoal Brook and other minor mineralized zones

Sample #	584004	584005	584082	584083	584116	584119
SiO2 (wt.%)	21.75	37.50	67.55	64.55	26.35	62.50
TiO2	0.17	0.20	0.51	0.43	0.25	0.29
Al2O3	6.27	5.37	10.60	8.84	7.51	5.86
Fe2O3(total)	39.77	31.34	9.01	12.35	37.42	8.39
MnO	0.14	0.08	0.06	0.07	0.03	0.15
MgO	1.11	0.69	1.48	1.05	1.00	1.20
CaO	2.95	1.89	0.47	0.52	0.30	8.43
Na2O	0.04	0.09	4.42	3.17	0.22	0.09
K2O	0.91	1.42	0.83	1.33	2.02	1.28
P2O5	0.02	0.03	0.09	0.08	0.05	0.03
LOI	22.96	18.50	4.60	6.50	21.81	7.77
Total	96.09	97.11	99.62	98.89	96.96	95.99
Cr(ppm)	7	6	7	7	7	5
Ni	-1	-1	7	4	-1	-1
Co	2	3	5	7	6	6
V	9	9	55	42	20	54
Cu	123	48	10	18	58	44
Pb	444	203	16	22	33	48
Zn	118	44	52	52	24	62
Cd	1.80	0.20	0.20	0.30	-0.10	0.40
Mo	5.00	3.00	5.00	61.00	8.00	5.00
Rb	16	25	9	15	41	86
Ba	149	261	203	308	302	124
Sr	157	76	58	58	2	102
Ga	46	39	22	22	43	14
Li	7.00	7.00	6.00	6.00	5.00	68.00
Nb	-1.0	-1.0	3.0	-1.0	-1.0	-1.0
Zr	117	120	209	153	157	45
Y	30	25	31	37	16	10
Th	1.00	-1.00	10.00	5.00	-1.00	9.00
La	10.00	11.00	15.00	15.00	3.00	9.00
Ce	46.00	38.00	59.00	50.00	45.00	23.00
F	139.00	175.00	1640.00	160.00	183.00	181.00
Be	0.90	0.70	1.10	1.10	1.20	0.70
Ag	13.4	4.2	0.4	0.8	12.4	5.3
Au(ppb)	-5.0	10.0	-5.0	-5.0	550.0	1100.0

Appendix III. (continued)

Carbonate and Calc-silicate samples

Winter Hill

Sample #	584039	584059	584054	584021	584024	584025	584027
SiO2 (wt.%)	61.60	32.95	52.20	13.55	40.35	3.60	33.95
TiO2	0.27	1.43	0.14	0.01	0.02	0.01	0.23
Al2O3	9.85	17.15	16.55	0 39	1.32	0.12	9.43
Fe2O3	0.47	1.59	0.66	0.10	0.41	0.18	0.53
FeO	2.39	8.08	3.37	0.51	2.08	0.90	2.72
MnO	0.48	0.66	0.74	0.80	0.39	0.72	0.90
MgO	17.03	25.13	4.87	25.81	40.93	40.66	29.25
CaO	0.49	2.46	15.00	25.74	1.97	16.46	9.77
Na2O	0.38	0.25	3.59	0.01	0.01	0.01	0.01
K2O	0.36	0.03	0.68	0.01	0.01	0.01	0.01
P2O5	0.04	0.16	0.12	0.08	0.18	0.08	0.14
LOI	6.13	9.47	1.64	24.03	12.05	35.93	10.07
Total	99.48	99.36	99.56	91.04	99.72	98.68	97.01
Cr(ppm)	5	68	8	5	4	11	9
Ni	1	23	2	1	-1	2	1
Co	3	31	13	2	3	2	3
V	8	318	56	2	16	1	8
Cu	40	44	15	37	13	15	26
Pb	29	44	475	852	12	12	39
Zn	1280	950	2310	1850	725	3540	2554
Cd	4.00	5.60	15.50	8.00	0.70	12.60	1.40
Mo	2.00	2.00	11.00	3.00	-1.00	2.00	3.00
Rb	11	3	14	-1	-1	-1	-1
Ba	145	34	636	8	43	10	37
Sr	61	11	325	76	2	52	17
Ga	11	28	17	1	6	9	13
Li	189.00	21.00	14.00	3.00	7.00	2.00	3.00
Nb	7.0	-1.0	15.0	2.0	1.0	2.0	7.0
Zr	192	81	55	2	12	1	162
Y	24	19	17	4	4	1	29
Th	9.00	-1.00	2.00	9.00	2.00	3.00	8.00
La	10.00	10.00	25.00	37.00	2.00	2.00	11.00
Ce	29.00	15.00	58.00	2.00	6.00	1.00	36.00
F	1160.00	1090.00	117.00	1850.00	1150.00	6060.00	1410.00
Be	1.60	1.50	3.40	0.50	2.90	0.30	1.30
Ag	0.1	0.2	3.5	1.1	0.1	0.2	3.0
Au(ppb)	-5.0	na	na	-5.0	-5.0	-5.0	-5.0

Appendix III. (continued)

Carbonate and Calc-silicate samples

Winter Hill

Sample Name	584041	584045	584047	584056	584218	584227
SiO2 (wt.%)	54.25	18.15	49.90	38.45	47.40	41.90
TiO2	0.36	0.01	0.18	0.02	2.59	0.11
Al2O3	12.06	0.16	12.04	0.09	14.72	5.00
Fe2O3	0.55	0.37	0.49	0.48	0.71	0.12
FeO	2.82	1.88	2.51	2.43	3.63	0.63
MnO	0.49	0.94	0.56	0.77	0.49	0.63
MgO	18.52	10.73	19.01	16.91	6.24	26.77
CaO	0.29	35.89	8.12	22.51	18.67	16.15
Na2O	0.21	0.01	1.30	0.01	1.27	0.01
K2O	1.14	0.01	0.40	0.01	1.14	0.01
P2O5	0.02	0.06	0.02	0.08	0.19	0.06
LOI	8.67	24.67	4.20	9.65	2.15	8.87
Total	99.39	92.88	98.73	91.41	99.21	100.26
Cr(ppm)	7	7	9	4	22	4
Ni	2	3	2	-1	2	-1
Co	4	2	4	2	10	-1
V	2	1	1	4	379	3
Cu	241	228	9	256	10	6
Pb	100	395	92	8279	31	62
Zn	1970	3690	1510	7400	67	1260
Cd	8.90	24.10	7.30	31.00	0.50	5.10
Mo	3.00	4.00	9.00	5.00	21.00	3.00
Rb	45	-1	4	1	38	-1
Ba	122	10	257	7	791	3
Sr	21	70	123	17	214	17
Ga	15	4	18	6	15	1
Li	176.00	13.00	28.00	40.00	18.00	4.00
Nb	8.0	2.0	7.0	-1.0	-1.0	3.0
Zr	255	17	270	1	139	176
Y	8	2	41	3	44	33
Th	8.00	2.00	9.00	-1.00	-1.00	4.00
La	22.00	1.00	12.00	3.00	8.00	8.00
Ce	61.00	2.00	42.00	6.00	22.00	29.00
F	1400.00	777.00	2730.00	885.00	267.00	2050.00
Be	2.10	1.30	2.80	3.90	2.20	1.10
Ag	1.0	3.4	0.1	15.1	0.1	2.4
Au(ppb)	na	-5.0	na	20.0	na	na

Appendix III. (continued)

Carbonate and Calc-silicate samples

Winter Hill North			Prospect #5
Sample Name	584081	584231	584101
SiO2 (wt.%)	61.95	36.00	29.50
TiO2	0.25	0.17	0.01
Al2O3	9.21	6.46	0.12
Fe2O3	0.78	0.74	0.44
FeO	3.97	3.77	2.23
MnO	0.17	0.19	0.22
MgO	11.18	37.18	13.55
CaO	7.20	1.50	,9.79
Na2O	1.44	0.03	0.01
K2O	1.87	0.02	0.01
P2O5	0.04	0.06	0.01
LOI	1.77	13.97	29.88
Total	99.83	100.09	95.77
Cr(ppm)	7	4	4
Ni	2	-1	-1
Co	5	3	-1
V	20	6	3
Cu	10	40	5
Pb	7	22	28
Zn	159	137	109
Cd	0.20	0.60	0.50
Mo	4.00	2.00	4.00
Rb	116	1	1
Ba	245	21	13
Sr	145	10	75
Ga	22	22	-1
Li	16.00	4.00	4.00
Nb	5.0	3.0	-1.0
Zr	290	207	12
Y	59	40	3
Th	8.00	1.00	-1.00
La	21.00	11.00	2.00
Ce	69.00	25.00	6.00
F	2310.00	6110.00	95.00
Be	1.50	2.00	0.60
Ag	-0.1	0.4	0.3
Au(ppb)	na	-5.0	-5.0

Appendix IV. Rare earth and trace element concentrations (ppm) from selected samples from the Connaigre Bay Group. All samples analysed by ICP-MS except Zr (ICP-EM). Hf and Ta recalculated from Zr and Nb, respectively. (-1 = less than one, na = not analysed, nc = not calculated)

Sample #		Sc	Pb	Bi	W	Mo	Rb	Cs	Ba	Sr	Tl	Li
5840068		19	155	0.02	2.79	1.84	26	6.18	358	407	0.91	19.98
SS88-536		44	2	0.01	253.65	0.50	34	6.38	720	160	4.78	32.77
5840084		19	7	0.05	5.56	0.28	12	0.61	95	144	0.06	6.45
5840.93	Mafic tuffs	20	8	0.01	4.12	0.19	16	0.30	902	48	0.56	13.58
5840192	and flows	26	35	0.84	73.17	0.80	123	0.79	2329	39	7.37	3.84
SS88-176		40	3	0.11	285.88	0.53	1	0.04	97	219	0.03	9.23
SS88-201		34	4	0.25	74.65	0.58	6	0.44	106	208	0.07	18.84
SS88-379		27	923	0.02	141.52	1.77	20	1.96	1603	35	1.57	34.37
5840002		16	17	0.08	3.32	3.51	123	2.04	1414	69	1.87	5.11
5840003		7	16	0.08	16.00	0.65	30	0.34	395	45	0.46	0.73
5840105		7	14	0.24	20.94	3.28	8	0.06	272	45	-0.05	2.57
5840111		8	9	0.25	17.60	3.67	5	0.24	185	134	0.05	2.43
SS88-C01	Felsic flows	8	5	0.03	1237.08	2.29	50	0.70	612	58	0.67	4.42
SS88-016	and tuffs	8	25	0.06	1472.81	1.27	8	0.34	160	89	0.11	4.62
SS88-182		20	8	10.39	54.27	9.59	119	1.84	495	17	1.36	14.87
SS88-189		9	20	0.09	417.30	0.74	12	0.09	281	67	0.14	4.27
SS88-205		7	1	0.13	438.04	3.47	14	0.15	353	79	0.16	1.66
SS88-208		4	5	0.08	465.36	1.61	12	1.01	24	8	0.14	80.57
SS88-209		10	8	0.04	304.18	3.63	41	0.98	275	96	0.40	3.41
SS88-003	Older	33	5	0.03	79.43	3.12	232	0.81	100	123	0.30	14.88
SS88-402	Mafic Dv.es	20	9	0.03	175.75	0.49	24	1.41	361	401	0.72	7.12
5840048	Older	7	27	0.02	3.86	0.30	3	0.22	90	56	0.11	9.45
5840049	Felsic dykes	6	19	0.13	1.26	0.68	5	0.17	85	80	0.17	6.46
5840069		8	52	0.01	3.09	1.71	12	5.95	413	78	1.05	41.07
5840191		23	917	6.98	4.51	3.25	42	0.57	676	39	3.35	14.15
SS88-012		6	179	2.65	357.77	3.93	17	0.34	126	128	0.44	2.45
5840083	Mineralized	9	19	0.13	12.56	69.66	23	0.60	93	56	0.30	2.93
5840106	Tickle Point	6	19	1.24	5.41	7.47	6	0.38	87	10	-0.10	17.55
5840104	Formation	7	8	0.35	11.16	3.62	54	0.28	790	45	0.50	7.41
5840103	samples	3	32	7.73	14.21	4.91	-1	0.11	4	1	0.35	5.68
5840102		5	67	15.30	47.16	7.89	-1	0.19	5	47	-0.10	7.10
5840113		5	11	0.34	11.68	1.77	10	0.49	137	42	-0.10	1.82
5840037		5	>10000	0.19	6.39	7.90	1	0.62	4	2	13.22	26.66
5840046		1	7368	15.10	3.99	1.73	1	0.43	6	10	6.85	25.53
5840067		2	3537	0.03	2.67	11.36	-1	0.11	12	22	2.27	4.95
5840076		1	7272	2.97	6.08	0.99	-1	0.37	7	3	9.82	2.27
5840078	Mineralized	32	2212	0.26	11.03	0.65	9	5.80	83	11	3.40	41.08
SS88-106	Sam Head	-1	>10000	0.36	56.03	109.54	-1	0.07	3	1	12.60	1.69
SS88-115	Formation	8	45	1.63	303.40	0.01	65	1.88	339	5	1.09	11.57
SS88-120	samples	15	229	1.48	300.31	1.50	112	2.46	427	8	1.65	19.06
SS88-123		34	69	0.02	333.78	1.04	1	0.38	256	65	5.56	39.95
SS88-124		10	11	0.02	59.94	2.24	69	51.73	436	35	65.73	101.15
5840041	Mg-silicate	13	187	0.04	2.60	1.34	63	23.99	123	21	0.82	215.42
5840074	f.g. sediment	24	55	0.19	9.67	0.71	26	2.30	223	138	0.75	10.36

Sample #		Ta	Nb	Hf	Zr	Y	Th	U	La	Ce	Pr	Nd
5840068		0.45	7.7	4.46	165	29	1.99	0.38	16.30	37.28	5.10	21.??
SS88-536		0.14	2.3	nc	na	21	0.22	0.05	3.10	8.68	1.50	7.28
5840084		0.25	4.3	5.41	200	46	2.37	0.45	13.48	32.16	4.85	21.31
5840193	Mafic tuffs	0.04	0.7	0.86	32	11	0.18	0.05	1.67	4.64	0.77	3.97
5840192	and flows	0.04	0.7	1.08	40	7	0.24	0.07	1.37	3.67	0.54	2.52
SS88-176		0.12	2.1	nc	na	24	0.70	0.14	5.69	15.14	2.32	10.5?
SS88-201		0.21	3.5	nc	na	27	1.03	0.21	9.06	21.93	3.23	13.??
SS88-379		0.05	0.9	nc	na	12	0.25	0.05	1.75	5.27	0.85	4.19
5840002		0.49	8.3	8.51	315	63	3.41	0.61	22.97	55.84	7.81	32.3?
5840003		0.20	3.4	5.84	216	12	2.41	0.42	4.39	10.96	1.52	6.03
5840105		0.21	3.5	4.30	159	30	4.26	0.83	18.22	35.78	4.63	17.60
5840111		0.39	6.7	7.49	277	53	4.77	0.93	24.31	55.88	7.45	29.75
SS88-001		0.16	2.8	nc	na	20	3.13	0.60	19.23	52.65	6.26	24.00
SS88-016	Felsic flows	0.21	3.5	nc	na	22	2.68	0.51	29.63	66.21	7.83	28.??
SS88-182	and tuffs	0.66	11.2	nc	na	59	7.31	1.47	32.64	77.92	10.50	41.3?
SS88-189		0.23	3.9	nc	na	41	5.65	0.95	18.02	40.56	5.32	21.02
SS88-205		0.18	3.1	nc	na	40	4.45	0.84	19.58	45.31	6.06	24.38
SS88-208		0.08	1.4	nc	na	16	3.45	0.80	10.71	28.44	4.09	17.25
SS88-209		0.25	4.3	nc	na	29	3.19	0.63	22.05	55.98	8.18	34.00
SS88-003	Mafic Dykes	0.08	1.4	nc	na	16	0.29	0.08	2.85	7.88	1.27	6.12
SS88-402		0.41	6.9	nc	na	40	2.53	0.62	16.08	36.53	5.05	21.93
5840048		0.39	6.6	7.68	284	30	5.34	0.84	19.44	46.53	6.31	24.82
5840049	Felsic dykes	0.36	6.1	6.51	241	49	4.82	0.91	19.48	43.97	6.11	23.80
5840069		0.44	7.4	7.95	294	21	5.41	1.12	15.71	36.44	4.90	18.68
5840191		0.05	0.8	1.30	48	12	0.20	0.08	2.33	5.83	0.95	4.23
SS88-012	Mineralized	0.20	3.4	nc	na	23	1.83	0.30	10.38	24.00	3.17	12.60
5840083	Tickle Point	0.25	4.2	4.14	153	34	1.83	0.34	11.27	28.27	3.95	15.91
5840106	Formation	0.28	4.8	4.14	153	26	3.83	1.00	11.96	26.86	3.61	14.50
5840104	samples	0.29	5.0	4.08	151	27	4.60	0.96	14.22	31.40	4.20	15.72
5840103		0.10	1.7	2.35	87	11	1.68	0.44	5.18	12.14	1.54	6.26
5840102		0.20	3.4	4.22	156	24	2.33	0.50	9.78	23.30	3.00	11.97
5840113		0.20	3.4	5.38	199	20	4.03	0.84	4.97	13.36	1.69	6.64
5840037		0.04	0.7	1.30	48	4	0.36	0.79	1.46	3.73	0.54	2.16
5840046		0.01	0.2	0.03	1	3	0.07	0.46	1.68	3.61	0.49	1.94
5840067		0.02	0.4	1.05	39	4	0.50	0.23	2.81	6.04	0.75	2.89
5840076		0.01	0.1	0.24	9	2	0.12	0.08	1.08	1.78	0.21	0.81
5840078	Mineralized	0.09	1.5	1.49	55	18	0.67	0.14	3.41	9.00	1.38	6.77
SS88-106	Sam Head	0.02	0.3	nc	na	3	0.17	0.20	1.06	3.42	0.55	2.27
SS88-115	Formation	0.12	2.1	nc	na	11	2.45	0.42	7.52	18.71	2.58	10.30
SS88-120	samples	0.22	3.8	nc	na	19	4.13	0.70	14.99	35.08	4.85	19.55
SS88-123		0.59	10.1	nc	na	19	0.24	0.27	2.07	5.98	1.06	5.61
SS88-124		0.01	0.2	nc	na	8	0.42	0.04	3.16	10.26	1.52	6.79
5840041	Mg-silicate	0.36	6.1	6.08	225	20	6.06	0.97	23.06	51.87	6.73	25.64
5840074	f.g. sediment	0.76	13.0	3.49	129	22	1.70	0.37	12.98	28.95	3.83	15.87

Sample #		Sm	Eu	Gd	Tb	Dy	Ho	Er	Tm	Yb	Lu	Be
5840068		5.49	1.55	5.19	0.91	5.58	1.12	3.43	0.46	2.86	0.41	1.15
SS88-536		2.66	0.84	3.34	0.63	4.17	0.88	2.56	0.36	2.24	0.33	0.44
5840084		6.16	2.21	8.39	1.47	9.79	1.97	5.16	0.72	4.32	0.58	1.08
5840193	Mafic tuffs	1.34	0.61	2.00	0.31	2.05	0.43	1.16	0.16	1.06	0.16	0.56
5840192	and flows	1.37	0.67	0.93	0.17	1.16	0.24	0.75	0.11	0.78	0.12	0.65
SS88-176		3.45	1.31	3.80	0.72	4.69	0.98	2.81	0.39	2.26	0.31	0.73
SS88-201		4.31	1.52	4.69	0.87	5.51	1.10	3.13	0.41	2.47	0.32	1.25
SS88-379		1.46	0.10	2.09	0.32	2.11	0.45	1.38	0.20	1.25	0.19	0.66
5840002		9.31	2.28	9.54	1.94	12.59	2.54	7.07	0.96	5.73	0.72	1.08
5840003		1.56	0.31	1.43	0.27	2.06	0.53	1.94	0.33	2.55	0.39	0.85
5840105		4.55	1.32	5.07	0.92	5.91	1.23	3.57	0.51	3.26	0.51	1.18
5840111		7.94	1.63	7.80	1.47	9.47	1.94	5.80	0.89	5.72	0.86	1.67
SS88-001		5.55	1.15	4.56	0.72	4.28	0.91	2.93	0.46	3.17	0.49	0.54
SS88-016	Felsic flows	5.79	1.34	4.78	0.82	4.78	0.96	2.89	0.42	2.82	0.45	0.48
SS88-182	and tuffs	9.85	2.12	9.79	1.79	11.39	2.32	7.10	1.02	6.48	0.94	1.34
SS88-189		5.87	1.67	5.76	1.17	7.82	1.68	5.15	0.75	4.77	0.70	1.58
SS88-205		6.39	1.24	6.08	1.18	7.63	1.60	4.75	0.70	4.57	0.70	1.40
SS88-208		4.49	0.86	2.97	0.44	2.34	0.56	2.00	0.36	2.76	0.47	0.36
SS88-209		8.84	1.57	6.69	1.01	5.56	1.13	3.47	0.53	3.41	0.53	2.24
SS88-003	Mafic Dykes	2.19	0.86	2.55	0.50	3.17	0.65	1.82	0.25	1.71	0.23	0.56
SS88-402		6.07	1.67	6.35	1.15	7.17	1.54	4.59	0.65	4.10	0.62	1.23
5840048		6.24	0.85	5.07	0.90	5.65	1.20	3.98	0.63	4.48	0.73	1.16
5840049	Felsic dykes	6.15	1.15	6.28	1.25	8.44	1.80	5.72	0.82	5.32	0.80	1.11
5840069		4.45	0.54	3.12	0.55	3.42	0.80	3.11	0.53	4.05	0.71	1.19
5840191		1.37	0.67	1.59	0.29	2.03	0.41	1.19	0.17	1.08	0.16	0.91
SS88-012	Mineralized	3.51	0.88	3.57	0.66	4.05	0.82	2.33	0.31	1.75	0.22	0.09
5840083	Tickle Point	4.71	2.04	6.03	1.06	6.53	1.31	3.26	0.42	2.55	0.37	1.05
5840106	Formation	3.67	0.85	4.06	0.78	4.98	1.03	3.25	0.47	3.03	0.45	0.60
5840104	samples	4.24	0.95	4.31	0.83	5.40	1.15	3.64	0.53	3.50	0.53	1.00
5840103		1.80	0.28	1.97	0.37	2.38	0.47	1.32	0.22	1.50	0.21	0.65
5840102		3.14	0.65	3.59	0.72	4.76	1.02	2.91	0.42	2.79	0.43	0.63
5840113		1.85	0.45	2.17	0.49	3.22	0.78	2.79	0.47	3.48	0.59	1.06
5840037		0.61	0.19	0.57	0.10	0.64	0.13	0.44	0.06	0.47	0.07	2.50
5840046		0.43	0.17	0.38	0.07	0.40	0.10	0.28	0.05	0.30	0.04	1.79
5840067		0.67	0.28	0.63	0.11	0.72	0.16	0.54	0.08	0.56	0.09	0.77
5840076		0.22	0.20	0.20	0.04	0.31	0.05	0.17	0.03	0.25	0.03	1.31
5840078	Mineralized	2.25	1.04	2.83	0.50	3.12	0.66	1.76	0.26	1.67	0.26	7.89
SS88-106	Sam Head	0.59	0.22	0.53	0.09	0.54	0.11	0.30	0.04	0.24	0.04	0.20
SS88-115	Formation	2.53	0.46	2.17	0.34	1.97	0.44	1.42	0.24	1.74	0.29	1.04
SS88-120	samples	4.94	0.95	3.72	0.55	3.38	0.73	2.44	0.39	2.99	0.51	2.06
SS88-123		2.12	0.63	2.83	0.54	3.58	0.76	2.26	0.31	2.11	0.31	1.91
SS88-124		2.19	0.42	2.19	0.40	2.31	0.44	1.27	0.16	0.99	0.13	1.67
5840041	Mg-silicate	5.67	1.12	3.83	0.61	3.82	0.83	2.77	0.44	3.38	0.56	2.14
5840074	f.g. sediment	4.15	1.42	4.01	0.69	4.18	0.82	2.40	0.32	1.92	0.26	0.94

APPENDIX V

ANALYTICAL TECHNIQUES

V.1. Induced Coupled Plasma/Mass Spectrometry (ICP/MS) Techniques

Rock samples weighing 1-2 kg were broken with a steel hammer into pieces weighing approximately 100 g. Two or three of these pieces were then fed through a steel jaw crusher. The chips produced in this crusher were then powdered to -100 mesh size using a bowl and puck assembly. Between samples, the jaw crusher was cleaned with a pressurized air gun and then with methanol. To remove sample remnants from the bowl and puck, granular silica was powdered between samples. The silica powder was then removed and the bowl and puck were cleaned with the air gun and methanol.

ICP/MS analytical techniques were used to analyse for selected trace and rare earth elements (see Introduction, Chapter 3 for the trace element list). Approximately 0.1 g of sample was weighed into a 100 ml teflon beaker. Ten to 15 ml of hydrofluoric (HF) and 10-15 ml of concentrated nitric acid (HNO_3) were added to the beaker and evaporated to near dryness. Ten ml of 8N HNO_3 were then added and again evaporated to near dryness. If any residue remained after this preparation, equal amounts of 8N HNO_3 and 6N hydrochloric acid (HCl) were added and then evaporated. A final evaporation with 8N HNO_3 was then undertaken. The samples were put into

solution by adding approximately 10 ml of 0.2N HNO_3 and heated, if necessary. More 0.2N HNO_3 was then added to bring the volume up to 90 ml. If the sample did not contain any silicate minerals, then an initial dissolution with 6N HCl and 8N HNO_3 was used instead of the HF and HNO_3 dissolution.

Two tubes were used in the final analysis. Tube #1 contained 9 g of sample solution and 1 gram of 0.2N HNO_3. Tube #2 contained 9 g of sample solution and 1 g of a mixed spike solution.

Established values and averages for the analysed rare earth and trace elements for the university standard (SY-2) are listed in Table V.1.

V.2. Newfoundland Department of Mines and Energy Geochemical Laboratory

Major and trace element analyses (except for LOI, F, and Au) were determined by either atomic absorption spectrophotometry (AAS) or by inductively coupled plasma emission spectrometry (ICP/ES). The majority of the major element analyses are determined using AAS whereas trace elements are analysed mainly by ICP/ES (Wagenbauer, 1988, 1989). The method of preparation for the major elements, taken from Wagenbauer et al. (1983) is as follows:

A 0.1 g portion of sample is fused in graphite crucible with 0.5 g of lithium metaborate at 1000°C. The hot melt is poured into a 250 ml polycarbonate bottle containing 25 ml of

Table V.1. Established values for sample standard SY-2 and the average of four analyses for the same sample. All analyses are in ppm.

ELEMENT	STANDARD VALUE	ANALYTICAL AVERAGE	ELEMENT	STANDARD VALUE	ANALYTICAL AVERAGE
Li	96	92.449	Gd	14.9	14.547
Be	24	22.47	Tb	2.86	2.891
Sc	7	7.638	Dy	19.5	19.955
Rb	220	227.67	Ho	4.5	4.485
Sr	271	267.91	Er	15	15.047
Y	114	113.526	Tm	2.4	2.406
Zr	265	257.066	Yb	17.3	17.346
Nb	30	29.82	Lu	2.89	2.893
Mo	0.8	0.822	Hf	8.5	8.189
Cs	2.68	2.674	Ta	1.8	2.237
Ba	447	442.786	W	6	7.447
La	69	67.915	Tl	1.54	1.527
Ce	157	154.676	Pb	80	80.24

4 vol.% HCl and 5 ml of concentrated HF, then digested at 90°C for 1.5 hours. After the contents have cooled to room temperature, 50 ml of 50 g/l boric acid is added to complex the excess HF and the same is digested again at 90°C for 1.5 hours. The solution is transferred into a 100 ml polyethylene volumetric flask, made to volume, and mixed.

The method of preparation for the trace element analyses is similar to that described in section V.1. A summary of methods used and the detection limits is presented in Table V.2.

LOI is determined at 1000°C by the method outlined by Hillebrand et al. (1953), whereas F is measured using fluoride-ion specific electrodes and a digital ionanalyser (Wagenbauer et al., 1983).

Au assays are determined by Chemex Laboratories using a fire assay and atomic absorption method. The detection limit for Au is 5 ppb.

V.3. Electron Microprobe Analysis

Analysis of individual minerals was carried out on an automated JEOL JXA-50A electron probe microanalyser, equipped with Krisel Control through a PDP-11 computer. The probe has an operating potential of 15 kilovolts and a 1 micron wide beam with a current of approximately 20 microamperes. Compositions of the probed minerals were calculated by reference to calibration curves based on the analysis of a

Table V.2. Summary of methods used and detection limits achieved for trace elements in silicate
rocks by atomic absorption spectrophotometry (AAS) and by inductively coupled plasma
emission spectrometry (ICP/EM).

Element	Digestion	AAS (ppm)	ICP/EM (ppm)
Ag	HF-HCl-HClO4	0.1	.
Ba	HF-HCl-HClO4	10	2
Be	HF-HCl-HClO4	0.1	0.1
Cd	HF-HCl-HClO4	0.1	.
Ce	HF-HCl-HClO4	.	2
Co	HF-HCl-HClO4	2	.
Cr	HF-HCl-HClO4	2	.
	LiBO4 fusion	.	10
Cu	HF-HCl-HClO4	2	.
Ga	HF-HCl-HClO4	.	2
La	HF-HCl-HClO4	.	2
Li	HF-HCl-HClO4	0.1	0.1
Mo	HF-HCl-HClO4	2	.
Nb	HF-HCl-HClO4	.	2
Ni	HF-HCl-HClO4	2	.
Pb	HF-HCl-HClO4	2	.
Rb	HF-HCl-HClO4	2	.
Sr	HF-HCl-HClO4	2	2
Th	HF-HCl-HClO4	.	2
V	HF-HCl-HClO4	5	2
Y	HF-HCl-HClO4	.	2
Zn	HF-HCl-HClO4	2	.
Zr	LiBO4 fusion	.	5

standard material (a pyroxene standard - ACPX05).

The thin sections entered into the microprobe were first polished, then coated with a thin carbon film in a Varium vacuum evaporator.

V.4. Scanning Electron Microscope Mineral Identification

Polished, carbon-coated thin sections were examined in a Hitachi S570 scanning electron microscope (SEM) at a voltage of 15 kilovolts. Backscatter images were obtained with a GW Electronic type 113 solid state Backscatter Electron Detector. Semi-quantitative X-ray analyses were performed with a Tracer Northern 5500 Energy Dispersive X-ray Analyser equipped with a spectral resolution of 145 electron volts.